MASARYK UNIVERSITY

FACULTY OF SCIENCE

DEPARTMENT OF EXPERIMENTAL BIOLOGY

ROLE OF SKP2 IN CYTOKINETICS OF CANCER STEM CELLS

Ph.D. Dissertation

Šárka Šimečková

Supervisor: Mgr. Karel Souček, Ph.D.

Brno 2018

BIBLIOGRAPHIC ENTRY

Author:	Mgr. Šárka Šimečková Faculty of Science, Masaryk University Department of Experimental Biology
Title of dissertation:	Role of Skp2 in cytokinetics of cancer stem cells
Degree programme:	Biology
Field of study:	Animal Physiology
Supervisor:	Mgr. Karel Souček, Ph.D. Faculty of Science, Masaryk University Department of Experimental Biology
Academic year:	2018
Number of pages:	184
Key words:	Prostate cancer, cancer stem cells, Skp2, MLN-4924, multiparametric flow cytometry

BIBLIOGRAFICKÝ ZÁZNAM

Autor:	Šárka Šimečková Přírodovědecká fakulta, Masarykova univerzita Ústav experimentální biologie
Název práce:	Úloha Skp2 v cytokinetice nádorových kmenových buněk
Studijní program:	Biologie
Studijní obor:	Fyziologie živočichů
Školitel:	Mgr. Karel Souček, Ph.D. Přírodovědecká fakulta, Masarykova univerzita Ústav experimentální biologie
Akademický rok:	2018
Počet stran:	184
Klíčová slova:	Rakovina prostaty, nádorové kmenové buňky, Skp2, MLN-4924, mnohoparametrická průtoková cytometrie

DECLARATION

Hereby I declare that I worked on this Ph.D. dissertation on my own under the supervision of my supervisor Mgr. Karel Souček, Ph.D. and I used only primary and secondary literature, which is properly cited and listed in the reference section.

In Brno Šárka Šimečková

ABSTRACT

A tumour is recognized as a neoplastic tissue consisting of various cell types and a substantial degree of heterogeneity is found in a tumour mass within cancer cells. Well accepted concepts contributing to such heterogeneity and tumour plasticity are cancer stem cells (CSCs) and the process of epithelial-to-mesenchymal transition (EMT). Both CSCs and EMT were shown to be involved in prostate cancer (PCa) progression. Moreover, the acquisition of a mesenchymal phenotype causing appearance of CSC-like characteristics in PCa was described. Since the CSCs are described as a subpopulation within a tumour that is responsible for tumour heterogeneity and drug resistance, they represent an attractive target for anticancer therapy.

S-phase kinase-associated protein 2 (Skp2) was previously described as an oncogene and its overexpression was detected in various cancers including PCa. It is involved in the regulation of cytokinetics - processes encompassing cell cycle, apoptosis, and differentiation. However, the role of Skp2 in CSCs is not well described yet. Thus, in our study, we focused on the role of Skp2 in prostate CSCs. We found that high nuclear expression of Skp2 and mesenchymal phenotype correlated with high Gleason score in PCa patients. *In vitro*, increased Skp2 expression was observed in PCa cell lines with mesenchymal and CSC-like phenotype compared to their epithelial counterparts. Conversely, the CSC-like phenotype was less represented in cells, in which *SKP2* expression was silenced. Furthermore, we observed that Skp2 downregulation led to increased expression of CSCs markers CD24 and CD44. Additionally, we showed that high expression levels of both CD24 and CD44 was associated with favourable recurrence-free survival for PCa patients. Pharmacological inhibition of SCF^{Skp2} activity resulted in cell cycle arrest, induced late apoptosis in $CD24^{+}$ cells, and affected the clonogenic ability of single cells in 2D condition.

The importance of complex analysis of cellular response to experimental treatments in samples with a limited number of cells (*e.g.,* rare populations like CSCs) prompted us to establish a multiparametric flow cytometric assay. This facilitates the

complex analysis of cellular phenotype-dependent response to an experimental treatment on a single cell level. Herein, we describe a seven-parameter flow cytometric assay that could complement routine cell-based tests and bring valuable information to the analysis of complex cellular response in phenotypically characterized cell populations.

In this thesis, we propose that high expression of Skp2 is associated with mesenchymal phenotype concomitant with the CSCs-like characteristics of the cells. Skp2 downregulation or pharmacological inhibition of SCF^{Skp2} affect cancer CSCs-like properties and change surface expression of CSC markers. Furthermore, we introduce a powerful flow cytometric assay for complex analysis of cellular phenotype after anti-cancer treatments that enables to distinguish a response of a small subset of cells defined by CD surface antigens within heterogeneous samples.

ABSTRAKT

Nádor je abnormální tkáň, která se skládá z různých buněčných typů. Samotné nádorové buňky jsou různorodé. K heterogenitě nádorové tkáně přispívají nádorové kmenové buňky (NKB) a proces epiteliálně mesenchymálního přechodu (EMT). Úloha NKB i EMT ve vývoji rakoviny prostaty již byla prokázána. Mimo to byla popsána souvislost mezi ziskem mesenchymálního fenotypu a fenotypu NKB u nádorových buněk prostaty. I když NKB tvoří jen malou populaci buněk v nádoru, byla popsána jejich rezistence k terapeutikům a jejich podíl na heterogenitě nádoru, a proto představují zajímavý cíl pro protinádorovou terapii.

S-phase kinase-associated protein 2 (Skp2) je onkogen, jehož zvýšená hladina byla popsána u mnoha nádorových onemocnění včetně rakoviny prostaty. Skp2 se podílí na řízení cytokinetiky - buněčných procesů zahrnujících buněčný cyklus, apoptózu či diferenciaci. Jelikož funkce Skp2 u NKB není stále dobře známá, zaměřili jsme se na úlohu Skp2 u NKB prostaty. Výsledky prezentované v předkládané disertační práci ukazují, že zvýšená jaderná hladina Skp2 a mesenchymální fenotyp buněk koreluje s vyšším Gleasonovým skóre pacientů. V *in vitro* podmínkách jsme pozorovali zvýšenou hladinu Skp2 u buněk s mezenchymálním fenotypem, které navíc vykazovaly znaky typické pro NKB. Snížení hladiny Skp2 v buňkách naopak vedlo ke zvýšení četnosti buněk pozitivních na znaky CD24 a CD44. Ukázali jsme, že u pacientů s rakovinou prostaty je zvýšená hladina těchto znaků spojena s příznivou prognózou bez recidivy. Farmakologická inhibice komplexu SCF^{Skp2} vedla k zástavě buněčného cyklu, způsobila buněčnou smrt u $CD24^{+}$ buněk a snížila klonogenní kapacitu buněk kultivovaných ve 2D podmínkách.

Naším dalším cílem bylo ustanovit metodu, pomocí které bychom byli schopni komplexně vyšetřit buněčnou odpověď na působení terapeutik i u malých populací buněk (např. NKB) v heterogenních vzorcích. Průtoková cytometrie, která byla za tímto účelem použita, umožňuje vyšetřit sedm parametrů na úrovni jedné buňky a může tak přinést více informací o odpovědi specifických buněk ve vzorku.

Výsledky prezentované v této práci tedy souhrnně popisují asociaci proteinu Skp2 s horší prognózou pacientů s rakovinou prostaty a spojitost s mezenchymálním fenotypem buněk, který je dále spjat s fenotypem NKB prostaty. Snížení hladiny Skp2 nebo farmakologická inhibice SCF^{Skp2} vedla k ovlivnění těchto vlastností a ke změně jejich fenotypu. Dále jsme popsali zavedení účinné cytometrické metody ke sledování komplexní odpovědi buněk s definovaným fenotypem na experimentální působení protinádorové terapie.

ACKNOWLEDGEMENTS

I would like to thank my supervisor, Mgr. Karel Souček, Ph.D., for the opportunity to join his team and work on many interesting projects. Thank you for your help and advice, and creating superbly equipped labs for us. Thank you for the possibility to attend inspiring scientific meetings and conferences. Many thanks to Prof. Jan Vondráček, Ph.D, Prof. Jiřina Hofmanová, CSc., and Prof. Alois Kozubík, CSc., for leading the whole Department of Cytokinetisc during my studies.

I would like to thank my dear colleagues, especially Zuzka and Eva, for teaching me most of the methods and for her help during my studies. Thanks to Jano for being always there to give scientific advice, to help and to share a piece of chocolate when needed. Thanks to Radek for his friendship, technical support, and for not losing his enthusiasm even in the times when nothing seemed to work. My thanks further belong to Lucia and Ximena for the creative-scientific happenings and being there to help with anything; thanks to the whole EZKA team and all the others from our lab who contributed to creating our work environment. Special thanks belong to Iva, Martina and Katka for their technical support. Many thanks to our collaborators Assoc. Prof. Jan Bouchal, Ph.D., MUDr. Gvantsa Kharaishvili, Ph.D., from the University Palackého, and to MUDr. Milan Král, PhD., for their cooperation in our projects.

Special thanks belong to my beloved family – especially to my mum, dad, Ondra and my grannies. Thank you for being there always for me; for your love, care, support, understanding and prayers during my studies.

I would love to thank my dear friends Jana, Ivan, Hanka, Ivka, Mercedes, Sarah, Gábi and the 24-7 Prayer family, namely Šárka T., Simča, Radka, Beth, Magda, Zdeňka, Ivana Š. Alena, Edita, Ivana M., Darina, Martin, Daniel V., Veronika & Mirek, and Daniel R. Also, I am grateful for meeting Jenny, Beth, Bev, Tim, Sam, Hannah, Georgina, Danielle, Sahr, 24-7 Ibiza team, and all the boiiis during my journey. Thank you all! You came at the right time and you have been such a blessing for me. Thank you for your great support, your love, and all the fun that we have had together. Thank you for reminding me who I am, and what really matters. Thank you for making me laugh, listening in the times of despair, your encouragement and your prayers.

FINANCIAL SUPPORT

The studies included in this dissertation were supported by grants AZV ČR 15-28628A, 17-28518A & 15-33999A, HistoPARK (CZ.1.07/2.3.00/20.0185), and by project no. LQ1605 from the National Program of Sustainability II (MEYS CR), ICRC-ERA-HumanBridge a.k.a. „REGPOT“ (Grant agreement no. 316 345) from the European Regional Development Fund and MZČR 17-28518A.

© Šárka Šimečková, Masaryk University, 2018

CONTENTS

Abstract 4
Abstrakt 6
Contents 11
List of abbreviations 15
1. Introduction 17
1.1. Prostate gland, prostate cancer and prostate cancer stem cells 17
1.1.1. Prostate 17
1.1.1.1. Prostate development 17
1.1.1.2. Prostate Epithelium 18
1.1.1.3. Prostate stem cells and epithelial cell differentiation 19
1.1.2. Prostate cancer 21
1.1.2.1. Prostate cancer treatment and drug resistance 23
1.1.3. Prostate cancer stem cells 24
1.1.3.1. Characterisation of prostate cancer stem cells – functional test 26
1.1.3.2. Detection and isolation of prostate cancer stem cells 28
1.1.4. Cancer cell plasticity 30
1.1.4.1. Epithelial-to-mesenchymal transition and prostate cancer 31
1.1.4.2. Epithelial-to-mesenchymal transition and prostate cancer stem cells 31
1.2. Ubiquitin ligases in the biology of the mammalian cells 33
1.2.1. Cullin-RING ubiquitin ligases 34
1.2.2. Function of SCF^{Skp2} ubiquitin ligase in the cells 37
1.2.2.1. Skp2 regulation 37
1.2.2.2. Skp2 function 38
1.2.2.3. Role of Skp2 in cancer 40
1.2.3. SCF^{Skp2} as a target for anticancer therapy 41
1.2.3.1. Pharmacological inhibition of Cullin neddylation 41
1.2.3.2. Pharmacological inhibition of Skp2 42
2. Hypothesis and Aims of the work 45
2.1. Hypothesis 45
2.2. Specific Aims of the Thesis 47

3. Material and Methods 49
3.1. Cells and Cell Culture 49
3.1.1. DU 145 and PC3 49
3.1.1.1. Preparation of DU 145 SKP2 Knock-down cell lines 49
3.1.2. cE2 and E2 50
3.1.3. HCT 116 50
3.1.4. SU-DHL-4 50
3.1.5. Cell culture 50
3.2. Chemicals 51
3.3. Treatments 51
3.3.1. Pharmacological inhibition of SCFSkp2 in DU 145 51
3.3.2. Establishment of the multiparametric flow cytometric assay 51
3.4. Methods 52
3.4.1. Skp2 overexpression 52
3.4.2. Spheroid formation assay 52
3.4.3. Tumourigenic potential of SKP2 KD cell lines 52
3.4.4. Western blot 53
3.4.5. Immunofluorescence microscopy 54
3.4.6. Cell painting and morphology analysis 55
3.4.7. Immunoprecipitation 55
3.4.8. RNA isolation and qPCR analysis 56
3.4.9. Flow cytometry 57
3.4.9.1. ALDH1 activity detection assay 57
3.4.9.2. Annexin V assay 57
3.4.9.3. Cell cycle analysis 57
3. 4.9.4. Immunophenotype analysis 57
3. 4.9.5. Intracellular detection of Skp2 59
3.4.9.6. Multiparametric analysis 59
3.4.9.7. Instrumentation and data analysis 60
3.4.9.8. Compensation controls 60
3.4.10. Immunohistochemistry of clinical samples 61
3.4.11. Survival analysis 62
3.4.12. Statistical analysis 62

4. Results 63
4.1. High Skp2 expression associates with a mesenchymal phenotype and increases tumourigenic potential of prostate cancer cells 63
4.1.1. High nuclear Skp2 expression and mesenchymal phenotype are associated with high Gleason score in patients with prostate cancer 63
4.1.2. Increased Expression of Skp2 is associated with mesenchymal phenotype of prostate cancer cells 65
4.1.3. Mesenchymal DU 145 cells exhibit characteristics of cancer stem-like cells 68
4.1.3.1. The expression of CD24 is increased in DU 145 epithelial cells 68
4.1.3.2. Functional tests confirming the CSC-like phenotype of DU 145 mesenchymal cells 70
4.1.4. Analysis of CSC-like properties of the cells with downregulated expression of Skp2 71
4.1.4.1. The Skp2 downregulation leads to upregulation of cell cycle inhibitors 72
4.1.4.2. The expression of CD24 is increased in *SKP2* KD cells 74
4.1.4.3. Skp2 downregulation reverses CSC-like properties of DU 145 mesenchymal cells 74
4.1.4.4. Skp2 overexpression causes a decrease of CD24 in DU 145 76
4.1.4.5. High CD24 and CD44 expression associates with favourable recurrence-free survival 77
4.1.5. Pharmacological inhibition of SCF^{Skp2} 78
4.1.5.1. Analysis of cytokinetics in DU 145 after inhibition of neddylation 79
4.1.5.2. The decrease of CD24 positive cells incidence after inhibition of neddylation 82
4.1.5.3. Clonogenic capacity of the $CD24^-$ single cells is decreased after inhibition of neddylation 86
4.2. Establishment of a tool for analysis of cellular response to experimental drug treatment in heterogeneous samples (in CSC-like cells) 88
4.2.1. Protocol workflow and optimization 88
4.2.1.1. Surface marker selection 91
4.2.1.2. Optimization of permeabilisation 91
Effect of permeabilisation on surface markers detection 91
Effect of permeabilisation on intracellular markers detection 92
4.2.1.3. Intracellular markers selection 94

4.2.1.4. Optimization of DNA stain 94
4.2.2. Application of the protocol to various models of cancer cell lines.....96
4.2.3. Analysis of response to experimental treatment in a heterogeneous sample 100
5. Discussion 104
6. Conclusions 112
7. References 114
8. List of publications and meeting contributions 130
8.1. Articles published in peer-reviewed journals with IF 130
8.1.1. first author 130
8.1.2. Co-author 130
8.2. Manuscripts 131
8.2.1. Manuscripts first author 131
8.2.2. Manuscripts co-author 132
8. 2. 3. Meeting contributions 132
8. 2.3.1. poster presentations (first author only) 132
8. 2.3.2. lectures 134
Appendices 135

LIST OF ABBREVIATIONS

ABC	ATP-binding cassette transporter
ADT	androgen deprivation therapy
Akt	protein kinase B
ALDH	aldehyd dehydrogenase
APC	anaphase-promoting complex
AR	androgen receptor
ATP	adenosine tri-phosphate
BPH	benign prostatic hyperplasia
BRCA	breast cancer type 1 susceptibility protein
CAND1	cullin associated and neddylation-dissociated 1
CARNS	castration-resistant Nkx3-1-expressing cells
CC3	cleaved caspase-3
CD	cluster of differentiation
CDC25a	cell division cycle 25
CDH1	Cdc20-homologue 1
CDK	cyclin-dependent kinase
Cdt1	chromatin licensing and DNA replication factor 1
CK	cytokeratin
CKIs	cyclin-dependent kinases inhibitors
COP9	constitutive photomorphogenesis 9
CRISPR	Clustered Regularly Interspaced Short Palindromic Repeats
CRL	cullin-RING ubiquitin ligase
CRPC	castration-resistant prostate cancer
CSCs	cancer stem cells
CTCs	cirkulating tumour cells
DAPI	4′,6-Diamidine-2′-phenylindole dihydrochloride
DNA	deoxyribonucleic acid
EdU	5-Ethynyl-2′-deoxyuridine
EGF	epidermal growth factor
EMT	epithelial-to-mesenchymal transition
EpCAM	epithelial cell adhesion molecule
FACS	fluorescence-activated cell sorting
FDA	food and drug administration
FoxM1	forkhead box M1
GABP	GA-binding protein transcription factor
GS	gleason score
HSC	hematopoietic stem cell
MAPK	mitogen-activated protein kinase
MDM2	mouse double minute 2
MEF	mouse embryonic fibroblast
MET	mesenchymal-to-epithelial transition
Myc	myelocytomatosis oncogene cellular homolog
NAE	nedd8 activating enzyme
NEDD8	neural precursor cell-expressed developmentally downregulated protein
PCA	principal component analysis
PCSCs	prostate CSCs
PFA	paraformaldehyde
PI3K	phosphatidylinositol-3-kinase
PIN	prostate intraepithelial neoplasia

PTEN	phosphatase and tensin homolog
RING	really interesting new gene
Rbx1/2	RING-box protein 1/2
RNA	ribonucleic acid
RT	room temperature
SCF	Skp1–Cullin–F-box
SP	Side population
TGF-β	transforming growth factor-β
TRAIL	TNF-related apoptosis-inducing ligand
Trop-2	trophoblast cell surface antigen 2
t-SNE	t-distributed stochastic neighbor embedding
Ub	ubiquitin
UGS	urogenital sinus
Xic1	*Xenopus* cyclin dependent kinase inhibitor
ZEB1	zinc-finger E-box binding homeobox

1. INTRODUCTION

1.1. PROSTATE GLAND, PROSTATE CANCER AND PROSTATE CANCER STEM CELLS

1.1.1. PROSTATE

The prostate is a part of male reproductive system, and its physiological function is to produce secretions that are part of the semen fluid and thereby enhance male fertility. The human prostate is a walnut-sized tubuloalveolar gland that is located below the bladder and surrounds the urethra. It consists of a fibromuscular stroma, a peripheral zone, a transition zone, and a central zone (Figure 1.1).

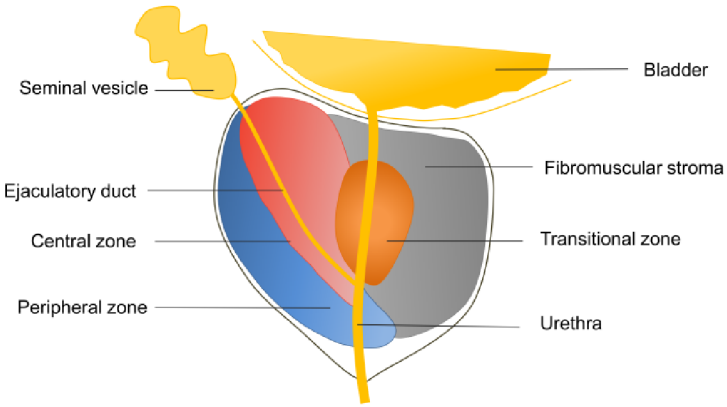

Figure 1.1 Overview of prostate anatomy

Schema depicts the adult human prostate. Key structures and regions of the prostate are indicated. Adapted from (1).

1.1.1.1. PROSTATE DEVELOPMENT

The development of the prostate is initiated during embryogenesis, and it arises from the primitive urogenital sinus (UGS) (2). The prostate is formed through

epithelial budding from the UGS starting approximately at 10 weeksof gestation in humans. The prostate organogenesis continues by the direct response of prostate epithelial cells to circulating androgens or by indirect response via stromal cells through birth and prepubertal stages, until the prostate achieves its maturity during puberty (reviewed in (2, 3)).

1.1.1.2. PROSTATE EPITHELIUM

The prostate epithelium is heterogeneous and is composed of several distinct epithelial cell types - basal cells, luminal cells, neuroendocrine cells and transit amplifying cells (Figure 1.2). The basal cells exhibit the proliferative role during epithelial renewal (4), the luminal cells are terminally differentiated secretory cells that produce prostate specific proteins in response to androgens, and the neuroendocrine cells secrete neuropeptides and hormones such as chromogranin A, neuron specific enolase, serotonin, and others (5). The different cell types can be distinguished by expression of various markers (6) including Cytokeratins (CK) (7). The basal cells express CK5 and CK14, and very low level of androgen receptor (AR). The luminal cells express CK8, CK18, AR, and secrete Prostate specific antigen (PSA) and prostatic acid phosphatase, while the neuroendocrine cells are androgen receptor negative, and express Chromogranin A and Synaptophysin (Figure 1.2).

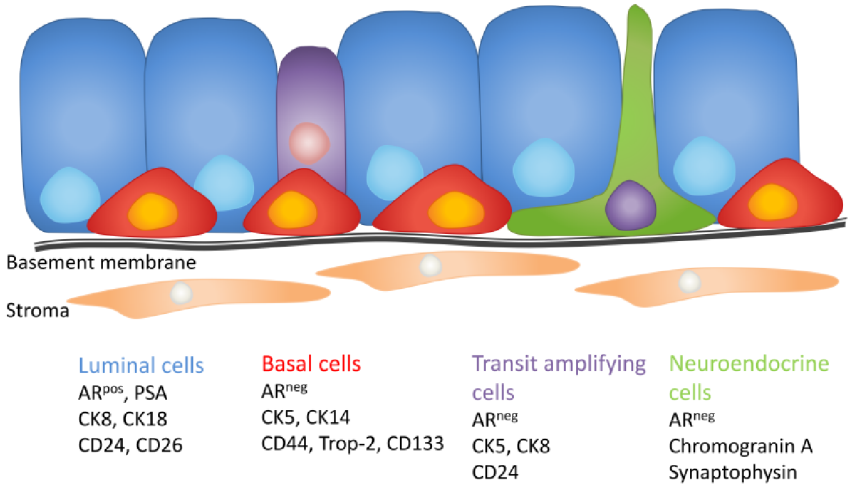

Figure 1.2 Prostate epithelium. Scheme illustrates the prostate epithelium composed of basal, luminal, transit amplifying cells and neuroendocrine cells. Below, typical markers characterizing distinct cell types are depicted. Adapted from (2) and (8).

The distinct prostate epithelial cells can also be distinguished based on expression of surface markers, mostly represented by CD (cluster of differentiation) markers that often function as receptors and adhesion molecules. Luminal cells are characterised by CD9, CD24, and integrin α_2 (CD49b) expression, while CD44, integrin α_2 (CD49b), integrin α_3 (CD49c), integrin α_6 (CD49f), and Trop-2 are expressed in basal cells specifically (9-11). Expression of CD44 and CD133 markers was documented on the surface of neuroendocrine cells (12, 13). Moreover, combined expression of particular surface markers was shown to define the differentiation status of prostate epithelial cells. Specifically, CD24 was described as a marker that distinguished between low differentiated and transit-amplifying cells in the basal layer of human prostate (8). The detection of surface markers expression is useful for identification and isolation of viable cells from the tissue with the possibility of further cultivation of these cells.

1.1.1.3. PROSTATE STEM CELLS AND EPITHELIAL CELL DIFFERENTIATION

In the prostate tissue, presence of stem cells has been reported. Normal stem cells in adult somatic tissue are characterized by their ability of self-renewal and capability to differentiate into specialized cell types. The evidence of the presence of the prostate stem cells was first described in rats in 1980s. The initial experiments demonstrated that the rat prostate underwent regression after androgen deprivation; however, a distinct subset of androgen independent basal cells survived and mediated the prostate regeneration after androgen replacement (14).

Since then, several prostate epithelium differentiation models have been suggested, and three generally accepted models are depicted in Figure 1.3 and summarized in (15). In the linear hierarchical model, the undifferentiated basal cells give rise to one copy of stem cell and a multipotent progenitor cell by asymmetric division (16). The progeny then differentiates to luminal orneuroendocrine cell through the intermediate cell. In the nonlinear hierarchical differentiation model, a common stem cell gives rise to lineage-specific progenitors, which then give rise to the distinct lineage cell types (17). The third model (independent lineage

differentiation model) suggests a presence of multiple stem cells within the epithelium and includes the luminal stem cells (so called CARNS - castration-resistant Nkx3-1-expressing cells) and basal stem cells (18). The stem cells independently give rise to basal, luminal, and neuroendocrine cells. Moreover, the stem cells are possibly multipotent and are able to generate the opposing lineage cells as well.

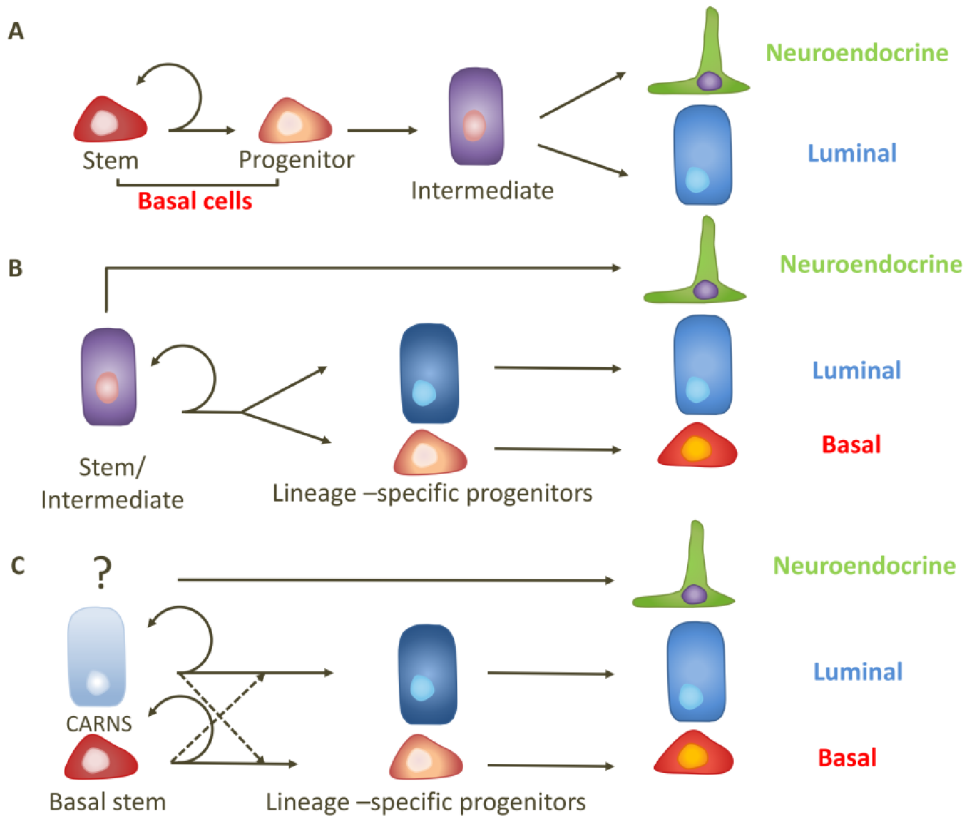

Figure 1.3 Hypothetic models of prostate cells differentiation. Scheme summarizes the models of prostate epithelium differentiation. A) linear hierarchical differentiation model, B) nonlinear hierarchical differentiation model, and C) independent lineage differentiation model. Adapted from (15).

Postnatal prostate development in mice revealed that the prostate epithelium contained multipotent progenitors, as well as unipotent stem cells that generated only basal or luminal cells, and also bipotent basal stem cells with the capability to generate basal and luminal cells (19, 20). Furthermore, in murine and human tissue, the existence of bipotent progenitors was demonstrated within both basal and luminal populations (11). Interestingly, a recent study revealed that adult prostate epithelium relies upon multipotent basal stem cells that are located in a discrete niche at the

junction between proximal ducts and urethra. They constantly undergo self-renewal, giving rise to bipotent basal progenitors that migrate along the proximal-distal axis of ducts, and are giving rise to luminal cells that replace those lost continually through apoptosis (21). The precise regulation of stem cells cytokinetics (proliferation, differentiation and apoptosis) is critical for proper development and maintenance of the prostatic tissue and its deregulation can lead to neoplastic transformations.

1.1.2. PROSTATE CANCER

Prostate cancer is the second leading cause of cancer-related death in men in Western countries (22). The majority of prostate cancer cases is represented by carcinomas (23) that mainly arise in the peripheral zone of the prostate, while the benign prostatic hyperplasia (BPH) characterised by non-malignant overgrowth of the prostatic tissue originates most frequently in the transition zone (24). These two diseases are the most prevalent neoplastic transformations in prostate and exhibit similarities in clinical manifestations. However, the association between BPH and increased prostate cancer risk is controversial, and yet not fully elucidated (25, 26). The prostate intraepithelial neoplasia (PIN), on the other hand, is widely accepted as the precursor of prostate cancer, and is characterised by luminal epithelial hyperplasia, reduction in basal cells, and enlargement of nuclei and nucleoli (27). The role of inflammation has been implicated in the progression of both, BPH and prostate cancer (28).

Prostate cancer is a multifocal disease, for the primary tumours contain multiple histopathological foci. The lesions exhibit different genetic abnormalities (29), and arise from both basal and luminal cells (30, 31). In the prostate gland, multiple transforming neoplastic events result in latent prostate cancer that does not progress into a clinically detectable disease (32). Human prostate cancers are pathologically classified as adenocarcinoma, with the vast majority corresponding to AR positive acinar adenocarcinoma (32). In the course of the disease progression, metastasis occur. Bones, lungs, and liver are the most frequent sites of distant prostate cancer metastasis (33).

The severity of the prostate cancer is mainly determined by the spread into the body and is defined by the stage of the disease. The stage of prostate cancer is estimated based on the results of staging and diagnostics tests, including detection of PSA level in blood and Gleason score (based on histopathological grading of the biopsy) (34) (Figure 1.4). In stage I, prostate cancer is found in one-half or less of one lobe of the prostate. The Gleason Score (GS) is 6 or lower and PSA level in the blood is lower than 10 ng/ml. In stage II, cancer is more advanced than in stage I but has not spread outside the prostate. The blood level of PSA is between 10 and 20, and the GS is 7 or lower and can be found in one-half or more than one-half of the prostate. The stage III is characterised by the spread of the disease out of the prostate and may disseminate into seminal vesicles, the PSA level, and GS can vary. In stage IV, cancer spreads beyond the seminal vesicles to nearby tissue or organs, metastasis to distant organs may occur, and the PSA level and GS vary.

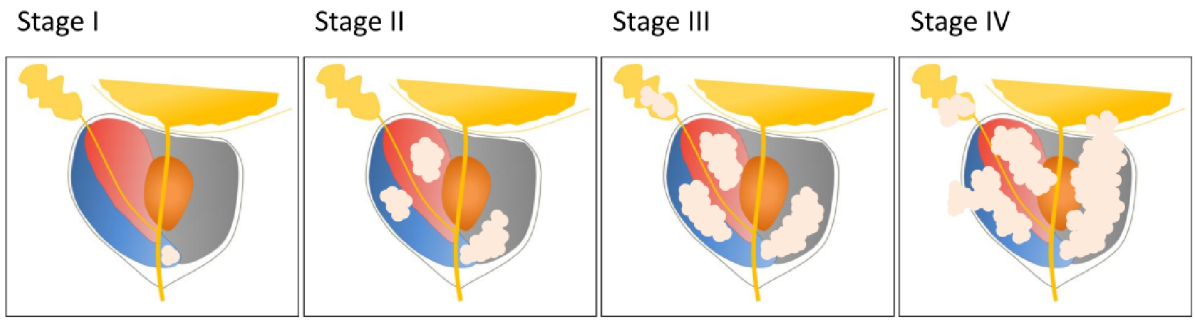

Figure 1.4 Prostate cancer staging. The scheme summarises the progression of the prostate cancer. Adapted from (34).

The highest incidence of prostate cancer was reported in North America and Oceania, in the opposite, the lowest occurrence was recorded in Asia (35). Latest statistics available for the Czech Republic show that in 2015, 7 049 new cases of prostate cancer were diagnosed, and 1 440 prostate cancer related deaths were recorded (36). Prostate cancer incidence increases significantly with age of the patients; typically, older men are diagnosed with higher grade and stage of prostate cancer than younger men. A significant correlation between Gleason score ≥ 8 and age

above 80 years was demonstrated (37). Moreover, increased risk of prostate cancer specific-mortality was shown in older patients (>70 years) with Gleason score 6 and 7, compared to younger patients (38). In another study, biologically more aggressive tumours were found in patients aged >70 years. However, higher age was not an independent predictor of survival after radical prostatectomy, whereas adverse prostate cancer features and severe comorbidities were (39).

Risk factors for prostate cancer, such as increasing age, African American race and family history, are recognized (40). Despite the apparent link between prostate cancer and advanced age of the patients, there is an increasing evidence of disease detection in younger men in western countries (35). Recently, increased prostate cancer detection across all age groups with a high-grade disease in younger patients (<50 years) was reported (41). Furthermore, Lin *et al.* showed that among men who had tumours with a Gleason score between 5 and 7, overall survival was worse with advancing age. Conversely, among men with high Gleason score or locally advanced cancer at diagnosis, the youngest (ages 35-44 years) were at the highest risk of all-cause and cancer-specific death (42). Hereditary prostate cancer accounts for a greater proportion of early onset of prostate cancer (men ≤55 years at diagnosis) (43). Thus, prostate cancer is not only a problem of elderly men but there is an increasing evidence of aggressive disease detected in younger men.

1.1.2.1. PROSTATE CANCER TREATMENT AND DRUG RESISTANCE

Early-stage prostate cancer is usually slow-growing, and may take years to cause any symptoms. The treatment options for early-stage prostate cancer include surgery, radiation therapy and active surveillance (44).

If the disease progresses into an advanced or metastatic prostate cancer, androgen deprivation therapy (ADT) is a critical component of the cure (45). Interestingly, the surgical or medical castration was the first prostate cancer treatment described in the 1940s (46). However, despite the initial tumour regression after ADT, the majority of patients develop castration-resistant disease (45). Current standard treatment of patients with castration-resistant prostate cancer (CRPC) is the anti-

mitotic agent docetaxel (47). Unfortunately, the patients can further develop docetaxel resistance, and therefore, new agents like cabazitaxel, abirateron or enzalutamide to treat patients with acquired docetaxel resistance are under investigation (45, 48, 49). Resistance to conventional treatments and development of CRPC remain challenging in prostate cancer therapy. Therefore, a better understanding of the processes that are behind the CRPC development can lead to the identification of new possible targets to treat this disease.

1.1.3. PROSTATE CANCER STEM CELLS

Cancer stem cells (CSCs) were initially documented in leukaemia and multiple myeloma as a small subset of cells that were capable of extensive proliferation and colony formation *in vitro* (50). Later on, the CSCs (or cancer stem-like cells) were also described in solid tumours (51, 52) including prostate cancer (53). The prostate CSCs displayed a significant capacity for self-renewal, extensive proliferation, differentiation, and invasion.

In principle, cancer stem cells are described as a small subset of transformed cells within a tumour with the properties of normal stem cells. The resemblance of CSCs to normal stem cells (reviewed in (54)), is shown in Figure 1.5. The CSCs possess the ability of self-renewal and can produce more differentiated progenitors. CSCs further exhibit increased resistance to drugs, avoid apoptosis, and can undergo unlimited division due to active telomerase. The proliferation of CSCs can be switched from quiescence to active proliferation. CSCs are located in an environment called onco-niche that contributes to sustaining their stem cell phenotype. Interestingly, it was shown that stromal cells isolated from the peripheral zone, but not the transitional zone of human prostate, promoted tumourigenic potential of prostatic CSCs (55). In consequence of their features, CSCs are involved in tumour maintenance, contribute to tumour heterogeneity, and promote disease progression (56), metastasis and chemoresistance (summarised in (57)). Moreover, signalling pathways that are essential for maintenance of stem cell phenotype, such as Wnt,

Notch, Hedgehog, PI3K/Akt, Ras/MAPK or STAT3 pathways, may be activated in cancer stem cells (56, 58).

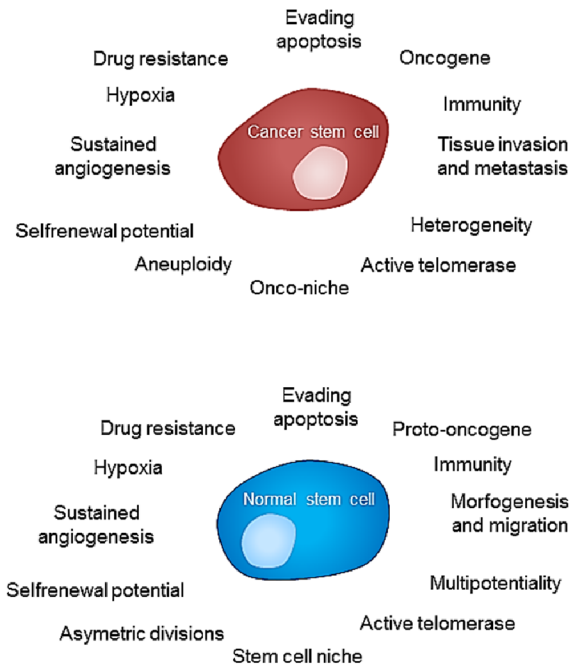

Figure 1.5 Properties of cancer stem cells and normal stem cells. The scheme illustrates feature similarities among the normal stem cells and cancer stem cells. Adapted from (54).

Despite the considerable progress in the field of CSCs biology, the origin of the CSCs is still a matter of debate and remains to be fully elucidated. Up to date, there are several theories describing the CSCs origin (59). The similarity of the CSCs to normal stem cells suggests that they can originate directly from the adult stem cell or more differentiated progenitors/transit amplifying cells that undergo oncogenic transformation. Another possibility is that CSCs can originate from embryonic stem cells (60). As mentioned previously, there is evidence that prostate cancer can arise from both basal and luminal cells. The normal prostate stem cells are located in basal layer of the epithelium (21), and several studies described the prostate cancer stem cells (PCSCs) as those exhibiting characteristics of basal cells (53, 61, 62). On the other hand, luminal cells with stem cells properties were also identified, suggesting that PCSCs arise from luminal progenitors (63) or CARN cells (18).

The role of PCSCs in prostate cancer progression and development of CRPC was suggested in several studies (64, 65). Rybak *et al.* proposed a model of CRPC development comprising the PCSC (Figure 1.6). They suggested that low-risk prostate cancer progresses in heterogeneous tumours during the active surveillance, and that administration of ADT causes the elimination of androgen-responsive cells resulting in tumour regression. However, ADT insensitive PCSCs remain in the tumour. They could be eventually activated, and subsequently initiate the progression of CRPC (56). Thus, PCSCs represent a target of interest for further studies to describe their characteristics in detail, with the potential of targeting them in cancer treatment (66, 67).

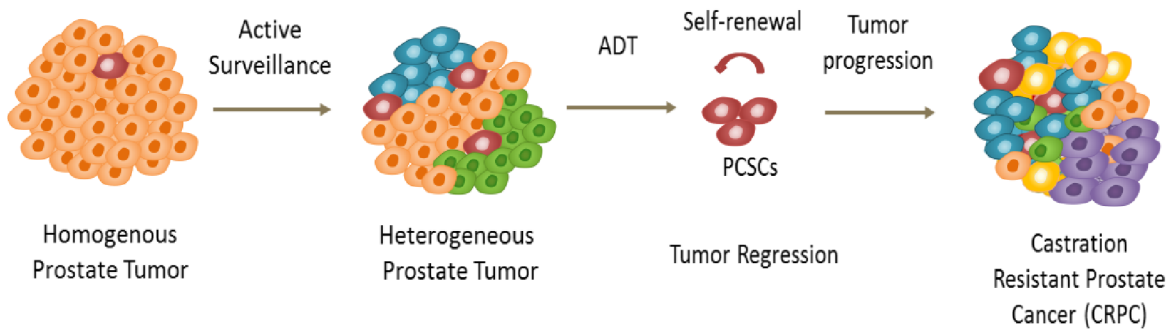

Figure 1.6 Prostate cancer stem cells and CRPC development. The scheme demonstrates the development of CRPC and the role of PCSCs in this process. Adapted from (56).

1.1.3.1. CHARACTERISATION OF PROSTATE CANCER STEM CELLS – FUNCTIONAL TEST

To comprehend the role of CSCs in carcinogenesis and cancer progression, we need tools that enable their investigation. The gold standard method confirming the presence of CSCs within a human tumour is a serial transplantation of tumour cells into immunodeficient mice, where the CSCs give rise to a tumour recapitulating the phenotype of the original tumour (68).

The *in vitro* approaches used for detection of CSCs comprise functional assays that reflect the CSCs properties such as self-renewal and drug resistance. To confirm CSCs phenotype *in vitro*, the self-renewal of CSCs is verified by the ability of single

cells to form colonies in 2D conditions (69, 70) or by the formation of tumourspheres in 3D culture. To evaluate the clonogenic capacity of the cells in 2D culture, cells are seeded in low density, and the ability of the single cells to form colonies is analysed. Moreover, the clonogenic capacity of a single cell with a specific immunophenotype can be examined (70). Using this method, a single cell from a heterogeneous sample with defined phenotype is sorted per well in a multi-well plate by fluorescence-activated cell sorting (FACS). The ability of single cells to form colonies is counted. Moreover, microscopic analysis of the phenotype of single-cell-derived colonies is possible (71).

Since the discovery that neural tissue contains a population of stem cells capable to form neurospheres *in vitro* (72), sphere-forming assays have been adapted for various solid tumours, including prostate cancer (11, 53, 69). In the initial experiments, the cells were cultivated in liquid media, which resulted in cell aggregation, and therefore, the spheres raised from cell aggregates rather than from single cells. To overcome this issue and to promote the growth of single cell-derived spheres, cells may be seeded in low density into a semi-solid medium (73) onto an agar bottom layer. In addition, critical parameters are cell density, medium composition, volume, culture dish, *etc.* (74).

Another different approach typically used for detection of CSCs is measurement of aldehyde dehydrogenase (ALDH) activity. ALDHs are a group of enzymes that are involved in modulation of several cell functions such as proliferation, differentiation, survival, and response to oxidative stress (summarised in (75)). Originally, this assay was developed to detect hematopoietic stem cells (76) and later on, it was also adapted for identification of PCSCs (77-79). ALDH1A1 activity was linked to cancer stem cells phenotype and worse prognosis of the patients (80-82). High expression of ALDH1 was also correlated with poor prognosis of the patients with prostate cancer (83) as well as with high activity of ALDH1 in the PCSCs (77, 84), and resulting in promotion of radioresistance (85). The principle of this assay is based on a conversion of non-fluorescent substrate to a fluorescent product by the

activity of ALDH (76). The fluorescent signal of individual cells is then detected by flow cytometry.

The chemoresistance of the CSCs is further, at least partially, caused by high expression of ATP Binding Cassette (ABC) transporters, particularly ABCG2 and ABCG1. These transporters are involved in efflux of the xenobiotics, and represent a major cause of multidrug resistance of these cells (86). The CSCs expressing high levels of ABCG2 were identified in primary tumours from patients with various malignancies (87). Castillo et al. showed high expression and activity of ABCG2 in prostate CSCs that were isolated from patients and cultivated as tumourspheres. These cells manifested the character of basal cells with cancer stem cell properties, including resistance to drugs (69). The assay used for detection of the CSCs based on the ABCG2 activity utilizes the ability of the cells to expel the DNA binding dye Hoechst 33342. These cells are then defined as a "Side population" (SP) (88). Pateawala *et al.* showed that the SP was enriched in CSCs and expressed a higher level of ABCG2. Surprisingly, they demonstrated that $ABCG2^+$ and $ABCG2^-$ cells exhibited similar tumourigenic properties (89).

1.1.3.2. DETECTION AND ISOLATION OF PROSTATE CANCER STEM CELLS

For detection and isolation of CSCs from the tissue of interest or in experimental conditions *in vitro,* a variety of markers presented on the cellular surface is used. These molecules mainly function as receptors and adhesion molecules. The phenotype of the cells is complex, and therefore, the cells are often identified based on a combination of several markers. PCSCs and tumour initiating cells share common features with normal stem cells (Figure 1.5), including molecules expressed on their surface. Over time, several markers defining prostate stem cells in normal tissue were described and applied to identification of PCSCs. For instance, Goldstein *et al.* described that both human and mouse prostate epithelial cells positive for Trop-2 and CD49f were capable to differentiate into basal, luminal and neuroendocrine cells *in vitro* and could regenerate prostatic tubules *in vivo* (10). Subsequently, in the study of Garraway *et al.,* it was shown that cells isolated from prostate cancer tissue with the

$CD44^+/CD49f^+/Trop2^+$ phenotype possessed high spheroid formation ability, and were able to differentiate and form tubular structures *in vivo* (90). In human, basal prostate CSCs with the $CD44^+/\alpha_2\beta_1^{high}/CD133^+$ phenotype were identified (53). Further, the cells with $CD44^+CD24^-$ phenotype are commonly used to define prostate cancer stem cells (91-93). Next, it was shown that expression of cancer stem cell markers CD49b, CD49f and c-met in primary prostate tumors was associated with progression of bone metastasis (94). Selected markers of prostate CSCs are listed in Table 1.1.

Table 1.1 Selected prostate cancer stem cells markers

Marker	Function	Species Human/Mouse	Citation
$CD24^{neg}$	Cell-to cell adhesion and cell-matrix interactions	Human	(8, 91)
CD44	Transmembrane glycoprotein Cell-to cell adhesion and cell-matrix interactions	Human, Mouse	(53, 95, 96)
CD49f	Integrin subunit α_6 mediates adhesion and migration	Human, Mouse	(97-99)
CD117	c-kit, receptor-tyrosin kinase	Mouse	(96)
CD133	Suggested role in glukose metabolism and cytoskeleton alteration	Human, Mouse	(53, 96, 100)
EpCAM	Epithelial cell adhesion molecule	Human	(101)
Integrin $\alpha_2\beta_1$	Mediates adhesion and migration	Human	(53)
Trop-2	Tumour-associated calcium signal transducer 2 Cell-to-cell adhesion	Human, Mouse	(10)
Sca-1	Stem cell antigen-1 Cell-to-cell interaction	Mouse	(10, 96-98, 102)

1.1.4. CANCER CELL PLASTICITY

Solid tumours are recognized as neoplastic heterogeneous tissue comprising tumour parenchyma that is represented by tumour cells, and tumour stroma that is composed of stromal cells, immune cells and endothelial cells (103). The tumour heterogeneity results also from differences between individual tumor cells. The intra-tumour phenotypic heterogeneity is a consequence of tumour tissue evolution driven by heritable and non-heritable causes. Two major concepts contributing to non-heritable development of intratumoural heterogeneity are CSCs and cellular plasticity.

Epithelial-to-mesenchymal transition (EMT) is a physiological process critical for fetal development from early stages of the embryogenesis (104). EMT is further recognised as a physiological response to injury, employed in wound healing, and involved in organ regeneration. In pathological conditions, this process is tightly linked to inflammation, and if the inflammation persists, fibrosis of the tissue leading to tissue degeneration can occur (105). The process of EMT is exploited in cancer by neoplastic cells and contributes to tumour heterogeneity and plasticity, favouring migration and metastasis (106).

Most of the cancer patients develop a carcinoma – cancer of epithelial origin. The epithelial cells are confined within a basement membrane and are characterised by tight cell-to-cell interaction and apical-basal polarity. During the process of EMT, the cells undergo multiple changes - they lose their epithelial features, undergo cytoskeletal reorganisation, gain the ability to migrate, and thus enable initiation of metastasis (104). Furthermore, there is an evidence of a reverse process to EMT - a transition from a mesenchymal to an epithelial state (MET) that occurs when tumour cells colonise distant sites (107). These transitions are a consequence of cellular changes that are driven at molecular level. The functional markers used for EMT detection are then molecules involved in the regulation of cell adhesion (E-cadherin, EpCAM), motility (N-cadherin) or cytoskeletal reorganisation (vimentin).

1.1.4.1. EPITHELIAL-TO-MESENCHYMAL TRANSITION AND PROSTATE CANCER

Downregulation of the major adhesion molecule E-cadherin is a well-established hallmark of EMT in many cancers including prostate and is associated with poor prognosis of prostate cancer patients (108, 109). It was shown that epigenetic suppression of E-cadherin expression facilitated by Zeb1 in prostate cancer cells promoted EMT and resulted in cell migration and metastasis (110, 111). Indeed, EMT was described as a crucial step in the progression and metastasis of prostate cancer (112, 113).

The cellular plasticity is represented by the ability of the cells to switch from one state to another. In cancer, this plasticity can be manifested by the EMT status of circulating tumour cells (CTCs) (114, 115). These cells, released from the tumour to the blood stream, are significant predictors of the overall survival of prostate cancer patients (with the number of ≥5 CTC/7.5ml of peripheral blood) (116). CTCs can exist in the epithelial, mesenchymal or intermediate state expressing both epithelial and mesenchymal markers (115, 117). Thus, these data suggest that EMT and MET play a role in the dissemination of prostate cancer cells and could be partial and reversible (118).

1.1.4.2. EPITHELIAL-TO-MESENCHYMAL TRANSITION AND PROSTATE CANCER STEM CELLS

The link between EMT and CSCs phenotype was first described in breast cancer (119). Mani et al. observed that EMT generated cells with the properties of cancer stem cells, demonstrated by increased self-renewal and tumourigenic potential. Furthermore, the acquisition of a mesenchymal phenotype concomitant with a CSCs phenotype was described also in prostate cancer. Sun *et al.* described that in both mouse and human prostate cancer cells, ADT promoted EMT as well as CSC characteristics of the cells, suggesting the link between EMT and PCSCs (120). Kong *et al.* showed that PCSCs with mesenchymal phenotype displayed stem-cell like features such as increased expression of stem cell related transcription factors Sox2, Nanog, Oct4 and/or Notch1, and exhibited enhanced clonogenic and sphere-forming

ability. This phenotype was regulated by miRNAs from miR-200 family (121). Further, an enrichment of cells with $CD24^{-}CD44^{+}$ phenotype was observed in prostate cancer cells that acquired docetaxel resistance and underwent EMT (122, 123). Moreover, the low expression of CD24 was correlated with shorter biochemical progression-free survival of the patients (123). Interestingly, in a model of a primary tumour-derived human prostate cells, it was demonstrated that not all cells having a potential for EMT exhibited stem cell-like properties (124). Altogether, emergence of CSCs is tightly linked with EMT and contributes to tumour heterogeneity and cancer cell plasticity, resulting in drug resistance (Figure 1.6), prostate cancer progression, and metastasis.

1.2. UBIQUITIN LIGASES IN THE BIOLOGY OF THE MAMMALIAN CELLS

Proteasome-mediated degradation is a critical mechanism responsible for maintaining the protein homeostasis in the cells. It is crucial for transmission and processing of both extrinsic and intrinsic signals and mediating communication between the cells. Ubiquitin-mediated proteolysis plays an irreplaceable role in the regulation of many cellular processes including cell cycle, differentiation, DNA repair, immune response, transcriptional regulation and others (125). Dysregulation of these processes may lead to serious disorders. Deregulated proteasomal degradation results in accumulation of impaired or misfolded proteins that leads to development of diseases including cancer (126), sickle cell anaemia, and neurodegenerative diseases such as Huntington disease, Alzheimer disease or Parkinson disease.

Degradation of a protein via the ubiquitin-proteasome pathway involves tagging the substrate by covalent attachment of a poly-ubiquitin chain, and degradation of the tagged substrate in the proteasome. Conjugation of ubiquitin to a substrate is a three-step cascade mechanism that is mediated by E1, E2, and E3 enzymes. E1 activates ubiquitin in an ATP-dependent manner. An ubiquitin-conjugating enzyme E2 transfers activated ubiquitin to an E3 ubiquitin ligase which is responsible for recognition of specific substrates and for tagging them by poly-ubiquitin chain (125).

Cell cycle regulation is tightly controlled by expression and activity of cyclin-dependent kinases (CDKs), cyclins and CDK inhibitors (CKIs) (127), as illustrated in Figure 1.7. The level of cyclins and CKIs oscillates during the cell cycle as a result of ubiquitin-mediated proteolysis (128). There are two major ubiquitin ligases involved in the regulation of the cell cycle progression, APC^{Cdh1} and SCF^{Skp2} (Figure 1.7) (129). Skp2, a variable component of SCF ligase responsible for specific substrate recognition, is targeted for polyubiquitination and subsequent degradation by APC^{Cdh1} during the G1 phase of the cell cycle (130). Conversely, it was shown that the SCF complex plays a role in the degradation of Cdh1 during the S phase (131).

Therefore, the activities of SCF^{Skp2} and APC^{Cdh1} ubiquitin ligases oscillate during the cell cycle. The APC^{Cdh1} complex is active in the late M and G1 phases, whereas the SCF^{Skp2} complex is active in the S and G2 phases (Figure 1.7) (132).

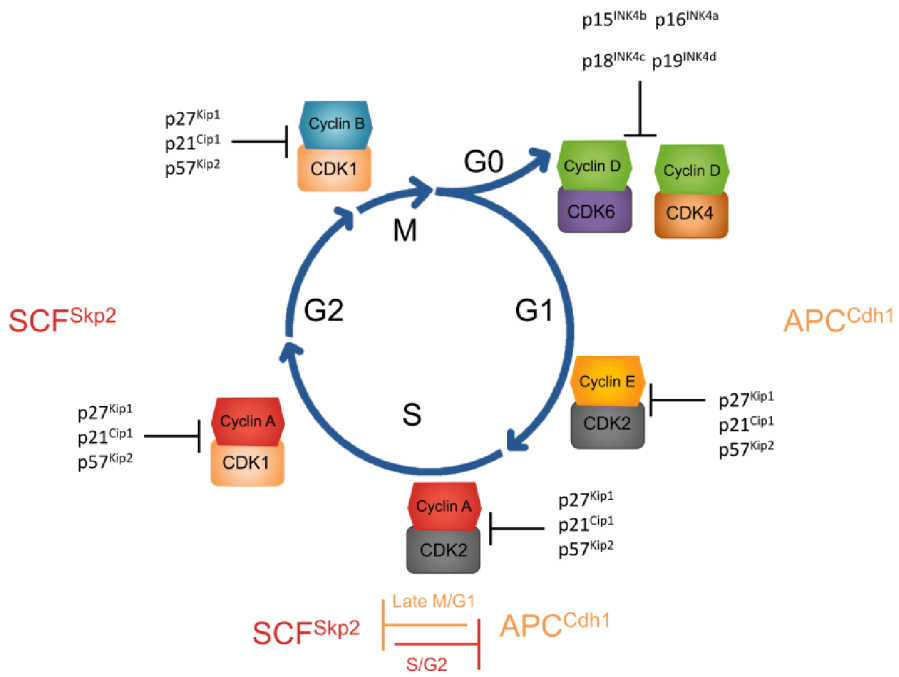

Figure 1.7 Basic principles of cell cycle regulation. The cell cycle is regulated by the activity of cyclin-dependent kinases (CDKs), cyclins and CDK inhibitors (CKIs). Specific CDK-cyclin complexes are required in various phases of the cell cycle. The activity of cyclin-CDKs complexes is further negatively controlled by the activity of CKIs: $p27^{Kip1}$, $p21^{Cip1}$, $p57^{Kip2}$, $p15^{INK4b}$, $p16^{INK4a}$, $p18^{INK4c}$, and $p19^{INK4d}$. The level of CKIs is regulated by their ubiquitination and proteasomal degradation. Two main ubiquitin ligases are involved in cell cycle progression, SCF^{Skp2}, and APC^{Cdh1} that negatively regulate one another and therefore, their activity oscillates during the cell cycle. Adapted from (133).

1.2.1. CULLIN-RING UBIQUITIN LIGASES

The Cullin-RING ubiquitin ligases (CRLs) belong to the largest family of E3 ubiquitin ligases, and approximately 20 % of the proteasome-dependent protein degradation is mediated by CRLs-ubiquitination (134). CRLs represent a superfamily of multi-component protein complexes, all sharing a common molecular structure. Scaffold proteins from a Cullin family form the core of these complexes that are nucleated with a catalytic subunit, adaptor protein, and substrate receptors. Human cells express Cullin 1, 2, 3, 4A, 4B, 5 and 7, and each of them forms a multisubunit

ubiquitin ligase (135). The catalytic subunit is supplied by RING proteins Rbx1 or Rbx2, bound to a C-terminal domain of the Cullins, and is responsible for recruiting the ubiquitin-conjugating enzyme E2 (136-138). The adaptor proteins, mediating the interaction with substrate receptors, bind to an N-terminal stalk of Cullins (139, 140). A key feature of CRLs is that they can assemble with numerous substrate receptors, thus facilitate formation of ubiquitin ligases that share a common catalytic core but recruit different substrates (135). Thus, CRLs mediate specific ubiquitination of a large number of functionally and structurally various substrates, and regulate various biological processes, as depicted in the following scheme (Figure 1.8).

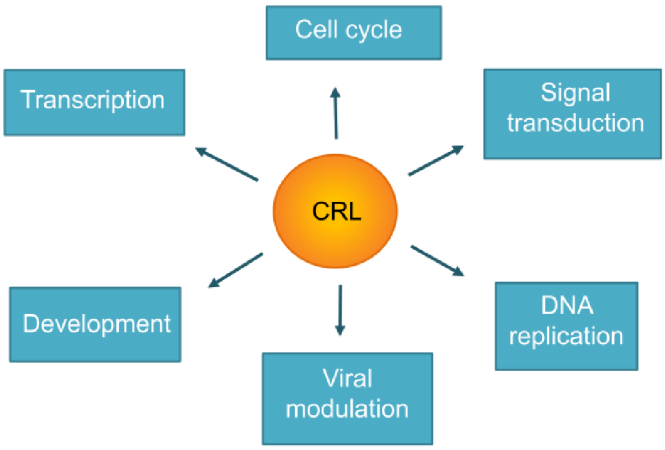

Figure 1.8 The Role of Cullin–RING ligases in multiple cellular processes. Cullin–RING ligases (CRLs) have been implicated in the regulation of various cellular processes via ubiquitination of multiple targets. Adapted from (135).

The assembly of the CRLs is a highly dynamic process that is regulated by several mechanisms. Posttranslational modification of Cullins by NEDD8 (neural precursor cell-expressed developmentally downregulated protein) promotes a conformational change of Cullin and therefore plays a central role in CRLs assembly (135). Except Cullin 7 (141), all Cullins can be modified by covalent attachment of NEDD8 (142).

NEDD8 is an 81 amino acid polypeptide which is 80% homologous to ubiquitin (143). Analogous to ubiquitination, the NEDD8 conjugation is a cascade process involving enzymes (144), as illustrated in Figure 1.9. First, NEDD8 is activated in an ATP-dependent manner by the NEDD8-activating enzyme (NAE) (145), linked to a NEDD8-conjugating substrate, and then transferred to substrates forming an isopeptide bond (reviewed in (146)). Cullins are the best-known substrates

for neddylation (147-149); however, this posttranslational modification affects the function and activity of various proteins including tumour suppressors p53, p73, and their ubiquitin ligase MDM2 (150, 151). Nonetheless, like ubiquitin, NEDD8 can be involved in tagging proteins for their degradation in proteasome (152, 153).

An opposite mechanism involved in CRLs regulation is Cullin deneddylation, the process of NEDD8 detachment operated by COP9 signalosome complex (154). There is evidence of Cullins sequestration that results in inhibition of the CRLs. Protein CAND1 binds unneddylated adaptor-free Cullin-RING complexes resulting in their inactivation (155-157).

However, another study introduced an alternative model of CRL dynamics, showing that only a small fraction of Cullin 1 was associated with CAND1 independently of its neddylation status. The assembly of the CRL complex was driven primarily by the adaptor binding, suggesting that the abundance of adaptor proteins, rather than cycles of neddylation and CAND1 binding drives CRL network organization (158).

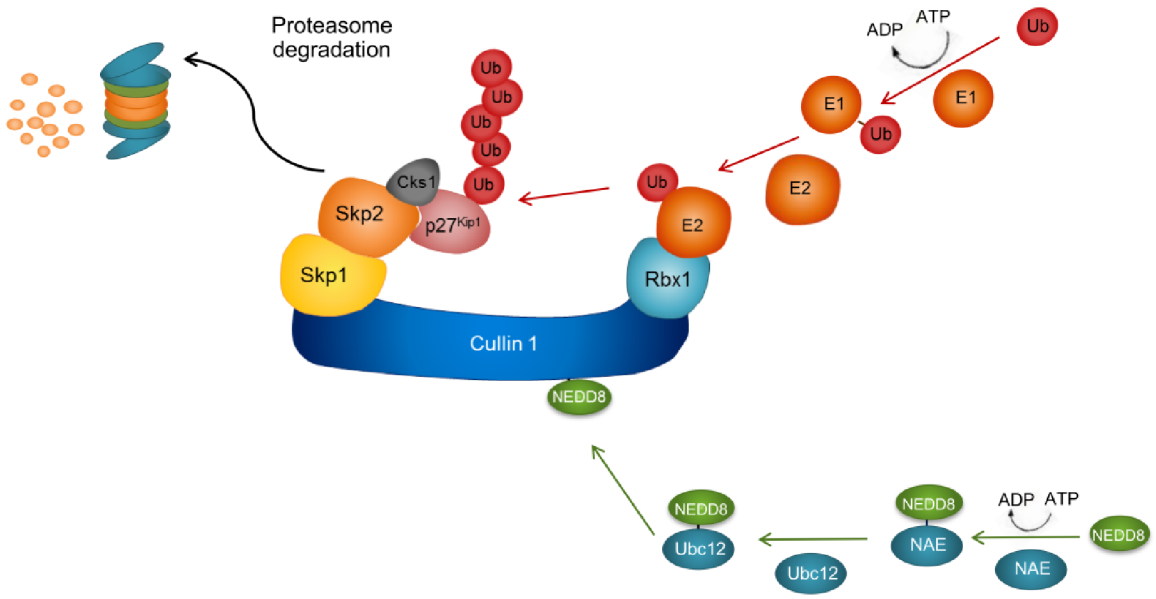

Figure 1.9 Ubiquitination and neddylation pathways are involved in proteasomal degradation. For proteasomal degradation, poly-ubiquitination of the target protein is required. Ubiquitin (Ub) is first activated by E1 and then transferred to E3 ubiquitin ligase via E2 enzyme. A posttranslational modification of the core complex protein,

Cullin 1 with an ubiquitin-like molecule, NEDD8, is critical for the activity of SCF^{Skp2} ubiquitin ligase. The process of neddylation is analogous to the ubiquitination. First, NEDD8 needs to be activated by NAE, and then enzymatically transferred by Ubc12 to the target protein. Adapted from (159).

1.2.2. FUNCTION OF SCF^{Skp2} UBIQUITIN LIGASE IN THE CELLS

The SCF^{Skp2} (Skp1–Cullin–F-box protein) is composed of scaffold protein Cullin 1 which interacts with all three subunits of the complex – Rbx1, Skp1 and Skp2 (160). Skp1 serves as an adaptor protein (161) that binds a specific substrate recognition subunit Skp2 through a conserved structural motif called F-box (162, 163). Skp2 is a variable component of SCF^{Skp2} responsible for recognition of specific substrates that are targeted for degradation in the proteasome (164).

1.2.2.1. SKP2 REGULATION

There is evidence of various mechanisms that control Skp2 expression and activity. In cycling cells, Skp2 mRNA and protein expression is regulated in a cell cycle-dependent manner - it is high in S phase and low in G1 and G2/M phase (165, 166). On the contrary, in cells released from quiescence, Skp2 mRNA is detectable in all phases of the cell cycle (167). The expression of Skp2 is regulated by several transcription factors, such as CBF1, GABP, and FoxM1 (168), and the upstream signalling pathway involved in the regulation of Skp2 expression is PI3K/Akt (169-172).

Based on *in vitro* studies, various stimuli involved in the regulation of Skp2 expression were proposed. For example, adhesion to the extracellular matrix was required for Skp2 expression (173). Recently, it was shown that mechanical cues stimulated Skp2 transcription in human breast cancer cells via Hippo signalling (174). Further, the role of epidermal growth factor (EGF) was implicated in activation of PI3K/Akt pathway and subsequent Skp2 upregulation (175). Moreover, a Skp2 autoinduction loop during G1 was described (176).

Protein phosphorylation is one of the most important and well-studied posttranslational modification. An important role of protein phosphorylation in the regulation of Skp2 function was reported. Gao *et al.* showed that Akt1-mediated phosphorylation of Skp2 at Ser72 promoted its cytoplasmic localization and impaired APC^{Cdh1}-mediated destruction of Skp2 (171). Lin *et al.* showed that Skp2 phosphorylation by Akt triggered SCF complex formation resulting in E3 ligase activity, cytoplasmic relocalization, and promotion of cell migration (177).

Acetylation, another posttranscriptional modification, leads to increased Skp2 stability, promotes its cytoplasmic retention and oncogenic function (178). Recently, the Hippo signalling pathway was implicated in the induction of Skp2 acetylation, cytosolic retention and promotion of cell polyploidy (179). Regarding Skp2 localization and protein stability regulation, a role of TGF-β1 cytokine was proposed. TGF-β1 induced Skp2 nuclear translocation and subsequent ubiquitination by APC^{Cdh1}, resulting in growth inhibition (180).

Degradation of Skp2 in G1 is regulated by APC^{Cdh1} (130). Besides, enrolment of gap junction protein in the regulation of Skp2 stability was reported. Connexin 43 was described as a negative regulator of Skp2 protein stability via promotion of its ubiquitination and degradation (181). Next, the interaction of Skp2 with Connexin 50 was shown to result in Skp2 cytoplasmic retention, its auto-ubiquitination and proteasomal degradation (182).

1.2.2.2. SKP2 FUNCTION

The regulation of Skp2 expression is tightly linked to the cell cycle, and Skp2 itself is involved in cell cycle regulation, as mentioned in previous chapters. For a deeper insight into Skp2 physiological function, genetically engineered mice with Skp2 deletion were prepared (183). The Skp2 deletion resulted in reduced body weight of the Skp2 knockout mice compared to their littermate controls, yet both male and female were fertile with no evidence of any illness. However, tissue abnormalities manifested by increased nuclei size concomitant with the accumulation of Skp2 substrates, $p27^{Kip1}$, and cyclin E were observed. Changes in DNA content and severe

proliferation defects induced by loss of Skp2 were reverted in $p27^{kip1}$ knockout hepatocytes to normal (184).

Skp2 is a significant player in the cell cycle machinery through targeting cell cycle regulators for proteasomal degradation. The timely precise degradation of these regulators is critical for proper cell cycle progression. Skp2 is essential for entry in S phase (165) via regulating the stability of Cyclin E (185), S/G2 transition (186), and also G2/M progression (187) in a p53 dependent manner (188). The prominent Skp2 substrate is the CKI, $p27^{Kip1}$. Apart from this major substrate, Skp2 also regulates multiplecell cycle regulators, regulators of apoptosis, DNA damage, DNA repair and DNA recombination (168). These substrates are listed in Table 1.2. In accordance with the function of these substrates, Skp2 deregulation is manifested in proliferation, differentiation and other cellular processes tightly linked to the cell cycle.

Table 1.2 Skp2 substrates and their function

Skp2 substrates	Main function	Reference
p27, p21, p57	Cell cycle inhibition	(172, 189-195)
E2F	Transcription	(196)
Cyclins D, E, A	Cell cycle progression	(185, 190)
Myc	Cell cycle/Apoptosis	(197, 198)
Cdt1, Orc1	DNA replication	(199-201)
BRCA2	DNA repair	(202)
Rag-2	DNA recombination	(203)
CDK9	Transcriptional elongation	(204)
Foxo1	Apoptosis	(205)

Apart from the role of Skp2 in the regulation of the cell cycle *per se*, it is implicated in the regulation of other cellular processes such as differentiation, survival, apoptosis or migration (206). Skp2 was shown to play a role in maintaining

the pool of hematopoietic stem cells (HSCs). Inactivation of Skp2 in HSC and progenitor cells resulted in delayed entry into the cell cycle, enhanced HSC quiescence, increased pool size, and increased HSC maintenance. The impaired ability to rapidly enter the cell cycle diminished the ability of HSC and progenitor cells to regenerate haematopoiesis after bone marrow transplantation (207).

The engagement of Skp2 in cellular differentiation was demonstrated in several models. For instance, Skp2 promotes adipocyte differentiation via a $p27^{Kip1}$ independent mechanism in MEFs (208). In adipocyte tissue, Skp2 was likewise shown to control adipocyte proliferation during the development of obesity (209). The role of Skp2 was further described in neural differentiation in Xenopus model. Skp2 regulated differentiation independent of the cell cycle via degradation of CDKI Xic1 (210).

In addition, Skp2 was implicated in the regulation of cell survival and apoptosis. In both non-transformed and transformed cells, induction of apoptosis after Skp2 depletion was observed (183, 211-214). The involvement of Skp2 in apoptosis regulation may be, at least partially, explained by degradation of its substrate FOXO1, a protein from forkhead transcription family, that promotes apoptosis signaling (205, 215).

1.2.2.3. ROLE OF SKP2 IN CANCER

One of the cancer hallmarks is excessive proliferation of the transformed cells (103). Due to the involvement of Skp2 in the degradation of cell cycle inhibitors, it has been recognized as an oncogene and its overexpression was detected in various cancers including prostate (216), breast (217), gastric (218), cholangiocarcinoma (175), colon (219-221) and metastasis (222).

In prostate cancer, several signaling pathways involved in Skp2 deregulation were described, including androgen receptor (223), PTEN (216) and PI3K/Akt (169) signaling pathways. In a mouse model, the essential role of Skp2 in the development of prostate cancer was described. It was shown that overexpression of Skp2 in prostate gland induced hyperplasia, dysplasia and low-grade carcinoma (224). High expression

of Skp2 in tumours accompanied by $p27^{Kip1}$ downregulation was correlated with poor prognosis in patients and it was implicated as a prognostic marker in many cancers including prostate (216, 225-231).

In non-small-cell-lung cancer, Skp2 amplification and overexpression were associated with presence of lymph node metastases (232). Further, cytoplasmic Skp2 was shown to enhance E-Cadherin ubiquitination and destruction, resulting in cellular migration (178). Conversely, downregulation of Skp2 inhibited the growth and metastasis of gastric cancer cells *in vitro* and *in vivo* (233). In combination with oncogenic stress, Skp2 downregulation restricted prostate cancer development *in vivo* (221). The above-described involvement of Skp2 in tumourigenesis, its overexpression in various cancers and correlation with worse prognosis and metastasis in patients, makes Skp2 an appealing target for anticancer therapy.

1.2.3. SCF^{Skp2} AS A TARGET FOR ANTICANCER THERAPY

The process of protein turnover is an attractive target in anticancer therapy. The first proteasomal inhibitor tested in humans, bortezomib (234), was approved by Food and Drug Administration (FDA) for treatment of multiple myeloma in 2008. Apart from Bortezomib, two other proteasome inhibitors were recently approved by FDA: carfilzomib, and ixazomib (235). However, as anti-cancer drugs, they are limited to lymphomas and multiple myeloma. Therefore, there is an interest in developing drugs with reduced toxicity that can be used to target proteasome also in non-haematological tumours (236). One possibility how to achieve this goal is to block the upstream components of the ubiquitin-proteasome system.

1.2.3.1. PHARMACOLOGICAL INHIBITION OF CULLIN NEDDYLATION

Cullin1 neddylation is a crucial step for SCF^{Skp2} assembly (155, 156). Therefore, one of the ways how to inhibit the activity of this complex is the disruption of the neddylation process. MLN-4924 (Pevonedistat), a potent ATP competitive inhibitor targets selectively the NAE enzyme (134) (Figure 1.10). This inhibitor is recently in phase III clinical trials for haematological malignancies and in the second

phase for several haematological cancers and solid tumour malignancies (237). As an alternative to MLN-4924, a natural product-like inhibitor (238) and a metal-based inhibitor (239) blocking NAE activity were described, but both were tested only *in vitro*, so far.

In vitro and *in vivo* studies demonstrate that inhibition of the neddylation process via MLN-4924 results in multiple cell type-dependent effects, caused by the accumulation of CRL substrates. Nevertheless, cell cycle deregulation, growth restriction, induction of apoptosis, and cellular senescence are the most common cellular responses to MLN-4924 treatment (134, 221, 240-245). Further, inhibition of migration after MLN-4924 treatment was described (246, 247). Interestingly, Swords *et al.* showed that MLN-4924 significantly reduced the viability of leukemic cells compared to peripheral blood mononuclear cells from healthy donors. (248).

The radiosensitization effect of MLN-4924 on cancer cells was demonstrated *in vitro* and/or *in vivo* in the models of breast cancer (249), nasopharyngeal carcinoma (250), head and neck squamous carcinoma (251), and pancreatic cancer (252). Moreover, in pancreatic cancer, it was shown that MLN-4924 treatment suppressed angiogenesis, tumour growth and metastasis (253). Apart from radiosensitization, enhanced response to other pro-apoptotic stimuli in neoplastic B-cells (254) or cervical carcinoma (255) was described. Further, the ability of MLN-4924 to sensitize cisplatin resistant ovarian cancer cells (256, 257), paclitaxel-resistant lung adenocarcinoma cells (258), or pancreatic cells to apoptosis (259) was demonstrated by *in vitro* studies.

1.2.3.2. PHARMACOLOGICAL INHIBITION OF SKP2

The activity of SCF^{Skp2} E3 ligase can be selectively targeted (Figure 1.10). Based on the SCF^{Skp2} structure, inhibitors targeting specifically the protein-protein interactions within the SCF^{Skp2} complex were designed. The Skp1 and Skp2 interaction represents a target for pharmacological inhibition to prevent SCF^{Skp2} activity. Indeed, several agents targeting this interaction were identified. Compound A, tested in multiple myeloma, induced cell cycle arrest, cell death and even overcame resistance

to drugs including bortezomib (260). Further example of a drug targeting Skp1 and Skp2 interaction is compound #25. Treatment with this agent resulted in specific inhibition of SCF^{Skp2}, accumulation of $p27^{Kip1}$ and $p21^{Cip1}$ proteins, led to the restriction of CSCs population and tumours regression *in vivo* (261). Moreover, it induced resensitization of castration-resistant prostate cancer cells to chemotherapeutics such as paclitaxel or doxorubicin (262).

Another approach to inhibit SCF^{Skp2} activity is to target the interaction of Skp2 with its substrates specifically. As described above, the prominent substrate of Skp2 is $p27^{Kip1}$. To be recognised by Skp2, $p27^{Kip1}$ needs to be phosphorylated (195), and it requires the accessory protein Cks1 to be bound to Skp2 (263, 264). An *in silico* screen identified series of inhibitors SKPin C1-C20 that target the binding interface for $p27^{Kip1}$ on Skp2/Cks1 (265). These molecules selectively inhibited Skp2-mediated $p27^{Kip1}$ degradation, resulting in cell cycle arrest. Besides the cell cycle arrest and $p27^{Kip1}$ accumulation, the ability of SKPin C1 to inhibit tumour growth *in vivo* was shown (266).

Furthermore, natural compounds isolated from plants like curcumin (267-269), caffeic acid (270), rottlerin (271) or genistein (272) were tested *in vitro* and exhibited anti-tumour activity manifested by cell cycle arrest, apoptosis or inhibition of migration via Skp2 downregulation. Thus, targeting the activity of SCF^{Skp2} is a promising approach in anti-cancer therapies.

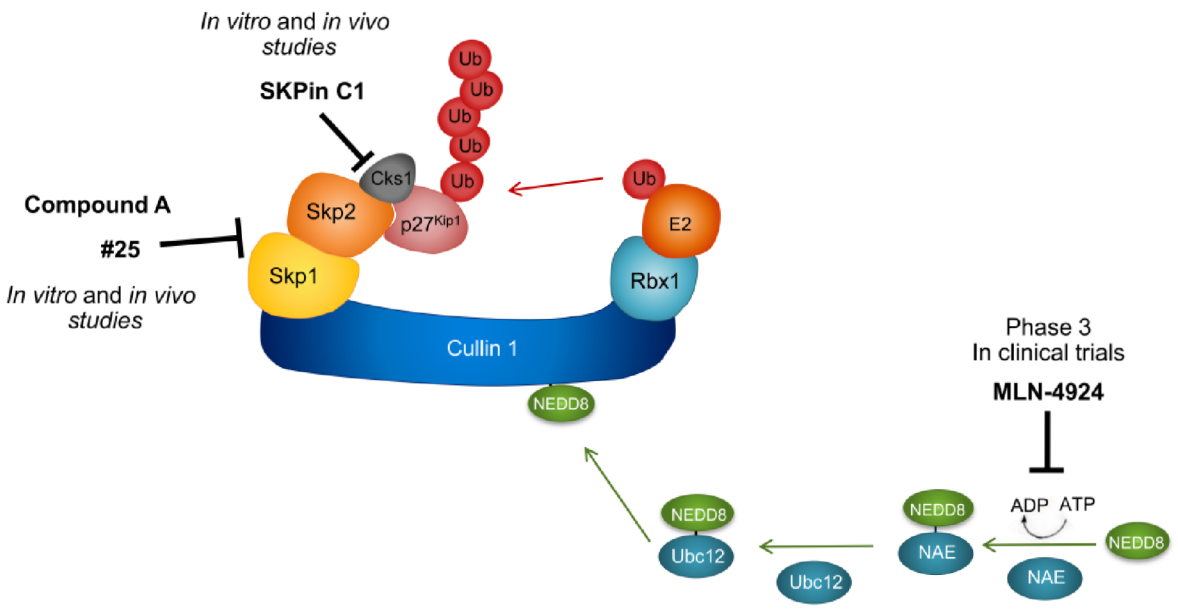

Figure 1.10 Pharmacological inhibition of SCF^{Skp2}. Several compounds that inhibit the activity of SCF^{Skp2} ubiquitin ligase were described. MLN-4924, an inhibitor of the neddylation process, abrogate the SCF^{Skp2} assembly. Compounds A and #25 target Skp1 and Skp2 interaction. The SKPin C1 inhibitor specifically targets p27^{Kip1} binding to Skp2/Cks1 interface. Adapted from (159).

2. HYPOTHESIS AND AIMS OF THE WORK

2.1. HYPOTHESIS

The Role of Skp2 in Prostate Cancer Stem-like Cells

Prostate cancer is a heterogeneous disease, characterized by multifocal lesions (29), and arising from both basal and luminal cells (30, 31). The CSCs are considered to be responsible for disease progression and can cause the relapse of the disease (56). CD24 was described as a marker distinguishing between low differentiated and transit-amplifying cells in the basal layer of human prostate (8). Moreover, prostate cancer cells with $CD24^{-}CD44^{+}$ phenotype are considered CSCs (122, 123).

One of the cancer hallmarks is excessive proliferation of the transformed cells (103). Skp2 is involved in cell cycle regulation, mainly via the degradation of CKIs. Therefore, it has been recognized as an oncogene, and its overexpression was detected in various cancers including prostate (216).

Based on the published results, we postulated the following hypothesis:

- High expression of Skp2 is associated with the progression of the prostate cancer and the EMT status.

- The expression of Skp2 is increased in the prostate CSC-like cells compared to non CSC-like cells. The downregulation of Skp2 will abrogate the CSC-like properties of the cells.

- Pharmacological modulation of SCF^{Skp2} will affect cytokinetics of CSC-like cells. The cells with CSC phenotype $CD44^{+}CD24^{-}$ will be more sensitive to MLN-4924 treatment than $CD44^{+}CD24^{+}$ cells.

- Pharmacological inactivation of the SCF^{Skp2} complex will decrease self-renewal capability of prostate CSCs.

Establishment of a tool for analysis of cellular response to experimental drug treatment in heterogeneous samples (in CSC-like cells)

Based on the high advantage of flow cytometry as a methodological approach to detect various cytokinetic parameters cell populations, and the possibility of analysis of such parameters on single cell level, we hypothesised that:

- The introduction of a multiparametric protocol for the assessment of complex cellular responses to experimental treatments on single cell level will serve as a powerful tool in experimental work.

- In a heterogenous sample, various subpopulations including CSC-like cells are present. These subpopulations respond differently to experimental treatment.

2.2. SPECIFIC AIMS OF THE THESIS

Aim 1: The Role of Skp2 in Prostate Cancer Stem-like Cells

- To examine the localization and expression of Skp2 in patients with prostate cancer and its correlation with the disease grading.

- To evaluate the EMT status of the cells in the prostate cancer.

- To analyse Skp2 expression, EMT status and CSC characteristics in *in vitro* cultures. To describe the effect of Skp2 downregulation on the CSC-like properties of the cells.

- To examine the biological effects of SCF^{Skp2} pharmacological inhibition.

- To disclose the potential of pharmacological inactivation of SCF^{Skp2} complex to affect CSC-like characteristics of prostate cancer cells (expression of CSC-like markers and self-renewal capacity).

Aim 2: Establishment of a tool for analysis of cellular response to experimental drug treatment in heterogeneous samples (in CSC-like cells)

- To establish a multiparametric flow cytometric assay to analyse the cellular response to experimental drug treatment of the cells. To comprehend simultaneous detection of surface markers for immunophenotyping, proliferation (based on the cell cycle and measurement of DNA synthesis), DNA damage, and cell death (determined by viability and apoptosis markers) to depict the complex response of the cells to the experimental treatment.

- To optimize critical steps necessary for establishment of the assay.

- To analyse the effects of the experimental drug treatment in various subpopulations within the heterogeneous samples.

3. MATERIAL AND METHODS

3.1. CELLS AND CELL CULTURE

3.1.1. DU 145 AND PC3

DU 145 human cancer cells (ATCC) derived from brain metastases of prostate cancer and PC3 human cancer cells derived from bone metastasis of prostate cancer were cultivated in RPMI 1640 (Thermo Fisher Scientific [TSF], Waltham, MA, USA) supplemented with 10% fetal bovine serum (FBS) (TFS), penicillin (100 U/ml), and streptomycin (0.1 mg/ml; Biosera, Nuaille, France). PC-3 AC (age control) and PC-3 DR (docetaxel resistant) cells were obtained from prof. Watson (Dublin, Ireland) and cultivated as described (273).

3.1.1.1. PREPARATION OF DU 145 SKP2 KNOCK-DOWN CELL LINES

DU 145 were transfected with Skp2 p45 CRISPR/Cas9 KO Plasmid (h) (sc-400534) and Skp2 p45 CRISPR/Cas9 KO Plasmid HDR (sc-400534) using Lipofectamine 3000 (TFS Scientific, USA) to prepare *SKP2* knock-down (KD) cell lines or with Control CRISPR/Cas9 Plasmid (sc-418922, all Santa Cruz Biotechnology, Inc.; SCBT) and empty vector pIRES puro2 (kindly provided by Prof. V. Bryja, Ph.D., Masaryk University, Brno, Czech Republic) to prepare control cells. Cells were selected in media with puromycin (300 ng/ml; TFS Scientific) for one week. RFP positive single cells (indicating insertion of plasmid with puromycin resistance in a site of CRISPR deletion) were sorted using FACSAria II Sorp system and 100-µm nozzle (20 psi) to obtain single cell-derived *SKP2* KD clones. Post-sorting purity was determined immediately after sorting. In the control group, viable cells were sorted.

3.1.2. cE2 AND E2

Mouse prostate adenocarcinoma cells (274) (a generous gift from Dr. Pradip Roy Burman, University of Southern California, Los Angeles, CA), were cultivated in Dulbecco's modified Eagle medium (DMEM) (TFS) supplemented with recombinant human (rh) epidermal growth factor (rh-EGF) (6 ng/ml; Sigma-Aldrich, St. Luis, MO, USA), rh-insulin (5 µg/ml; Sigma-Aldrich), bovine pituitary extract (25 µg/ml; Hammond Cell Tech, Windsor, CA, USA), 10 % FBS, penicillin, and streptomycin.

3.1.3. HCT 116

Human colon adenocarcinoma cells (a generous gift from Dr. Bert Vogelstein, Johns Hopkins University, Baltimore, MD) were cultivated in McCoy´s medium (TFS) containing 10 % heat-inactivated FBS, penicillin, and streptomycin.

3.1.4. SU-DHL-4

Human diffuse large B-cell lymphoma cells (a kind gift from Dr. Martin Trbušek, Masaryk University, Czech Republic), were cultivated in RPMI 1640 supplemented with 10 % FBS, penicillin, and streptomycin.

3.1.5. CELL CULTURE

All adherent cell lines were cultivated in TPP (Trasadingen, Switzerland) or FALCON™ (TFS) cultivation flasks and plates in a humidified incubator at 37°C in an atmosphere of 5% CO_2. The cells (except SU-DHL-4 growing in suspension) were harvested by washing with 0.05% EDTA in PBS followed by trypsinization (0.05 % w/v trypsin/0.53 mM Trypsin-EDTA; GE Healthcare Life Sciences, Little Chalfont, UK). The AmpFLSTR® Identifiler® PCR Amplification Kit (TFS) was used to verify the origin of cell lines.

3.2. CHEMICALS

MLN-4924 was obtained from Active Biochem (Hong Kong, China); dimethyl sulfoxide (DMSO), MG-132, Triton X-100, and phosphate-buffered saline (PBS) were obtained from Sigma-Aldrich; TRAIL was kindly provided by Dr. Ladislav Anděra, Institute of Molecular Genetics, CAS, Prague, Czech Republic. The staining buffer for flow cytometry was 1% bovine serum albumin (BSA; Serva Electrophoresis GmbH, Heidelberg, Germany) in PBS with 0.1% NaN_3 (Sigma-Aldrich). A buffered, 4% formaldehyde solution in PBS was prepared in-house from powder (Fluka). Fumitremorgin C (Abcam, ab144258) was used for ABCG2 inhibition.

3.3. TREATMENTS

3.3.1. PHARMACOLOGICAL INHIBITION OF SCFSKP2 IN DU 145

Cells were treated in subconfluent conditions 24 hours after seeding with MLN-4924 inhibitor or vehicle (DMSO). The concentration range varied from 0.04 μM to 3 μM. The cells were treated for 24 to 96 hours as indicated in individual experiments. In clonogenic assay, single cells were sorted in medium containing 0.04 μM MLN-4924 and cultivated for 3 weeks.

3.3.2. ESTABLISHMENT OF THE MULTIPARAMETRIC FLOW CYTOMETRIC ASSAY

For the induction of DNA damage and/or apoptosis, exponentially growing cells were treated with experimental drugs. cE2 and SU-DHL-4 were treated with lethal concentrations of MG-132 (1 μM and 5 μM, respectively) for 24 hours. DU 145 and HCT 116 were treated with lethal concentration of TRAIL (50 ng/ml) for 2 hours. All cell lines were treated with MLN-4924 (DU 145 and HCT 116 0.33 μM,

SU-DHL-4 1 μM, cE2 5 μM) for 24 hours. Concentrations were selected based on pilot experiments. In all cases, corresponding vehicle at the appropriate dilution was applied in the control groups.

3.4. METHODS

3.4.1. SKP2 OVEREXPRESSION

DU 145 cells were transfected using Neon transfection system (TFS) with control plasmid (pcDNA3.1) or Skp2 (pcDNA3 Skp2-Myc) plasmid that was a gift from Axel Brunger (Addgene Plasmid #19947) (275), incubated for two days and harvested for flow cytometric analysis to detect surface markers.

3.4.2. SPHEROID FORMATION ASSAY

For spheroid formation assay, DU 145 (control and *SKP2* KD) cells were seeded in semisolid media (0.1% agarose) in plates precoated with 0.5% agar and cultured for three weeks. Cells were seeded in low density, 500 cells/well in a 6 well plate. Spheroids were stained with MTT (276) and counted using ImageJ software. For analysis of cancer stem cells markers, cells were seeded in high density (10 000 cells/well in a 6 well plate) in semisolid media (0.1% agarose) on plates precoated with 0.5% agar and cultivated for three weeks. Spheroids were harvested, incubated with prewarmed PBS/EDTA and Trypsin to obtain single cell suspension. Cells were then stained with antibodies according to standard procedure and analysed by a flow cytometer.

3.4.3. TUMOURIGENIC POTENTIAL OF SKP2 KD CELL LINES

Suspension of 1×10^6 cells per mice (in Growth factor reduced Matrigel; 354230; BD Biosciences, Franklin Lakes, NJ, USA) were injected into the right flank of male SHO mice (Crl:SHO-PrKD$^{scid/Hrhr}$). 10 mice per group were used. Six weeks

after injection, mice were sacrificed. Tumour formation rate was then calculated for both control and *SKP2* KD cells. The rate was calculated as a ratio of number of mice inoculated with cancer cell and number of mice bearing tumours. Animal experiments were approved by the Academy of Sciences of the Czech Republic (AVCR 2013/13); supervised by the local ethical committee of the Institute of Biophysics of the Czech Academy of Sciences and performed by certified individuals.

3.4.4. WESTERN BLOT

Samples for western blot were prepared as described previously (277). Proteins were separated using sodium dodecyl sulphate polyacrylamide gel electrophoresis (SDS-PAGE) and detected by specific primary antibodies and secondary antibodies (Table 3.1). Signals were detected using the Immobilon Western HRP Substrate (Merck Millipore, Billerica, MA, USA) and visualized on X-ray films (Agfa, Mortsel, Belgium).

Table 3.1 List of antibodies used for western blot

Primary Antibody	Supplier	Source	Cat. No.	Dilution
α-tubulin	Sigma-Aldrich	Mouse	T9026	1:4000
β-actin	Sigma-Aldrich	Mouse	A5441	1:8000
CDK1	SCBT	Mouse	SC-8395	1:500
CDK2	SCBT	Rabbit	SC-163	1:500
CDK4	SCBT	Rabbit	SC-601	1:500
cleaved caspase-3	Cell Signaling	Rabbit	9661	1:500
E-Cadherin	BD Pharmingen	Mouse	610182	1:5000
γH2A.X	Cell Signaling	Rabbit	9718	1:1000
N-Cadherin	BD Pharmingen	Mouse	610920	1:2500
Nedd8	Cell Signaling	Rabbit	2754	1:1000
$p21^{Cip1}$	SCBT	Rabbit	SC-397	1:500
$p27^{Kip1}$	SCBT	Rabbit	SC-528	1:500

$p27^{Kip1}$	Cell Signaling	Rabbit	2552	1:1000
Skp2	Cell Signaling	Rabbit	4313	1:1000
Slug	Cell Signaling	Rabbit	9585	1:500
Snail	Bioss	Rabbit	1371	1:500
Trop-2	R&D	Mouse	AF650	1:250
Trop-2	R&D	Goat	AF1122	1:250
vimentin	Sigma-Aldrich	Mouse	V6389	1:500
vimentin	Sigma-Aldrich	Rabbit	SAB300676	1:500
Zeb1	Bethyl	Rabbit	A301-922A	1:500
Zeb2	Bethyl	Rabbit	A302-474A	1:500
Secondary Antibody	**Supplier**		**Cat. No.**	**Dilution**
[HRP]-linked anti-rabbit IgG1	Amersham	Sheep	NA934V	1:3000
HRP-linked anti-mouse IgG1	Amersham	Sheep	NA931	1:4000
Mouse TrueBlot®: Anti-Mouse IgG HRP	TFS	Rat	188817	1:1000
Rabbit TrueBlot®: Anti-Rabbit IgG HRP	TFS	Mouse	188816	1:1000

Table 3.1 continued

3.4.5. IMMUNOFLUORESCENCE MICROSCOPY

DU 145 control cells and *SKP2* KD cells were seeded on 10 mm cover slips coated with 0.1% gelatine. After 24 hrs, cells were treated with 0.11 µM MLN-4924 or DMSO for another 24 hrs. Then, cells were washed with 1 ml of HBSS, fixed with 4% PFA for 15 min at room temperature (RT), incubated in permeabilising and blocking solution (0.3% Triton X-100 and 5% Donkey serum) for 1 hour, RT. Afterwards, cells were incubated overnight with Skp2 (1:200, Cell Signaling, 4313) and p27 (1:100, Transduction Laboratories, 610242) antibodies and stained with secondary antibody the following day. The secondary antibodies were Donkey anti-Mouse IgG (H+L) Highly Cross-Adsorbed Secondary Antibody, Alexa Fluor 647 (TFS, A31571, 1:500 and Donkey anti-Rabbit IgG (H+L) Highly Cross-Adsorbed Secondary Antibody, Alexa Fluor 488, TFS, A21206, 1:500). Prior to microscopic analysis, cells were stained with DNA probe and cover slips were anchored to

microscopic slide with Mowiol ® 40-88 (Sigma-Aldrich). Between each step, washing with HBSS (3x5 min) was performed. Fluorescent imaging was performed using Olympus FV10i confocal microscope. Images were processed using CellProfiler v2.2.0 software (278).

3.4.6. CELL PAINTING AND MORPHOLOGY ANALYSIS

The cells were seeded in density 50 000 cells/cm^2 into 4 wells per clone into 384 black well plate (Falcon, #353962) and grown for 2 days at standard conditions. Next, cells were stained with Hoechst 33342, concanavalin A, SYTO14, phalloidin, wheat germ agglutinin and MitoTracker as described previously (279) using epMotion 5075 liquid handling workstation (Eppendorf, Hamburg, Germany). Images were acquired with an ImageXpress Micro (Molecular Devices; San Jose, CA, USA) fluorescence microscope (40x objective). Briefly, 5 fluorescence channels – using DAPI, Cy3, GFP, TxRed, Cy5 filters were captured from 35 sites in each well or 1000 cells per well were acquired with adaptive acquisition set up. Spill overs of fluorescence from different channels were compensated by subtraction of dim signal based on single stained compensation controls. Representative images were artificially colored and scale bar was added to images using ImageJ 1.51p (NIH). Acquired images were processed based on the original cell painting protocol (279). Objects of nuclei, cytoplasm and whole cell areas were segmented and together 1785 features were calculated from 5 fluorescence channels on these three objects using CellProfiler v2.2.0 software. Data was scaled, missing data and constant values in specific features were removed before principal component analysis and t-SNE analysis (perplexity 1605, nr. of iterations 500, minimum cost value 0.5) were performed and plots were produced in R (RStudio, Inc., Boston, MA, USA).

3.4.7. IMMUNOPRECIPITATION

Control DU 145 cells and *SKP2* KD cells were treated for 24 hours with 0.11μM MLN-4924 or DMSO. Lysates were prepared using lysis buffer (50 mM

TRIS pH 7.4, 150 mM NaCl, 1 mM EDTA, 8 mM Glycerol, 0.5% IGEPAL® CA-630), incubated with Protein G Sepharose Beads 4® Fast Flow (GE Healthcare, 17-0618-01) to preclean samples. Then, supernatants were incubated with 1 µg control (Unlabeled Rabbit IgG1, Southern Biotech, 0111-01) or $p27^{Kip1}$ (Santa Cruz, sc-528) antibody for 2 hours at 4°C. Lysates were subsequently incubated with Protein G Sepharose Beads 4® Fast Flow overnight at 4°C. The next day, lysates were washed and prepared for western blot analysis. Between each step, cells were washed with TBS buffer (50 mM Tris-HCl pH 7.8, 150 mM NaCl, 1mM EDTA pH 8).

3.4.8. RNA ISOLATION AND qPCR ANALYSIS

Total RNA was isolated using High Pure RNA Isolation Kit (Roche; Basel, Switzerland) and quantified on BioSpectrometer (Eppendorf). Equal amount of RNA was transcribed to cDNA using High-Capacity RNA-to-cDNA Kit (Applied Biosystems; Foster City, CA, USA). mRNA levels were quantified with gene-specific primers in combination with UPL hydrolysis probes using Roche LightCycler 480 system (Roche). Relative expression levels of CD24 and CD44 were normalized to the housekeeping gene *POLR2A*. Primers used for qPCR analysis are listed in Table 3.2.

Table 3.2 List of primers used for PCR

Gene	Accesion #	F primer	R primer	Probe
CD24	NM_013230.2	TGGATTTGACATTGCATTTGA	TGGGGGTAGATTCTCATTCATC	#37
CD44	NM_000610.3	TCACATTAAGTTTGCATGACCTG	AATAGGGCCAGCCTCTATGAA	#57
POLR2A	NM_000937.3	CACGTCGACAGGAACATCAG	GCAAATTCACCAAGAGAGACG	#1

3.4.9. FLOW CYTOMETRY

3.4.9.1. ALDH1 ACTIVITY DETECTION ASSAY

Cells were stained according to manufacturer's protocol (Aldehyde dehydrogenase-based cell detection kit; 01700 Stem Cell; Vancouver, Canada). Briefly, cells were harvested, resuspended in Aldefluor buffer, incubated with Fumitremorgin C (Abcam) for 5 min (15 µM). Then, activated aldefluor reagent was added and cells were split into negative control (incubated with DEAB) and stained sample. Cells were incubated for 30 min at 37°C. To discriminate dead cells from analysis, propidium iodide was added to samples prior to the analysis by flow cytometry.

3.4.9.2. ANNEXIN V ASSAY

All cells (adherent and floating) were harvested 48 hours after MLN-4924 treatment, and stained according to manufacturer's recommendation. First, cells were stained with CD24 antibody or isotype control for 20 min at 4°C. Subsequently, cells were stained with AnnexinV and propidium iodide for 15 min at RT and analysed by flow cytometry.

3.4.9.3. CELL CYCLE ANALYSIS

Cells were harvested and fixed with 70% ethanol and stored at 4°C for at least 30 min. Then, cells were washed from ethanol and incubated in Vindelov´s solution (280) for 30 minutes at 37 °C. Cell cycle was analysed using Modfit software LT 3.3 (Verity software House, Topsham, ME, USA). Dead cells, aggregates and debris were excluded from analysis.

3. 4.9.4. IMMUNOPHENOTYPE ANALYSIS

Cells were harvested using PBS/EDTA and Trypsin, 1×10^6 cell were stained in 100 µl of antibody/antibodies cocktail solution for 20 min at 4°C. Then, cells were stained with LIVE/DEAD Fixable Dead Cell Stain kit according to the Manufacturer´s

recommendation to discriminate dead cells from analysis. Antibodies and probes used for flow cytometric analysis are enlisted in Table 3.3.

Table 3.3 List of the antibodies used for flow cytometry

Antibody	Fluorochrome	Supplier	Source	Cat. No	Dilution
Surface markers					
CD19	Brilliant Blue 515	BD Horizon	BD Horizon	564456	1:20
CD20	APC/Cy7	Mouse	BioLegend	302314	1:20
CD24	Alexa Fluor 488	Mouse	Sony	2155540	1:20
CD24	Brilliant Violet 421	Mouse	BioLegend	311122	1:20
CD24	PE/Cy7	Mouse	BioLegend	311122	1:20
CD44	APC/Cy7	Rat	BioLegend	103 028	1:100
Prominin-1	APC	Rat	Miltenyi Biotec	130-102-197	1:11
Trop-2	-	Mouse	R&D	MAB650	1:50
Trop-2 biotin	-	Mouse	R&D	BAF1122	1:50
Intracellular markers					
Cleaved Caspase 3	-	Rabbit	Cell Signalling	9661S	1:800
Cleaved PARP	-	Rabbit	Cell Signalling	9544	1:25
γH2A.X	PE	Rabbit	Cell Signalling	5763	1:50
Skp2	-	Rabbit	Cell Signalling	4313	1:100
Secondary antibodies and Isotype controls					
anti-Rabbit	Alexa Fluor 488	Donkey	TFS	A21202	1:1500
anti-Rabbit	Alexa Fluor 594	Donkey	TFS	A-21207	1:500
anti-Rabbit	PerCP	Donkey	Jackson ImmunoResearch	711-126-152	1:25
IgG1	Brilliant Blue 515	Mouse	BD Horizon	564416	1:20
IgG1	APC	Rat	Miltenyi Biotec	130-102-646	1:11
IgG2a	Alexa Fluor 488	Mouse	Sony	2601165	1:20
IgG2a	Brilliant Violet 650	Mouse	BioLegend	711-126-152	1:25
IgG2a	PE/Cy7	Mouse	BioLegend		1:20
IgG2b	APC/Cy7	Rat	BioLegend	400624	1:100
IgG XP®	PE	Rabbit	Cell Signaling	5742S	1:100
Streptavidin	Brilliant Violet 421	-	BioLegend	405 226	1:1500
Streptavidin	Brilliant Violet 650	-	BioLegend	405 231	1:1500
Streptavidin	PE	-	eBioscience	12-4317	1:2000

Viability					
LIVE/DEAD® Fixable Dead Cell Stain Kit	Far Red	-	TFS	L10120	1:1000
LIVE/DEAD® Fixable Dead Cell Stain Kit	Green	-	TFS	L23101	1:1000
LIVE/DEAD® Fixable Dead Cell Stain Kit	Violet	-	TFS	L34955	1:1000
LIVE/DEAD® Fixable Dead Cell Stain Kit	Yellow	-	TFS	L34959	1:1000
Probes					
AnnexinV	FITC Propidium iodide	-	Exbio	ED7044	
Aldehyde dehydrogenase-based cell detection kit			StemCell	01700	
DAPI	-	-	AppliChem	A4099	1:2000
PO-PRO-1			TFS	P3581	1:10 000
Click-iT® EdU	Alexa Fluor® 488	-	TFS	C10420	-
Click-iT® EdU	Alexa Fluor® 647	-	TFS	C10424	-

Table 3.3 continued

3. 4.9.5. INTRACELLULAR DETECTION OF SKP2

Cells were harvested and stained with CD24 surface antibody and with LIVE/DEAD Fixable Dead Cell Stain kit as described in 3.4.9.4. Subsequently, cells were fixed with 4% PFA for 15 min at RT, and permeabilised with 0.25% Triton X-100 solution for another 15 min at RT. Then, cells were incubated with Skp2 antibody over night at 4°C. The next day, cells were stained with secondary antibody for 1 hour at RT and analysed by flow cytometry.

3.4.9.6. MULTIPARAMETRIC ANALYSIS

This assay is described in details in (281). Briefly, cells treated as described in 3.3.2., were incubated with 10 µM EdU (ethyl deoxyuridine) one hour prior to

harvesting. Cells were harvested and stained for surface markers and with LIVE/DEAD Fixable Dead Cell Stain kit as described in 3.4.9.4. Then, cells were fixed in 4% PFA for 15 min at RT and permeabilised for another 15 min with 0.25% Triton X-100 solution at RT. Cells were subsequently stained with probes and antibodies detecting proliferation (EdU click-iT reaction), and intracellular markers such as cleaved caspase-3 (over-night at 4°C) followed by incubation with secondary antibody for 1 hour at RT. Then, cells were stained with γH2A.X antibody for 1 hour at RT to detect DNA damage and with PO-PRO-1 for analysis of the cell cycle (45 min, RT).

3.4.9.7. INSTRUMENTATION AND DATA ANALYSIS

The sorting of the cells and multiparametric analyses were performed on a BD FACSAria II Sorp system (BD Biosciences) equipped with five lasers (excitation wavelengths: 355, 405, 488, 561, and 639 nm). Cytometric data were recorded using FACSDiva software (Version 6.1.3; BD Biosciences). Other experiments and optimization experiments for establishment of multiparametric assay were performed using a BD FACSVerse (BD Biosciences) equipped with three lasers (excitation wavelengths: 405, 488, and 640 nm) where cytometric data were recorded using FACSuite software (Version 1.0.5.3841 and 1.0.6; BD Biosciences). The quality of the instrument was regularly tested using BD FACSuite CS&T Research Beads (BD Biosciences) before each measurement. Data analysis was performed using FlowJo software (Version 10.0.7, Tree Star, Ashland, OR, USA). Gating strategy for selection of viable (Live/Dead low) single cells (FSC-A vs. FSC-H) without debris (FSC-A vs. SSC-A) was applied to all samples that were analysed by flow cytometry. List mode data from the publication "Multiparametric analysis of complex cellular response" were uploaded into the FlowRepository database of flow cytometry experiments (http://flowrepository.org /id/FR-FCM-ZZS3).

3.4.9.8. COMPENSATION CONTROLS

For compensation setup, single colour controls (beads or cells) were recorded on a BD FACSAria II Sorp system and compensation matrix was calculated by

FACSDiva software. Compensation beads or cells (positive controls) were stained with appropriate antibodies and probes. Anti-rat and anti-hamster Ig,κ/negative control, anti-mouse Ig,κ/negative control compensation beads (BD Biosciences), Sphero™ Goat anti-Rabbit and Sphero™ Biotin Polystyrene Particles (Spherotech, Lake Forest, IL, USA) labelled with specific antibodies in the appropriate dilutions were used. Arc™ Amine Reactive Compensation Bead Kit beads (TFS) were stained using the LIVE/DEAD® Fixable fluorescent reactive dye kit according to manufacturer´s recommendation. As compensation control for DNA staining, fixed and permeabilised cells with and without the appropriately diluted DNA probe were used. As a compensation control for DNA proliferation, cells pretreated with EdU were stained with Click-iT reaction cocktail. Cells were stained under the same conditions (time, temperature) as samples in protocol. Compensation beads were stained with primary antibodies for 20 min at 4°C. In case of secondary detection, beads were stained with primary antibodies (20 min, 4°C) followed by secondary detection (20 min, 4°C). Isotype controls (ISO) were prepared and recorded for all samples. Gates were set according to the isotype controls or untreated cells (for γH2A.X and cleaved caspase-3).

3.4.10. IMMUNOHISTOCHEMISTRY OF CLINICAL SAMPLES

Retrospective analysis of tissue samples was performed in three independent sets of patients with prostate carcinoma. The main set included 187 tissue samples (33 samples of BPH, 101 samples of PCa, 35 samples of cancer outgrowths into seminal vesicles and 18 cancer positive lymph nodes). Samples were examined for expression of Skp2, E-Cadherin and Slug. Samples were obtained from patients who signed written informed consent, in the University Hospital Olomouc, and the study was approved by the Ethics Committee of the University Hospital and Medical Faculty of Palacky University in Olomouc. The specimens were assessed semi-quantitatively using the histoscore (H-score), considering percentage of positive cells (0–100%) multiplied by staining intensity (0–3), which results in a final H-score between 0 and

300. Immunostaining was performed using routine immunostaining procedures with validated antibodies specified in Table 3.4.

Table 3.4 List of antibodies used for immunohistochemistry

Primary Antibody	Supplier	Source	Clone	Cat. No.	Dilution	Method
Skp2	Invitrogen	Mouse	2C8D9	18-7334	1:75	Ventana
Slug	Cell Signaling	Rabbit	C19G7	9585	1:100	MW, citrate, pH 6.0
E-cadherin	Dako	Mouse	NCH-38	IR05961-2	1:50	MW, citrate, pH 6.0
vimentin	Dako	Mouse	V9	IR63061-2	1:10	MW, citrate, pH 6.0

3.4.11. SURVIVAL ANALYSIS

Data were retrieved from (282). Data were plotted and re-analysed in Prism (v6, GraphPad, La Jolla, California, United States) using logrank Mantel-Cox test. Threshold for CD24 and CD44 was set to 'low 25%'.

3.4.12. STATISTICAL ANALYSIS

Statistical analysis was performed using STATISTICA for Windows (StatSoft, Prague, Czech Republic) or in Prism (v6, GraphPad, La Jolla, CA, United States) using Student´s t-test. *P* values were calculated using paired *t* test (two-tailed) or multiple comparison *t* test with Holm-Sidak correction.

4. RESULTS

4.1. HIGH SKP2 EXPRESSION ASSOCIATES WITH A MESENCHYMAL PHENOTYPE AND INCREASES TUMOURIGENIC POTENTIAL OF PROSTATE CANCER CELLS

Overexpression of Skp2 has been detected in various cancers including prostate. The process of EMT as well as CSCs contribute to the plasticity of prostate cancer cells and disease progression. Acquisition of a mesenchymal phenotype that results in a CSC phenotype in prostate cancer was described.

4.1.1. HIGH NUCLEAR SKP2 EXPRESSION AND MESENCHYMAL PHENOTYPE ARE ASSOCIATED WITH HIGH GLEASON SCORE IN PATIENTS WITH PROSTATE CANCER

To elucidate the role of Skp2 in prostate cancer progression, we performed a retrospective analysis of Skp2 expression in patients with benign hyperplasia and prostate carcinoma (Figure 4.1 A). Our results show that the nuclear expression of Skp2 was significantly increased in prostate cancer tissues compared to benign hyperplasia tissues (Figure 4.1 B) and that high Gleason score ($\geq$ 7) was associated with high nuclear, but not cytoplasmic, Skp2 expression (Figure 4.1 C-D).

A

Clinical characteristics of the patients				
Number of patients	101			
Age	49-60	61-70	71-76	
	36	57	8	
Serum PSA (ng/ml)	<4	4–10	>10	missing
	11	40	45	5
Gleason scores	<7	7	>7	
	22	49	30	
Cancer stages	pT2a-c	pT3a-b	pT4	
	42	50	9	
Lymph node status	pN1	pN0	pNx*	
	29	65	7	
*without lymphadenectomy or no information				

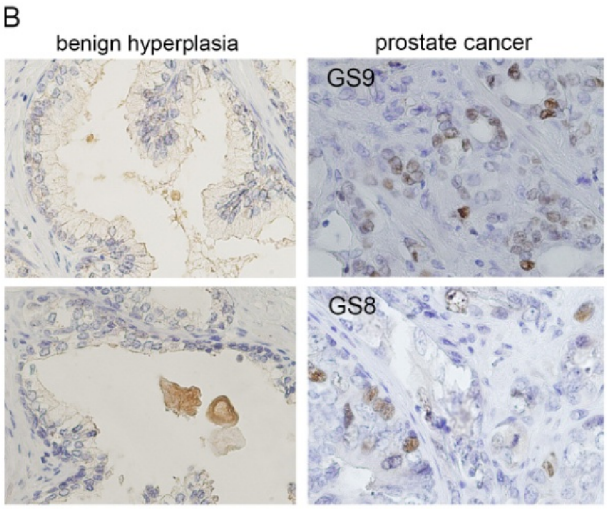

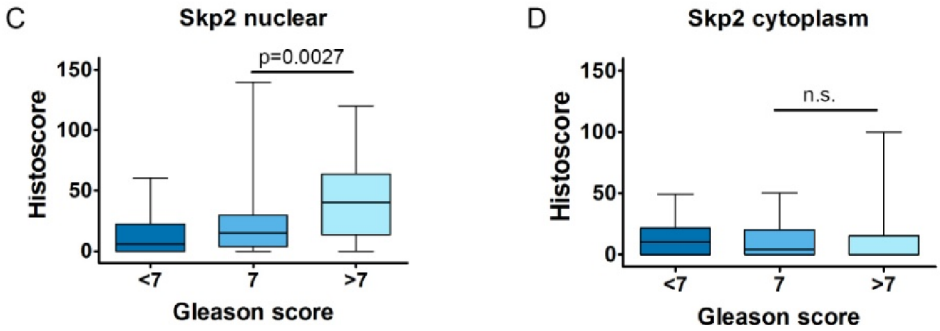

Figure 4.1. Nuclear Skp2 expression is associated with a high Gleason score in prostate cancer patients. (A) Clinical characterization of the patients. (B) Patient samples from primary prostate carcinoma with Gleason score (GS) 8 and 9, and benign hyperplasia were stained with anti-Skp2 antibody. Magnification: 40×. (C) Nuclear expression of Skp2 in patients with prostate cancer. (D) Cytoplasmic Skp2 expression in patients with prostate cancer. Box plots show median of Histoscore for selected markers, error bars represent min to max values.

Moreover, high Gleason score was associated with a mesenchymal phenotype, as demonstrated by decreased expression of epithelial marker E-cadherin and increased expression of mesenchymal marker vimentin (Figure 4.2 A-B). Thus, we showed that nuclear expression of Skp2 is significantly increased in patients with high Gleason score (≥ 7) whose cancer cells exhibit characteristics of the mesenchymal state.

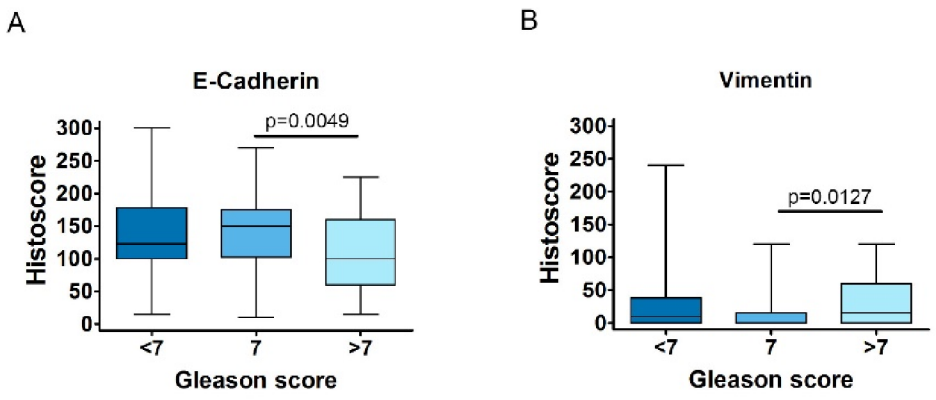

Figure 4.2 Expression of the EMT-related markers (E-cadherin and vimentin) correlate with Gleason score. Patient samples from primary prostate carcinoma and benign hyperplasia were stained with anti-E-Cadherin (A) and Vimentin (B) antibody. Box plots show median of Histoscore for selected markers, error bars represent min to max values.

4.1.2. Increased Expression of Skp2 is associated with mesenchymal phenotype of prostate cancer cells

To assess the connection between Skp2 expression and a mesenchymal phenotype in prostate cancer cells, we employed three sets of prostate epithelial cell lines and their mesenchymal counterparts. First, we compared human DU 145 epithelial and mesenchymal sublines that were previously prepared in our laboratory (71). We documented the differences in morphology of mesenchymal and epithelial sublines. In subconfluent conditions, the mesenchymal cells are spindle shaped and scattered. The epithelial cells are characterized by a polygonal, cobblestone morphology, and they grow in clusters (Figure 4.3 A-B). Moreover, we also documented the differences in morphology when we analysed more than 1700 parameters of mesenchymal and epithelial sublines using the cell painting protocol (279) and unsupervised image analysis with t-SNE and PCA algorithms (Figure 4.3 C-E).

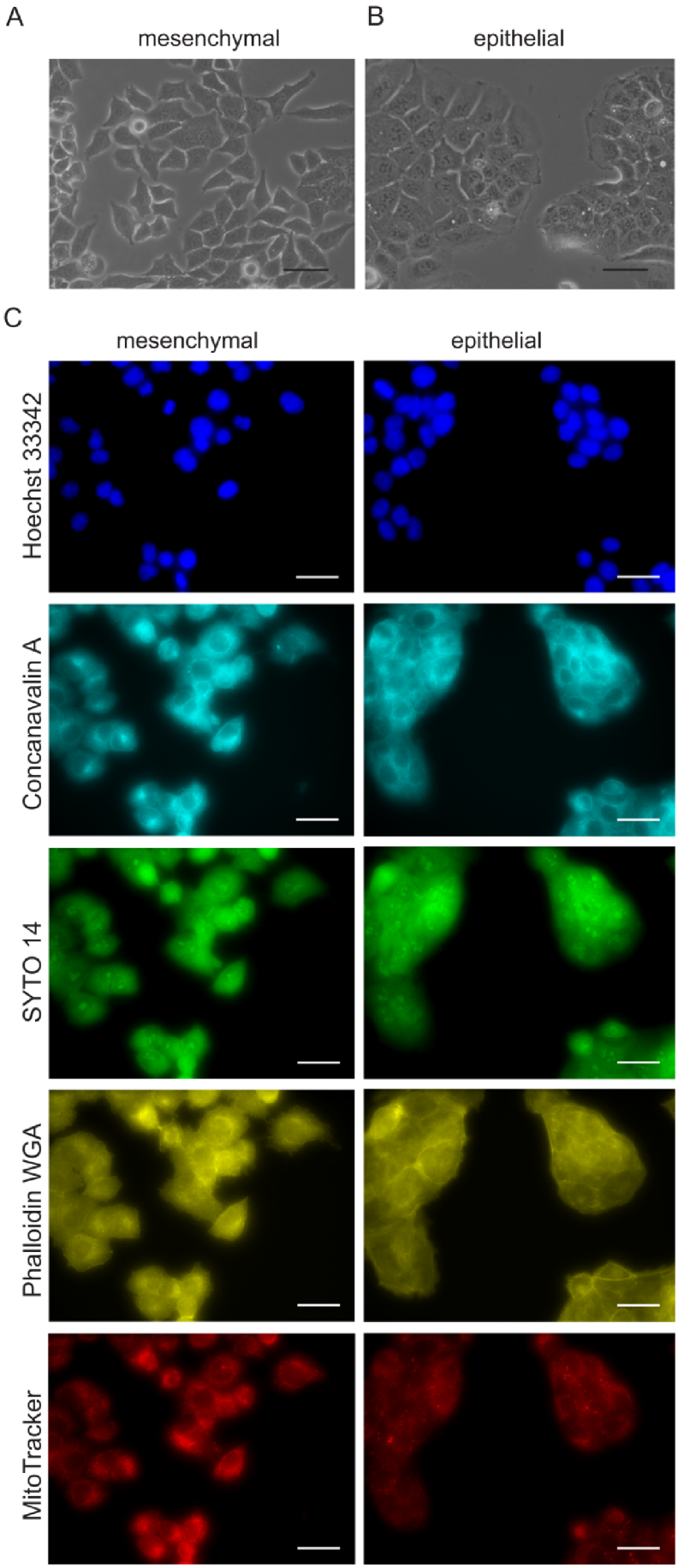
A
mesenchymal
B
epithelial
C
mesenchymal
epithelial
Hoechst 33342
Concanavalin A
SYTO 14
Phalloidin WGA
MitoTracker

Figure 4.3 (Continued)

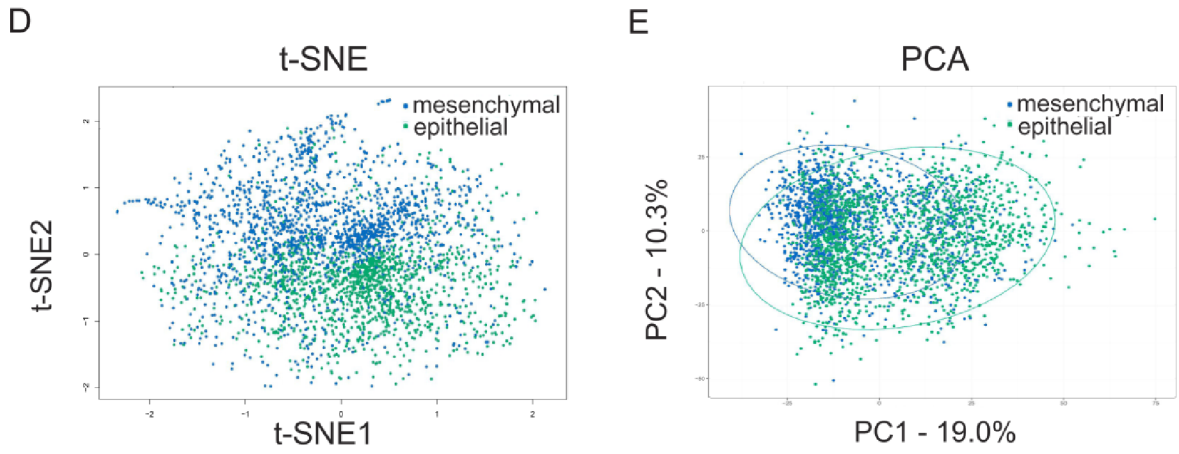

Figure 4.3 The cellular morphology differs in established mesenchymal and epithelial DU 145 subclones. (A-B) Morphology of the cells. Scale bar represents 50 µm. (C) Representative images of mesenchymal and epithelial sublines (scale bar size 30 µm). The nuclei (Hoechst 33342), endoplasmic reticulum (Concanavalin A), nucleoli and cytoplasmic RNA (SYTO 14), actin, Golgi apparatus, plasma membrane (Phalloidin&WGA) and mitochondria (MitoTracker) were visualized according to the cell painting protocol. (E) t-distributed stochastic neighbour embedding (t-SNE) and Principal component analysis (PCA) from 1761 morphology parameters of mesenchymal and epithelial cells. Ellipse in principal component analysis plot marks 95% confidence interval. Partial separation of confidence intervals in PCA and objects clustering into 2 groups in t-SNE plot (D) shows different phenotype based on morphology of mesenchymal and epithelial cell lines.

We analysed the Skp2 expression in these sublines and in cell lines, in which an EMT phenotype was achieved by different processes. We used age-control PC-3 cells (AC; epithelial) and docetaxel-resistant PC-3 cells (DR; mesenchymal), in which the acquisition of docetaxel resistance was accompanied by EMT (273). Next, we employed mouse prostate adenocarcinoma cell lines with a biallelic *PTEN* deletion: cE2 (epithelial, androgen independent) and E2 (mesenchymal, androgen dependent) (274, 283). To verify the epithelial characteristics of these cells, we confirmed the expression of both E-cadherin and Trop-2, which belong to the same gene family as does EpCAM, and whose overexpression has been described in various human epithelial cancers. The mesenchymal phenotype was defined by the expression of vimentin, N-cadherin and transcription repressor of E-cadherin, ZEB1. We found that the mesenchymal phenotype of prostate cancer cells was accompanied by an increase

in Skp2 levels in all selected pairs of cell lines (Figure 4.4). For further studies, we selected the DU 145 cell line and established sublines resulting from their natural heterogeneity in CSC markers expression CD24 and Trop-2, respectively (Figures 4.5, 4.28 A and 4.30 A).

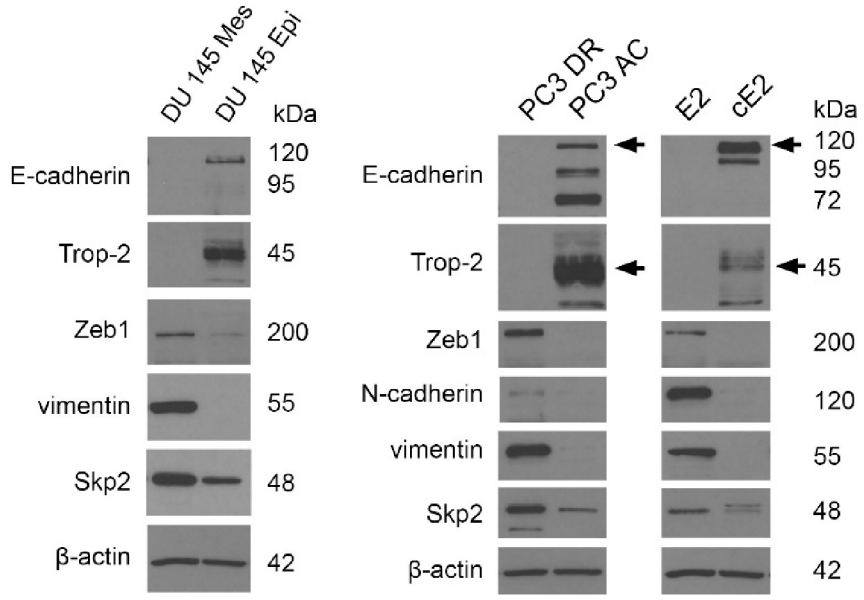

Figure 4.4 Increased Skp2 expression is associated with the mesenchymal phenotype of prostate cancer cells. Western blot analysis of Skp2 expression and EMT markers in prostate cancer cell lines: DU 145 Mesenchymal (Mes), DU 145 Epithelial (Epi), PC3 docetaxel-resistant (DR), PC3 age-control (AC), and mouse prostate adenocarcinoma cells with mesenchymal (E2) and epithelial (cE2) phenotypes. Representative results from three independent repetitions are shown. β-actin was used as a loading control. Arrows point to the specific signal.

4.1.3. MESENCHYMAL DU 145 CELLS EXHIBIT CHARACTERISTICS OF CANCER STEM-LIKE CELLS

4.1.3.1. THE EXPRESSION OF CD24 IS INCREASED IN DU 145 EPITHELIAL CELLS

As mentioned in the chapter 1.1.4.2., the EMT is often concomitant with the CSCs phenotype of prostate cancer cells. The $CD44^{+}CD24^{-}$ phenotype is commonly used to define prostate cancer stem cells (91-93). Thus, we investigated expression of these markers in epithelial and mesenchymal sublines established from DU 145 cells.

We observed that the $CD44^{+}CD24^{-}$ population is more abundant in mesenchymal cells (Figure 4.5 A-C). Increased expression of CD24 in epithelial cells was also confirmed at the mRNA level (Figure 4.6). These data suggest the cancer stem-like cell nature of DU 145 mesenchymal cells.

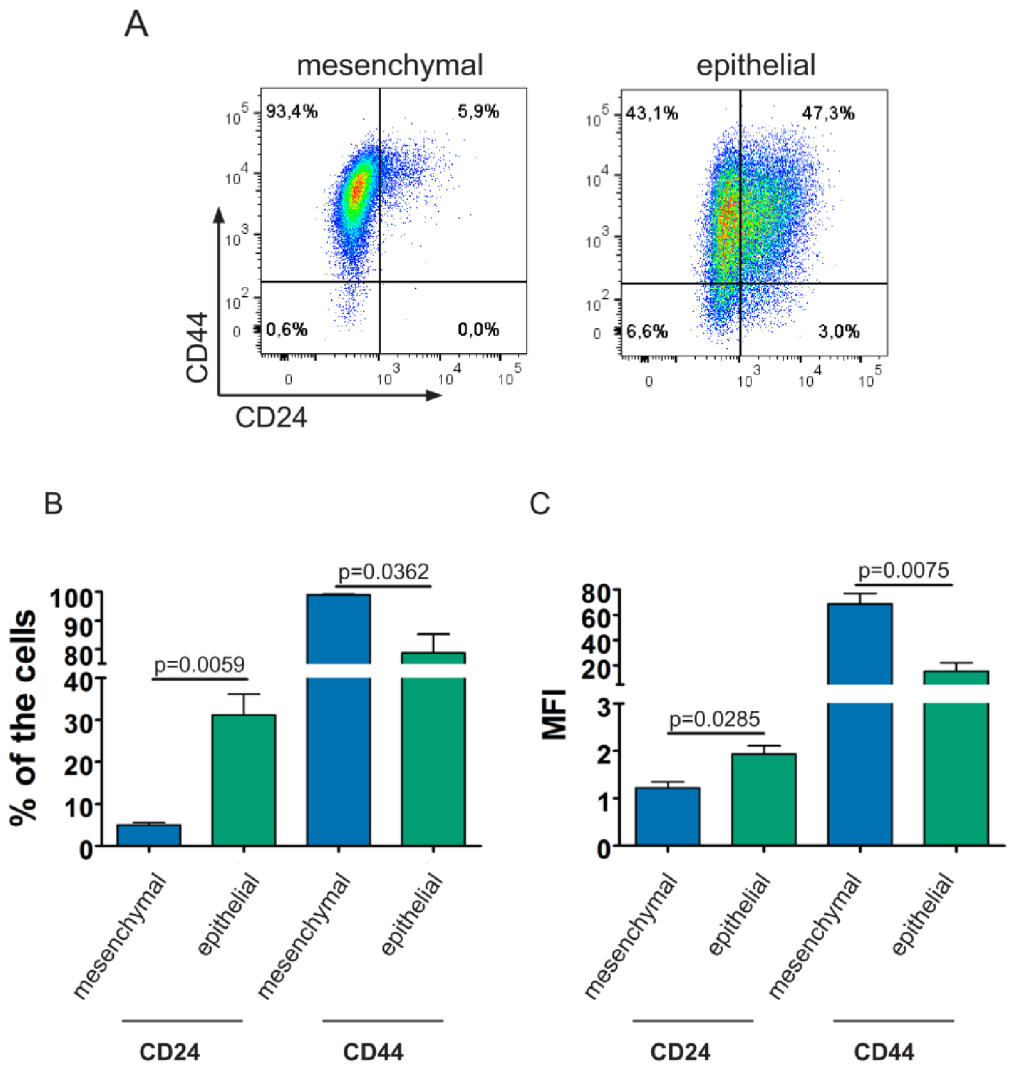

Figure 4.5 Expression of CSCs markers CD24 and CD44 is altered in DU 145 cells with a mesenchymal phenotype. (A) Expression of CD24 and CD44 markers in DU 145 mesenchymal and epithelial cells was analysed by flow cytometry. Graphs are in a logarithmic scale. (B) Quantification of results shown in (A). Bars show the mean ± SD of the percentage of positive cells for both markers. Results are from three independent repetitions. (C) Expression of CD24 and CD44 measured as the median fluorescence index (MFI) that was calculated as a ratio of a fluorescent intensity signal from samples stained with specific antibody and isotype control. Bars show the mean ± SD values for the MFI of selected markers from three independent experiments.

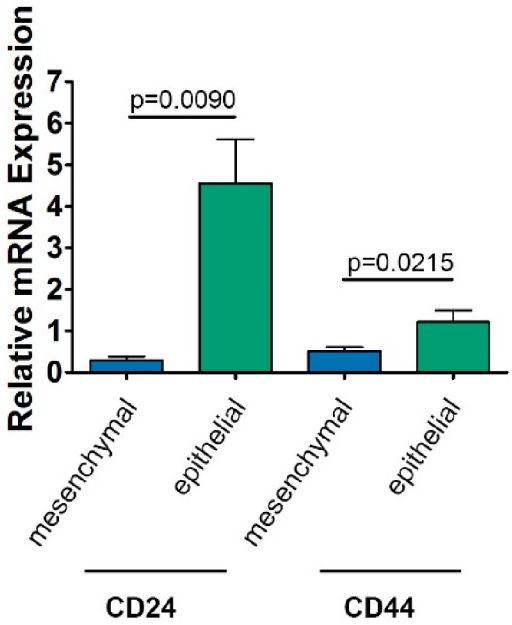

Figure 4.6 CD24 and CD44 mRNA expression is increased in epithelial cells. qRT-PCR analysis of *CD24* and *CD44* relative expression in mesenchymal and epithelial cells. Data represent the mean ± SD of five independent experiments. The relative expression of the markers was normalized to *POLR2A* expression.

4.1.3.2. FUNCTIONAL TESTS CONFIRMING THE CSC-LIKE PHENOTYPE OF DU 145 MESENCHYMAL CELLS

To further validate the cancer stem-like phenotype of the mesenchymal cells, the epithelial and mesenchymal cells were seeded at low densities in semisolid media to examine their ability to grow in anchorage-independent conditions and form spheroids. The cancer stem-like phenotype of the mesenchymal cells was illustrated by their increased ability to form spheroids (Figure 4.7 A-B). This phenomenon was not caused by increased proliferation, as there was no significant difference in proliferation between mesenchymal and epithelial cells (Figure 4.7 C). The cancer stem-like properties of mesenchymal DU 145 cells were further confirmed by the increased activity of ALDH1 (Figure 4.7 D). Thus, we showed that DU 145 cells with the mesenchymal phenotype and high expression of Skp2 exhibit CSC-like characteristics compared to their epithelial counterparts.

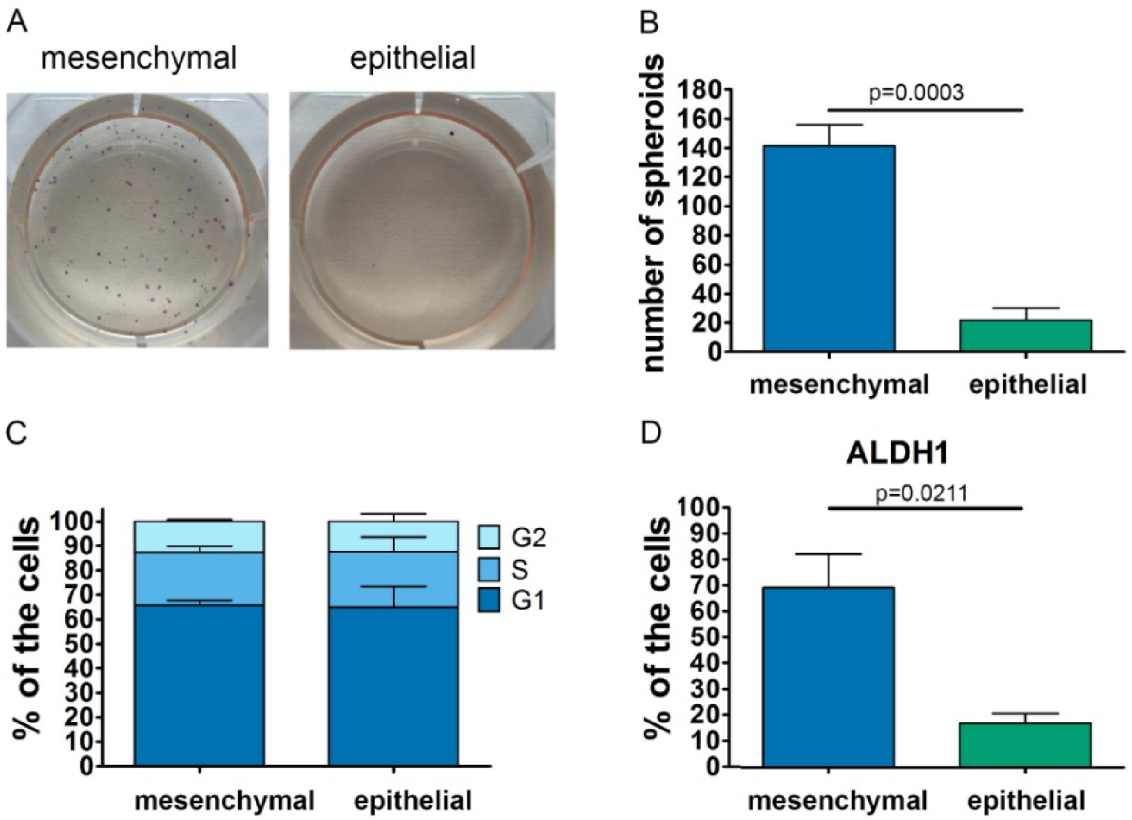

Figure 4.7 CSC-like characteristics of DU 145 mesenchymal and epithelial cells. (A) Spheroid formation and growth in anchorage-independent conditions in DU 145 mesenchymal and epithelial cells. (B) Quantification of results shown in (A). Data are shown as the mean ± SD of the number of spheroids per well. Results are from three independent repetitions. (C) Cell cycle analysis determined by flow cytometry. Results are from three independent experiments. (D) ALDH1 activity in DU 145 mesenchymal and epithelial cells was analysed by flow cytometry. Data are presented as the mean ± SD of the percentage of cells with active ALDH1. Results are from three independent repetitions.

4.1.4. Analysis of CSC-like properties of the cells with downregulated expression of Skp2

Skp2 is overexpressed in prostate cancer (216) and high expression of Skp2 correlates with high Gleason score (Figure 4.1). Conversely, its downregulation was shown to restrict prostate cancer development *in vivo* (221). Since CSCs are considered to be crucial for cancer progression, we decided to examine whether targeting of Skp2 would affect the CSC-like properties of the cells and their tumourigenic potential.

4.1.4.1. THE SKP2 DOWNREGULATION LEADS TO UPREGULATION OF CELL CYCLE INHIBITORS

To ascertain the role of Skp2 in cancer stem-like cells, we decided to knock down Skp2 expression in DU 145 mesenchymal cells (DU 145 *SKP2* KD cells) and analyse their tumourigenic capacity *in vitro*. Silencing of Skp2 resulted in the accumulation of its substrates $p27^{Kip1}$ and $p21^{Cip1}$ (Figure 4.8 A). However, the cell cycle was not significantly affected (Figure 4.8 B). Therefore, we decided to investigate whether the accumulated cell cycle inhibitor $p27^{Kip1}$ is functional and is able to form complexes with CDKs. The immunoprecipitation analysis confirmed the ability of $p27^{Kip1}$ to bind CDK1, CDK2 and CDK4 in *SKP2* KD cells (Figure 4.8 C). As positive controls, we used two different inductors of the cell cycle arrest - the inhibitor MLN-4924 (134) or starvation followed by treatment with *all-trans retinoic acid* (ATRA) (284).

We also investigated the localization of $p27^{Kip1}$ and Skp2 in *SKP2* KD cells. We observed that the level of Skp2 was decreased both in nucleus and cytoplasm in *SKP2* KD cells (Figure 4.8 D-F), and was accompanied by accumulation of $p27^{Kip1}$ in the nucleus and cytoplasm (Figure 4.8 G-H). Thus, we showed that Skp2 downregulation resulted in accumulation of the cell cycle inhibitors, however, the proliferation of the cells was not significantly affected.

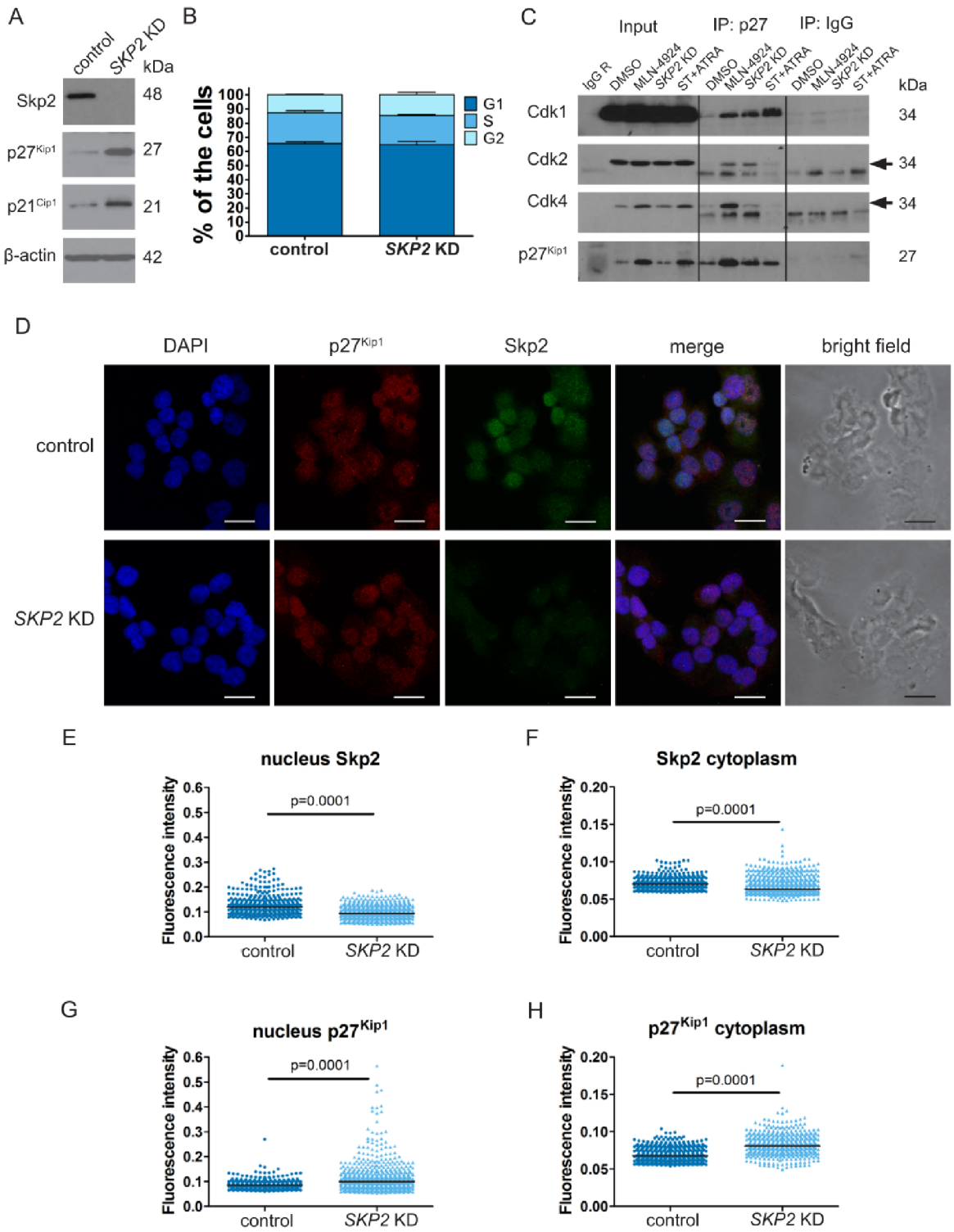

Figure 4.8 Skp2 downregulation results in accumulation of cell cycle inhibitors. (A) Skp2, p27^{Kip1} and p21^{Cip1} expression in *SKP2* KD cells was determined by western blot. Representative images are from three independent experiments. β-actin was used as a loading control. (B) Cell cycle was analysed by flow cytometry. Data are from three independent experiments. (C) Immunoprecipitation (IP) of p27^{Kip1} followed by western blot detection of CDKs. Results were obtained from three independent experiments. Arrows denote specific signals. (D) Immunocytochemistry

staining for Skp2 and $p27^{Kip1}$ in control and *SKP2* KD cells. Scale bar size represent 20 µm. (E-H) Quantification of the data from (D). Data are presented as Fluorescence intensity and each dot represents the signal from one cell. Results are from three independent experiments. The bars represent the medians of each group.

4.1.4.2. THE EXPRESSION OF CD24 IS INCREASED IN *SKP2* KD CELLS

We have previously observed an increase of $CD44^{+}CD24^{+}$ population in DU 145 epithelial cells, where the level of Skp2 is lower than in mesenchymal cells (Figure 4.5) Therefore, we hypothesised that the level of CD24 and CD44 will be increased in the DU 145 mesenchymal cells with Skp2 knock down. Indeed, we observed that the expression of CD24 and CD44 was significantly increased in *SKP2* KD cells both at the protein and mRNA level (Figure 4.9 A-C). Moreover, the cells cultivated in 3D conditions as spheroids maintained their phenotype in terms of CD24 and CD44 expression (Figure 4.9. D-E). Thus, we confirmed that Skp2 down-regulation affected the expression of CSC-like markers in terms of increase of $CD44^{+}CD24^{+}$ subpopulation in cells cultivated both in 2D and 3D conditions.

4.1.4.3. SKP2 DOWNREGULATION REVERSES CSC-LIKE PROPERTIES OF DU 145 MESENCHYMAL CELLS

To assess the role of Skp2 in self-renewal, we tested the ability of the cells with downregulated Skp2 to grow in the anchorage-independent conditions and form spheroids from single cells. We found that the sphere-forming ability of *SKP2* KD cells was significantly decreased (Figure 4.10 A-B), whereas Skp2 knock-down itself did not impair cellular proliferation (Figure 4.8 B). Next, we investigated the tumourigenic potential of *SKP2* KD cells. The cells were injected into immunodeficient mice, and the rate of xenograft formation was recorded. Our results showed that Skp2 knock-down significantly decreased the tumourigenic potential of DU 145 mesenchymal cells (Figure 4.10 C). Furthermore, the activity of ALDH1 was decreased in these cells (Figure 4.10 D). In conclusion, our data confirm that Skp2 silencing decreases the tumourigenic potential of mesenchymal DU 145 cells and affects the functional properties of cancer stem-like cells.

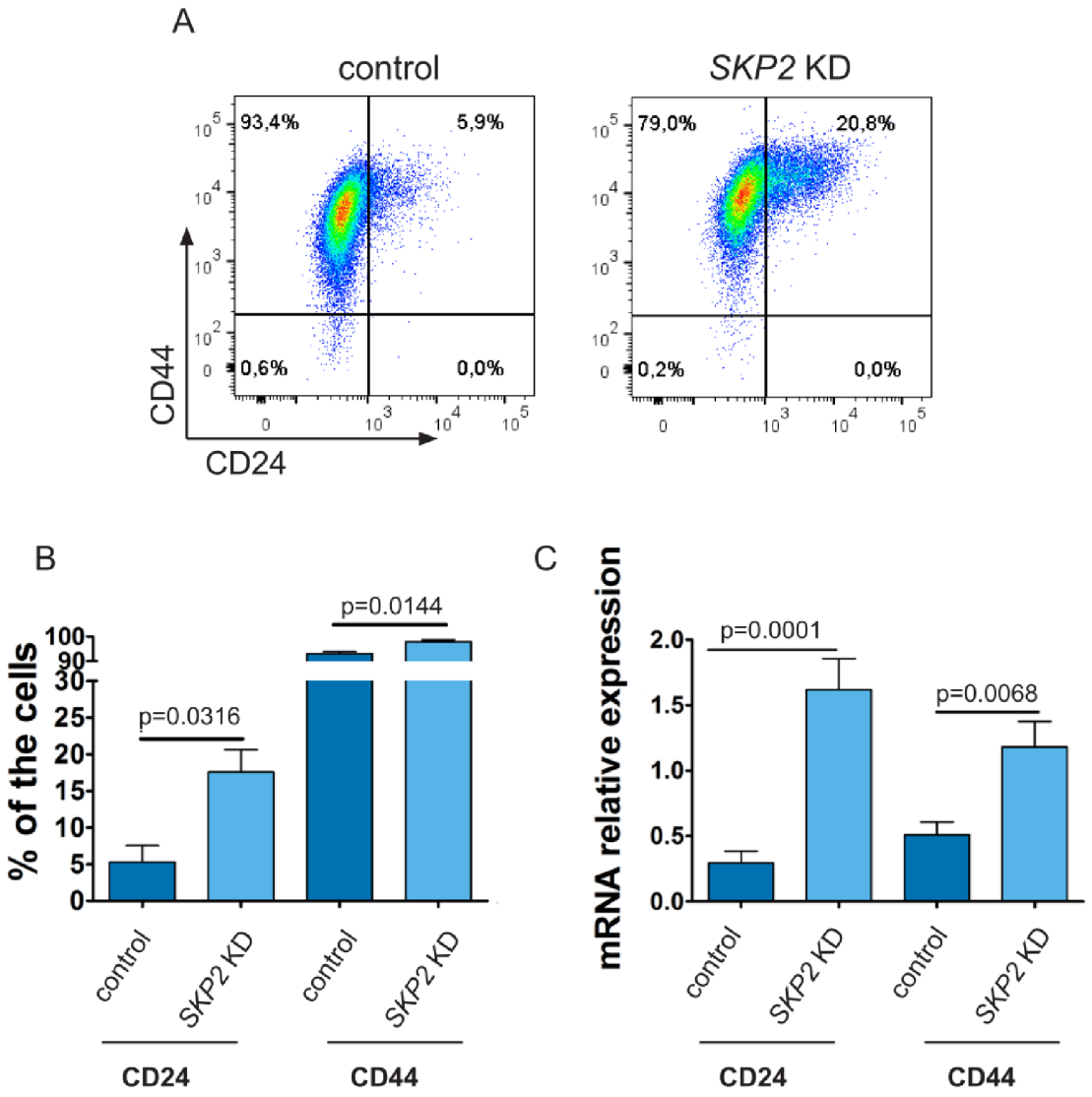

Figure 4.9 Expression of CD24 and CD44 is increased in DU 145 *SKP2* KD cells cultivated in both 2D and in anchorage-independent conditions. (A) Expression of CD24 and CD44 in control and *SKP2* KD cells analysed by flow cytometry. Graphs are in a logarithmic scale (B) Quantification of results shown in (A). Data are presented as the mean ± SD of the percentage of positive cells for the selected markers. Representative images are from three independent experiments. (C) qRT-PCR analysis of CD24 and CD44 markers in DU 145 *SKP2* KD cells and control cells. Data represent the mean ± SD of three independent experiments. The relative expression of the markers was normalized to POLR2A expression. (D) Expression of CD24 and CD44 in cells cultivated in anchorage-independent conditions analysed by flow cytometry. Results are from three independent repetitions. (E) Quantification of results shown in (D). Bars show the mean ± SD of the percentage of positive cells for both markers. Graphs are in a logarithmic scale.

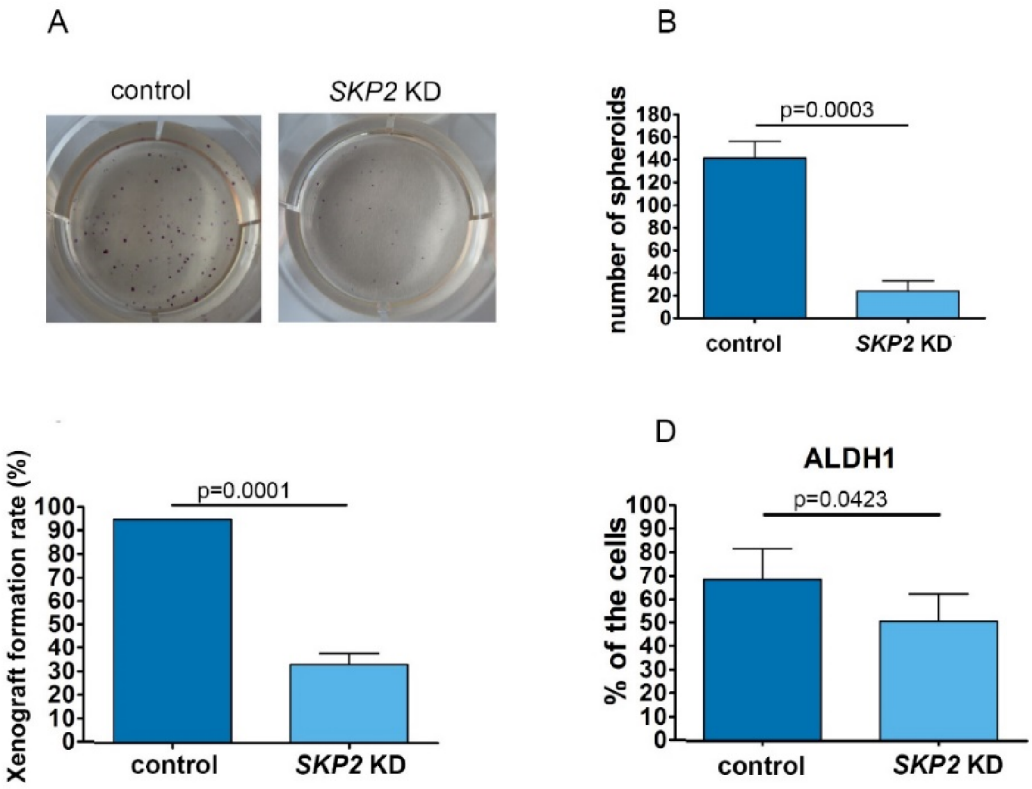

Figure 4.10 The clonogenic and tumourigenic potential is decreased in DU 145 *SKP2* KD cells. (A) Spheroids formation and growth in anchorage-independent conditions in *SKP2* KD cells and control cells. (B) Quantification of results shown in (A). Data are shown as the mean ± SD of the number of spheroids per well. Results are from three independent repetitions. (C) Xenograft formation rate of *SKP2* KD cells in SHO mice. Tumour formation rate was calculated for control and *SKP2* KD cells as a ratio of number of mice inoculated with cancer cells and number of mice bearing tumours. Number of mice per group, n = 10. (D) ALDH1 activity in DU 145 control and *SKP2* KD cells was analysed by flow cytometry. Data are presented as the mean ± SD of the percentage of cells with active ALDH1. Results are from three independent experiments.

4.1.4.4. SKP2 OVEREXPRESSION CAUSES A DECREASE OF CD24 IN DU 145

In our study, we observed a negative correlation between the decreased expression of Skp2 and the increased expression of CD24 in epithelial DU 145 cells compared to their mesenchymal counterparts (Figures 4.5 A-C). Importantly, CD24 expression was increased in DU 145 *SKP2* KD cells (Figure 4.9). Therefore, we hypothesized that Skp2 overexpression will lead to decreased CD24 expression in the DU 145 parental cell line. Indeed, we observed that in cells with transient Skp2

overexpression (Figure 4.11 A), CD24 expression was decreased (Figure 4.11 B). Thus, we showed that Skp2 is important for maintaining the cancer stem-like phenotype of DU 145 mesenchymal cells in terms of the expression of the CSC marker CD24.

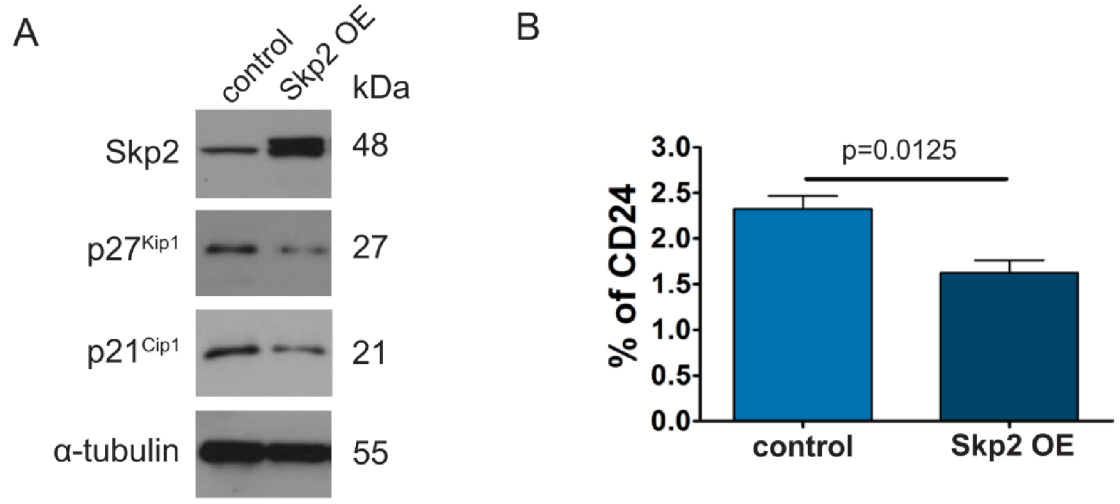

Figure 4.11. CD24 is decreased in DU 145 cells after Skp2 overexpression (OE). (A) Western blot analysis of Skp2, $p27^{Kip1}$ and $p21^{Cip1}$ protein expression. Representative images are from three independent experiments. α-tubulin was used as a loading control. (B) Expression of CD24 in DU 145 cells overexpressing Skp2 and control cells was analysed by flow cytometry. Data are presented as the mean ± SD of the percentage of CD24-positive cells. Results are from three independent experiments.

4.1.4.5. HIGH CD24 AND CD44 EXPRESSION ASSOCIATES WITH FAVOURABLE RECURRENCE-FREE SURVIVAL

CD24 was described as a marker that distinguished between low differentiated and transit-amplifying cells in the basal layer of human prostate (8). Moreover, prostate cancer cells with $CD24^{-}CD44^{+}$ phenotype are considered CSCs (122, 123). In order to validate the clinical relevance of CD24 and CD44 in prostate cancer, we examined the association of CD24 and CD44 expression with the prognosis of patients with prostate cancer.

Our results suggest that the high expression of CD24 is linked to the epithelial and less aggressive phenotype of metastatic prostate cancer cells, and accompanied by the low expression of Skp2. Conversely, low CD24 expression is linked to the

mesenchymal phenotype of metastatic prostate cancer cells that have characteristics of cancer stem-like cells, associated with high Skp2 expression. As Skp2 overexpression has been correlated with poor prognosis in prostate cancer patients, we wanted to reveal whether high CD24 expression would be associated with a better prognosis. To investigate the association of CD24 and CD44 expression with recurrence-free survival, we analysed cohorts of prostate cancer patients (282) and confirmed that high expression levels of both markers (CD24 and CD44) were associated with favourable recurrence-free survival (Figure 4.12).

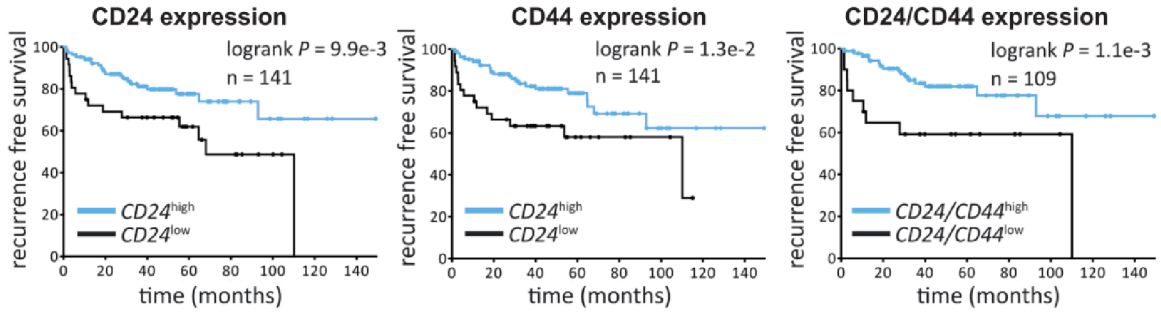

Figure 4.12 CD24 and CD44 expression is associated with better prognosis for prostate cancer patients. The graphs show an analysis of recurrence-free survival analysis in a cohort of prostate cancer patients, according to high or low CD24 (left), CD44 (middle), and CD24/CD44 (right) expression levels. Data was retrieved from (282). Data were plotted and reanalysed using Prism (v6, GraphPad) using the log rank Mantel-Cox test. The threshold for CD24 and CD44 was set to 'low 25%.'

4.1.5. PHARMACOLOGICAL INHIBITION OF SCF^{Skp2}

Based on our observation that Skp2 downregulation has significant influence on the CSC-like phenotype of the cells, we aimed to test another approach to target the activity of SCF^{Skp2} in parental DU 145 cells. We took advantage of an inhibitor of neddylation, MLN-4924, which blocks SCF^{Skp2} assembly and is currently in clinical trials for multiple malignancies (237). We hypothesized that pharmacological inhibition of SCF^{Skp2} would affect cytokinetics of the cells, that $CD44^{+}CD24^{-}$ cells would be more sensitive to MLN-4924 treatment than $CD44^{+}CD24^{+}$ cells, and that pharmacological inactivation of the SCF^{Skp2} complex will decrease the self-renewal capacity of prostate cancer stem-like cells.

4.1.5.1. ANALYSIS OF CYTOKINETICS IN DU 145 AFTER INHIBITION OF NEDDYLATION

First, we determined the cytotoxic effect of the inhibitor on the cells. We observed decreased viability and number of the cells in a time and concentration dependent manner. The viability did not decrease under 50% even after 96 hours of the treatment (Figure 4.13 A). However, the numbers of the cells were significantly decreased (Figure 4.13 B), suggesting that the cells respond to the inhibition of neddylation by proliferation arrest rather than cell death.

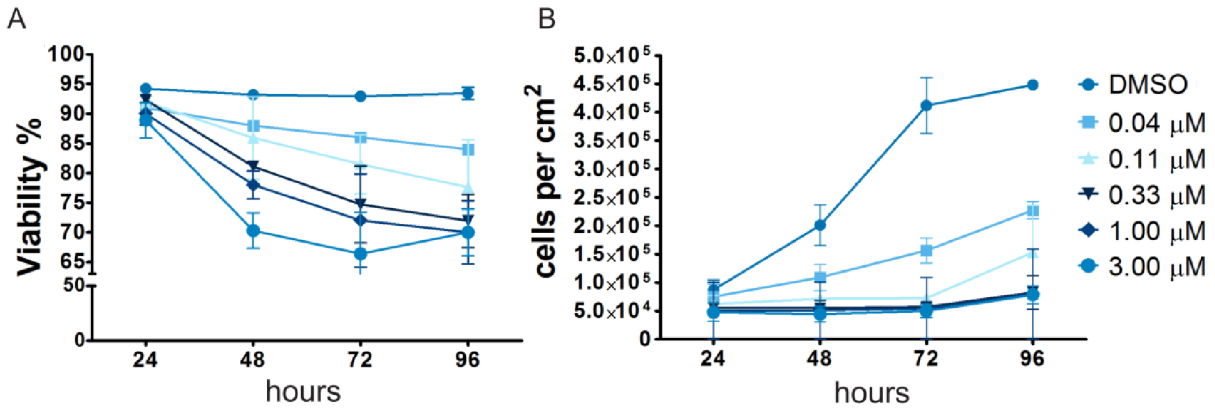

Figure 4.13 Inhibition of neddylation leads to decreased viability and cell counts. In DU 145 parental cell line, the viability (A) and cell counts (B) were determined by CASY Cell Counter after DMSO (vehicle) or MLN-4924 treatment at indicated time points. Data is presented as the mean ± SD of the viable cells (A) or number of the cells per cm^2 (B), and was obtained from two independent experiments. The statistical significance ($p \leq 0.05$) was observed at all concentrations used from 48 hours post treatment on.

For further analysis of the effect of the MLN-4924 inhibitor on cytokinetics and CSC-like properties of prostate cancer cells, we selected the two lowest concentration of the inhibitor – 0.04 μM and 0.11 μM for their low toxicity, yet significant inhibition of proliferation of the cells at 24-96 hours of the treatment. The effect of the MLN-4924 was confirmed by decreased binding of Nedd8 to Cullins at all selected time points in both concentrations used (Figure 4.14). Interestingly, the level of Skp2 itself was slightly upregulated after MLN-4924 treatment. An accumulation of Skp2 substrates, the cell cycle inhibitors $p27^{Kip1}$ and $p21^{Cip1}$ was observed, however, accumulation of another Skp2 substrate, Cdt1, was not detected.

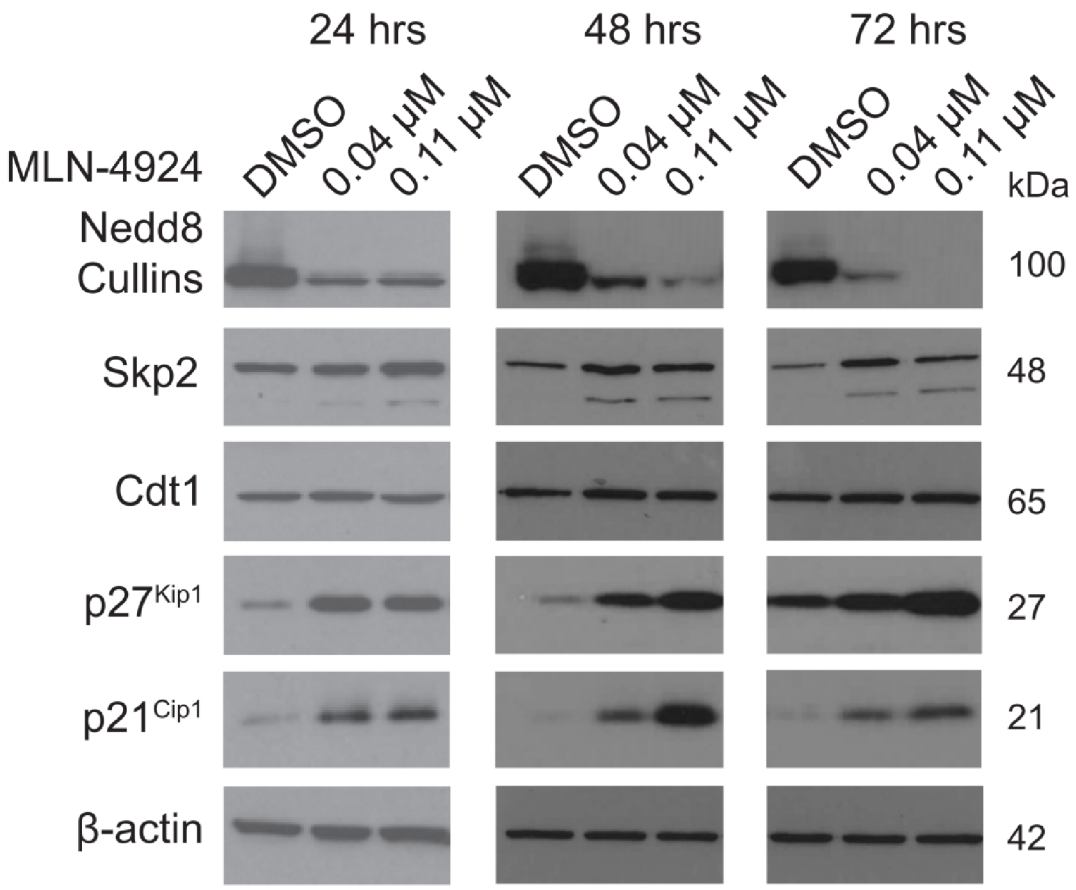

Figure 4.14 Inhibition of neddylation results in accumulation of SCF^{Skp2} substrates. Western blot analysis of Skp2 expression and expression of SCF^{Skp2} substrates after DMSO (vehicle) or 0.04 μM and 0.11 μM MLN-4924.

The decrease in cell counts and accumulation of the cell cycle inhibitors suggested an induction of cell cycle arrest in the cells after the MLN-4924 treatment. Indeed, we observed that the treatment with both 0.04 μM and 0.11 μM concentrations for 24 hours resulted in cell cycle arrest, and graded with the prolonged time of the treatment (Figure 4.15 A-B). The cells were preferentially arrested in the G2 phase of the cell cycle.

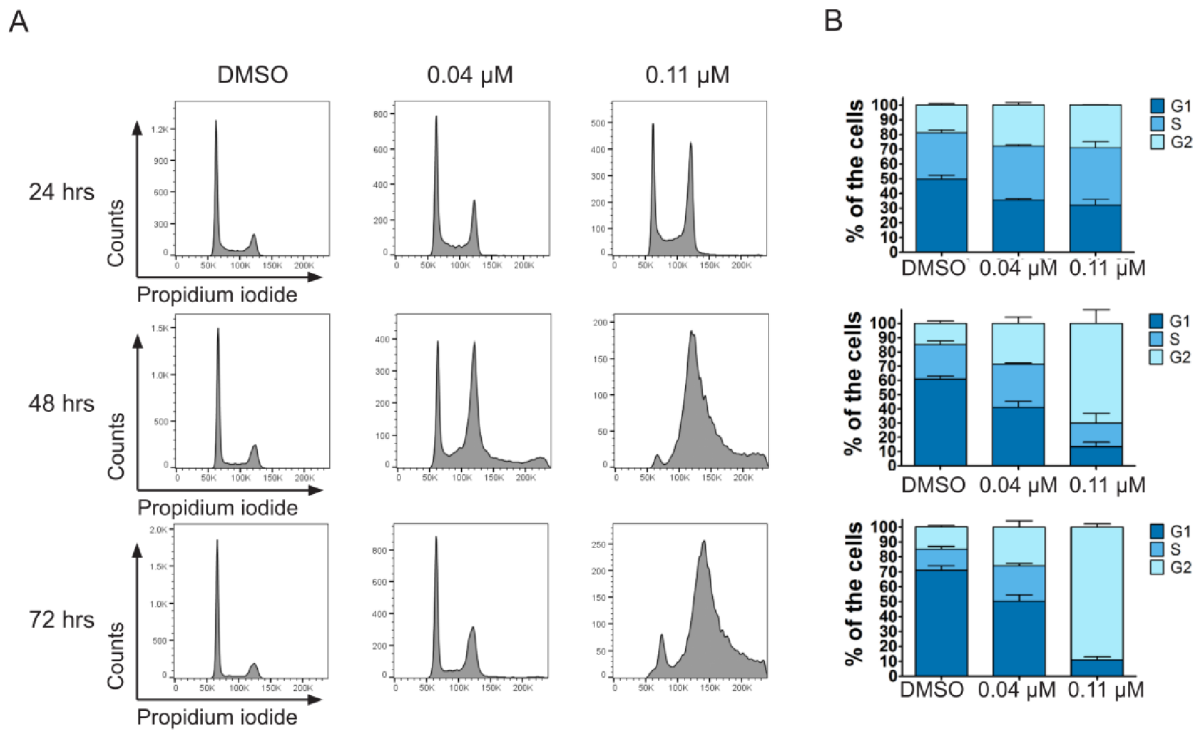

Figure 4.15 Inhibition of neddylation induces cell cycle arrest. (A) Histograms show the cell cycle after treatment with DMSO (vehicle) or 0.04 μM and 0.11 μM MLN-4924. Graphs are in a linear scale. (B) Quantification of (A). Bars represent the mean ± SD from at least three independent experiments.

We further examined whether MLN-4924 also induces DNA damage and cell death in DU 145 cells. Our results show that both DNA damage and cell death are induced after 48 hours of the treatment, and not earlier (Figure 4.16). The MLN-4924 inhibitor exerts pleiotropic effects on the cells (summarized in the chapter 1.2.3.1.). In our experimental model, we observed decreased viability, cell cycle arrest, DNA damage and cell death induction in a time and concentration dependent manner.

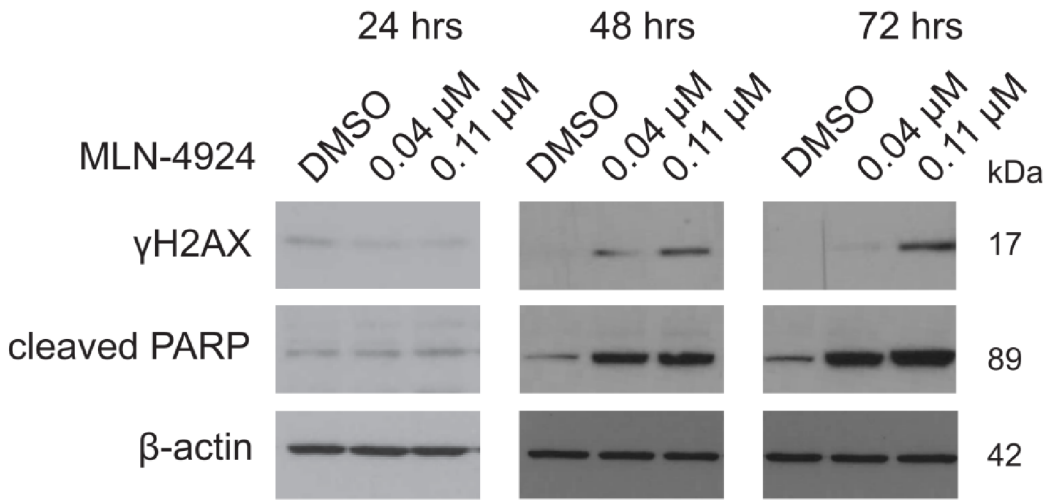

Figure 4.16 Inhibition of neddylation induces DNA damage and cell death. Western blot analysis of γH2A.X as a marker of DNA damage and cleaved PARP as a marker of programmed cell death after DMSO (vehicle) or 0.04 µM and 0.11 µM MLN-4924 treatment in selected time points. Representative results from three independent repetitions are shown. β-actin was used as a loading control.

4.1.5.2. THE DECREASE OF CD24 POSITIVE CELLS INCIDENCE AFTER INHIBITION OF NEDDYLATION

As we have previously observed an association of decreased Skp2 expression with increased CD24 and CD44, we examined the expression of the CSC markers CD44 and CD24 after the MLN-4924 treatment at selected time points. There was no change in CD44 expression at all selected time points and both MLN-4924 concentrations (Figure 4.17 A). After 24 hours of the treatment, there was no change in CD24 expression either (Figure 4.17 A-B, upper row). Unexpectedly, instead of an increase in CD24 expression, we observed significant decrease in CD24 after 48 hours and 72 hours of the treatment with both concentrations of the MLN-4924 inhibitor (Figure 4.17 A-B, middle and bottom row).

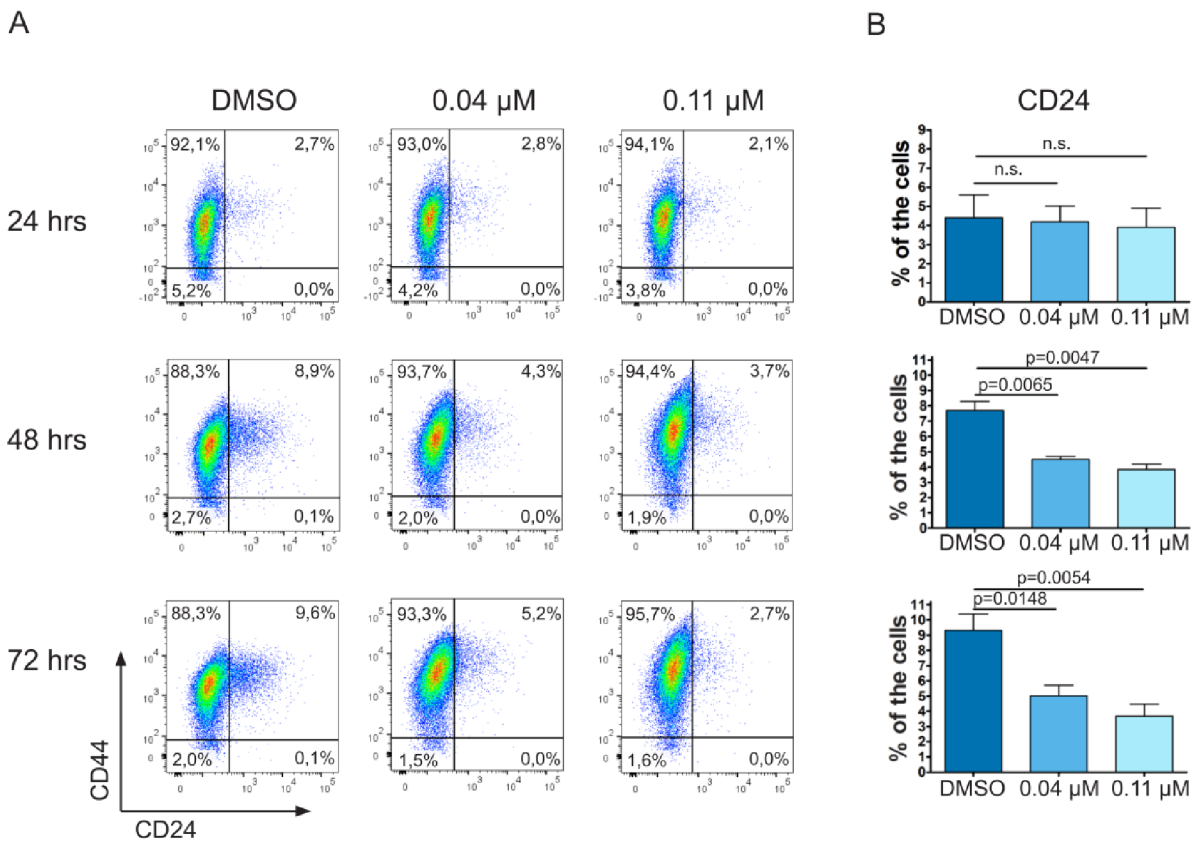

Figure 4.17 Inhibition of neddylation decreases the CD44$^+$CD24$^+$ subpopulation. (A) Expression of CD24 and CD44 in DU 145 analysed by flow cytometry. Cells were treated with DMSO (vehicle) or 0.04 μM and 0.11 μM MLN-4924 inhibitor for indicated time. Graphs are in a logarithmic scale. (B) Quantification of results shown in (A). Data is presented as the mean ± SD of the percentage of cells positive for the selected markers. Representative images are from three independent experiments.

When we noticed the drop in CD24 positive cells after MLN-4924 treatment, we questioned whether these cells could be more sensitive to the treatment and die preferentially. Therefore, we selected the time point when we first observed the initiation of cell death (48 hours) (Figure 4.16), and we analysed induction of the cell death by AnnexinV assay in combination with a CD24 marker (Figure 4.18 A). There was no early apoptosis induced in either CD24$^-$ or CD24$^+$ cells after MLN-4924 treatment (Figure 4.18 A-B), however, we detected induction of late apoptosis/necrosis in CD24$^+$ cells (Figure 4.18 A, C). Thus, we showed that CD24$^+$ cells were more susceptible to induction of late apoptosis/necrosis than CD24$^-$ cells in short-term treatment (48 hours).

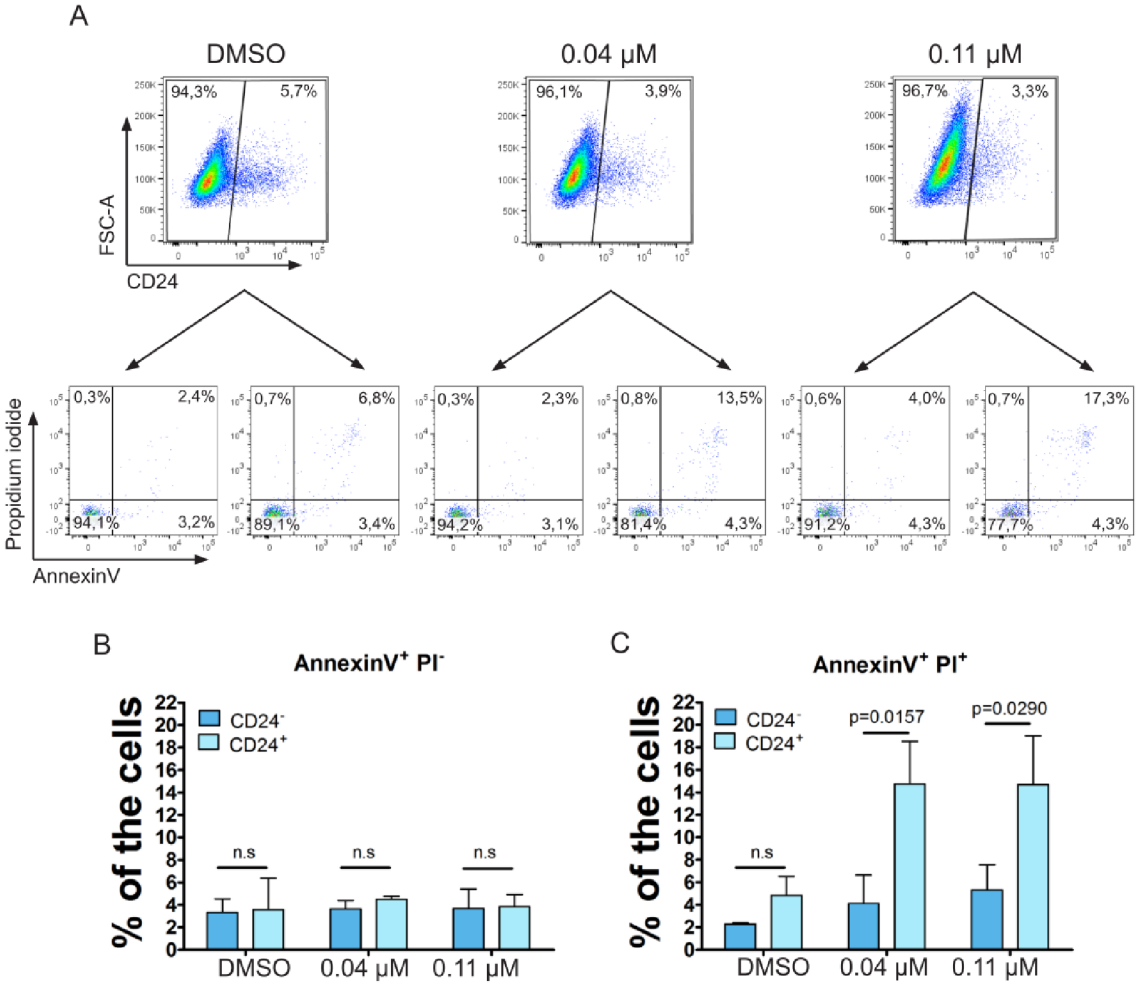

Figure 4.18 Inhibition of neddylation induces late apoptosis/necrosis in CD24$^+$ cells. (A) Induction of cell death in CD24$^+$ and CD24$^-$ cells. Cells were treated with DMSO (vehicle) or 0.04 μM and 0.11 μM MLN-4924 inhibitor for 48 hours. Cell death was assessed by AnnexinV and Propidium iodide (PI) positivity by flow cytometry. Graphs are in a logarithmic scale (CD24, Propidium iodide and AnnexinV) and in a linear scale (FSC-A). (B-C) Quantification of results shown in (A). Data is presented as the mean ± SD of the percentage of cells positive for the selected markers. Representative images are from three independent experiments.

To elucidate whether the different sensitivity of CD24$^+$ and CD24$^-$ cells to the MLN-4924 inhibitor could be caused by different expression of Skp2 in these cells, we examined the Skp2 protein level in those two subpopulations. The Skp2 expression was analysed by flow cytometry in CD24$^+$ and CD24$^-$ cells (Figure 4.19 A). However, we did not observe significant change in Skp2 expression (Figure 4.19 B). We also sorted CD24$^-$ and CD24$^+$ cells and analysed Skp2 protein level in those cells by

western blotting. Again, we did not detect any difference in the Skp2 protein between these subpopulations (Figure 4.19 C). Therefore, we did not confirm that the protein level of Skp2 is responsible for the high sensitivity to the MLN-4924 treatment in the $CD24^+$ subpopulation. Thus, the mechanism behind the high sensitivity of $CD24^+$ cells remains to be revealed.

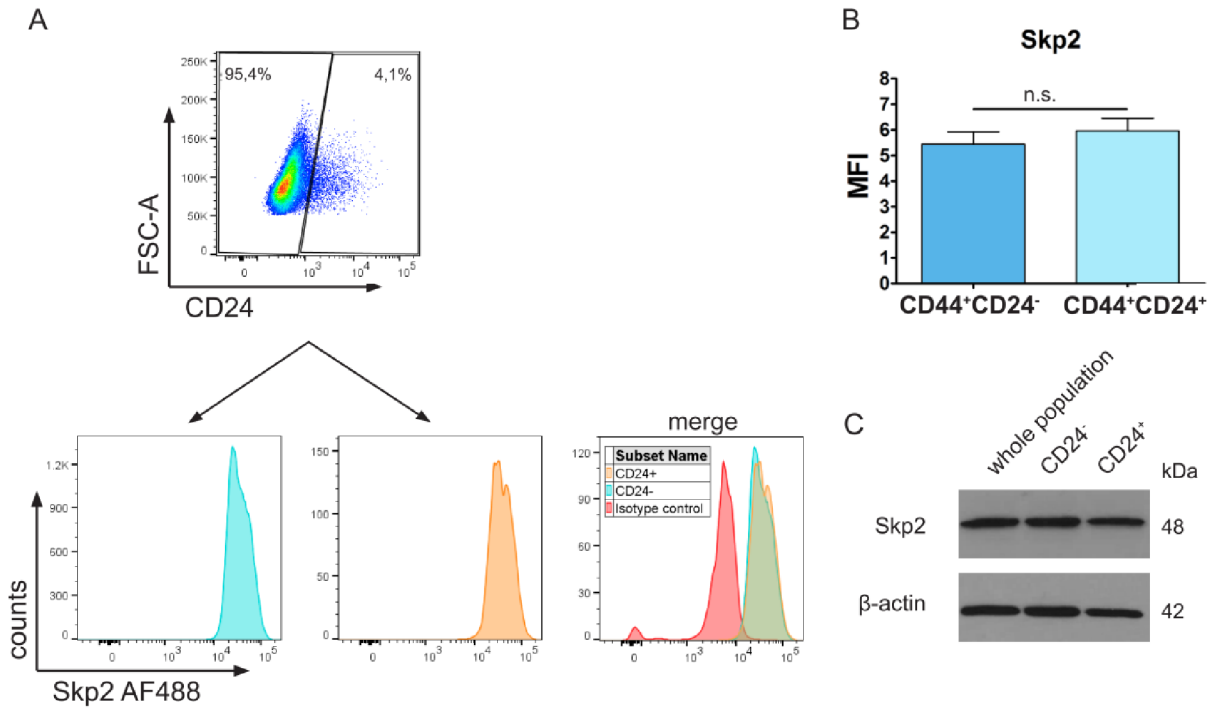

Figure 4.19 Skp2 protein level is equal in $CD24^-$ and $CD24^+$ cells. (A) The expression of Skp2 was analysed in $CD24^-$ (green histogram) and $CD24^+$ (orange histogram) subpopulations of DU 145 cells by flow cytometry. Graphs are in logarithmic scale. Histogram of Skp2 expression in $CD24^-$ and $CD24^+$ cells was merged with histogram from isotype control (red). Graphs are in logarithmic scale. (B) Quantification of results shown in (A). Data is presented as the mean ± SD of MFI for Skp2 that was calculated as a ratio of a fluorescent intensity signal from samples stained with specific antibody and isotype control. Representative images are from two independent experiments. (C) Western blot analysis of Skp2 protein level in $CD24^-$ and $CD24^+$ subpopulations in DU 145 cells. β-actin was used as a loading control.

4.1.5.3. CLONOGENIC CAPACITY OF THE CD24$^-$ SINGLE CELLS IS DECREASED AFTER INHIBITION OF NEDDYLATION

To assess whether pharmacological inhibition of SCF^{Skp2} affects the self-renewal of the cells, the ability of single cells to grow and form colonies in 2D culture was examined. CD44$^+$CD24$^-$ and CD44$^+$CD24$^+$ single cells were sorted into wells containing complete growth medium with vehicle (DMSO) or MLN-4924 inhibitor. After three weeks of growth, the colonies were analysed. We observed a comparable clonogenic capacity of the CD44$^+$CD24$^-$ and CD44$^+$CD24$^+$ in control medium, however, the clonogenic capacity of the cells with CSC-like phenotype CD44$^+$CD24$^-$ was significantly decreased when the cells were cultured in the presence of MLN-4924 inhibitor (Figure 4.20).

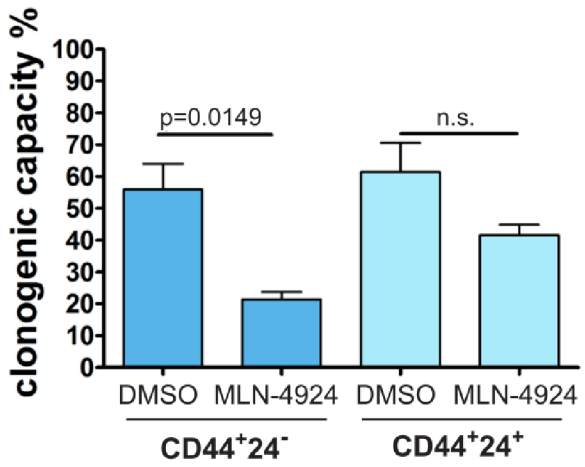

Figure 4.20 Clonogenic capacity of the CD44$^+$CD24$^-$ single cells is decreased after inhibition of neddylation. DU 145 single cells with CD44$^+$CD24$^-$ and CD44$^+$CD24$^+$ phenotype were sorted into a medium containing DMSO (vehicle) or 0.04 µM MLN-4924. After three weeks of cultivation, the colonies were counted. Results are from three independent repetitions. Bars represent the mean ± SD of the clonogenic capacity.

We further assessed the ability of the cells to grow in anchorage-independent conditions and form spheroids from single cells after MLN-4924 treatment. We observed a trend of decreased number of spheroids and significant decrease in size of the spheroids after MLN-4924 treatment in cells with both CD44$^+$CD24$^-$ and CD44$^+$CD24$^+$ phenotype. Thus, contrarily to short-term treatment with the MLN-4924, the long-term treatment with low concentration of the inhibitor resulted in robust inhibition of clonogenic ability of the cells with the CSCs phenotype cultivated in 2D conditions. In 3D conditions, the number and size of the spheroids was decreased in cells with both CD44$^+$CD24$^-$ and CD44$^+$CD24$^+$ phenotype.

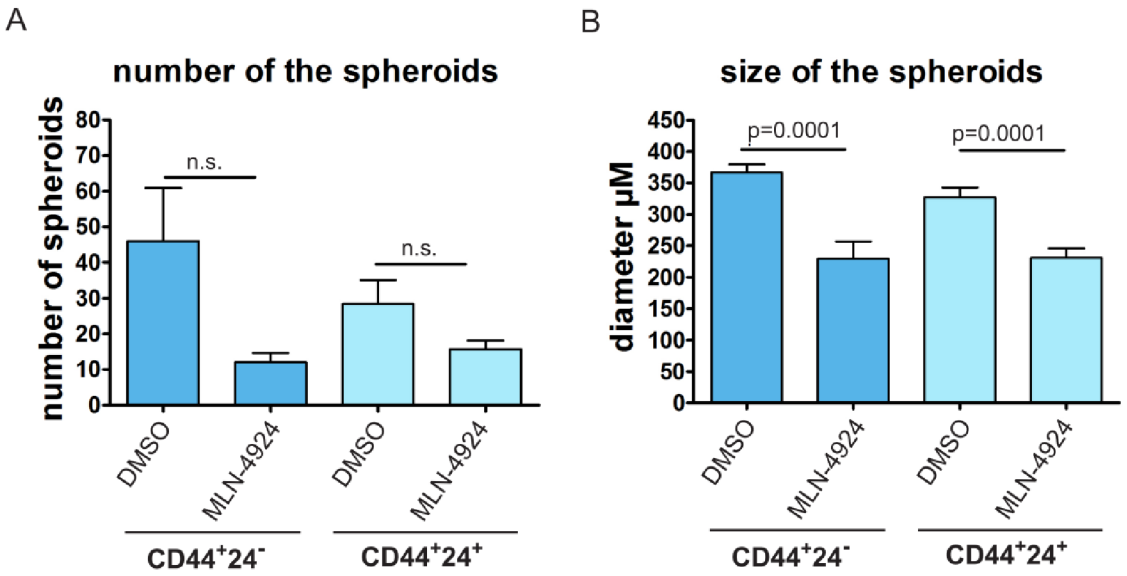

Figure 4.21 The size of the spheres is decreased after MLN-4924 treatment. (A) DU 145 single cells with $CD44^{+}CD24^{-}$ and $CD44^{+}CD24^{+}$ phenotype were sorted and seeded into semisolid medium. The next day, cells were treated with DMSO (vehicle) or 0.11 µM MLN-4924. After three weeks of cultivation, the spheroids were stained with MTT and counted using ImageJ software. Results are from three independent repetitions. Data is presented as the mean ± SD of the number of spheroids per well. Results are from three independent repetitions. (B) The size of the spheroids was measured using ImageJ software. Data is shown as the mean ± SD of the diameter of the spheroids. Results are from three independent repetitions.

4.2. ESTABLISHMENT OF A TOOL FOR ANALYSIS OF CELLULAR RESPONSE TO EXPERIMENTAL DRUG TREATMENT IN HETEROGENEOUS SAMPLES (IN CSC-LIKE CELLS)

Multicolour flow cytometry is an advanced methodological approach that can provide detailed information about the phenotype of the cells at the single-cell level, and elucidate the functions of identified cell populations through analysis of a variety of parameters. Nevertheless, design and optimization challenges remain in multiparametric flow cytometry protocols to detect markers present in various cellular compartments such as surface, cytoplasm and/or nucleus. For these protocols, it is critical to not only acquire good compensation control data, but also to consider the selection of appropriate markers and probes that are technically and biologically compatible with the staining procedure. Further, the fixation and permeabilisation agents need to be gentle to the labelled surface markers, and simultaneously sufficient to provide access to intracellular antigens (285).

4.2.1. PROTOCOL WORKFLOW AND OPTIMIZATION

A comprehensive description of the cellular response to a drug treatment is important to better understand the mechanisms of action of anticancer drugs. In this respect, flow cytometry is acknowledged as an irreplaceable methodology, not only in experimental biology but also in clinical and diagnostic applications. The advantage of flow cytometry over many other methods is the capability to perform multiparametric analysis at the single-cell level in a single tube/assay. Patient tumour samples as well as *in vitro* cultured cells are heterogeneous in terms of surface markers expression (286). Moreover, small subpopulations such as CSCs, defined by expression of distinct surface markers, can be identified within the heterogeneous samples.

Therefore, we introduced a multiparametric protocol for the assessment of complex cellular responses to experimental treatments, with the potential of distinguishing the response of the cells from distinct subpopulations in the heterogeneous samples. We established an assay for simultaneous detection of fluorescence parameters including surface markers for immunophenotyping, proliferation based on the cell cycle and measurement of DNA synthesis, DNA damage, and cell death determination using viability and apoptosis markers. Using various cell lines (mouse and human, suspension and adherent) and experimental treatments, the feasibility and robustness of the protocol was demonstrated. An overview of the assay workflow is depicted in Figure 4.22.

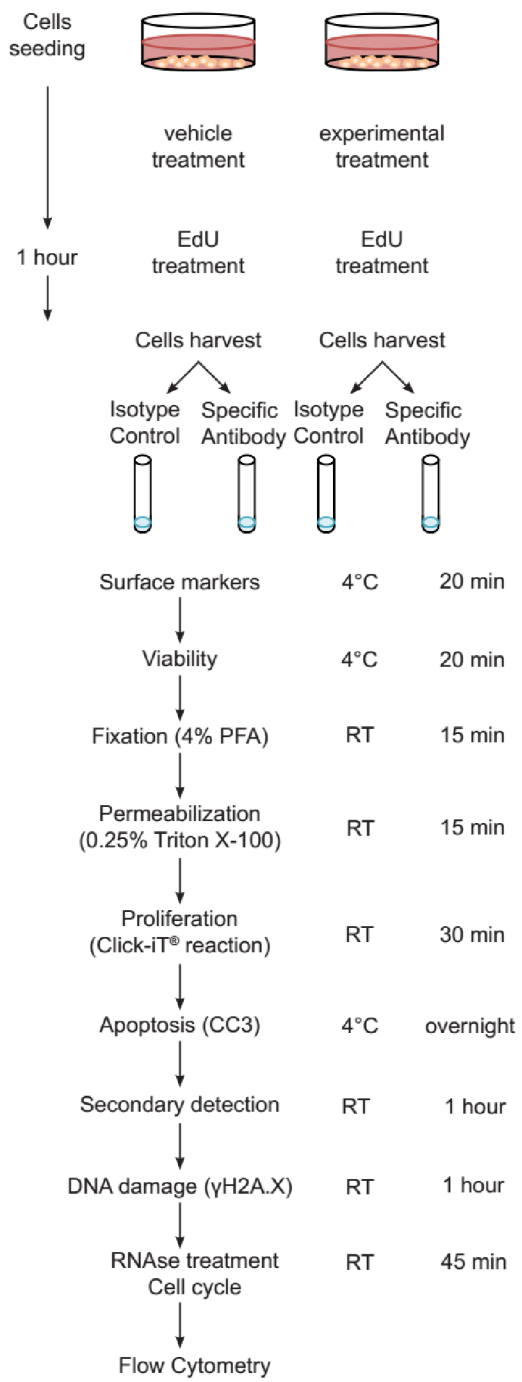

Figure 4.22 Scheme of experimental design and procedure. Cells were seeded and treated with experimental drugs as described in the Material and Methods. Before harvesting, all cells were treated with EdU. Harvested cells were split and stained with isotype controls or specific antibodies detecting surface markers, followed by viability stain. Next, cells were fixed, permeabilised, and the Click-iT® reaction was performed. Subsequently, cells were stained with cleaved caspase-3 (CC3) antibody, to detect apoptosis and γH2A.X antibody for the detection of DNA damage. Last, cells were stained with DNA-binding dye PO-PRO-1 with RNAse and analysed by flow cytometry. Figure from (281).

4.2.1.1. SURFACE MARKER SELECTION

Multiple optimization steps were performed before the above described final workflow and protocol was reached. The initial step in our design was the selection of fluorescently labelled antibodies for surface marker detection that are compatible with the subsequent azide-alkyne coupling (Click-iT® EdU) reaction. During our optimization procedure, we realized that the performance of Click-iT® EdU compatible antibody conjugates (e.g., allophycocyanin [APC]) might be significantly affected upon permeabilisation followed by the Click-iT® EdU reaction. For example, when we detected the surface marker Prominin-1 in cE2 cells using APC-labeled anti-Prominin-1 antibody, a visible drop in both the number of positive cells and MFI after the permeabilisation and Click-iT® EdU reaction steps was observed (Figure 4.23 A-B).

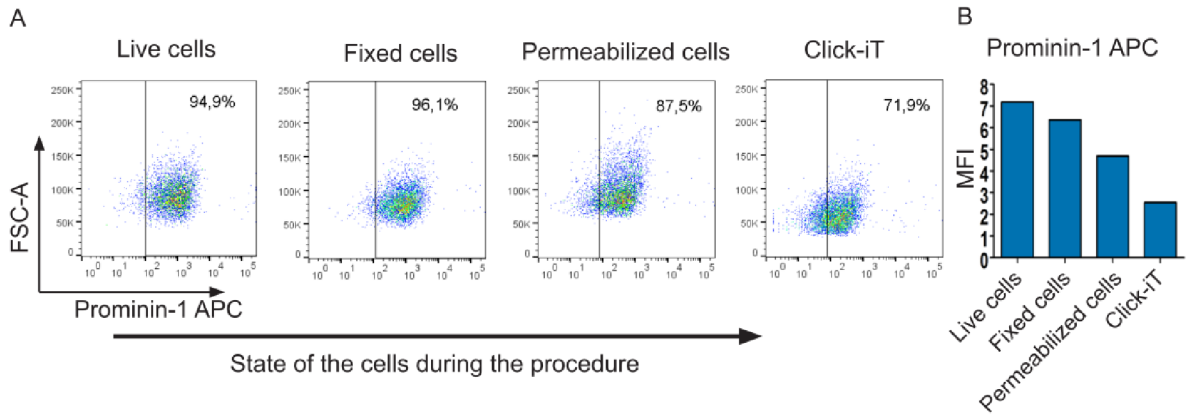

Figure 4.23 Stability of surface marker Prominin-1 in particular steps during the procedure decreases. (A) The signal stability of the Prominin-1 APC antibody during the procedure was analysed by flow cytometry. Graphs are in logarithmic scale. (B) The decrease of Prominin-1 APC signal in cE2 cells during the procedure was confirmed by MFI that was calculated as a ratio of a fluorescent intensity signal from samples stained with specific antibody and isotype control. Figure adapted from (281).

4.2.1.2. OPTIMIZATION OF PERMEABILISATION

Effect of permeabilisation on surface markers detection

Fixation and permeabilisation are crucial steps during sample processing that are necessary for successful detection of intracellular markers (287, 288). Here, we tested several permeabilising agents, such as 0.25% Triton X-100, digitonin (300 µg/ml), and saponin-based reagents from two different commercial kits (Mouse

Pluripotent Stem Cell Transcription Factor Analysis Kit, BD 560585 and Click-iT® detection kit). In case of saponin permeabilisation, we followed the manufacturer's recommendation (dilution, incubation time). Because we aimed to analyse intracellular markers simultaneously with surface markers, we also examined how the tested agents affect the detection of a surface marker Trop-2 (10) in cE2 cells. Cells treated with all permeabilisation reagents exhibited 100% positivity for Trop-2, however, based on MFI, the most gentle permeabilisation reagent was 0.25% Triton X-100 (Figure 4.24).

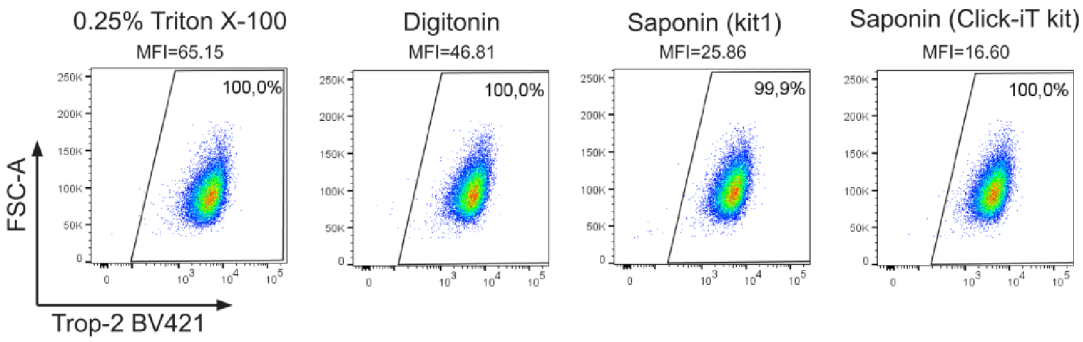

Figure 4.24 MFI but not the percentage of Trop-2 positive cells decreases after permeabilisation. The cE2 cells were stained with Trop-2 antibody and viability stain, fixed with 4% PFA and permeabilised with 0.25% Triton X-100, digitonin [300 µg/ml], or saponin-based reagents from the Mouse Pluripotent Stem Cell Transcription Factor Analysis Kit [BD Biosciences 560585; kit 1] or the Click-iT® detection kit [TFS 405231]).The positivity for Trop-2 was assessed by flow cytometry. The MFI was calculated as a ratio of a fluorescent intensity signal from samples stained with specific antibody and isotype control. Graphs are in logarithmic scale. Figure from (281).

Effect of permeabilisation on intracellular markers detection

Beside the surface markers, we compared detection of intracellular markers using similar permeabilisation agents. We observed that saponin was not sufficient for the detection of intracellular markers, such as cleaved caspase-3 (CC3) or γH2A.X (Figure 4.25 A-B). The best results in the detection of the intracellular markers γH2A.X and CC3 (i.e., a good separation of positive and negative populations) in cells treated with a high dose of the proteasome inhibitor MG-132 occurred when 0.25% Triton X-100 was used (Figure 4.25 A-B).

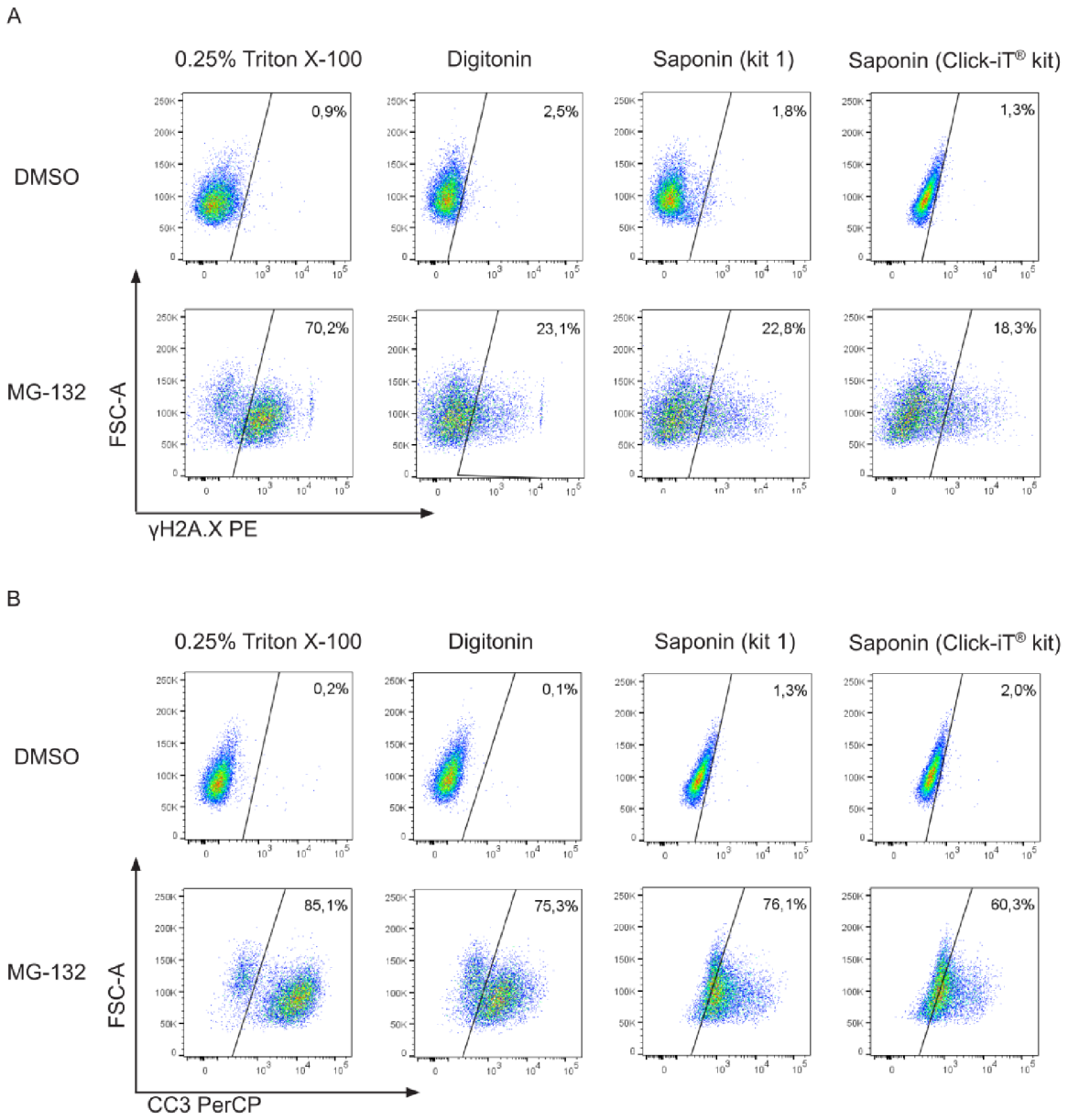

Figure 4.25 The best condition for detection of intracellular markers γH2A.X and CC3 provides permeabilisation with 0.25%Triton X-100. The cE2 cells were treated with DMSO (vehicle) or MG-132. Cells were stained with viability probe, fixed and permeabilised with indicated agents and stained with markers of DNA damage or apoptosis. (A) Detection of DNA damage by induction of γH2A.X was assessed by flow cytometry. Graphs are in a logarithmic scale (γH2A.X) or in a linear scale (FSC-A). (B) Detection of apoptosis in cE2 cells via induction of CC3 was assessed by flow cytometry. Graphs are in a logarithmic scale (CC3) or in a linear scale (FSC-A).

4.2.1.3. INTRACELLULAR MARKERS SELECTION

Establishing the optimal permeabilisation conditions was a prerequisite for successful implementation of detection of intracellular markers of apoptosis induction: cleaved PARP (C.PARP), a substrate of executive caspases, and cleaved caspase-3 (CC3), both of which are commonly used as indicators of ongoing apoptosis (289, 290). Positivity for both markers was detected in cells treated with MG-132; however, CC3 exhibited better separation of positive and negative populations (Figure 4.26). Therefore, we decided to use CC3 as a marker of ongoing apoptosis in the protocol.

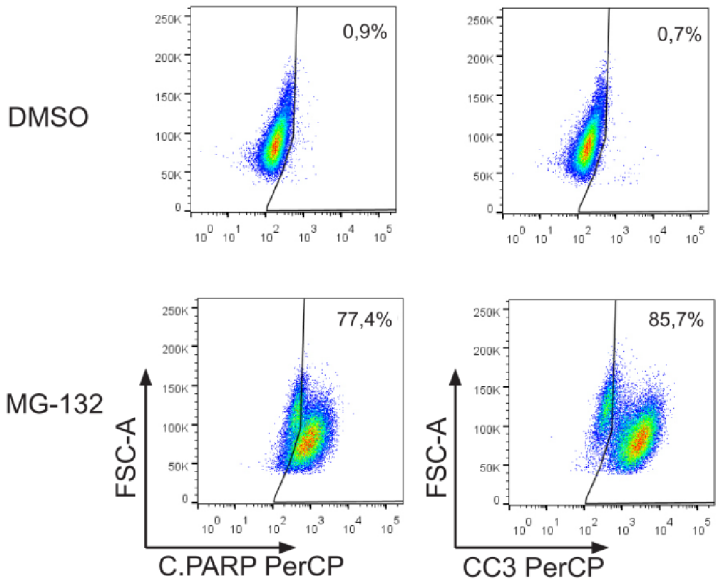

Figure 4.26 Cleaved caspase-3 antibody provides better separation of positive and negative cells than cleaved PARP. cE2 cells were treated with DMSO (vehicle) or MG-132. Cells were fixed in 4% PFA and permeabilised by 0.25% Triton X-100. Next, the cells were stained with primary antibody to cleaved PARP or CC3 and analysed by flow cytometry. Graphs are in a logarithmic scale (C-PARP PerCP and CC3 PerCP) and in a linear scale (FSC-A). Figure from (281).

4.2.1.4. OPTIMIZATION OF DNA STAIN

One of the most challenging steps in the assay optimization was to find an appropriate DNA stain to use in combination with other selected parameters. Nowadays, a broad spectrum of DNA-binding fluorescent dyes is available. Commonly used dyes intercalate into the DNA (ethidium bromide, propidium iodide, 7AAD) or bind to the minor groove of the DNA. The latter group includes 4',6-

diamidino-2-phenylindole (DAPI), which binds preferentially to the AT site of DNA (291), and Hoechst, which can be used to visualize DNA content in live cells. For this application, we found that the fluorescent signal of some DNA dyes is too strong, with high background, and impossible to compensate (e.g., FxCycle Far Red and APC/Cy7; data not shown). Next, we observed that DAPI, which is routinely used in single-parameter analysis of the cell cycle, was not suitable for our multiparametric assay due to its broad emission spectrum. Although the emission maximum of DAPI is around 450 nm, we found it impossible to use in combination with fluorochromes with an emission maximum around 650 nm (both excited by 405 nm laser) due to the high spillover of DAPI (Figure 4.27 A). When we analysed cE2 cells that are fully positive for the Trop-2 surface marker (Figure 4.27 B) in combination with DAPI, it increased background in isotype control (ISO) and the cells appeared as Trop-2 negative (gate set based on ISO with/without DAPI) (Figure 4.27 A). Therefore, we tested the dye PO-PRO-1, which is a bright and photostable cyanine monomer that intercalates nonspecifically into DNA (292). Implementation of PO-PRO-1 into our protocol was suitable for cell cycle analysis in a multiparametric assay (Figure 4.27 C).

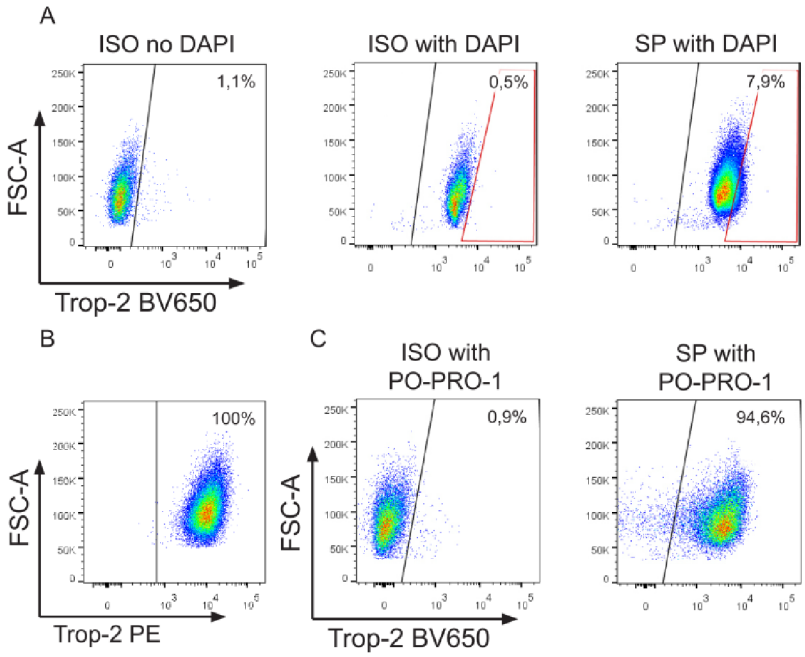

Figure 4.27 DAPI is incompatible with the BV650 fluorochrome. (A) Cells were stained with Trop-2 antibody (SP) or isotype control (ISO), fixed with 4% PFA, permeabilised with 0.25% Triton X-100, and stained with DAPI. Indication of high spillover of DAPI into BV650 fluorochrome. (B) Uniform Trop-2 expression in cE2

cells detected by flow cytometry. (C) Cells were stained with Trop-2 antibody (SP) or isotype control (ISO), fixed with 4% PFA, permeabilised with 0.25% Triton-X, and stained with PO-PRO-1. Graphs are in logarithmic scale (Trop-2), in case of FSC-A in linear scale.

4.2.2. APPLICATION OF THE PROTOCOL TO VARIOUS MODELS OF CANCER CELL LINES

When all the crucial steps were optimized, we aimed to demonstrate the ability of our assay to examine the complex cellular response to the experimental treatment in cancer cell lines of various origin. We treated the cells with selected concentrations of well-established inducers of cell cycle arrest or apoptosis MLN-4924, MG-132, or TRAIL, and applied the complete staining procedure (Figure 4.22). Changes in cellular viability, expression of surface markers, cell cycle progression and markers of apoptosis induction are depicted in Figure 4.28 and described in Table 4.1.

Altogether, most effects were in accordance with expected outcomes of drug treatment, but our analysis revealed several interesting phenomena. An apparent lack of effect of TRAIL on cellular viability probably results from the sustained integrity of the cellular membrane in the early phases of apoptosis in DU 145 and HCT 116 cells (Figure 4.28 A and D, row a) (293). In terms of surface marker expression, we detected an effect of particular treatments on expression of surface markers in all studied cell lines (Figure 4.28 A-D, row b; and Table 4.1). Cell cycle analysis based on the DNA amount stained with probe PO-PRO-1 indicated changes in the cell cycle progression; however, the cell cycle profile showed relatively high coefficient of variation. Alternatively, cell cycle phases can be visualized and determined accurately in a dot plot showing a combination of DNA stain versus DNA synthesis (Click-iT® EdU). Our analysis revealed different responses of selected cell lines to the MLN-4924 inhibitor, as depicted in Figures 4.28, row c, and Table 4.1. Proliferation was abolished in cE2 and SU-DHL-4 treated with MG-132 (Figure 4.28, row c, and summarized in Table 4.1). Interestingly, proliferation was not affected in DU 145 and

HCT 116 cells following TRAIL treatment, and these cells exhibited an unchanged cell cycle profile as seen in control (Figure 4.28 A and D, row c).

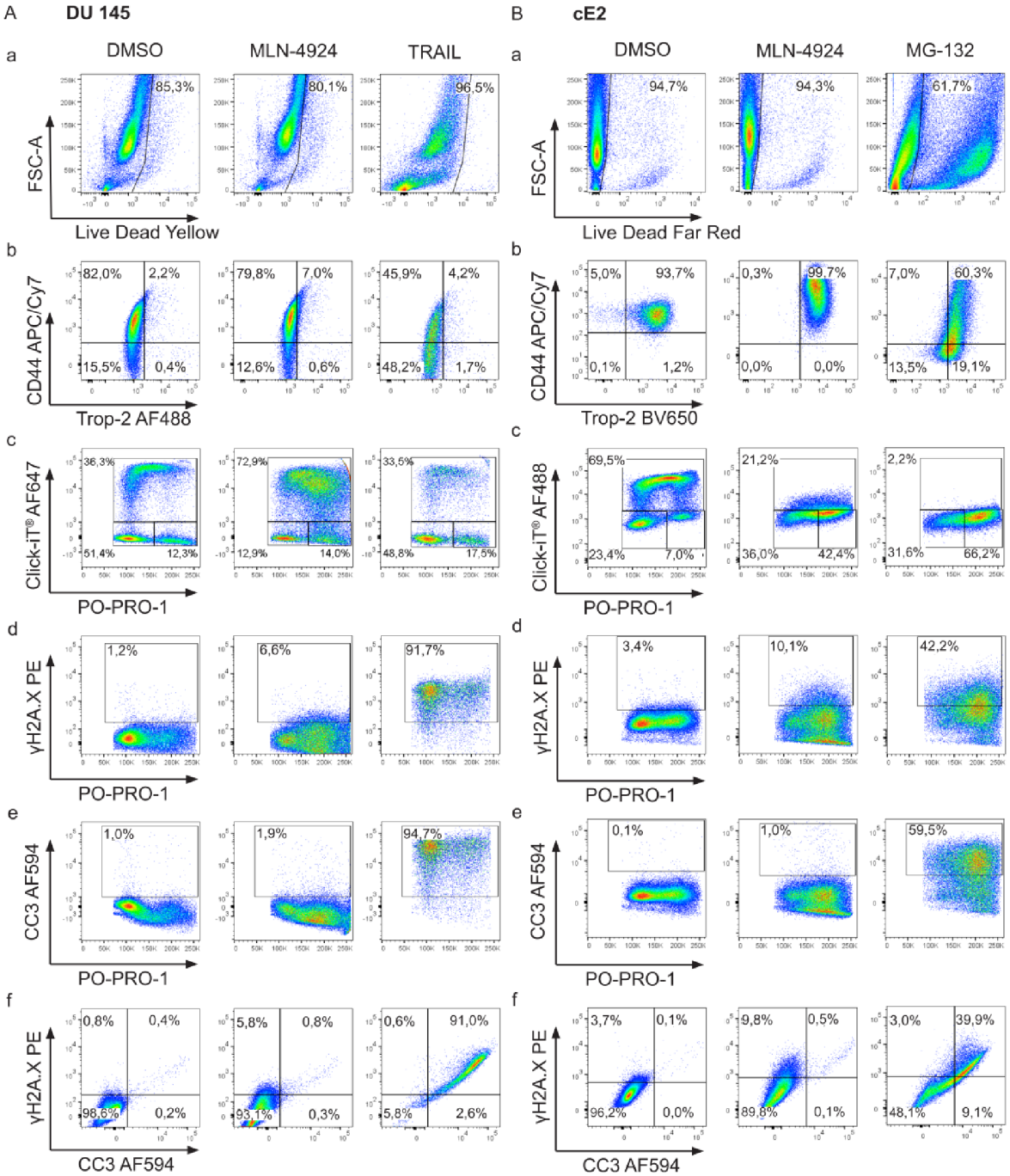

Figure 4.28 The established assay provides complex analysis of cellular response to MLN-4924, TRAIL or MG-132 treatment. DU-145, cE2, SU-DHL-4, and HCT 116 cells we treated with DMSO (vehicle), MLN-4924, and MG-132 or TRAIL. Following parameters were examined by flow cytometry: the viability of the cells (row a in A-D), surface markers expression (row b in A-D), proliferation defined in dot plots with PO-PRO-1/Click-iT® EdU (row c in A-D), DNA damage denoted by

γH2A.X positivity (row d, f in A-D) and apoptosis determined by CC3 (row e, f). Graphs are in logarithmic scale, FSC-A is in linear scale. Figure from (281).

Figure 4.28 (Continued)

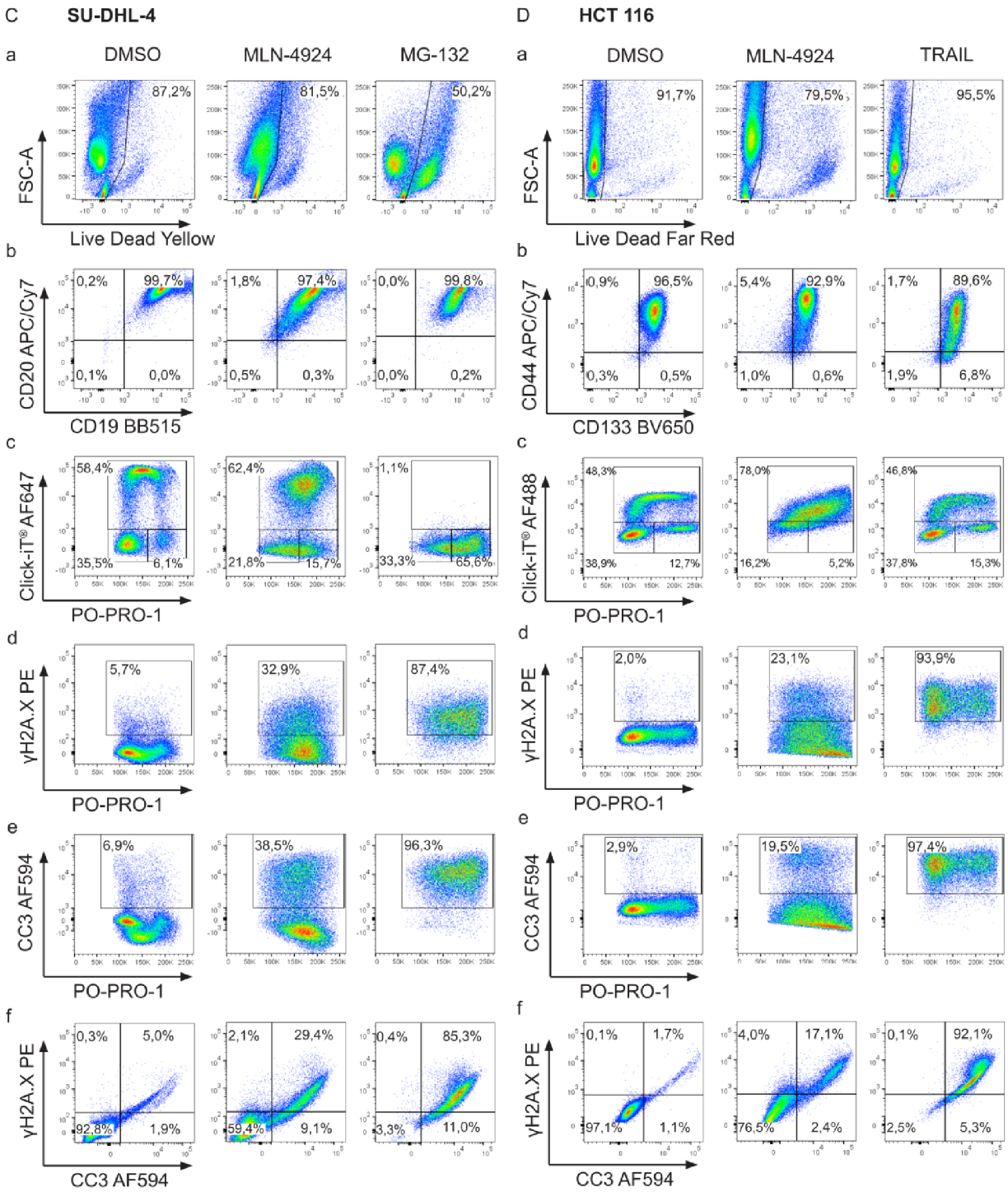

Table 4.1 Summarised biological effects of experimental treatments on multiple cellular parameters in different cell lines shown in Figure 4.28.

	DU 145	cE2	SU-DHL-4	HCT 116
Cell viability				
Figure	4.28 A/a	4.28 B/a	4.28 C/a	4.28 D/a
MLN-2924	Decreased	Decreased	Decreased	Decreased
MG-132		Decreased	Decreased	
TRAIL	Unaffected			Unaffected
Surface markers				
Figure	4.28 A/b	4.28 B/b	4.28 C/b	4.28 D/b
Markers	CD44 + Trop-2	CD44 + Trop-2	CD19 + CD20	CD44 + CD133
MLN-2924	Unaffected	Unaffected	Unaffected	Unaffected
MG-132		Decreased	Unaffected	
TRAIL	Decreased			Unaffected
Cell cycle				
Figure	4.28 A/c	4.28 B/c	4.28 C/c	4.28 D/c
MLN-2924	S phase accumulation	G2 phase arrest	Shift to G2 phase	S phase accumulation
MG-132		G2 phase arrest	G2 phase arrest	
TRAIL	Unaffected			Unaffected
DNA damage				
Figure	4.28 A/d, f	4.28 B/d, f	4.28 C/d, f	4.28 D/d, f
MLN-2924	Induced	Induced	Induced	Induced
MG-132		Induced	Induced	
TRAIL	Induced			Induced
Apoptosis				
Figure	4.28 A/e, f	4.28 B/e, f	4.28 C/e, f	4.28 D/e, f
MLN-2924	Unaffected	Unaffected	Induced	Induced
MG-132		Induced	Induced	
TRAIL	Induced			Induced

Our analysis confirmed the ability of MLN-4924 to induce DNA damage in all studied cell lines (Figure 4.28 A-D, rows d, f and Table 4.1), and to induce apoptosis in SU-DHL-4 and HCT 116 cells (Figure 4.28 C-D, rows e, f). Both induction of DNA damage and apoptosis was observed in samples treated with MG-132 or TRAIL (Figure 4.28, rows d-f, Table 4.1) and confirmed also on protein level by western blot (Figure 4.29). These results demonstrated the robustness of our assay and its capability to describe a broad spectrum of cell responses using a complex set of different parameters at the single-cell level.

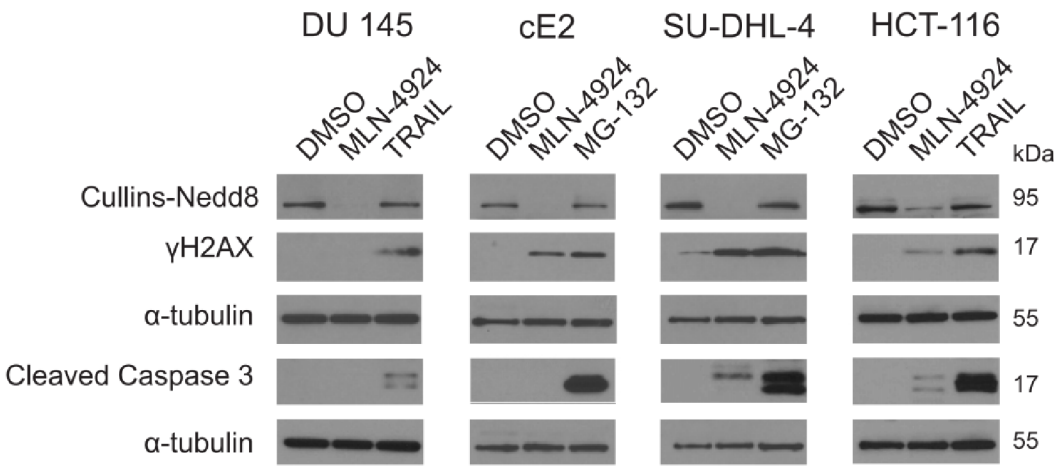

Figure 4.29 DNA damage and apoptosis was induced in cells treated with MLN-4924, TRAIL or MG-132, respectively. estern blot analysis of samples paired to those analysed by flow cytometry. The activity of the MLN-4924 inhibitor was confirmed by abrogated NEDD8 binding to Cullins. Induction of DNA damage was confirmed by detection of γH2A.X, apoptosis was detected by CC3. α-tubulin was used as a loading control. Figure adapted from (281).

4.2.3. ANALYSIS OF RESPONSE TO EXPERIMENTAL TREATMENT IN A HETEROGENEOUS SAMPLE

To demonstrate the applicability of our protocol in the complex analysis of heterogeneous samples, we took advantage of the DU 145 cell line, where we observed a consistent presence of a subpopulation of cells expressing Trop-2 (Figure 4.28 A, row b). Therefore, we employed the established protocol to investigate the response of cells that differ in Trop-2 expression status to MLN-4924 or TRAIL treatment. We observed that the expression of Trop-2 itself did not change following MLN-4924 or TRAIL treatment (Figure 4.30 A, 4.31 A and Table 4.2), but we noted differences in cell cycle progression in Trop-2 positive and negative subpopulations (Figure 4.30 B, 4.31 B and Table 4.2). The induction of DNA damage was proportionate in Trop-2$^-$ and Trop-2$^+$ cells following TRAIL and MLN-4924 treatment (Figure 4.30 C and E, 4.31 C and Table 4.2). Induction of apoptosis was significantly increased in Trop-2$^-$ cells compared to Trop-2$^+$ cells following TRAIL treatment (Figure 4.30 D-E, 4.31 D and Table 4.2). Thus, these data demonstrate that our approach is useful in complex analysis of cellular responses in a heterogeneous

sample, and has the potential to reveal differences in the responses of precisely defined phenotypic subpopulations.

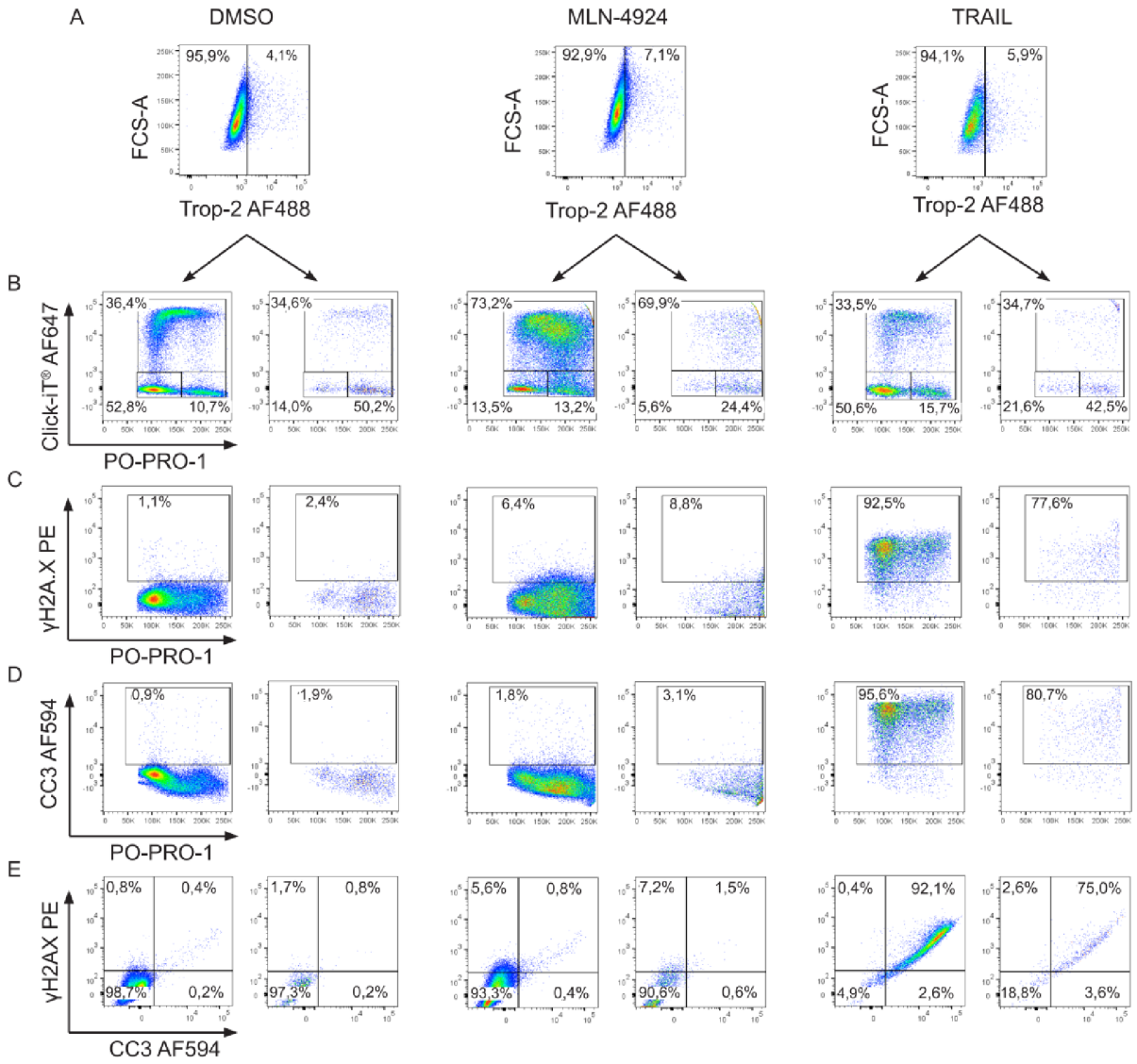

Figure 4.30 Trop-2^{+} cells are less sensitive to apoptosis induction compared to Trop-2^{-} cells. Response to treatment was analysed separately in the Trop-2^{-} andTrop-2^{+} subpopulations in the DU 145 cell line (A). Differences in proliferation (B), DNA damage (C, E), and induction of apoptosis (D, E) were examined. Gates shown in Figure 4.28A were applied to Trop-2 subpopulations of DU 145 cells in Figure 4.30. Figure from (281).

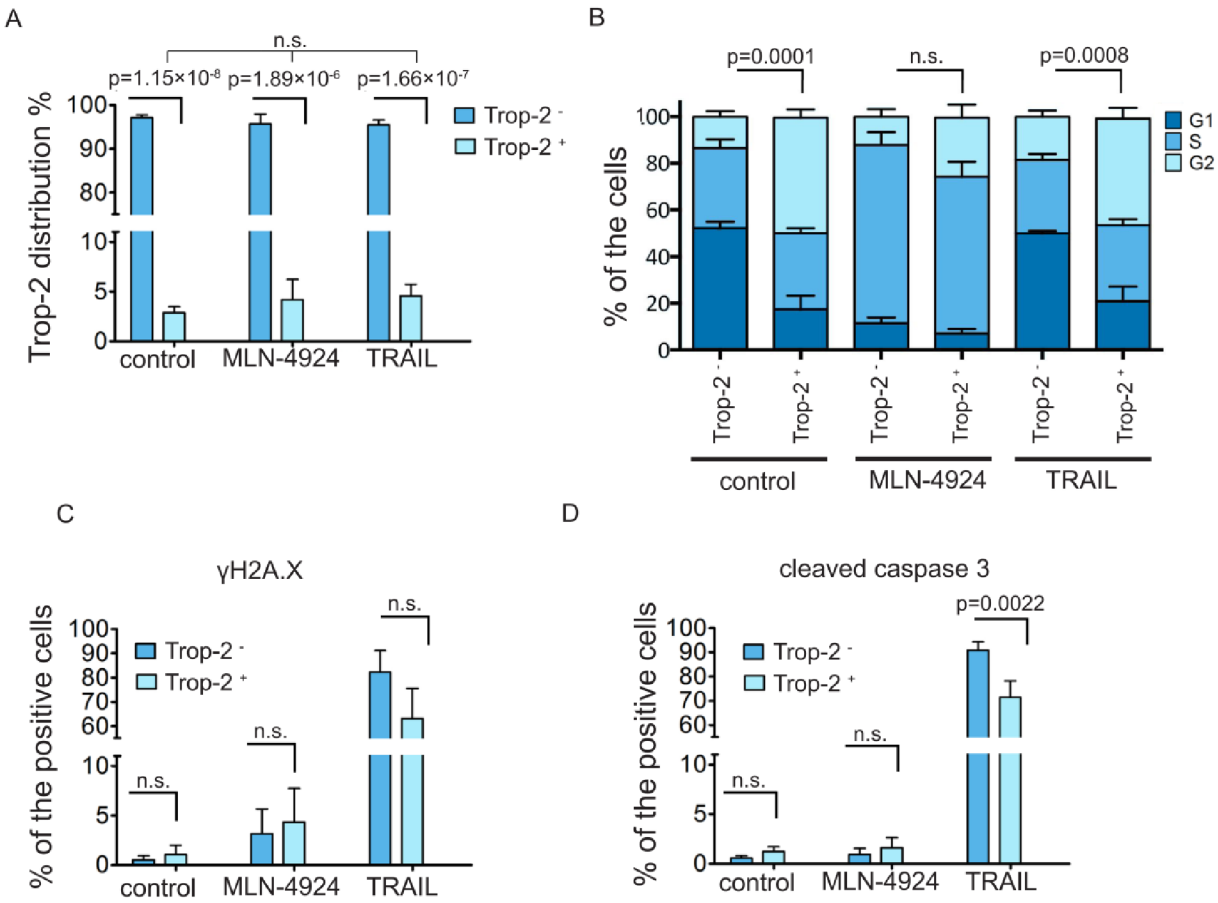

Figure 4.31 Trop-2$^-$ and Trop-2$^+$ subpopulations in DU 145 respond differently to TRAIL treatment. (A) Quantification of Trop-2 distribution in DU 145 cells treated with DMSO (vehicle), MLN-4924 and TRAIL shown in Figure 4.30 A. Data is presented as the mean ± SD of the percentage of positive cells for the selected marker. Representative images are from three independent experiments. (B) Cell cycle analysis of Trop-2$^-$ and Trop-2$^+$ subpopulations after indicated treatments shown in Figure 4.30 B. (C) Quantification of DNA damage (shown in Figure 4.30 C) after MLN-4924 and TRAIL treatment. Data is presented as the mean ± SD of the percentage of positive cells for the selected marker. Representative images are from three independent experiments. (D) Quantification of apoptosis induction (shown in Figure 4.30 D) after MLN-4924 and TRAIL treatment. Data is presented as the mean ± SD of the percentage of positive cells for the selected marker. Representative images are from three independent experiments. Figure adapted from (281).

Table 4.2 Summarised biological effects of experimental treatments on defined cellular subpopulations shown in Figure 4.30 and 4.31.

	DU 145 Trop-2$^-$	DU 145 Trop-2$^+$
Trop-2 expression		
Figure	4.30 A, 4.31 A	
MLN-2924	Unaffected	Unaffected
TRAIL	Unaffected	Unaffected
Cell cycle		
Figure	4.30 B, 4.31 B	
Untreated		G2 accumulation
MLN-2924		Increased G2, decreased S
TRAIL		Increased G2, unchanged S
DNA damage		
Figure	4.30 C, E; 4.31C	
MLN-2924	Proportionate	Proportionate
TRAIL	Proportionate	Proportionate
Apoptosis		
Figure	4.30 D, E; 4.31D	
MLN-2924	Not induced	Not induced
TRAIL	Increased	Decreased

5. DISCUSSION

The Role of Skp2 in Prostate Cancer Stem-like Cells

In our work, we have focused on describing the role of Skp2 in prostate cancer stem-like cells. Skp2 has been described as an oncogene and its overexpression was detected in various cancers including prostate cancer (216). We showed that Skp2 expression was increased in cancerous prostate tissue compared to benign prostate tissue. Specifically in tumours with a high Gleason score (≥ 7), nuclear but not cytoplasmic Skp2 expression was increased. As a crucial step of prostate cancer progression and metastasis, altered expression of EMT markers was described, indicating the ongoing process of EMT (112, 113). In our study, we observed increased incidence of low expression levels of E-cadherin and high levels of vimentin in the cohort of patients with high Gleason score (≥ 7), suggesting the ongoing EMT of prostate cancer cells. To our knowledge, we demonstrate for the first time the link between high Skp2 expression and mesenchymal phenotype in patients with advanced prostate cancer.

The process of EMT contributes to cell state plasticity and intra-tumoural heterogeneity (294). In our laboratory, we observed heterogeneity of metastatic DU 145 cells based on expression of Trop-2, a surface molecule from EpCAM family (295). Thus, we established epithelial and mesenchymal sublines from the parental cell line based on the Trop-2 positivity or negativity, as described previously (71). We showed that Skp2 expression was increased in the mesenchymal DU 145 subline. Moreover, this phenomenon was confirmed in two other mesenchymal human and mouse prostate cancer cell lines, where the EMT status resulted from resistance to docetaxel or castration, respectively. Accordingly, the acquisition of the mesenchymal phenotype was associated with increased Skp2 expression in paclitaxel-resistant breast cancer cells (296) and TGF-β1-induced EMT in melanoma cells (297). Importantly, Ruan *et al*. revealed that Skp2 regulates castration-resistant prostate cancer through

Twist-mediated oncogenic functions including EMT and acquisitions of CSC-like properties (262).

Since EMT was confirmed to be associated with cancer stem cells, we questioned whether the mesenchymal DU 145 subline exhibits CSC-like properties. We have successfully detected CSC-like properties such as decreased expression levels of CD24, increased ability to form spheroids, and high ALDH1 activity in mesenchymal DU 145 cells. These results are consistent with the acquisition of the $CD44^{+}CD24^{-}$ CSC-like phenotype, which correlates with the mesenchymal state of the cancer cells. The $CD44^{+}CD24^{-}$ phenotype has been associated with CSCs and the mesenchymal phenotype in several cancers, including breast cancer (298, 299), ovarian cancer (300), and oral squamous carcinoma (301). Similarly, prostate cancer cells with the $CD44^{+}CD24^{-}$ phenotype have been described as mesenchymal (302). These results are in agreement with the work of Cremers *et al.* who showed that CD24 was not required for tumour initiation and growth in murine models of breast cancer and prostate cancer (303). The mesenchymal state resulting from docetaxel resistance in DU 145 and PC3 cells was also linked to the acquisition of the $CD44^{+}CD24^{-}$ phenotype (122, 123). Further, it was shown that the overexpression of the mesenchymal-related genes *ZEB1* and *VIM* correlated with shorter radiologic progression, whereas low expression levels of CD24 correlated with shorter biochemical recurrence-free survival of patients with prostate cancer (123).

As our previous results showed that high Skp2 level correlates with the mesenchymal state of cancer cells and acquisition of CSC-like properties, we next aimed to downregulate Skp2 to ascertain whether it would affect CSC-like properties of cancer cells. Knock-down of *SKP2* significantly reduced the ability of these cells to form spheroids *in vitro* and decreased tumourigenic potential *in vivo*. Our findings are in agreement with the work of Lu *et al.* who found that Skp2 deficiency led to the suppression of prostate tumourigenesis. These authors showed that Skp2 was involved in tumourigenesis via the repression of H3K4-specific demethylase JARID1B (304). Another study showed that Skp2 deficiency blocked tumourigenesis in the pRb/p53 double-deficient prostate tissue, suggesting that Skp2 was a promising target for drug

treatment in pRb/p53-deficient tumours (305). In addition to the decreased tumourigenicity of *SKP2* KD cells, we observed the upregulation of CD24 expression and the decreased activity of ALDH1. These findings are in line with those of Zhao *et al.*, where Skp2 downregulation or its pharmacological inhibition decreased the activity of ALDH1 (305).

Since we observed that the CSC-like phenotype $CD44^{+}CD24^{-}$ correlated with mesenchymal phenotype of prostate cancer cells and their increased tumourigenicity, we aimed to validate the CD44 and CD24 expression in clinical samples. An analysis of biochemical recurrence-free survival revealed that high expression levels of CD24 and CD44 were associated with a better prognosis for patients. These findings are in line with the work of Marin-Aguilera *et al.* who showed that low mRNA levels of CD24 correlated with shorter biochemical recurrence-free survival of patients with prostate cancer (123). A decreased number of CD24-positive cells was also associated with the mesenchymal phenotype and DU 145 cell chemoresistance (123, 306). Furthermore, prostate cancer cells with low CD24 expression levels displayed high tumourigenic potential (307), which is in line with our findings. In conclusion, our results suggest that CSCs in prostate cancer can be targeted via modulation of Skp2.

As we showed that down-regulation of Skp2 expression affects CSC-like properties *in vitro*, we questioned whether pharmacological targeting of the neddylation pathway, that is crucial for Skp2 activity, would exhibit comparable effects. For this purpose, we used MLN-4924 inhibitor, that blocks SCF^{Skp2} assembly, and is currently in the third phase of clinical trials (reviewed in chapter.

Interestingly, MLN-4924 was shown to decrease the viability selectively in leukemic cells but not in the normal blood cells (248). The decreased viability was shown also *in vitro* in lymphoma cells (241, 244) and in prostate cancer cells (243). Even though we used similar concentrations of the MLN-4924 inhibitor and the final post treatment time point (96 hours) as Wang *et al.*, (243) , we did not observe a drop of the viability under 50 % in our experimental set up. This discrepancy could be explained by different cell seeding density, as higher seeding density in our

experimental setup may enhance cell survival after MLN-4924 treatment. Moreover, different timing of experimental treatment may be responsible for the outcome. Rather than reduction of cellular viability, we noted decreased cell counts caused by the cell cycle arrest, resulting from accumulation of the cell cycle inhibitors. However, we did not observe accumulation of another Skp2 substrate, the replication licensing factor Cdt1 (200, 201), that would result in induction of re-replication. The Cdt1 accumulation after MLN-4924 was previously shown in prostate cancer cell lines (243), colon, glioblastoma, lung cancer cells (242) or lymphoma cells (241). Yet, our preliminary flow cytometric data confirmed Cdt1 accumulation in HeLa FUCCI cells after treatment with MLN-4924 (data not shown), suggesting a cell type specific context of Cdt1 accumulation.

The pleiotropic effect caused by inhibition of neddylation has been described in many cancer cells (summarized in chapter 1.2.3.1.). In our model, we further observed induction of DNA damage and cell death in a time and concentration-dependent manner. Even though some works describe cleavage of caspases after MLN-4924, indicating ongoing apoptosis, we did not observe caspase-3 cleavage in prostate cancer cells, suggesting either that another mechanism of cell death is involved, or that the programmed cell death is caspase-3 independent (308).

Prostate CSCs contribute to the tumour heterogeneity and disease progression. Therefore, they represent a target of interest in cancer therapy (66, 67). Our data demonstrated that pharmacological inhibition of SCF^{Skp2} did not reduce $CD44^{+}CD24^{-}$ cells but resulted in a significant decrease of $CD44^{+}CD24^{+}$ cells after the treatment with MLN-4924 inhibitor. This effect was caused by induction of late apoptosis/necrosis in $CD24^{+}$ cells after the treatment. The preferential induction of late apoptosis/necrosis after MLN-4924 treatment has been recently described in lung adenocarcinoma cells (258) or oesophageal cancer cells (258, 309). Our findings showing the lower susceptibility of $CD44^{+}CD24^{-}$ cells to cell death are in line with data recently published by Jaworska and Szliszka, who observed increased apoptosis in $CD44^{+}CD24^{-}$ CSCs subpopulation in PC3 but not DU 145 cells after co-treatment of taxanes and TRAIL (93). Nevertheless, we were unable to confirm that the protein

level of Skp2 was a determining factor for the high sensitivity to the MLN-4924 treatment in the $CD24^+$ subpopulation. However, our preliminary data indicate an increase in G1 phase of the cell cycle of $CD24^-$ cells compared to $CD24^+$ cells, which could underlie the difference in sensitivity to the SCF^{Skp2} assembly inhibitor. Still, further studies that would explain this phenomenon are needed.

The self-renewal of CSC-like cells is experimentally addressed by the ability of a single cell to form a colony in 2D conditions or a spheroid in 3D conditions. The decreased clonogenic potential after MLN-4924 was documented in prostate cancer cells in 2D (243). In our work, we aimed to investigate the effect of this inhibitor on the clonogenic capacity in both 2D and 3D conditions with emphasis on CSC-like cells. Despite the higher susceptibility of the $CD24^+$ cells to apoptosis induction after short-time (48 hours) of MLN-4924 treatment, we observed that long term cultivation of sorted single cells in medium containing low concentration of MLN-4924 significantly decreased the clonogenic capacity of the cells with CSCs phenotype $CD44^+CD24^-$ in 2D condition. MLN-4924 decreased the size of all spheroids regardless of their CD24 expression. This data is in line with former work by Chan *et al*. who described decreased size of spheroids formed by prostate cancer cells after pharmacological inhibition of Skp2 by the compound #25 that targets Skp2-Skp1 interaction (261), which was further corroborated by Twist overexpression (262). Importantly, it has been shown that inhibition of SCF^{Skp2} with a compound #25 also resulted in restriction of tumour growth *in vivo* (261). Altogether, we observed that inhibition of SCF^{Skp2} affects cytokinetic parameters of prostate cancer cells and decreases the clonogenic potential of CSC-like cells.

In summary, we propose a new connection between Skp2, EMT and CSCs in prostate cancer. In our study, we used a model of androgen-independent metastatic DU 145 cells, representing an advanced stage of prostate cancer. We discovered that the mesenchymal phenotype of the cells was accompanied by increased Skp2 level and CSCs phenotype, which was reverted by Skp2 downregulation. Moreover, pharmacological inhibition of SCF^{Skp2} decreased the clonogenic capacity of the cells

cultivated in 2D and spheroids size in 3D conditions. Therefore, we suggest Skp2 as a promising target in prostate cancer stem cells.

Multiparametric assay for detection of cytokinetics of small subpopulations after experimental treatment

The tumour cells *in vivo* as well as established cell cultures *in vitro* are heterogeneous in terms of molecules expressed on their surface, which reflects their state and function. Therefore, detection of specific markers on the surface of the cells is used to capture small subpopulations, *e.g.* CSCs within the sample. In our work, we observed heterogeneity in DU 145 cells in terms of expression of CSC markers CD24 and Trop-2, and a different sensitivity of the defined subpopulations to experimental treatments. A complex analysis of the cell fate following the experimental treatment is important not only for understanding the treatment effects but also for identification of sensitive or resistant cell types with a specific phenotype. Compared to conventional methodological approaches in experimental work (*e.g.* PCR or western blotting), multiparametric flow cytometry provides deep insight in the cytokinetics of the defined subpopulations in heterogeneous samples. Although flow cytometry is an irreplaceable approach for multiparametric single-cell analyses, it is not frequently used for "single-tube" analysis of complex cellular response to the experimental therapy. This type of analysis can be very useful in case of limited amount of biological material, such as clinical samples or end-point *in vivo* studies. Major obstacle for simple multiplex detection of different biomarkers of cellular functions is the necessity to perform several optimizing steps and verifications. In this study, we aimed to employ full advantage of the multicolor flow cytometry to establish a protocol for complex analysis of cellular response together with the immunophenotype and functional characteristics of the treated cells.

The crucial step is the selection of fluorescently labelled antibodies for surface marker detection that are compatible with subsequent azide-alkyne coupling (Click-iT® EdU) reaction. Azide-alkyne coupling (click chemistry) has become a powerful

coupling method for chemoselective ligation (310). However, copper and reactive oxygen species-mediated damage to fluorescent proteins prevents the simultaneous detection of EdU with GFP or R-phycoerythrin (R-PE) fluorescence. Moreover, here we showed that fluorescent intensity of Click-iT® EdU compatible APC conjugate is affected upon permeabilisation followed by the Click-iT® EdU reaction. This limitation might be overcome in second-generation Click-iT® Plus EdU kits with "copper-safe" catalysis of the click reaction (311). With respect to the compatibility with the Click-iT® chemistry, the protocol allows high degree of customization by the end user. For instance, other antibodies for apoptosis detection (such as cPARP) can be suitable for different experimental models.

Detergents such as saponin, Triton X-100, and Tween-20 are widely used to permeabilise cells in flow cytometry (312). Saponin has been described as a favourable permeabilisation reagent for simultaneous detection of surface antibodies and proliferation in T cells with no alteration of membrane antigens. In addition, saponin has been described as a sensitive reagent for the detection of intranuclear antigens (313). Seminal study comparing different cellular fixation and permeabilisation techniques for intracellular stainings published by Krutzik and Nolen is not systematically dealing with permeabilisation in combination with surface antigen detection (314). Therefore, we concentrated in our work on finding a condition which would preserve the surface antigen pattern and give optimal result of intracellular stainings not only in the intact cells, but also in drug treated groups. Triton X-100 in 0.25% concentration was gentle enough to the tested surface proteins and at the same time provided a good separation of positive and negative populations for the intracellular markers γH2A.X and CC3. This result is in line with a recent study, where Triton X-100 was shown to be a more convenient permeabilisation reagent compared to saponin in the immunocytochemical detection of phospho-specific antibodies (315).

Analysis of the cell cycle progression by flow cytometry is a frequently used technique. Nowadays, a broad spectrum of DNA-binding fluorescent dyes is available, including intercalating dyes (ethidium bromide, propidium iodide, 7AAD) and minor

groove binders (DAPI and Hoechst). In our case, the fluorescent signal of FxCycle Far Red stain was impossible to compensate with some other fluorochromes. Therefore, we searched for a dye suitable for our experimental setup. Next, we found that DAPI, which is routinely used in single-parameter analysis of the cell cycle, was not suitable for our multiparametric assay due its broad emission spectrum resulting in high spillover of DAPI into other channels. Therefore, we implemented the PO-PRO-1 dye (292, 316) into our protocol. It gave suitable results of cell cycle analysis when it was combined with EdU-Click-iT assay and overall it was functional in our multiparametric assay. However, we are aware of the existing scope for further improvement of DNA staining in this protocol.

In summary, we have established a multiparametric flow cytometric assay for the complex analysis of cellular phenotypes in response to experimental therapy. Using this assay, we are able to simultaneously detect changes in viability, cell cycle profile, DNA synthesis and damage, and apoptosis in cells characterized by the expression of two surface markers. Obviously, the main benefit of this approach is that various biological responses to a specific treatment can be evaluated in a single assay on a single-cell level. Furthermore, we demonstrate the possible application of this established procedure to analyse heterogeneous samples and to compare the effects of drugs on different subsets of cell lines. Moreover, the protocol can be applied to both human and mouse cells, and to adherent and non-adherent cells. This creates an opportunity to efficiently analyse mixed cell populations including infiltrating host cells in xenografts. Further benefit of this assay is that for the complex analysis of the cellular phenotype, a low number of cells is needed. Parallel examination of these parameters by different methods would require a much higher number of the cells. Thus, we suggest that this assay is useful for complex analysis of rare populations, *e.g.* CSCs or CTCs in patient samples.

In conclusion, we have established a useful protocol for complex phenotype analysis of specifically defined cell populations and for investigation of their responses to drug treatment in a single assay.

6. CONCLUSIONS

Conclusions related to the first aim of the Thesis: The Role of Skp2 in Prostate Cancer Stem-like Cells

- The nuclear expression of Skp2 was associated with a high Gleason score in prostate cancer patients. High Skp2 expression was further associated with the mesenchymal phenotype in prostate cancer patients.

- High expression of Skp2 was associated with the mesenchymal state and CSCs characteristics of prostate cancer cells *in vitro*.

- Skp2 downregulation attenuated CSC-like properties of the cells *in vitro*.

- Pharmacological inhibition of the SCF^{Skp2} complex resulted in cell cycle arrest and accumulation of $p27^{Kip1}$ and $p21^{Cip1}$ cell cycle inhibitors.

- MLN-4924 induced late apoptosis/necrosis in $CD44^{+}CD24^{+}$ cells but not in $CD44^{+}CD24^{-}$ CSC-like cells**.** Clonogenic capacity of the cells with CSC-like phenotype $CD44^{+}CD24^{-}$ was significantly decreased when the cells were cultured in media with MLN-4924 inhibitor.

Conclusions related to the second aim of the Thesis: Establishment of a tool for analysis of cellular response to experimental drug treatment in heterogeneous samples (in CSC-like cells)

The results presented in this Thesis led us to the following conclusions:

- The critical steps necessary for assay establishment such as permeabilisation and probes or antibodies selection were optimized.

- A multiparametric flow cytometric assay for complex analysis of cellular phenotypes in response to experimental therapy was established. The main benefit of this approach is that various biological responses to a specific treatment can be evaluated in a single assay on a single-cell level.

- A possible application of this established procedure to analyse heterogeneous samples and to compare the effects of drugs on different subsets in heterogeneous samples was demonstrated.

7. REFERENCES

1. Verze, P., T. Cai, and S. Lorenzetti, *The role of the prostate in male fertility, health and disease.* Nat Rev Urol, 2016. **13**(7): p. 379-86.
2. Toivanen, R. and M.M. Shen, *Prostate organogenesis: tissue induction, hormonal regulation and cell type specification.* Development, 2017. **144**(8): p. 1382-1398.
3. Cunha, G.R., et al., *Normal and abnormal development of the male urogenital tract. Role of androgens, mesenchymal-epithelial interactions, and growth factors.* J Androl, 1992. **13**(6): p. 465-75.
4. Bonkhoff, H., U. Stein, and K. Remberger, *The proliferative function of basal cells in the normal and hyperplastic human prostate.* Prostate, 1994. **24**(3): p. 114-8.
5. Li, Q., C.S. Zhang, and Y. Zhang, *Molecular aspects of prostate cancer with neuroendocrine differentiation.* Chin J Cancer Res, 2016. **28**(1): p. 122-9.
6. Hudson, D.L., *Epithelial stem cells in human prostate growth and disease.* Prostate Cancer Prostatic Dis, 2004. **7**(3): p. 188-94.
7. Hudson, D.L., et al., *Epithelial cell differentiation pathways in the human prostate: identification of intermediate phenotypes by keratin expression.* J Histochem Cytochem, 2001. **49**(2): p. 271-8.
8. Petkova, N., et al., *Surface CD24 distinguishes between low differentiated and transit-amplifying cells in the basal layer of human prostate.* Prostate, 2013. **73**(14): p. 1576-90.
9. Liu, A.Y., M.P. Roudier, and L.D. True, *Heterogeneity in primary and metastatic prostate cancer as defined by cell surface CD profile.* Am J Pathol, 2004. **165**(5): p. 1543-56.
10. Goldstein, A.S., et al., *Trop2 identifies a subpopulation of murine and human prostate basal cells with stem cell characteristics.* Proc Natl Acad Sci U S A, 2008. **105**(52): p. 20882-7.
11. Karthaus, W.R., et al., *Identification of multipotent luminal progenitor cells in human prostate organoid cultures.* Cell, 2014. **159**(1): p. 163-175.
12. Richardson, G.D., et al., *CD133, a novel marker for human prostatic epithelial stem cells.* J Cell Sci, 2004. **117**(Pt 16): p. 3539-45.
13. Palapattu, G.S., et al., *Selective expression of CD44, a putative prostate cancer stem cell marker, in neuroendocrine tumor cells of human prostate cancer.* Prostate, 2009. **69**(7): p. 787-98.
14. English, H.F., R.J. Santen, and J.T. Isaacs, *Response of glandular versus basal rat ventral prostatic epithelial cells to androgen withdrawal and replacement.* Prostate, 1987. **11**(3): p. 229-42.

15. Taylor, R.A., R. Toivanen, and G.P. Risbridger, *Stem cells in prostate cancer: treating the root of the problem.* Endocr Relat Cancer, 2010. **17**(4): p. R273-85.
16. Isaacs, J.T. and D.S. Coffey, *Etiology and disease process of benign prostatic hyperplasia.* Prostate Suppl, 1989. **2**: p. 33-50.
17. Wang, Y., et al., *Cell differentiation lineage in the prostate.* Differentiation, 2001. **68**(4-5): p. 270-9.
18. Wang, X., et al., *A luminal epithelial stem cell that is a cell of origin for prostate cancer.* Nature, 2009. **461**(7263): p. 495-500.
19. Ousset, M., et al., *Multipotent and unipotent progenitors contribute to prostate postnatal development.* Nat Cell Biol, 2012. **14**(11): p. 1131-8.
20. Wuidart, A., et al., *Quantitative lineage tracing strategies to resolve multipotency in tissue-specific stem cells.* Genes Dev, 2016. **30**(11): p. 1261-77.
21. Moad, M., et al., *Multipotent Basal Stem Cells, Maintained in Localized Proximal Niches, Support Directed Long-Ranging Epithelial Flows in Human Prostates.* Cell Rep, 2017. **20**(7): p. 1609-1622.
22. Siegel, R.L., K.D. Miller, and A. Jemal, *Cancer statistics, 2018.* CA Cancer J Clin, 2018. **68**(1): p. 7-30.
23. Oh WK, H.M., D'Amico AV, et al. , *Biology of Prostate Cancer.* Kufe DW, Pollock RE, Weichselbaum RR, et al., editors. Holland-Frei Cancer Medicine. 6th edition. Hamilton (ON), (BC Decker; 2003.): p. Available from: https://www.ncbi.nlm.nih.gov/books/NBK13217/.
24. Lawrentschuk N, P.M., *Benign Prostate Disorders.* De Groot LJ, Chrousos G, Dungan K, et al., editors. Endotext [Internet]. South Dartmouth (MA): MDText.com, Inc.; 2000-, 2016.
25. Orsted, D.D., et al., *Association of clinical benign prostate hyperplasia with prostate cancer incidence and mortality revisited: a nationwide cohort study of 3,009,258 men.* Eur Urol, 2011. **60**(4): p. 691-8.
26. Schenk, J.M., et al., *Association of symptomatic benign prostatic hyperplasia and prostate cancer: results from the prostate cancer prevention trial.* Am J Epidemiol, 2011. **173**(12): p. 1419-28.
27. Bostwick, D.G., et al., *High-grade prostatic intraepithelial neoplasia.* Rev Urol, 2004. **6**(4): p. 171-9.
28. De Nunzio, C., et al., *The controversial relationship between benign prostatic hyperplasia and prostate cancer: the role of inflammation.* Eur Urol, 2011. **60**(1): p. 106-17.
29. Macintosh, C.A., et al., *Precise microdissection of human prostate cancers reveals genotypic heterogeneity.* Cancer Res, 1998. **58**(1): p. 23-8.
30. Goldstein, A.S., et al., *Identification of a cell of origin for human prostate cancer.* Science, 2010. **329**(5991): p. 568-71.
31. Park, J.W., et al., *Prostate epithelial cell of origin determines cancer differentiation state in an organoid transformation assay.* Proc Natl Acad Sci U S A, 2016. **113**(16): p. 4482-7.
32. Shen, M.M. and C. Abate-Shen, *Molecular genetics of prostate cancer: new prospects for old challenges.* Genes Dev, 2010. **24**(18): p. 1967-2000.
33. Bubendorf, L., et al., *Metastatic patterns of prostate cancer: an autopsy study of 1,589 patients.* Hum Pathol, 2000. **31**(5): p. 578-83.
34. National, C., Institute, *Stages of Prostate Cancer.* 2018: p. https://www.cancer.gov/types/prostate/patient/prostate-treatment-pdq#section/_120.

35. Zhou, C.K., et al., *Prostate cancer incidence in 43 populations worldwide: An analysis of time trends overall and by age group.* Int J Cancer, 2016. **138**(6): p. 1388-400.
36. Dušek Ladislav, M.J., Kubásek Miroslav, Koptíková Jana, Žaloudík Jan, Vyzula Rostislav, *Epidemiologie zhoubných nádorů v České republice [online] . Masarykova univerzita, [2005], [cit. 2018-8-17].* http://www.svod.cz. . **Verze 7.0 [2007]**.
37. Pepe, P. and M. Pennisi, *Gleason score stratification according to age at diagnosis in 1028 men.* Contemp Oncol (Pozn), 2015. **19**(6): p. 471-3.
38. Russo, A.L., et al., *Advancing age within established Gleason score categories and the risk of prostate cancer-specific mortality (PCSM).* BJU Int, 2012. **110**(7): p. 973-9.
39. Kunz, I., et al., *Tumour characteristics, oncological and functional outcomes in patients aged >/= 70 years undergoing radical prostatectomy.* BJU Int, 2013. **111**(3 Pt B): p. E24-9.
40. Salinas, C.A., et al., *Prostate cancer in young men: an important clinical entity.* Nat Rev Urol, 2014. **11**(6): p. 317-23.
41. Bhatt, N.R., et al., *Increasing detection of significant prostate cancer in younger men - ten year trends in prostate cancer risk profile in the Mid-West of Ireland.* Cent European J Urol, 2017. **70**(2): p. 143-147.
42. Lin, D.W., M. Porter, and B. Montgomery, *Treatment and survival outcomes in young men diagnosed with prostate cancer: a Population-based Cohort Study.* Cancer, 2009. **115**(13): p. 2863-71.
43. Carter, B.S., et al., *Mendelian inheritance of familial prostate cancer.* Proc Natl Acad Sci U S A, 1992. **89**(8): p. 3367-71.
44. Harris, W.P., et al., *Androgen deprivation therapy: progress in understanding mechanisms of resistance and optimizing androgen depletion.* Nat Clin Pract Urol, 2009. **6**(2): p. 76-85.
45. Chandrasekar, T., et al., *Targeting molecular resistance in castration-resistant prostate cancer.* BMC Med, 2015. **13**: p. 206.
46. Huggins C, S.R., Hodges CV, *Studies on prostatic cancer: II. The effects of castration on advanced carcinoma of the prostate gland.* Arch Surg., 1941. **43**: p. 209-223.
47. Shapiro, D. and B. Tareen, *Current and emerging treatments in the management of castration-resistant prostate cancer.* Expert Rev Anticancer Ther, 2012. **12**(7): p. 951-64.
48. Tassinari, D., et al., *Treatment of Metastatic, Castration-resistant, Docetaxel-resistant Prostate Cancer: A Systematic Review of Literature With a Network Meta-analysis of Randomized Clinical Trials.* Rev Recent Clin Trials, 2018. **13**(3): p. 226-237.
49. Ritch, C.R. and M.S. Cookson, *Advances in the management of castration resistant prostate cancer.* BMJ, 2016. **355**: p. i4405.
50. Park, C.H., D.E. Bergsagel, and E.A. McCulloch, *Mouse myeloma tumor stem cells: a primary cell culture assay.* J Natl Cancer Inst, 1971. **46**(2): p. 411-22.
51. Al-Hajj, M., et al., *Prospective identification of tumorigenic breast cancer cells.* Proc Natl Acad Sci U S A, 2003. **100**(7): p. 3983-8.
52. Singh, S.K., et al., *Identification of a cancer stem cell in human brain tumors.* Cancer Res, 2003. **63**(18): p. 5821-8.
53. Collins, A.T., et al., *Prospective identification of tumorigenic prostate cancer stem cells.* Cancer Res, 2005. **65**(23): p. 10946-51.
54. Tu, S.M. and S.H. Lin, *Prostate cancer stem cells.* Clin Genitourin Cancer, 2012. **10**(2): p. 69-76.

55. Peng, Y., et al., *Human Stromal Cells in the Peripheral Zone of the Prostate Promote Tumorigenesis of Prostatic Cancer Stem Cells through Up-regulation of C-Kit Expression.* J Cancer, 2015. **6**(8): p. 776-85.
56. Rybak, A.P., R.G. Bristow, and A. Kapoor, *Prostate cancer stem cells: deciphering the origins and pathways involved in prostate tumorigenesis and aggression.* Oncotarget, 2015. **6**(4): p. 1900-19.
57. Leao, R., et al., *Cancer Stem Cells in Prostate Cancer: Implications for Targeted Therapy.* Urol Int, 2017. **99**(2): p. 125-136.
58. Hu, Y. and L. Fu, *Targeting cancer stem cells: a new therapy to cure cancer patients.* Am J Cancer Res, 2012. **2**(3): p. 340-56.
59. Yu, C., et al., *Prostate cancer stem cell biology.* Minerva Urol Nefrol, 2012. **64**(1): p. 19-33.
60. Fujimori, H., et al., *Induction of cancerous stem cells during embryonic stem cell differentiation.* J Biol Chem, 2012. **287**(44): p. 36777-91.
61. Wang, S., et al., *Pten deletion leads to the expansion of a prostatic stem/progenitor cell subpopulation and tumor initiation.* Proc Natl Acad Sci U S A, 2006. **103**(5): p. 1480-5.
62. Rajasekhar, V.K., et al., *Tumour-initiating stem-like cells in human prostate cancer exhibit increased NF-kappaB signalling.* Nat Commun, 2011. **2**: p. 162.
63. Korsten, H., et al., *Accumulating progenitor cells in the luminal epithelial cell layer are candidate tumor initiating cells in a Pten knockout mouse prostate cancer model.* PLoS One, 2009. **4**(5): p. e5662.
64. Qin, J., et al., *The PSA(-/lo) prostate cancer cell population harbors self-renewing long-term tumor-propagating cells that resist castration.* Cell Stem Cell, 2012. **10**(5): p. 556-69.
65. Germann, M., et al., *Stem-like cells with luminal progenitor phenotype survive castration in human prostate cancer.* Stem Cells, 2012. **30**(6): p. 1076-86.
66. Li, P., R. Yang, and W.Q. Gao, *Contributions of epithelial-mesenchymal transition and cancer stem cells to the development of castration resistance of prostate cancer.* Mol Cancer, 2014. **13**: p. 55.
67. Yun, E.J., U.G. Lo, and J.T. Hsieh, *The evolving landscape of prostate cancer stem cell: Therapeutic implications and future challenges.* Asian J Urol, 2016. **3**(4): p. 203-210.
68. Nguyen, L.V., et al., *Cancer stem cells: an evolving concept.* Nat Rev Cancer, 2012. **12**(2): p. 133-43.
69. Castillo, V., et al., *Functional characteristics of cancer stem cells and their role in drug resistance of prostate cancer.* Int J Oncol, 2014. **45**(3): p. 985-94.
70. Fedr, R., et al., *Automatic cell cloning assay for determining the clonogenic capacity of cancer and cancer stem-like cells.* Cytometry A, 2013. **83**(5): p. 472-82.
71. Remsik, J., et al., *Trop-2 plasticity is controlled by epithelial-to-mesenchymal transition.* Carcinogenesis, 2018.
72. Reynolds, B.A. and S. Weiss, *Generation of neurons and astrocytes from isolated cells of the adult mammalian central nervous system.* Science, 1992. **255**(5052): p. 1707-10.
73. Lee, E.K., H. Cho, and C.W. Kim, *Proteomic analysis of cancer stem cells in human prostate cancer cells.* Biochem Biophys Res Commun, 2011. **412**(2): p. 279-85.
74. Weiswald, L.B., D. Bellet, and V. Dangles-Marie, *Spherical cancer models in tumor biology.* Neoplasia, 2015. **17**(1): p. 1-15.

75. Marchitti, S.A., et al., *Non-P450 aldehyde oxidizing enzymes: the aldehyde dehydrogenase superfamily.* Expert Opin Drug Metab Toxicol, 2008. **4**(6): p. 697-720.
76. Storms, R.W., et al., *Isolation of primitive human hematopoietic progenitors on the basis of aldehyde dehydrogenase activity.* Proc Natl Acad Sci U S A, 1999. **96**(16): p. 9118-23.
77. van den Hoogen, C., et al., *High aldehyde dehydrogenase activity identifies tumor-initiating and metastasis-initiating cells in human prostate cancer.* Cancer Res, 2010. **70**(12): p. 5163-73.
78. Jeter, C.R., et al., *NANOG promotes cancer stem cell characteristics and prostate cancer resistance to androgen deprivation.* Oncogene, 2011. **30**(36): p. 3833-45.
79. Le Magnen, C., et al., *Characterization and clinical relevance of ALDHbright populations in prostate cancer.* Clin Cancer Res, 2013. **19**(19): p. 5361-71.
80. Huang, E.H., et al., *Aldehyde dehydrogenase 1 is a marker for normal and malignant human colonic stem cells (SC) and tracks SC overpopulation during colon tumorigenesis.* Cancer Res, 2009. **69**(8): p. 3382-9.
81. Jiang, F., et al., *Aldehyde dehydrogenase 1 is a tumor stem cell-associated marker in lung cancer.* Mol Cancer Res, 2009. **7**(3): p. 330-8.
82. Tanei, T., et al., *Association of breast cancer stem cells identified by aldehyde dehydrogenase 1 expression with resistance to sequential Paclitaxel and epirubicin-based chemotherapy for breast cancers.* Clin Cancer Res, 2009. **15**(12): p. 4234-41.
83. Li, T., et al., *ALDH1A1 is a marker for malignant prostate stem cells and predictor of prostate cancer patients' outcome.* Lab Invest, 2010. **90**(2): p. 234-44.
84. Gangavarapu, K.J., et al., *Aldehyde dehydrogenase and ATP binding cassette transporter G2 (ABCG2) functional assays isolate different populations of prostate stem cells where ABCG2 function selects for cells with increased stem cell activity.* Stem Cell Res Ther, 2013. **4**(5): p. 132.
85. Cojoc, M., et al., *Aldehyde Dehydrogenase Is Regulated by beta-Catenin/TCF and Promotes Radioresistance in Prostate Cancer Progenitor Cells.* Cancer Res, 2015. **75**(7): p. 1482-94.
86. Zhou, S., et al., *The ABC transporter Bcrp1/ABCG2 is expressed in a wide variety of stem cells and is a molecular determinant of the side-population phenotype.* Nat Med, 2001. **7**(9): p. 1028-34.
87. Hirschmann-Jax, C., et al., *A distinct "side population" of cells with high drug efflux capacity in human tumor cells.* Proc Natl Acad Sci U S A, 2004. **101**(39): p. 14228-33.
88. Goodell, M.A., et al., *Isolation and functional properties of murine hematopoietic stem cells that are replicating in vivo.* J Exp Med, 1996. **183**(4): p. 1797-806.
89. Patrawala, L., et al., *Side population is enriched in tumorigenic, stem-like cancer cells, whereas ABCG2+ and ABCG2- cancer cells are similarly tumorigenic.* Cancer Res, 2005. **65**(14): p. 6207-19.
90. Garraway, I.P., et al., *Human prostate sphere-forming cells represent a subset of basal epithelial cells capable of glandular regeneration in vivo.* Prostate, 2010. **70**(5): p. 491-501.
91. Hurt, E.M., et al., *CD44+ CD24(-) prostate cells are early cancer progenitor/stem cells that provide a model for patients with poor prognosis.* Br J Cancer, 2008. **98**(4): p. 756-65.
92. Salvatori, L., et al., *Cell-to-cell signaling influences the fate of prostate cancer stem cells and their potential to generate more aggressive tumors.* PLoS One, 2012. **7**(2): p. e31467.

93. Jaworska, D. and E. Szliszka, *Targeting Apoptotic Activity Against Prostate Cancer Stem Cells.* Int J Mol Sci, 2017. **18**(8).
94. Colombel, M., et al., *Increased expression of putative cancer stem cell markers in primary prostate cancer is associated with progression of bone metastases.* Prostate, 2012. **72**(7): p. 713-20.
95. Patrawala, L., et al., *Hierarchical organization of prostate cancer cells in xenograft tumors: the CD44+alpha2beta1+ cell population is enriched in tumor-initiating cells.* Cancer Res, 2007. **67**(14): p. 6796-805.
96. Leong, K.G., et al., *Generation of a prostate from a single adult stem cell.* Nature, 2008. **456**(7223): p. 804-8.
97. Mulholland, D.J., et al., *Lin-Sca-1+CD49fhigh stem/progenitors are tumor-initiating cells in the Pten-null prostate cancer model.* Cancer Res, 2009. **69**(22): p. 8555-62.
98. Liao, C.P., et al., *Cancer-associated fibroblasts enhance the gland-forming capability of prostate cancer stem cells.* Cancer Res, 2010. **70**(18): p. 7294-303.
99. Yamamoto, H., et al., *CD49f is an efficient marker of monolayer- and spheroid colony-forming cells of the benign and malignant human prostate.* PLoS One, 2012. **7**(10): p. e46979.
100. Yang, C., et al., *Pentaspan membrane glycoprotein, prominin-1, is involved in glucose metabolism and cytoskeleton alteration.* Biochemistry (Mosc), 2007. **72**(8): p. 854-62.
101. Guo, C., et al., *Epcam, CD44, and CD49f distinguish sphere-forming human prostate basal cells from a subpopulation with predominant tubule initiation capability.* PLoS One, 2012. **7**(4): p. e34219.
102. Burger, P.E., et al., *Sca-1 expression identifies stem cells in the proximal region of prostatic ducts with high capacity to reconstitute prostatic tissue.* Proc Natl Acad Sci U S A, 2005. **102**(20): p. 7180-5.
103. Hanahan, D. and R.A. Weinberg, *Hallmarks of cancer: the next generation.* Cell, 2011. **144**(5): p. 646-74.
104. Lim, J. and J.P. Thiery, *Epithelial-mesenchymal transitions: insights from development.* Development, 2012. **139**(19): p. 3471-86.
105. Thiery, J.P., et al., *Epithelial-mesenchymal transitions in development and disease.* Cell, 2009. **139**(5): p. 871-90.
106. Kalluri, R. and R.A. Weinberg, *The basics of epithelial-mesenchymal transition.* J Clin Invest, 2009. **119**(6): p. 1420-8.
107. Chaffer, C.L., et al., *Mesenchymal-to-epithelial transition facilitates bladder cancer metastasis: role of fibroblast growth factor receptor-2.* Cancer Res, 2006. **66**(23): p. 11271-8.
108. Ross, J.S., et al., *E-cadherin expression in prostatic carcinoma biopsies: correlation with tumor grade, DNA content, pathologic stage, and clinical outcome.* Mod Pathol, 1994. **7**(8): p. 835-41.
109. Umbas, R., et al., *Decreased E-cadherin expression is associated with poor prognosis in patients with prostate cancer.* Cancer Res, 1994. **54**(14): p. 3929-33.
110. Byles, V., et al., *SIRT1 induces EMT by cooperating with EMT transcription factors and enhances prostate cancer cell migration and metastasis.* Oncogene, 2012. **31**(43): p. 4619-29.
111. Hou, L., et al., *SET8 induces epithelialmesenchymal transition and enhances prostate cancer cell metastasis by cooperating with ZEB1.* Mol Med Rep, 2016. **13**(2): p. 1681-8.
112. Sethi, S., et al., *Molecular signature of epithelial-mesenchymal transition (EMT) in human prostate cancer bone metastasis.* Am J Transl Res, 2010. **3**(1): p. 90-9.

113. Kolijn, K., E.I. Verhoef, and G.J. van Leenders, *Morphological and immunohistochemical identification of epithelial-to-mesenchymal transition in clinical prostate cancer.* Oncotarget, 2015. **6**(27): p. 24488-98.
114. Yu, M., et al., *Circulating breast tumor cells exhibit dynamic changes in epithelial and mesenchymal composition.* Science, 2013. **339**(6119): p. 580-4.
115. Satelli, A., et al., *EMT circulating tumor cells detected by cell-surface vimentin are associated with prostate cancer progression.* Oncotarget, 2017. **8**(30): p. 49329-49337.
116. de Bono, J.S., et al., *Circulating tumor cells predict survival benefit from treatment in metastatic castration-resistant prostate cancer.* Clin Cancer Res, 2008. **14**(19): p. 6302-9.
117. Armstrong, A.J., et al., *Circulating tumor cells from patients with advanced prostate and breast cancer display both epithelial and mesenchymal markers.* Mol Cancer Res, 2011. **9**(8): p. 997-1007.
118. Jadaan, D.Y., M.M. Jadaan, and J.P. McCabe, *Cellular Plasticity in Prostate Cancer Bone Metastasis.* Prostate Cancer, 2015. **2015**: p. 651580.
119. Mani, S.A., et al., *The epithelial-mesenchymal transition generates cells with properties of stem cells.* Cell, 2008. **133**(4): p. 704-15.
120. Sun, Y., et al., *Androgen deprivation causes epithelial-mesenchymal transition in the prostate: implications for androgen-deprivation therapy.* Cancer Res, 2012. **72**(2): p. 527-36.
121. Kong, D., et al., *Epithelial to mesenchymal transition is mechanistically linked with stem cell signatures in prostate cancer cells.* PLoS One, 2010. **5**(8): p. e12445.
122. Puhr, M., et al., *Epithelial-to-mesenchymal transition leads to docetaxel resistance in prostate cancer and is mediated by reduced expression of miR-200c and miR-205.* Am J Pathol, 2012. **181**(6): p. 2188-201.
123. Marin-Aguilera, M., et al., *Epithelial-to-mesenchymal transition mediates docetaxel resistance and high risk of relapse in prostate cancer.* Mol Cancer Ther, 2014. **13**(5): p. 1270-84.
124. Harner-Foreman, N., et al., *A novel spontaneous model of epithelial-mesenchymal transition (EMT) using a primary prostate cancer derived cell line demonstrating distinct stem-like characteristics.* Sci Rep, 2017. **7**: p. 40633.
125. Glickman, M.H. and A. Ciechanover, *The ubiquitin-proteasome proteolytic pathway: destruction for the sake of construction.* Physiol Rev, 2002. **82**(2): p. 373-428.
126. Liu, J., et al., *Targeting the ubiquitin pathway for cancer treatment.* Biochim Biophys Acta, 2015. **1855**(1): p. 50-60.
127. Lim, S. and P. Kaldis, *Cdks, cyclins and CKIs: roles beyond cell cycle regulation.* Development, 2013. **140**(15): p. 3079-93.
128. Nakayama, K.I. and K. Nakayama, *Ubiquitin ligases: cell-cycle control and cancer.* Nat Rev Cancer, 2006. **6**(5): p. 369-81.
129. Nakayama, K.I. and K. Nakayama, *Regulation of the cell cycle by SCF-type ubiquitin ligases.* Semin Cell Dev Biol, 2005. **16**(3): p. 323-33.
130. Wei, W., et al., *Degradation of the SCF component Skp2 in cell-cycle phase G1 by the anaphase-promoting complex.* Nature, 2004. **428**(6979): p. 194-8.
131. Benmaamar, R. and M. Pagano, *Involvement of the SCF complex in the control of Cdh1 degradation in S-phase.* Cell Cycle, 2005. **4**(9): p. 1230-2.
132. Sakaue-Sawano, A., et al., *Visualizing spatiotemporal dynamics of multicellular cell-cycle progression.* Cell, 2008. **132**(3): p. 487-98.
133. Fuster, J.J., et al., *Control of cell proliferation in atherosclerosis: insights from animal models and human studies.* Cardiovasc Res, 2010. **86**(2): p. 254-64.

134. Soucy, T.A., et al., *An inhibitor of NEDD8-activating enzyme as a new approach to treat cancer.* Nature, 2009. **458**(7239): p. 732-6.
135. Petroski, M.D. and R.J. Deshaies, *Function and regulation of cullin-RING ubiquitin ligases.* Nat Rev Mol Cell Biol, 2005. **6**(1): p. 9-20.
136. Tan, P., et al., *Recruitment of a ROC1-CUL1 ubiquitin ligase by Skp1 and HOS to catalyze the ubiquitination of I kappa B alpha.* Mol Cell, 1999. **3**(4): p. 527-33.
137. Ohta, T., et al., *ROC1, a homolog of APC11, represents a family of cullin partners with an associated ubiquitin ligase activity.* Mol Cell, 1999. **3**(4): p. 535-41.
138. Kamura, T., et al., *Rbx1, a component of the VHL tumor suppressor complex and SCF ubiquitin ligase.* Science, 1999. **284**(5414): p. 657-61.
139. Zimmerman, E.S., B.A. Schulman, and N. Zheng, *Structural assembly of cullin-RING ubiquitin ligase complexes.* Curr Opin Struct Biol, 2010. **20**(6): p. 714-21.
140. Duda, D.M., et al., *Structural regulation of cullin-RING ubiquitin ligase complexes.* Curr Opin Struct Biol, 2011. **21**(2): p. 257-64.
141. Skaar, J.R., et al., *PARC and CUL7 form atypical cullin RING ligase complexes.* Cancer Res, 2007. **67**(5): p. 2006-14.
142. Hori, T., et al., *Covalent modification of all members of human cullin family proteins by NEDD8.* Oncogene, 1999. **18**(48): p. 6829-34.
143. Kamitani, T., et al., *Characterization of NEDD8, a developmentally down-regulated ubiquitin-like protein.* J Biol Chem, 1997. **272**(45): p. 28557-62.
144. Liakopoulos, D., et al., *A novel protein modification pathway related to the ubiquitin system.* EMBO J, 1998. **17**(8): p. 2208-14.
145. Osaka, F., et al., *A new NEDD8-ligating system for cullin-4A.* Genes Dev, 1998. **12**(15): p. 2263-8.
146. Watson, I.R., M.S. Irwin, and M. Ohh, *NEDD8 pathways in cancer, Sine Quibus Non.* Cancer Cell, 2011. **19**(2): p. 168-76.
147. Kipreos, E.T., et al., *cul-1 is required for cell cycle exit in C. elegans and identifies a novel gene family.* Cell, 1996. **85**(6): p. 829-39.
148. Yu, H., et al., *Identification of a cullin homology region in a subunit of the anaphase-promoting complex.* Science, 1998. **279**(5354): p. 1219-22.
149. Zachariae, W., et al., *Mass spectrometric analysis of the anaphase-promoting complex from yeast: identification of a subunit related to cullins.* Science, 1998. **279**(5354): p. 1216-9.
150. Watson, I.R., et al., *Mdm2-mediated NEDD8 modification of TAp73 regulates its transactivation function.* J Biol Chem, 2006. **281**(45): p. 34096-103.
151. Xirodimas, D.P., et al., *Mdm2-mediated NEDD8 conjugation of p53 inhibits its transcriptional activity.* Cell, 2004. **118**(1): p. 83-97.
152. Oved, S., et al., *Conjugation to Nedd8 instigates ubiquitylation and down-regulation of activated receptor tyrosine kinases.* J Biol Chem, 2006. **281**(31): p. 21640-51.
153. Fan, M., R.M. Bigsby, and K.P. Nephew, *The NEDD8 pathway is required for proteasome-mediated degradation of human estrogen receptor (ER)-alpha and essential for the antiproliferative activity of ICI 182,780 in ERalpha-positive breast cancer cells.* Mol Endocrinol, 2003. **17**(3): p. 356-65.
154. Lyapina, S., et al., *Promotion of NEDD-CUL1 conjugate cleavage by COP9 signalosome.* Science, 2001. **292**(5520): p. 1382-5.
155. Liu, J., et al., *NEDD8 modification of CUL1 dissociates p120(CAND1), an inhibitor of CUL1-SKP1 binding and SCF ligases.* Mol Cell, 2002. **10**(6): p. 1511-8.
156. Zheng, J., et al., *CAND1 binds to unneddylated CUL1 and regulates the formation of SCF ubiquitin E3 ligase complex.* Mol Cell, 2002. **10**(6): p. 1519-26.

157. Goldenberg, S.J., et al., *Structure of the Cand1-Cul1-Roc1 complex reveals regulatory mechanisms for the assembly of the multisubunit cullin-dependent ubiquitin ligases.* Cell, 2004. **119**(4): p. 517-28.
158. Bennett, E.J., et al., *Dynamics of cullin-RING ubiquitin ligase network revealed by systematic quantitative proteomics.* Cell, 2010. **143**(6): p. 951-65.
159. Soucy, T.A., et al., *The NEDD8 Conjugation Pathway and Its Relevance in Cancer Biology and Therapy.* Genes Cancer, 2010. **1**(7): p. 708-16.
160. Zheng, N., et al., *Structure of the Cul1-Rbx1-Skp1-F boxSkp2 SCF ubiquitin ligase complex.* Nature, 2002. **416**(6882): p. 703-9.
161. Skowyra, D., et al., *F-box proteins are receptors that recruit phosphorylated substrates to the SCF ubiquitin-ligase complex.* Cell, 1997. **91**(2): p. 209-19.
162. Bai, C., et al., *SKP1 connects cell cycle regulators to the ubiquitin proteolysis machinery through a novel motif, the F-box.* Cell, 1996. **86**(2): p. 263-74.
163. Schulman, B.A., et al., *Insights into SCF ubiquitin ligases from the structure of the Skp1-Skp2 complex.* Nature, 2000. **408**(6810): p. 381-6.
164. Chen, L. and D.A. Tweddle, *p53, SKP2, and DKK3 as MYCN Target Genes and Their Potential Therapeutic Significance.* Front Oncol, 2012. **2**: p. 173.
165. Zhang, H., et al., *p19Skp1 and p45Skp2 are essential elements of the cyclin A-CDK2 S phase kinase.* Cell, 1995. **82**(6): p. 915-25.
166. Lisztwan, J., et al., *Association of human CUL-1 and ubiquitin-conjugating enzyme CDC34 with the F-box protein p45(SKP2): evidence for evolutionary conservation in the subunit composition of the CDC34-SCF pathway.* EMBO J, 1998. **17**(2): p. 368-83.
167. Wirbelauer, C., et al., *The F-box protein Skp2 is a ubiquitylation target of a Cul1-based core ubiquitin ligase complex: evidence for a role of Cul1 in the suppression of Skp2 expression in quiescent fibroblasts.* EMBO J, 2000. **19**(20): p. 5362-75.
168. Chan, C.H., et al., *Regulation of Skp2 expression and activity and its role in cancer progression.* ScientificWorldJournal, 2010. **10**: p. 1001-15.
169. van Duijn, P.W. and J. Trapman, *PI3K/Akt signaling regulates p27(kip1) expression via Skp2 in PC3 and DU145 prostate cancer cells, but is not a major factor in p27(kip1) regulation in LNCaP and PC346 cells.* Prostate, 2006. **66**(7): p. 749-60.
170. Auld, C.A., C.D. Caccia, and R.F. Morrison, *Hormonal induction of adipogenesis induces Skp2 expression through PI3K and MAPK pathways.* J Cell Biochem, 2007. **100**(1): p. 204-16.
171. Gao, D., et al., *Phosphorylation by Akt1 promotes cytoplasmic localization of Skp2 and impairs APCCdh1-mediated Skp2 destruction.* Nat Cell Biol, 2009. **11**(4): p. 397-408.
172. Mamillapalli, R., et al., *PTEN regulates the ubiquitin-dependent degradation of the CDK inhibitor p27(KIP1) through the ubiquitin E3 ligase SCF(SKP2).* Curr Biol, 2001. **11**(4): p. 263-7.
173. Carrano, A.C. and M. Pagano, *Role of the F-box protein Skp2 in adhesion-dependent cell cycle progression.* J Cell Biol, 2001. **153**(7): p. 1381-90.
174. Jang, W., et al., *Mechanical cue-induced YAP instructs Skp2-dependent cell cycle exit and oncogenic signaling.* EMBO J, 2017. **36**(17): p. 2510-2528.
175. Kim, J.Y., et al., *Epidermal growth factor upregulates Skp2/Cks1 and p27(kip1) in human extrahepatic cholangiocarcinoma cells.* World J Gastroenterol, 2014. **20**(3): p. 755-73.
176. Yung, Y., et al., *A Skp2 autoinduction loop and restriction point control.* J Cell Biol, 2007. **178**(5): p. 741-7.

177. Lin, H.K., et al., *Phosphorylation-dependent regulation of cytosolic localization and oncogenic function of Skp2 by Akt/PKB.* Nat Cell Biol, 2009. **11**(4): p. 420-32.
178. Inuzuka, H., et al., *Acetylation-dependent regulation of Skp2 function.* Cell, 2012. **150**(1): p. 179-93.
179. Zhang, S., et al., *Hippo Signaling Suppresses Cell Ploidy and Tumorigenesis through Skp2.* Cancer Cell, 2017. **31**(5): p. 669-684 e7.
180. Hu, D., et al., *Nuclear translocation of Skp2 facilitates its destruction in response to TGFbeta signaling.* Cell Cycle, 2011. **10**(2): p. 285-92.
181. Zhang, Y.W., K. Nakayama, and I. Morita, *A novel route for connexin 43 to inhibit cell proliferation: negative regulation of S-phase kinase-associated protein (Skp 2).* Cancer Res, 2003. **63**(7): p. 1623-30.
182. Shi, Q., et al., *Connexin Controls Cell-Cycle Exit and Cell Differentiation by Directly Promoting Cytosolic Localization and Degradation of E3 Ligase Skp2.* Dev Cell, 2015. **35**(4): p. 483-96.
183. Nakayama, K., et al., *Targeted disruption of Skp2 results in accumulation of cyclin E and p27(Kip1), polyploidy and centrosome overduplication.* EMBO J, 2000. **19**(9): p. 2069-81.
184. Kossatz, U., et al., *Skp2-dependent degradation of p27kip1 is essential for cell cycle progression.* Genes Dev, 2004. **18**(21): p. 2602-7.
185. Yeh, K.H., et al., *The F-box protein SKP2 binds to the phosphorylated threonine 380 in cyclin E and regulates ubiquitin-dependent degradation of cyclin E.* Biochem Biophys Res Commun, 2001. **281**(4): p. 884-90.
186. Auld, C.A., K.M. Fernandes, and R.F. Morrison, *Skp2-mediated p27(Kip1) degradation during S/G2 phase progression of adipocyte hyperplasia.* J Cell Physiol, 2007. **211**(1): p. 101-11.
187. Nakayama, K., et al., *Skp2-mediated degradation of p27 regulates progression into mitosis.* Dev Cell, 2004. **6**(5): p. 661-72.
188. Hu, R. and A.E. Aplin, *Skp2 regulates G2/M progression in a p53-dependent manner.* Mol Biol Cell, 2008. **19**(11): p. 4602-10.
189. Bornstein, G., et al., *Role of the SCFSkp2 ubiquitin ligase in the degradation of p21Cip1 in S phase.* J Biol Chem, 2003. **278**(28): p. 25752-7.
190. Yu, Z.K., J.L. Gervais, and H. Zhang, *Human CUL-1 associates with the SKP1/SKP2 complex and regulates p21(CIP1/WAF1) and cyclin D proteins.* Proc Natl Acad Sci U S A, 1998. **95**(19): p. 11324-9.
191. Kamura, T., et al., *Degradation of p57Kip2 mediated by SCFSkp2-dependent ubiquitylation.* Proc Natl Acad Sci U S A, 2003. **100**(18): p. 10231-6.
192. Polyak, K., et al., *Cloning of p27Kip1, a cyclin-dependent kinase inhibitor and a potential mediator of extracellular antimitogenic signals.* Cell, 1994. **78**(1): p. 59-66.
193. Toyoshima, H. and T. Hunter, *p27, a novel inhibitor of G1 cyclin-Cdk protein kinase activity, is related to p21.* Cell, 1994. **78**(1): p. 67-74.
194. Carrano, A.C., et al., *SKP2 is required for ubiquitin-mediated degradation of the CDK inhibitor p27.* Nat Cell Biol, 1999. **1**(4): p. 193-9.
195. Tsvetkov, L.M., et al., *p27(Kip1) ubiquitination and degradation is regulated by the SCF(Skp2) complex through phosphorylated Thr187 in p27.* Curr Biol, 1999. **9**(12): p. 661-4.
196. Marti, A., et al., *Interaction between ubiquitin-protein ligase SCFSKP2 and E2F-1 underlies the regulation of E2F-1 degradation.* Nat Cell Biol, 1999. **1**(1): p. 14-9.
197. Kim, S.Y., et al., *Skp2 regulates Myc protein stability and activity.* Mol Cell, 2003. **11**(5): p. 1177-88.

198. von der Lehr, N., et al., *The F-box protein Skp2 participates in c-Myc proteosomal degradation and acts as a cofactor for c-Myc-regulated transcription.* Mol Cell, 2003. **11**(5): p. 1189-200.
199. Mendez, J., et al., *Human origin recognition complex large subunit is degraded by ubiquitin-mediated proteolysis after initiation of DNA replication.* Mol Cell, 2002. **9**(3): p. 481-91.
200. Kondo, T., et al., *Rapid degradation of Cdt1 upon UV-induced DNA damage is mediated by SCFSkp2 complex.* J Biol Chem, 2004. **279**(26): p. 27315-9.
201. Li, X., et al., *The SCF(Skp2) ubiquitin ligase complex interacts with the human replication licensing factor Cdt1 and regulates Cdt1 degradation.* J Biol Chem, 2003. **278**(33): p. 30854-8.
202. Moro, L., et al., *Up-regulation of Skp2 after prostate cancer cell adhesion to basement membranes results in BRCA2 degradation and cell proliferation.* J Biol Chem, 2006. **281**(31): p. 22100-7.
203. Jiang, H., et al., *Ubiquitylation of RAG-2 by Skp2-SCF links destruction of the V(D)J recombinase to the cell cycle.* Mol Cell, 2005. **18**(6): p. 699-709.
204. Kiernan, R.E., et al., *Interaction between cyclin T1 and SCF(SKP2) targets CDK9 for ubiquitination and degradation by the proteasome.* Mol Cell Biol, 2001. **21**(23): p. 7956-70.
205. Huang, H., et al., *Skp2 inhibits FOXO1 in tumor suppression through ubiquitin-mediated degradation.* Proc Natl Acad Sci U S A, 2005. **102**(5): p. 1649-54.
206. Randle, S.J. and H. Laman, *F-box protein interactions with the hallmark pathways in cancer.* Semin Cancer Biol, 2016. **36**: p. 3-17.
207. Rodriguez, S., et al., *The SKP2 E3 ligase regulates basal homeostasis and stress-induced regeneration of HSCs.* Blood, 2011. **117**(24): p. 6509-19.
208. Okada, M., et al., *Skp2 promotes adipocyte differentiation via a p27Kip1-independent mechanism in primary mouse embryonic fibroblasts.* Biochem Biophys Res Commun, 2009. **379**(2): p. 249-54.
209. Sakai, T., et al., *Skp2 controls adipocyte proliferation during the development of obesity.* J Biol Chem, 2007. **282**(3): p. 2038-46.
210. Boix-Perales, H., et al., *The E3 ubiquitin ligase skp2 regulates neural differentiation independent from the cell cycle.* Neural Dev, 2007. **2**: p. 27.
211. Supriatno, et al., *Overexpression of p27(Kip1) induces growth arrest and apoptosis in an oral cancer cell line.* Oral Oncol, 2002. **38**(7): p. 730-6.
212. Yokoi, S., et al., *Down-regulation of SKP2 induces apoptosis in lung-cancer cells.* Cancer Sci, 2003. **94**(4): p. 344-9.
213. Harada, K., et al., *Down-regulation of S-phase kinase associated protein 2 (Skp2) induces apoptosis in oral cancer cells.* Oral Oncol, 2005. **41**(6): p. 623-30.
214. Kitagawa, M., S.H. Lee, and F. McCormick, *Skp2 suppresses p53-dependent apoptosis by inhibiting p300.* Mol Cell, 2008. **29**(2): p. 217-31.
215. Dehan, E. and M. Pagano, *Skp2, the FoxO1 hunter.* Cancer Cell, 2005. **7**(3): p. 209-10.
216. Yang, G., et al., *Elevated Skp2 protein expression in human prostate cancer: association with loss of the cyclin-dependent kinase inhibitor p27 and PTEN and with reduced recurrence-free survival.* Clin Cancer Res, 2002. **8**(11): p. 3419-26.
217. Signoretti, S., et al., *Oncogenic role of the ubiquitin ligase subunit Skp2 in human breast cancer.* J Clin Invest, 2002. **110**(5): p. 633-41.
218. Ma, X.M., et al., *Relation of overexpression of S phase kinase-associated protein 2 with reduced expression of p27 and PTEN in human gastric carcinoma.* World J Gastroenterol, 2005. **11**(42): p. 6716-21.

219. Shapira, M., et al., *The prognostic impact of the ubiquitin ligase subunits Skp2 and Cks1 in colorectal carcinoma.* Cancer, 2005. **103**(7): p. 1336-46.
220. Hershko, D.D., *Oncogenic properties and prognostic implications of the ubiquitin ligase Skp2 in cancer.* Cancer, 2008. **112**(7): p. 1415-24.
221. Lin, H.K., et al., *Skp2 targeting suppresses tumorigenesis by Arf-p53-independent cellular senescence.* Nature, 2010. **464**(7287): p. 374-9.
222. Chen, H., et al., *Interference of Skp2 effectively inhibits the development and metastasis of colon carcinoma.* Mol Med Rep, 2014. **10**(2): p. 1129-35.
223. Pernicova, Z., et al., *Androgen depletion induces senescence in prostate cancer cells through down-regulation of Skp2.* Neoplasia, 2011. **13**(6): p. 526-36.
224. Shim, E.H., et al., *Expression of the F-box protein SKP2 induces hyperplasia, dysplasia, and low-grade carcinoma in the mouse prostate.* Cancer Res, 2003. **63**(7): p. 1583-8.
225. Osoegawa, A., et al., *Regulation of p27 by S-phase kinase-associated protein 2 is associated with aggressiveness in non-small-cell lung cancer.* J Clin Oncol, 2004. **22**(20): p. 4165-73.
226. Sonoda, H., et al., *Significance of skp2 expression in primary breast cancer.* Clin Cancer Res, 2006. **12**(4): p. 1215-20.
227. Traub, F., et al., *Prognostic impact of Skp2 and p27 in human breast cancer.* Breast Cancer Res Treat, 2006. **99**(2): p. 185-91.
228. Nguyen, P.L., et al., *The impact of Skp2 overexpression on recurrence-free survival following radical prostatectomy.* Urol Oncol, 2011. **29**(3): p. 302-8.
229. Wang, J., et al., *E3-ligase Skp2 predicts poor prognosis and maintains cancer stem cell pool in nasopharyngeal carcinoma.* Oncotarget, 2014. **5**(14): p. 5591-601.
230. Yang, C., et al., *High Skp2/Low p57(Kip2) Expression is Associated with Poor Prognosis in Human Breast Carcinoma.* Breast Cancer (Auckl), 2015. **9**(Suppl 1): p. 13-21.
231. Calvisi, D.F., et al., *SKP2 and CKS1 promote degradation of cell cycle regulators and are associated with hepatocellular carcinoma prognosis.* Gastroenterology, 2009. **137**(5): p. 1816-26 e1-10.
232. Yokoi, S., et al., *Amplification and overexpression of SKP2 are associated with metastasis of non-small-cell lung cancers to lymph nodes.* Am J Pathol, 2004. **165**(1): p. 175-80.
233. Wei, Z., et al., *Downregulation of Skp2 inhibits the growth and metastasis of gastric cancer cells in vitro and in vivo.* Tumour Biol, 2013. **34**(1): p. 181-92.
234. Adams, J. and M. Kauffman, *Development of the proteasome inhibitor Velcade (Bortezomib).* Cancer Invest, 2004. **22**(2): p. 304-11.
235. Drugs.com, *Proteasome inhibitors.* 2018: p. https://www.drugs.com/drug-class/proteasome-inhibitors.html.
236. Landre, V., et al., *Screening for E3-ubiquitin ligase inhibitors: challenges and opportunities.* Oncotarget, 2014. **5**(18): p. 7988-8013.
237. ClinicalTrialsGov, *Bethesda (MD): National Library of Medicine (US).* 2018: p. http://www.clinicaltrials.gov.
238. Leung, C.H., et al., *A natural product-like inhibitor of NEDD8-activating enzyme.* Chem Commun (Camb), 2011. **47**(9): p. 2511-3.
239. Zhong, H.J., et al., *A metal-based inhibitor of NEDD8-activating enzyme.* PLoS One, 2012. **7**(11): p. e49574.
240. Jia, L., M.S. Soengas, and Y. Sun, *ROC1/RBX1 E3 ubiquitin ligase silencing suppresses tumor cell growth via sequential induction of G2-M arrest, apoptosis, and senescence.* Cancer Res, 2009. **69**(12): p. 4974-82.

241. Milhollen, M.A., et al., *MLN4924, a NEDD8-activating enzyme inhibitor, is active in diffuse large B-cell lymphoma models: rationale for treatment of NF-{kappa}B-dependent lymphoma.* Blood, 2010. **116**(9): p. 1515-23.
242. Jia, L., H. Li, and Y. Sun, *Induction of p21-dependent senescence by an NAE inhibitor, MLN4924, as a mechanism of growth suppression.* Neoplasia, 2011. **13**(6): p. 561-9.
243. Wang, X., et al., *Targeting the neddylation pathway to suppress the growth of prostate cancer cells: therapeutic implication for the men's cancer.* Biomed Res Int, 2014. **2014**: p. 974309.
244. Wang, Y., et al., *Targeting protein neddylation with an NEDD8-activating enzyme inhibitor MLN4924 induced apoptosis or senescence in human lymphoma cells.* Cancer Biol Ther, 2015. **16**(3): p. 420-9.
245. Wong, K.M., et al., *Targeting the protein ubiquitination machinery in melanoma by the NEDD8-activating enzyme inhibitor pevonedistat (MLN4924).* Invest New Drugs, 2017. **35**(1): p. 11-25.
246. Tong, S., et al., *MLN4924 (Pevonedistat), a protein neddylation inhibitor, suppresses proliferation and migration of human clear cell renal cell carcinoma.* Sci Rep, 2017. **7**(1): p. 5599.
247. Lan, H., et al., *Neddylation inhibitor MLN4924 suppresses growth and migration of human gastric cancer cells.* Sci Rep, 2016. **6**: p. 24218.
248. Swords, R.T., et al., *Inhibition of NEDD8-activating enzyme: a novel approach for the treatment of acute myeloid leukemia.* Blood, 2010. **115**(18): p. 3796-800.
249. Yang, D., et al., *The p21-dependent radiosensitization of human breast cancer cells by MLN4924, an investigational inhibitor of NEDD8 activating enzyme.* PLoS One, 2012. **7**(3): p. e34079.
250. Xie, P., et al., *Promoting tumorigenesis in nasopharyngeal carcinoma, NEDD8 serves as a potential theranostic target.* Cell Death Dis, 2017. **8**(6): p. e2834.
251. Vanderdys, V., et al., *The Neddylation Inhibitor Pevonedistat (MLN4924) Suppresses and Radiosensitizes Head and Neck Squamous Carcinoma Cells and Tumors.* Mol Cancer Ther, 2018. **17**(2): p. 368-380.
252. Wei, D., et al., *Radiosensitization of human pancreatic cancer cells by MLN4924, an investigational NEDD8-activating enzyme inhibitor.* Cancer Res, 2012. **72**(1): p. 282-93.
253. Yao, W.T., et al., *Suppression of tumor angiogenesis by targeting the protein neddylation pathway.* Cell Death Dis, 2014. **5**: p. e1059.
254. Paiva, C., et al., *Pevonedistat, a Nedd8-activating enzyme inhibitor, sensitizes neoplastic B-cells to death receptor-mediated apoptosis.* Oncotarget, 2017. **8**(13): p. 21128-21139.
255. Lin, W.C., et al., *MLN4924, a Novel NEDD8-activating enzyme inhibitor, exhibits antitumor activity and enhances cisplatin-induced cytotoxicity in human cervical carcinoma: in vitro and in vivo study.* Am J Cancer Res, 2015. **5**(11): p. 3350-62.
256. Nawrocki, S.T., et al., *Disrupting protein NEDDylation with MLN4924 is a novel strategy to target cisplatin resistance in ovarian cancer.* Clin Cancer Res, 2013. **19**(13): p. 3577-90.
257. Jazaeri, A.A., et al., *Overcoming platinum resistance in preclinical models of ovarian cancer using the neddylation inhibitor MLN4924.* Mol Cancer Ther, 2013. **12**(10): p. 1958-67.
258. Xu, Q., et al., *MLN4924 neddylation inhibitor promotes cell death in paclitaxel-resistant human lung adenocarcinoma cells.* Oncol Lett, 2018. **15**(1): p. 515-521.

259. Li, H., et al., *Inhibition of Neddylation Modification Sensitizes Pancreatic Cancer Cells to Gemcitabine.* Neoplasia, 2017. **19**(6): p. 509-518.
260. Chen, Q., et al., *Targeting the p27 E3 ligase SCF(Skp2) results in p27- and Skp2-mediated cell-cycle arrest and activation of autophagy.* Blood, 2008. **111**(9): p. 4690-9.
261. Chan, C.H., et al., *Pharmacological inactivation of Skp2 SCF ubiquitin ligase restricts cancer stem cell traits and cancer progression.* Cell, 2013. **154**(3): p. 556-68.
262. Ruan, D., et al., *Skp2 deficiency restricts the progression and stem cell features of castration-resistant prostate cancer by destabilizing Twist.* Oncogene, 2017. **36**(30): p. 4299-4310.
263. Ganoth, D., et al., *The cell-cycle regulatory protein Cks1 is required for SCF(Skp2)-mediated ubiquitinylation of p27.* Nat Cell Biol, 2001. **3**(3): p. 321-4.
264. Spruck, C., et al., *A CDK-independent function of mammalian Cks1: targeting of SCF(Skp2) to the CDK inhibitor p27Kip1.* Mol Cell, 2001. **7**(3): p. 639-50.
265. Wu, L., et al., *Specific small molecule inhibitors of Skp2-mediated p27 degradation.* Chem Biol, 2012. **19**(12): p. 1515-24.
266. Wen, Y., K. Wang, and K. Yang, *Inhibiting the role of Skp2 suppresses cell proliferation and tumorigenesis of human gastric cancer cells via the upregulation of p27kip1.* Mol Med Rep, 2016. **14**(4): p. 3917-24.
267. Sun, S.H., et al., *Cycle arrest and apoptosis in MDA-MB-231/Her2 cells induced by curcumin.* Eur J Pharmacol, 2012. **690**(1-3): p. 22-30.
268. Su, J., et al., *Curcumin inhibits cell growth and invasion and induces apoptosis through down-regulation of Skp2 in pancreatic cancer cells.* Am J Cancer Res, 2016. **6**(9): p. 1949-1962.
269. Feng, S., et al., *Curcumin exerts its antitumor activity through regulation of miR-7/Skp2/p21 in nasopharyngeal carcinoma cells.* Onco Targets Ther, 2017. **10**: p. 2377-2388.
270. Lin, H.P., et al., *Caffeic acid phenethyl ester induced cell cycle arrest and growth inhibition in androgen-independent prostate cancer cells via regulation of Skp2, p53, p21Cip1 and p27Kip1.* Oncotarget, 2015. **6**(9): p. 6684-707.
271. Yin, X., et al., *Rottlerin exerts its anti-tumor activity through inhibition of Skp2 in breast cancer cells.* Oncotarget, 2016. **7**(41): p. 66512-66524.
272. Ye, D., Z. Li, and C. Wei, *Genistein inhibits the S-phase kinase-associated protein 2 expression in breast cancer cells.* Exp Ther Med, 2018. **15**(1): p. 1069-1075.
273. O'Neill, A.J., et al., *Characterisation and manipulation of docetaxel resistant prostate cancer cell lines.* Mol Cancer, 2011. **10**: p. 126.
274. Liao, C.P., et al., *Mouse prostate cancer cell lines established from primary and postcastration recurrent tumors.* Horm Cancer, 2010. **1**(1): p. 44-54.
275. Ohta, T. and Y. Xiong, *Phosphorylation- and Skp1-independent in vitro ubiquitination of E2F1 by multiple ROC-cullin ligases.* Cancer Res, 2001. **61**(4): p. 1347-53.
276. Mosmann, T., *Rapid colorimetric assay for cellular growth and survival: application to proliferation and cytotoxicity assays.* J Immunol Methods, 1983. **65**(1-2): p. 55-63.
277. Slabakova, E., et al., *TGF-beta1-induced EMT of non-transformed prostate hyperplasia cells is characterized by early induction of SNAI2/Slug.* Prostate, 2011. **71**(12): p. 1332-43.
278. Carpenter, A.E., et al., *CellProfiler: image analysis software for identifying and quantifying cell phenotypes.* Genome Biol, 2006. **7**(10): p. R100.
279. Bray, M.A., et al., *Cell Painting, a high-content image-based assay for morphological profiling using multiplexed fluorescent dyes.* Nat Protoc, 2016. **11**(9): p. 1757-74.

280. Vindelov, L.L., *Flow microfluorometric analysis of nuclear DNA in cells from solid tumors and cell suspensions. A new method for rapid isolation and straining of nuclei.* Virchows Arch B Cell Pathol, 1977. **24**(3): p. 227-42.
281. Simeckova, S., et al., *Multiparameter cytometric analysis of complex cellular response.* Cytometry A, 2018. **93**(2): p. 239-248.
282. Taylor, B.S., et al., *Integrative genomic profiling of human prostate cancer.* Cancer Cell, 2010. **18**(1): p. 11-22.
283. Slabakova, E., et al., *Opposite regulation of MDM2 and MDMX expression in acquisition of mesenchymal phenotype in benign and cancer cells.* Oncotarget, 2015. **6**(34): p. 36156-71.
284. Dimberg, A., K. Nilsson, and F. Oberg, *Phosphorylation-deficient Stat1 inhibits retinoic acid-induced differentiation and cell cycle arrest in U-937 monoblasts.* Blood, 2000. **96**(8): p. 2870-8.
285. Jamur, M.C. and C. Oliver, *Permeabilization of cell membranes.* Methods Mol Biol, 2010. **588**: p. 63-6.
286. Remsik, J., et al., *Plasticity and intratumoural heterogeneity of cell surface antigen expression in breast cancer.* Br J Cancer, 2018. **118**(6): p. 813-819.
287. Pollice, A.A., et al., *Sequential paraformaldehyde and methanol fixation for simultaneous flow cytometric analysis of DNA, cell surface proteins, and intracellular proteins.* Cytometry, 1992. **13**(4): p. 432-44.
288. Schmid, I., C.H. Uittenbogaart, and J.V. Giorgi, *A gentle fixation and permeabilization method for combined cell surface and intracellular staining with improved precision in DNA quantification.* Cytometry, 1991. **12**(3): p. 279-85.
289. Kaufmann, S.H., et al., *Specific proteolytic cleavage of poly(ADP-ribose) polymerase: an early marker of chemotherapy-induced apoptosis.* Cancer Res, 1993. **53**(17): p. 3976-85.
290. Miura, M., et al., *Induction of apoptosis in fibroblasts by IL-1 beta-converting enzyme, a mammalian homolog of the C. elegans cell death gene ced-3.* Cell, 1993. **75**(4): p. 653-60.
291. Kubista, M., B. Akerman, and B. Norden, *Characterization of interaction between DNA and 4',6-diamidino-2-phenylindole by optical spectroscopy.* Biochemistry, 1987. **26**(14): p. 4545-53.
292. Hoshi, H., J. O'Brien, and S.L. Mills, *A novel fluorescent tracer for visualizing coupled cells in neural circuits of living tissue.* J Histochem Cytochem, 2006. **54**(10): p. 1169-76.
293. Wlodkowic, D., et al., *Apoptosis and beyond: cytometry in studies of programmed cell death.* Methods Cell Biol, 2011. **103**: p. 55-98.
294. Wahl, G.M. and B.T. Spike, *Cell state plasticity, stem cells, EMT, and the generation of intra-tumoral heterogeneity.* NPJ Breast Cancer, 2017. **3**: p. 14.
295. Fornaro, M., et al., *Cloning of the gene encoding Trop-2, a cell-surface glycoprotein expressed by human carcinomas.* Int J Cancer, 1995. **62**(5): p. 610-8.
296. Yang, Q., et al., *Acquisition of epithelial-mesenchymal transition is associated with Skp2 expression in paclitaxel-resistant breast cancer cells.* Br J Cancer, 2014. **110**(8): p. 1958-67.
297. Qu, X., et al., *A signal transduction pathway from TGF-beta1 to SKP2 via Akt1 and c-Myc and its correlation with progression in human melanoma.* J Invest Dermatol, 2014. **134**(1): p. 159-167.
298. Yan, W., et al., *Increased invasion and tumorigenicity capacity of CD44+/CD24- breast cancer MCF7 cells in vitro and in nude mice.* Cancer Cell Int, 2013. **13**(1): p. 62.

299. Li, W., et al., *Unraveling the roles of CD44/CD24 and ALDH1 as cancer stem cell markers in tumorigenesis and metastasis.* Sci Rep, 2017. **7**(1): p. 13856.
300. Meng, E., et al., *CD44+/CD24- ovarian cancer cells demonstrate cancer stem cell properties and correlate to survival.* Clin Exp Metastasis, 2012. **29**(8): p. 939-48.
301. Ghuwalewala, S., et al., *CD44(high)CD24(low) molecular signature determines the Cancer Stem Cell and EMT phenotype in Oral Squamous Cell Carcinoma.* Stem Cell Res, 2016. **16**(2): p. 405-17.
302. Klarmann, G.J., et al., *Invasive prostate cancer cells are tumor initiating cells that have a stem cell-like genomic signature.* Clin Exp Metastasis, 2009. **26**(5): p. 433-46.
303. Cremers, N., et al., *CD24 Is Not Required for Tumor Initiation and Growth in Murine Breast and Prostate Cancer Models.* PLoS One, 2016. **11**(3): p. e0151468.
304. Lu, Z., et al., *Skp2 suppresses apoptosis in Rb1-deficient tumours by limiting E2F1 activity.* Nat Commun, 2014. **5**: p. 3463.
305. Zhao, H., et al., *Skp2 deletion unmasks a p27 safeguard that blocks tumorigenesis in the absence of pRb and p53 tumor suppressors.* Cancer Cell, 2013. **24**(5): p. 645-59.
306. Puhr, M., et al., *PIAS1 is a crucial factor for prostate cancer cell survival and a valid target in docetaxel resistant cells.* Oncotarget, 2014. **5**(23): p. 12043-56.
307. Mulholland, D.J., et al., *Pten loss and RAS/MAPK activation cooperate to promote EMT and metastasis initiated from prostate cancer stem/progenitor cells.* Cancer Res, 2012. **72**(7): p. 1878-89.
308. Joza, N., et al., *Essential role of the mitochondrial apoptosis-inducing factor in programmed cell death.* Nature, 2001. **410**(6828): p. 549-54.
309. Lin, S., et al., *Neddylation inhibitor MLN4924 induces G2 cell cycle arrest, DNA damage and sensitizes esophageal squamous cell carcinoma cells to cisplatin.* Oncol Lett, 2018. **15**(2): p. 2583-2589.
310. Breinbauer, R. and M. Kohn, *Azide-alkyne coupling: a powerful reaction for bioconjugate chemistry.* Chembiochem, 2003. **4**(11): p. 1147-9.
311. Deveny, R., et al., *Improved click chemistry demonstrating EdU cell proliferation with GFP expressing cells and R-PE based immunophenotyping.(P3299).* . The Journal of Immunology, 2013. **190**(211.7).
312. Wilson, E.L., et al., Cytometry: Elsevier Science, 2000.
313. Jacob, M.C., M. Favre, and J.C. Bensa, *Membrane cell permeabilization with saponin and multiparametric analysis by flow cytometry.* Cytometry, 1991. **12**(6): p. 550-8.
314. Krutzik, P.O. and G.P. Nolan, *Intracellular phospho-protein staining techniques for flow cytometry: monitoring single cell signaling events.* Cytometry A, 2003. **55**(2): p. 61-70.
315. Molgaard, S., et al., *Detection of phosphorylated Akt and MAPK in cell culture assays.* MethodsX, 2016. **3**: p. 386-98.
316. Sabnis, R., *PO-PRO-1.* Handbook of Fluorescent Dyes and Probes: John Wiley & Sons,, 2015: p. 324-325.

8. LIST OF PUBLICATIONS AND MEETING CONTRIBUTIONS

8.1. ARTICLES PUBLISHED IN PEER-REVIEWED JOURNALS WITH IF

8.1.1. FIRST AUTHOR

- **Šárka Šimečková**, Radek Fedr, Ján Remšík, Zuzana Kahounová, Eva Slabáková, Karel Souček. **Multiparameter cytometric analysis of complex cellular response.** *Cytometry A. 2018 Feb; 93(2):239-248. doi: 10.1002/cyto.a.23295. IF 3.222 (2018)*
  Personal contribution (70 %): Conception and Design, Collection of data, Data analysis and interpretation, Manuscript writing

8.1.2. CO-AUTHOR

- Remšík Ján, Binó Lucia, Kahounová Zuzana., Kharaishvili Gvantsa, **Šimečková Šárka,** Fedr Radek., Kučírková Tereza, Lenárt Sára, Muresan Ximena Maria, Slabáková Eva, Knopfová Lucia, Bouchal Jan, Král Milan, Beneš Petr, Souček Karel. **Trop-2 plasticity is controlled by epithelial-to-mesenchymal transition.** *Carcinogenesis. 2018 Jul 16. doi: 10.1093/carcin/bgy095. IF 5.072 (2018)*
  Personal contribution (15 %): Conception and Design, Collection of data, Data analysis and interpretation

- Paculová Hana, Kramara Juraj, **Šimečková Šárka**, Souček Karel, Hylse Ondřej, Paruch Kamil, Svoboda Marek, Mastrík Martin, Kohoutek Jiří. **BRCA1 or CDK12 loss sensitizes cells to CHK1 inhibitors.** *Tumour Biology 2017 Oct;39(10):1010428317727479. doi: 10.1177/1010428317727479 IF 3.65 (2018)*; *Open acess*
  Personal contribution (10 %): Collection of data, Data analysis and interpretation

- Kahounová Zuzana, Kurfürstová Daniela, Bouchal Jan, Kharaishvili Gvantsa, Navrátil Jiří, Remšík Ján, **Šimečková Šárka**, Študent Vladimir, Kozubík Alois, Souček Karel. **The fibroblast surface markers FAP, anti-fibroblast, and FSP are expressed by cells of epithelial origin and may be altered during epithelial-to-mesenchymal transition.** *Cytometry A. 2017 Apr 6. doi: 10.1002/cyto.a.23101. IF 3.222 (2018)*
  Personal contribution (5 %): Collection of data

- Pernicová Zuzana, Slabáková Eva, Fedr Radek, **Šimečková Šárka**, Jaroš Josef, Suchánková Tereza, Bouchal Jan, Kharaishvili Gvantsa, Král Milan, Kozubík Alois, Souček Karel. **The role of high cell density in the promotion of neuroendocrine transdifferentiation of prostate cancer cells.** *Mol Cancer 2014 May 20;13:113. doi: 10.1186/1476-4598-13-113. IF 6.204 (2018); Open access*
  Personal contribution (10 %): Collection of data, Data analysis

8.2. MANUSCRIPTS

8.2.1. MANUSCRIPTS FIRST AUTHOR

- **Šimečková Šárka**, Kahounová Zuzana, Fedr Radek, Remšík Ján, Slabáková Eva, Bouchal Jan, Kharaishvili Gvantsa , Král Milan, Souček Karel. **High**

Skp2 expression is associated with mesenchymal and cancer stem-like cells phenotype. *Manuscript submitted to Scientific Report, under review*

Personal contribution (70 %): conception and design, collection of data, data analysis and interpretation, manuscript writing

8.2.2. MANUSCRIPTS CO-AUTHOR

- Radek Fedr, Zuzana Kahounová, Ján Remšík, **Šárka Šimečková**, Karel Souček. **Extent of autofluorescence, non-specific and specific immunofluorescence signals measured by flow cytometry associates with cell size and cell cycle progression.**
  manuscript in preparation

  Personal contribution (5 %): collection of data, data analysis and interpretation

8. 2. 3. MEETING CONTRIBUTIONS

8. 2.3.1. POSTER PRESENTATIONS (FIRST AUTHOR ONLY)

2017

Šárka Šimečková, Radek Fedr, Zuzana Kahounová, Ján Remšík, Eva Slabáková, Alena Mičková, Gvantsa Kharaishvili, Milan Král, Jan Bouchal, Karel Souček. Inhibition of SCF^{Skp2} affects characteristics of cancer stem-like cells. International Conference Analytical Cytometry IX, 14.-17. 10. 2017, Prague, Czech Republic, page 100, ISBN 978-80-88214-06-9

2016

Šimečková Šárka, Radek Fedr, Zuzana Pernicová, Eva Slabáková, Jan Bouchal, Gvantsa Kharaishvili, Milan Král, Alois Kozubík, Karel Souček. Inhibition of SCF^{Skp2} affects characteristics of cancer stem-like cells. The 12th Symposium & Workshop on Molecular Pathology and Histo(cyto)chemistry, 2.-3.6.2016, Olomouc, Czech Republic, page 42, ISBN 978-80-7471-150-3

Šimečková Šárka, Fedr Radek, Pernicová Zuzana, Slabáková Eva, Bouchal Jan, Kharaishvili Gvantsa, Král Milan, Kozubík Alois, Souček Karel. Inhibition of SCF^{Skp2} affects characteristics of cancer stem-like cells. EMBO meeting: Cellular signaling and Cancer therapy, 27.-31.5.2016, Dubrovnik, Croatia, page 220

2015

Šimečková Šárka, Fedr Radek, Pernicová Zuzana, Kozubík Alois, Souček Karel. Multiparametric analysis of complex cellular response to the experimental treatment using flow cytometry. V4 International Conference in Analytical Cytometry VIII, 3.10. -6.10.2015, Olomouc, Czech Republic, page 142, ISBN 978-80-906086-2-7

Šimečková Šárka, Remšík Ján, Pernicová Zuzana, Fedr Radek, Smějová Monika, Kozubík Alois, Souček Karel. Trop-2 expression defines prostate cancer cells in different EMT state. 11th World Congress on Urological Research, 10.-12.9.2015, Nijmegen, Netherlands, page 146

Šimečková Šárka, Remšík Ján, Pernicová Zuzana, Fedr Radek, Smějová Monika, Kozubík Alois, Souček Karel. Loss of Trop-2 expression is associated with mesenchymal phenotype in prostate cancer cells. 30th Congress of the International Society for Advancement of Cytometry, 26.-30.5.2015, Glasgow, United Kingdom, page 236

2014

Šimečková Šárka, Pernicová Zuzana, Fedr Radek, Bouchal Jan, Kharaishvili Gvantsa, Král Milan, Kozubík Alois, Souček Karel. Pharmacological inhibition of SCF^{Skp2} complex activity affects characteristics of cancer stem-like cells. EMBO meeting: Cellular signaling and Cancer therapy, 23.-27.5.2014, Dubrovnik, Croatia, page 239, ISBN 978-3-00-045429-5.

2013

Šimečková Šárka, Pernicová Zuzana, Fedr Radek, Eva Sedlmaierová, Kozubík Alois, Souček Karel. Pharmocological inhibition of Skp2-SCF complex activity as an approach to modulate characteristics of cancer stem-like cells. V4 International Conference Analytical Cytometry VII, Mikulov, 21.-24.9. 2013, page128, ISBN 978-80-905449-2-5

8. 2.3.2. LECTURES

2015

Pros and Cons of multiparametric flow cytometry. V4 International Conference in Analytical Cytometry VIII, 3. – 6. 10. 2015, Olomouc, Czech Republic

2014

Pharmacological inhibition of SCF^{Skp2} complex activity affects characteristics of cancer stem-like cells

OrganoNET 2014 Conference, 19.-20.6. 2014, Brno, Czech Republic

APPENDICES

Appendix I

High Skp2 expression is associated with a mesenchymal phenotype and increased tumorigenic potential of prostate cancer cells

Šárka Šimečková[1,2,3], Zuzana Kahounová[1], Radek Fedr[1,2], Ján Remšík[1,2,3*], Eva Slabáková[1], Jan Bouchal[4], Gvantsa Kharaishvili[4], Milan Král[5], Petr Beneš[2,3], Karel Souček[1,2,§]

[1]Department of Cytokinetics, Institute of Biophysics of the Czech Academy of Sciences, Brno, Czech Republic
[2]Center of Biomolecular and Cellular Engineering, International Clinical Research Center, St. Anne´s University Hospital Brno, Brno, Czech Republic
[3]Department of Experimental Biology, Faculty of Science, Masaryk University, Brno, Czech Republic
[4]Department of Clinical and Molecular Pathology, Institute of Molecular and Translational Medicine, Faculty of Medicine and Dentistry, Palacky University, Olomouc, Czech Republic
[5]Department of Urology, University Hospital, Olomouc, Czech Republic
[*]Current address: Human Oncology & Pathogenesis Program, Memorial Sloan Kettering Cancer Center, New York, New York 10065, USA
[§] corresponding author

Skp2 is a crucial component of SCF^{Skp2} E3 ubiquitin ligase and is often overexpressed in various types of cancer, including prostate cancer (PCa). The epithelial-to-mesenchymal transition (EMT) is involved in PCa progression. The acquisition of a mesenchymal phenotype that results in a cancer stem cell (CSC) phenotype in PCa was described. Therefore, we aimed to investigate the expression and localization of Skp2 in clinical samples from patients with PCa, the association of Skp2 with EMT status, and the role of Skp2 in prostate CSC. We found that nuclear expression of Skp2 was increased in patients with PCa compared to those with benign hyperplasia, and correlated with high Gleason score in PCa patients. Increased Skp2 expression was observed in PCa cell lines with mesenchymal and CSC-like phenotype compared to their epithelial counterparts. Conversely, the CSC-like phenotype was diminished in cells in which SKP2 expression was silenced. Furthermore, we observed that Skp2 downregulation led to the increase in expression of both CD24 and CD44. Finally, we showed that high expression levels of both CD24 and CD44 were associated with favorable recurrence-free survival for PCa patients. This study uncovered the Skp2-mediated CSC-like phenotype with oncogenic functions in PCa.

Introduction

Prostate cancer is the second leading cause of cancer-related deaths in men in western countries (1). Resistance to conventional treatments and development of castration-resistant prostate cancer remain challenges of current prostate cancer therapies. The need for identification of new targets to treat this disease is therefore tremendous.

The epithelial-to-mesenchymal transition (EMT) is a physiological process during embryogenesis that may become reactivated in cancer. It is characterized by the loss of cell-to-cell adhesion and apical-basal polarity, and the gain of migratory behavior (2). EMT has been described as a crucial step in the progression and metastasis of prostate cancer (3). Furthermore, the acquisition of a mesenchymal phenotype, concomitant with a cancer stem cell (CSC) phenotype, in prostate cancer has been shown previously (4-6). EMT and CSCs play important roles in the development of drug resistance in cases of prostate cancer (7).

CSCs have been described as a small subset of cells within a heterogeneous tumor that share a number of features with normal stem cells. CSCs are characterized by self-renewal, the expression of specific surface markers, and aldehyde dehydrogenase (ALDH) activity (8,9); CSCs are also involved in tumor initiation, metastasis, and chemoresistance (10). The CSC marker CD24 has been described as a marker that distinguishes poorly differentiated cells from transit-amplifying cells in the basal layer of the human prostate (11). Cells with a $CD24^-$ $CD44^+$ phenotype are commonly used to define prostate CSCs (12,13).

The cyclin-dependent kinase inhibitor $p27^{Kip1}$ was shown to control both stem cell renewal and EMT in embryonic stem cells (14). Importantly, S-phase kinase-associated protein 2 (Skp2) is the main regulator of $p27^{Kip1}$ protein stability (15,16). High expression of Skp2 in tumors, accompanied by $p27^{Kip1}$ downregulation, has been correlated with poor prognosis in cancer patients; Skp2 has also been implicated as a prognostic marker in many types of cancer, including prostate cancer (17,18). Skp2 is a variable component of SCF^{Skp2} (Skp, Cullin, F-box containing complex) E3 ubiquitin ligase, which is responsible for recognizing many substrates that are targeted for degradation in the proteasome (19). The mechanisms that control Skp2 expression are not fully understood (20). In prostate cancer, putative regulatory mechanisms of Skp2 include those involving the androgen receptor (21), PTEN (17), and PI3K/Akt (22). In mice, an essential role of Skp2 in the development of prostate cancer was described as overexpression of Skp2 in the prostate gland induced hyperplasia, dysplasia, and

low-grade carcinoma (23). Conversely, Skp2 inactivation, together with senescence-induced oncogenic stress, was shown to profoundly restrict tumorigenesis in vivo (24).
The roles of Skp2 in both EMT and cancer stem-like cells in prostate cancer have not been fully elucidated. Herein, we show an association between elevated Skp2 levels and an EMT phenotype in patients with prostate cancer as well as in prostate cancer cell lines. Moreover, a mesenchymal phenotype was found to be associated with characteristics of cancer stem-like cells, including a DU 145 cell phenotype that was altered after Skp2 downregulation.

Material and Methods

Chemicals

DMSO (Sigma-Aldrich, St. Luis, MO, USA); 0.05% Trypsin-EDTA (GE Healthcare Life Sciences, Little Chalfont, UK); 1% BSA (Serva, Germany) in PBS with 0.01% NaN3 (Sigma-Aldrich); 0.25% Triton X-100 (Sigma-Aldrich) solution in PBS; 4% Paraformaldehyde solution (Sigma-Aldrich) in PBS; Aldehyde dehydrogenase-based cell detection kit (StemCell 01700); Fumitremorgin C (Abcam, ab144258); For detail specification regarding used antibodies - see Supplementary Table S1, S3, S4).

Cell culture

DU 145 cells were obtained from ATCC and cultivated in RPMI 1640 (Thermo Fisher Scientific, TFS, Waltham, MA, USA) with 10 % of fetal bovine serum (FBS; TFS), penicillin (100 U/ml) and streptomycin (0.1 mg/ml; Biosera, Nuaille, France). PC-3 cells were cultivated in Ham's F12 media (TFS) with 10 % of FBS, penicillin and streptomycin. E2 and cE2 murine prostate adenocarcinoma cells (25) (a generous gift from Dr. Pradip Roy Burman, University of Southern California, Los Angeles, CA), were cultivated as described in (25). PC-3 AC and PC-3 DR12 cells were obtained from prof. Watson (Dublin, Ireland) and cultivated as described (26).
All cell lines were cultivated in TPP (Trasadingen, Switzerland), flasks, and, plates in a humidified incubator at 37°C in an atmosphere of 5% CO2. The cells were harvested by washing with 0.05% EDTA in PBS followed by trypsinization (0.05 % w/v trypsin/0.53 mM Trypsin-EDTA). The AmpFLSTR® Identifiler® PCR Amplification Kit (TFS) was used to verify the origin of cell lines.

Electrophoresis and western blotting

The procedure was performed as described previously (27). Antibodies used for western blot are listed in Supplementary Table S1.

RNA isolation and qPCR analysis

Total RNA was isolated using a High Pure RNA Isolation Kit (Roche) and equal amounts of RNA were reverse transcribed using a High Capacity RNA-to-cDNA Kit (Life Technologies). Quantitative RT-PCR was carried out as described previously (27) using TaqMan assays with primers and conditions specified in Supplementary Table S2. Relative changes in gene expression were calculated using the E-method based on real efficiency values obtained from calibration curves (28).

Preparation of SKP2 KD cell lines

DU 145 were transfected with Skp2 p45 CRISPR/Cas9 KO Plasmid (h) (sc-400534) and Skp2 p45 CRISPR/Cas9 KO Plasmid HDR (sc-400534) using Lipofectamine 3000 (TFS) as recommended to prepare *SKP2* KD cell lines or with Control CRISPR/Cas9 Plasmid (sc-418922, all SCBT) and empty vector pIRES puro2 (kindly provided by V. Bryja, Masaryk University, Brno, Czech Republic) to prepare control cells. Cells were selected in media with puromycin (300 ng/ml; TFS) for one week. RFP positive single cells (indicating insertion of the plasmid with puromycin resistance in a site of CRISPR deletion) were sorted using FACSAria II Sorp system using a 100-µm nozzle (20 psi) to obtain single cell-derived SKP2 KD clones. To prepare control cell lines, cells underwent the same procedure as *SKP2* KD cells. Therefore, viable single cells were sorted. Post-sorting purity was determined immediately after sorting. The protein level of Skp2 in *SKP2* KD and control cells was examined by western blot.

Spheroids formation assay

For spheroid formation assay, cells were seeded in semisolid media (0.1% agarose in complete culture media) on plates precoated with 0.5% agar and cultured for three weeks. Cells were seeded in low density, 500 cells/well in a 6-well plate. Spheroids were stained with MTT (29) and counted using ImageJ software (NIH). For analysis of cancer stem cells markers in 3D, cells were seeded in high density (10 000 cells/well in 6 well plate) in semisolid media (0.1% agarose in complete culture media) on plates precoated with 0.5% agar and cultivated for three weeks. Spheroids were harvested, incubated with prewarmed PBS/EDTA and Trypsin to obtain a single cell suspension. Cells were then stained with antibodies according to standard procedure and analyzed on a flow cytometer.

Flow cytometry analysis

Sample acquisition was performed with using FACSVerse (BD Biosciences). Flow cytometric data were analyzed using FlowJo software (Version 10.0.7, Tree Star, Ashland, OR, USA). Details about antibodies used are listed in Supplementary Table S3. Immunophenotype analysis was performed as described previously (30). Cells were harvested using PBS/EDTA and Trypsin and stained with particular antibodies or probes. Cell cycle analysis was performed as described previously (21). ALDH1 activity was analyzed according to manufacturer's protocol and as described previously (31). Dead cells, aggregates, and debris were excluded from analysis.

Cell painting and morphology analysis

The cells were seeded in density 50 000 cells/cm2 into 4 wells per clone into 384 black well plate (Falcon, # 353962) and grown for 2 days at standard conditions. Next, cells were

stained with Hoechst 33342, concanavalin A, SYTO14, phalloidin, wheat germ agglutinin and MitoTracker as described previously (32) with using epMotion 5075 (Eppendorf) liquid handling workstation. Images were acquired with using ImageXpress Micro (Molecular Devices) fluorescence microscope (40x objective). Briefly, 5 fluorescence channels – using DAPI, Cy3, GFP, TxRed, Cy5 filters were captured from 35 sites in each well or 1000 cells per well were acquired with adaptive acquisition set up. Spill overs of fluorescence from different channels were compensated by subtraction of dim signal based on single stained compensation controls. Representative images were artificially colored and scale bar was burned into images using ImageJ 1.51p (NIH). Acquired images were processed based on the original cell painting protocol (32). Objects of nuclei, cytoplasm and whole cell areas were segmented and together 1785 features were calculated from 5 fluorescence channels on these three objects with using CellProfiler v2.2.0 software (33). Data were scaled, missing data and constant values in specific features were removed before principal component analysis and t-SNE analysis (perplexity 1605, nr. of iterations 500, minimum cost value 0.5) were performed. Plots were produced in R (RStudio, Inc., Boston, MA, USA).

Tumorigenic potential of SKP2 KD cell lines

The colony of severe combined immunodeficient animals (Crl:SHO-PrKDscid/Hrhr) was acquired from Charles River (Sulzfeld, Germany) and maintained according to the ARRIVE guidelines. Cells were injected into the right flank (1×106 cells/mice; 10 mice per group) and six weeks after injection, mice were sacrificed. Tumor formation rate was then calculated for both control and *SKP2* KD cells. The rate was calculated as a ratio of number of mice inoculated with cancer cell and number of mice bearing tumors. All procedures involving animals were performed according to the EU Directive 2010/63/EU for animal experiments and approved by the Academy of Sciences of the Czech Republic (AVCR 2013/13); supervised by the local ethical committee of the Institute of Biophysics of the Czech Academy of Sciences and performed by certified individuals.

Immunostaining of clinical samples

Retrospective analysis of tissue samples was performed in three independent sets of patients with prostate carcinoma. The main set included 187 tissue samples (33 samples of BPH, 101 samples of PCa, 35 samples of seminal vesicles and 18 positive lymph nodes). Samples were examined for expression of Skp2, E-Cadherin, and Slug. Samples were obtained from patients, who signed written informed consent, in the University Hospital Olomouc and the study was approved by the Ethics Committee of the University Hospital and Medical Faculty of Palacky University in Olomouc. Immunostaining was performed using routine immunostaining procedures with validated antibodies specified in Supplementary Table S4.

Skp2 overexpression analysis

Cells were transfected using Neon transfection system (TFS) with control plasmid (pcDNA3.1) or pcDNA3-myc-Skp2 that was a gift from Axel Brunger (Addgene Plasmid #19947) (34), incubated for two days and harvested for flow cytometric analysis to detect surface markers.

Survival data analysis

Data were retrieved from (35), (GEO accession no. GSE21032). Data for recurrence-free survival were re-analysed and plotted in Prism (v6, GraphPad, La Jolla, California, United States) using logrank Mantel-Cox test. The threshold for CD24 and CD44 was set to 'low 25%'.

Statistical analysis

Statistical analysis was performed using STATISTICA for Windows (StatSoft, Prague, Czech Republic) using Student´s t-test.

Results

High nuclear Skp2 expression and mesenchymal phenotype is associated with high Gleason score in patients with prostate cancer

To confirm the role of Skp2 in prostate cancer progression, we performed a retrospective analysis of Skp2 expression in patients with benign hyperplasia and prostate carcinoma (Table S5 and S6). Our results show that the nuclear expression of Skp2 was significantly increased in prostate cancer tissues compared to benign hyperplasia tissues (Figure 1A). High Gleason score (≥ 7) was associated with high nuclear, but not cytoplasmic, Skp2 expression (Figure 1B and Supplementary Figure 1). Moreover, high Gleason score was associated with a mesenchymal phenotype, as demonstrated by decreased E-cadherin expression and increased vimentin expression (Figure 1C). Thus, we showed that nuclear expression of Skp2 is significantly increased in patients with a high Gleason score (≥ 7) whose cancer cells exhibit characteristics of the mesenchymal state.

Increased Skp2 is associated with mesenchymal phenotype of prostate cancer cells

To assess the connection between Skp2 expression and a mesenchymal phenotype in prostate cancer cells, we employed three sets of prostate epithelial cell lines and their mesenchymal counterparts. To verify the epithelial characteristics of these cells, we confirmed the expression of both E-cadherin and Trop-2, which belong to the same gene family as does EpCAM, and whose overexpression has been described in various human epithelial cancers. The induction of mesenchymal phenotype was defined by the expression of vimentin, N-cadherin and transcription repressor of E-cadherin, ZEB1. Moreover we documented the differences in morphology of mesenchymal and epithelial sublines using cell painting protocol 32 and unsupervised image analysis (Figure 2A, Supplementary Figure 3D, E).

In the cell lines used, an EMT phenotype was induced

by different processes. We compared human DU 145 epithelial and mesenchymal sublines (Figure 2A and B, Supplementary Figure 3D, E) that were previously prepared in our laboratory (36). We then used age-control PC-3 cells (AC; epithelial) and docetaxel-resistant PC-3 cells (DR; mesenchymal), in which the acquisition of docetaxel resistance was accompanied by EMT (26). Lastly, we employed mouse prostate adenocarcinoma cell lines with a biallelic PTEN depletion: cE2 (epithelial, androgen independent) and E2 (mesenchymal, androgen dependent) (25,27) (Supplementary Figure 2). We found that the mesenchymal phenotype of prostate cancer cells was accompanied by an increase in Skp2 levels in all selected pairs of cell lines (Figure 2B, Supplementary Figure 2).

Mesenchymal DU145 cells exhibit characteristics of cancer stem-like cells

The properties of cancer stem-like cells were further investigated in epithelial and mesenchymal sublines established from DU 145 cells. We observed that mesenchymal cells are enriched in a $CD24^{-}CD44^{+}$ subpopulation (Figure 3A and B, Supplementary Figure 3A). Increased expression of CD24 in epithelial cells was also confirmed at the mRNA level (Supplementary Figure 3B). Thereafter, epithelial and mesenchymal cells were seeded at low densities in semisolid media to examine their ability to grow in anchorage-independent conditions and form spheroids. The cancer stem-like cell phenotype of the mesenchymal cells was illustrated by their increased ability to form spheroids (Figure 3C and D). This phenomenon was not caused by increased proliferation, as there were no differences in proliferation between mesenchymal and epithelial cells (Supplementary Figure 3C). The cancer stem-like properties of mesenchymal DU 145 cells were further confirmed by the increased activity of ALDH1 (Figure 3E). Thus, we showed that DU 145 cells with a mesenchymal phenotype and high expression of Skp2 exhibit CSC characteristics compared to their epithelial counterparts.

Decreased clonogenic and tumorigenic potential of DU 145 SKP2 KD cells is accompanied by increased CD24 and CD44 expression

To further ascertain the role of Skp2 in cancer stem-like cells, we decided to knock down Skp2 expression in DU 145 mesenchymal cells (DU 145 *SKP2* KD cells; Figure 4A) and analyze their tumorigenic capacity in vitro and in vivo. Silencing of Skp2 resulted in the accumulation of its substrate $p27^{Kip1}$ (Figure 4A). CD24 and CD44 expression was significantly increased in *SKP2* KD cells both at the protein (Figure 4B and C) and mRNA level (Supplementary

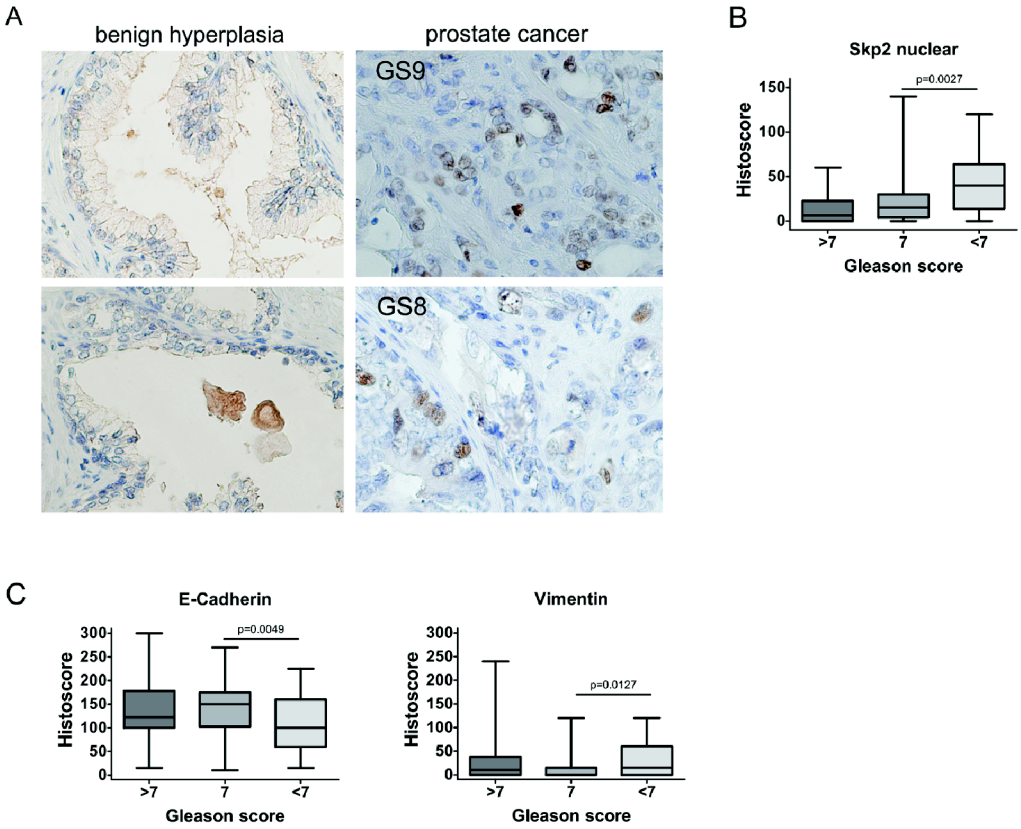

Figure 1. Nuclear Skp2 expression is associated with a high Gleason score in prostate cancer patients. (A) Patient samples from primary prostate carcinoma and benign hyperplasia were stained with anti-Skp2 antibody. Magnification: 40×. (B) Correlation of Skp2 with Gleason score. (C) Correlation of EMT-related marker (E-cadherin and vimentin) expression with Gleason score.

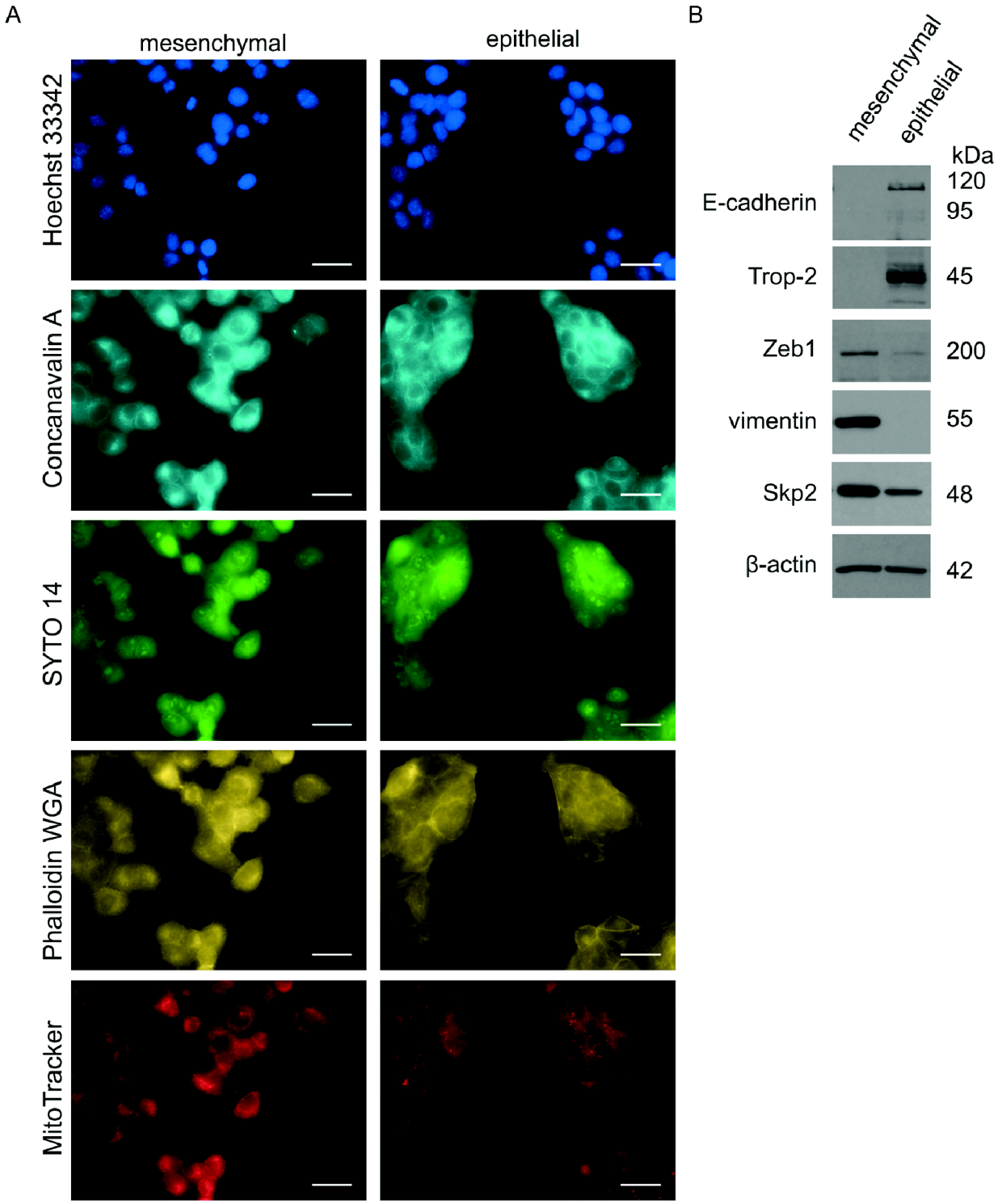

Figure 2. Increased Skp2 expression is associated with the mesenchymal phenotype of prostate cancer cells. (A) Representative images of mesenchymal and epithelial DU 145 sublines, scale bar size 30 µm. The nuclei (Hoechst 33342), endoplasmic reticulum (Concanavalin A), nucleoli and cytoplasmic RNA (SYTO 14), actin, Golgi apparatus, plasma membrane (Phalloidin&WGA) and mitochondria (MitoTracker) were visualized according cell painting protocol. (B) Expression of mesenchymal and epithelial markers and Skp2 in sublines of DU 145 cells by western blot. Representative images are from three independent experiments. β-actin was used as a loading control.

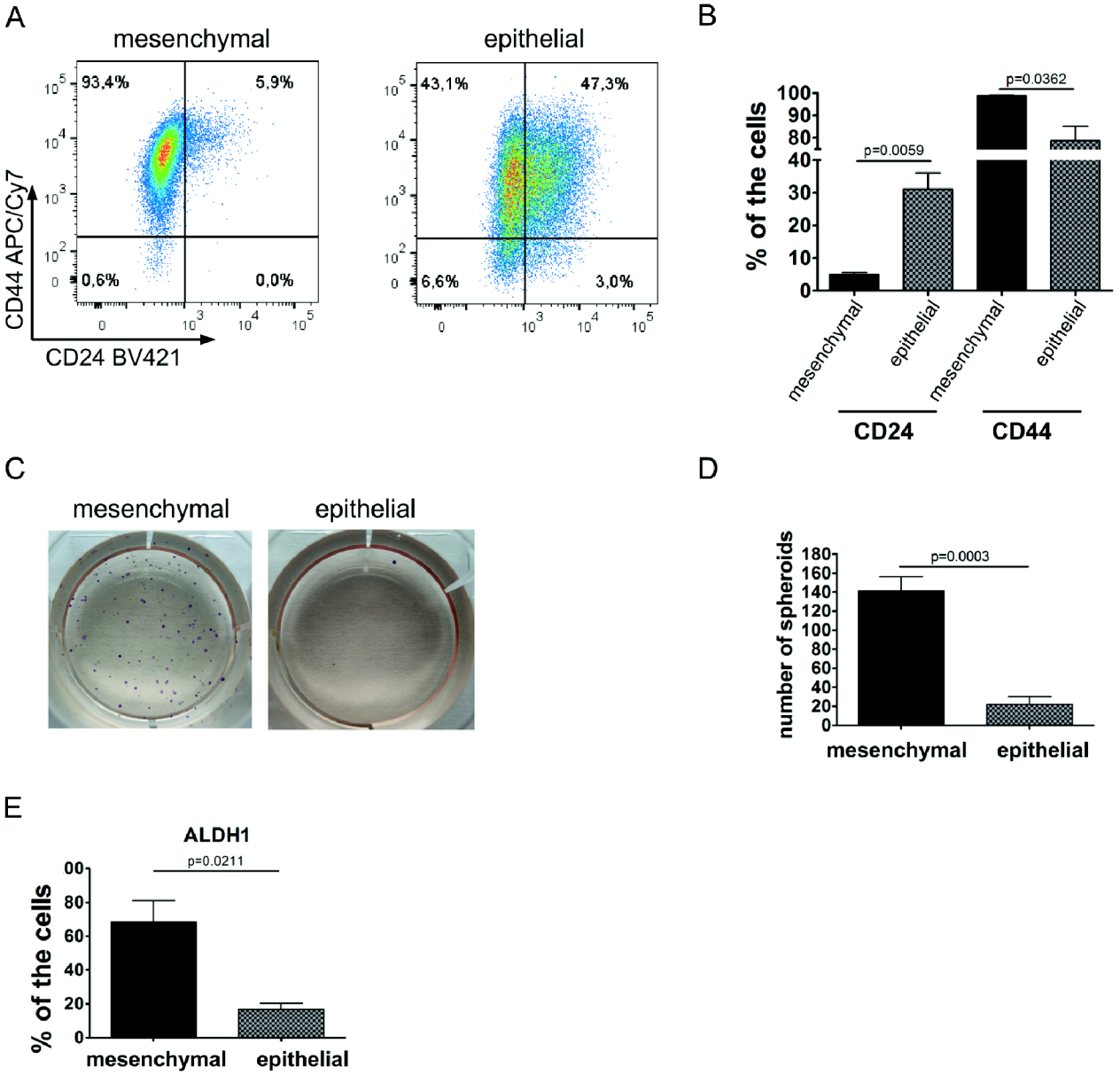

Figure 3. DU 145 cells with a mesenchymal phenotype are considered cancer stem-like cells. (A) Subpopulation of $CD24^{-}CD44^{+}$ CSCs in populations of mesenchymal and epithelial DU 145 cells. (B) Quantitation of results shown in (A). Bars show the mean ± SD of the percentage of positive cells for both markers. Results are from three independent repetitions. (C) Spheroid formation and growth in anchorage-independent conditions in DU 145 mesenchymal and epithelial cells. (D) Quantitation of results shown in (C). Data are shown as the mean ± SD of the number of spheroids per well. Results are from three independent repetitions. (E) ALDH1 activity in DU 145 mesenchymal and epithelial cells. Data are presented as the mean ± SD of the percentage of cells with active ALDH1. Results are from three independent repetitions.

Figure 4A).

We then examined the ability of these cells to grow in the anchorage-independent conditions and form spheroids. We found that the sphere-forming ability of *SKP2* KD cells was significantly decreased (Figure 4D and E), whereas Skp2 knock-down itself did not impair cellular proliferation (Supplementary Figure S4B). Moreover, the cells cultivated in 3D conditions maintained their phenotype in terms of CD24 and CD44 expression (Supplementary Figure 4C and D).

Next, *SKP2* KD cells were injected into immunodeficient mice, and the rate of xenograft formation was recorded. Our results showed that Skp2 knock-down significantly decreased the tumorigenic potential of DU 145 mesenchymal cells (Figure 4F). Furthermore, the activity of ALDH1 was decreased in these cells (Figure 4G). In conclusion, our data confirm that Skp2 silencing decreases the tumorigenic potential of mesenchymal DU 145 cells

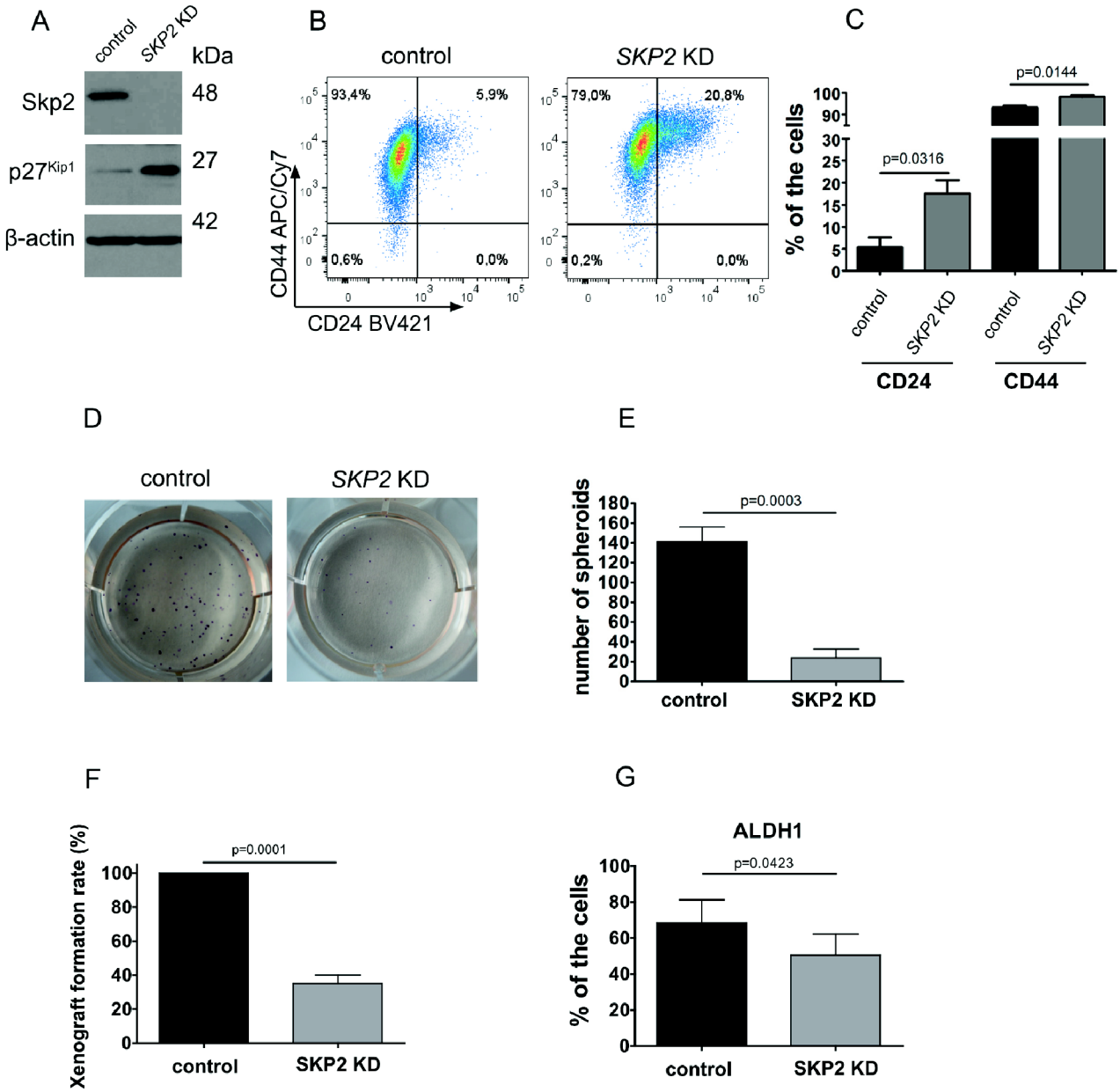

Figure 4. Decreased clonogenic and tumorigenic potential of DU 145 *SKP2* KD cells is accompanied by increases in CD24 and CD44 expression. (A) Skp2 and p27^{Kip1} expression in *SKP2* KD cells was determined by western blot. Representative images are from three independent experiments. β-actin was used as a loading control. (B) CD24 and CD44 expression in *SKP2* KD cells. (C) Quantitation of results shown in (B). Data are presented as the mean ± SD of the percentage of positive cells for the selected markers. Representative images are from three independent experiments. (D) Capability of spheroid formation and growth in anchorage-independent conditions in *SKP2* KD cells and control cells. (E) Quantitation of results shown in (D). Data are shown as the mean ± SD of the number of spheroids per well. Results are from three independent repetitions. (F) Xenograft formation rate of *SKP2* KD cells in SHO mice. Tumor formation rate was then calculated for control and *SKP2* KD cells. Number of mice per group, n = 10. (G) ALDH1 activity in DU 145 mesenchymal cells with Skp2 knocked down. Data are presented as the mean ± SD of the percentage of cells with active ALDH1. Results are from three independent experiments.

and affects the functional properties of cancer stem-like cells.

Skp2 overexpression induces decrease of CD24 in DU 145

In our study, we observed a negative correlation between the decreased expression of Skp2 and the increased expression of CD24 in epithelial DU 145 cells compared to their mesenchymal counterparts (Figures 2B and 3A). Importantly, CD24 expression was increased in DU 145 *SKP2* KD cells (Figure 4B and C, Supplementary Figure 4A). Therefore, we hypothesized that Skp2 overexpression

leads to decreased CD24 expression in the DU 145 parental cell line. Indeed, we observed that in cells with transient Skp2 overexpression (Supplementary Figure 5A), CD24 expression was decreased (Supplementary Figure 5B). Thus, we showed that Skp2 is important for maintaining the cancer stem-like phenotype of DU 145 mesenchymal cells in term of the expression of the CSC marker CD24. Our results suggest that the high expression of CD24 is linked to the epithelial and less aggressive phenotype of metastatic prostate cancer cells, accompanied by the low expression of Skp2. Conversely, low CD24 expression is linked to the mesenchymal phenotype of metastatic prostate cancer cells that have characteristics of cancer stem-like cells associated with high Skp2 expression. As Skp2 overexpression has been correlated with poor prognosis in prostate cancer patients, we wanted to reveal whether low CD24 expression would be associated with a better prognosis. To investigate the association of CD24 and CD44 expression with recurrence-free survival, we analyzed cohorts of prostate cancer patients (35) and confirmed that high expression levels of both markers (CD24 and CD44) were associated with favorable recurrence-free survival (Figure 5).

Discussion

In our work, we showed that Skp2 expression was increased in cancerous prostate tissue compared to benign prostate tissue, specifically in tumors with a high Gleason score (≥ 7). Poorly differentiated tumors also had lower expression levels of E-cadherin and higher levels of vimentin, suggesting the ongoing EMT of prostate cancer cells.

Our results confirmed that Skp2 expression was increased in mesenchymal prostate cancer cells compared to their epithelial counterparts. Yet, the acquisition of the mesenchymal phenotype was associated with increased Skp2 expression in paclitaxel-resistant breast cancer cells (37) and TGF-β1-induced EMT in melanoma cells (38). Importantly, Ruan et al. revealed that Skp2 regulates castration-resistant prostate cancer through Twist-mediated oncogenic functions including EMT and CSC acquisitions (6).

We demonstrated that the mesenchymal state of DU 145 cells exhibited CSC properties: decreased expression levels of CD24, increased ability to form spheroids, and high ALDH1 activity. These results are consistent with the acquisition of the CSC phenotype, which correlates with the mesenchymal state of the cancer cells. The $CD24^{-}CD44^{+}$ phenotype has been associated with CSCs, and the mesenchymal phenotype has been observed in several cancers, including breast cancer (39,40), ovarian cancer (41), and oral squamous carcinoma (42). Similarly, prostate cancer cells with the $CD24^{-}CD44^{+}$ phenotype have been described as mesenchymal (43). These results are in agreement with the work of Cremers et al. who showed that CD24 was not required for tumor initiation and growth in murine models of breast cancer and prostate cancer (44). The mesenchymal state caused by docetaxel resistance in DU 145 and PC3 cells was linked to the acquisition of the $CD24^{-}CD44^{+}$ phenotype (4,5). Further, it was shown that the overexpression of the mesenchymal-related genes ZEB1 and VIM correlated with shorter radiologic progression, whereas low expression levels of CD24 correlated with shorter biochemical recurrence-free survival of patients with prostate cancer (5).

To further assess the role of Skp2 in the tumorigenesis of the prostate cancer stem-like cells, we employed DU 145 cells in which *SKP2* had been knocked down. We confirmed that the knock-down of Skp2 significantly reduced the ability of these cells to form spheroids in vitro and decreased tumorigenic potential in vivo. Our findings are in agreement with the work of Lu *et al.* who found that Skp2 deficiency led to the suppression of prostate tumorigenesis. These authors showed that Skp2 was involved in tumorigenesis via the repression of H3K4-specific demethylase JARID1B (45). Another study showed that Skp2 deficiency blocked tumorigenesis in the pRb/p53 double-deficient prostate tissue, suggesting that Skp2 was a promising target for drug treatment in pRb/p53-deficient tumors (46). In addition to the decreased tumorigenicity of *SKP2* KD cells, we observed the upregulation of CD24

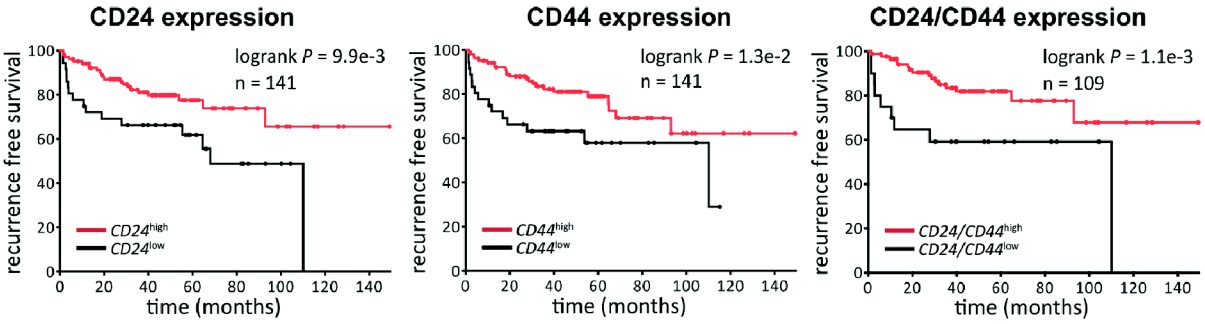

Figure 5. CD24 and CD44 expression is associated with better prognosis for prostate cancer patients. The graphs show an analysis of recurrence-free survival analysis in a cohort of prostate cancer patients, according to high or low CD24 (left), CD44 (middle), and CD24CD44 (right) expression levels. Data were retrieved from (35). Data were plotted and reanalyzed using Prism (v6, GraphPad) using the log rank Mantel-Cox test. The threshold for CD24 and CD44 was set to 'low 25%.'

expression and the decreased activity of ALDH1. These findings are in line with those of Zhao et al., where Skp2 downregulation or its pharmacological inhibition decreased the activity of ALDH1 (46).

An analysis of biochemical recurrence-free survival revealed that high expression levels of CD24 and CD44 were associated with a better prognosis for patients. These findings are in line with the work of Marin-Aguilera *et al.* who showed that low mRNA levels of CD24 correlated with shorter biochemical recurrence-free survival of patients with prostate cancer (5). A decreased number of CD24-positive cells were also associated with the mesenchymal phenotype and DU 145 cell chemoresistance (5,47). Furthermore, prostate cancer cells with low CD24 expression levels displayed high tumorigenic potential (48), which is in line with our findings.

Conclusion

In conclusion, we showed that the nuclear expression of Skp2 is associated with a high Gleason score. High Skp2 expression is further associated with the mesenchymal phenotype in prostate cancer patients and in vitro. Our results demonstrated that high expression levels of Skp2 were associated with the mesenchymal state and CSC characteristics. Lastly, we showed an inverse relationship between Skp2 and CD24 expression, suggesting that Skp2 is a promising marker for prostate cancer susceptibility. In overall, we demonstrated potential of Skp2 targeting in prostate cancer treatment.

Acknowledgment

This work was supported by grants GA CR P301/12/P407, IGA MZD NT13573-4/2012, and AZV ČR 15-28628A & 15-33999A, and supported by project no. LQ1605 from the National Program of Sustainability II (MEYS CR) and by European Union project ICRC-ERA-HumanBridge (No. 316345) and HistoPARK (CZ.1.07/2.3.00/20.0185) from the European Regional Development Fund. The authors would like to thank Iva Lišková, Kateřina Svobodová, and Martina Urbánková for superb technical assistance, Pavla Řezníčková and Dr. Nina Charvátová for maintenance of the animal facility, Prof. Vítězslav Bryja for providing the pIRESpuro2 plasmid, Dr. S.W. Hayward for providing CAFTD04 cells, Dr. Pradip Roy Burman for providing cE2 and E2 cells, Prof. William G. Watson for providing PC-3AC, PC-3DR8, and PC-3DR12 cells, and Prof. Radek Vrtěl for cell line authentication.

Disclosure of potential conflicts of interest

No potential conflicts of interest are disclosed.

Authors' Contributions

Conception and design: K. Souček, Š. Šimečková, Z. Kahounová, E. Slabáková

Cell lines experiments: Š. Šimečková, R. Fedr, P. Beneš

In vivo experiments: J. Remšík, Š. Šimečková

Analysis and evaluation of immunohistochemical samples: Jan Bouchal, Gvantsa Kharaishvili, Milan Král

Writing, review, and/or revision of the manuscript: Š. Šimečková, J. Bouchal, K. Souček

Study supervision: K. Souček,

REFERENCES

1. Siegel, R. L., Miller, K. D. & Jemal, A. Cancer statistics, 2018. CA Cancer J Clin 68, 7-30, doi:10.3322/caac.21442 (2018).

2. Oskarsson, T., Batlle, E. & Massague, J. Metastatic stem cells: sources, niches, and vital pathways. Cell Stem Cell 14, 306-321, doi:10.1016/j.stem.2014.02.002 S1934-5909(14)00053-8 [pii] (2014).

3. Sethi, S., Macoska, J., Chen, W. & Sarkar, F. H. Molecular signature of epithelial-mesenchymal transition (EMT) in human prostate cancer bone metastasis. Am J Transl Res 3, 90-99 (2010).

4. Puhr, M. et al. Epithelial-to-mesenchymal transition leads to docetaxel resistance in prostate cancer and is mediated by reduced expression of miR-200c and miR-205. Am J Pathol 181, 2188-2201, doi:10.1016/j.ajpath.2012.08.011 S0002-9440(12)00653-0 [pii] (2012).

5. Marin-Aguilera, M. et al. Epithelial-to-mesenchymal transition mediates docetaxel resistance and high risk of relapse in prostate cancer. Mol Cancer Ther 13, 1270-1284, doi:10.1158/1535-7163.MCT-13-0775 1535-7163.MCT-13-0775 [pii] (2014).

6. Ruan, D. et al. Skp2 deficiency restricts the progression and stem cell features of castration-resistant prostate cancer by destabilizing Twist. Oncogene 36, 4299-4310, doi:10.1038/onc.2017.64 onc201764 [pii] (2017).

7. Li, P., Yang, R. & Gao, W. Q. Contributions of epithelial-mesenchymal transition and cancer stem cells to the development of castration resistance of prostate cancer. Mol Cancer 13, 55, doi:10.1186/1476-4598-13-55 1476-4598-13-55 [pii] (2014).

8. Habib, K., Kumar, S., Manikar, N., Zutshi, S. & Fatma, T. Biochemical effect of carbaryl on oxidative stress, antioxidant enzymes and osmolytes of cyanobacterium Calothrix brevissima. Bull Environ Contam Toxicol 87, 615-620, doi:10.1007/s00128-011-0410-0 (2011).

9. Gangavarapu, K. J. et al. Aldehyde dehydrogenase and ATP binding cassette transporter G2 (ABCG2) functional assays isolate different populations of prostate stem cells where ABCG2 function selects for cells with increased stem cell activity. Stem Cell Res Ther 4, 132, doi:10.1186/scrt343 scrt343 [pii] (2013).

10. Leao, R. et al. Cancer Stem Cells in Prostate Cancer: Implications for Targeted Therapy. Urol Int 99, 125-136, doi:10.1159/000455160 000455160 [pii] (2017).

11. Petkova, N. et al. Surface CD24 distinguishes between low differentiated and transit-amplifying cells in the basal layer of human prostate. Prostate 73, 1576-1590, doi:10.1002/pros.22708 (2013).

12. Hurt, E. M., Kawasaki, B. T., Klarmann, G. J., Thomas, S. B. & Farrar, W. L. CD44+ CD24(-) prostate cells are early cancer progenitor/stem cells that provide a model for patients with poor prognosis. Br J Cancer 98, 756-765, doi:10.1038/sj.bjc.6604242 6604242 [pii]

(2008).
13. Salvatori, L. et al. Cell-to-cell signaling influences the fate of prostate cancer stem cells and their potential to generate more aggressive tumors. PLoS One 7, e31467, doi:10.1371/journal.pone.0031467
PONE-D-11-10345 [pii] (2012).
14. Menchon, C., Edel, M. J. & Izpisua Belmonte, J. C. The cell cycle inhibitor p27Kip(1) controls self-renewal and pluripotency of human embryonic stem cells by regulating the cell cycle, Brachyury and Twist. Cell Cycle 10, 1435-1447, doi:15421 [pii] 10.4161/cc.10.9.15421 (2011).
15. Polyak, K. et al. Cloning of p27Kip1, a cyclin-dependent kinase inhibitor and a potential mediator of extracellular antimitogenic signals. Cell 78, 59-66, doi:0092-8674(94)90572-X [pii] (1994).
16. Toyoshima, H. & Hunter, T. p27, a novel inhibitor of G1 cyclin-Cdk protein kinase activity, is related to p21. Cell 78, 67-74, doi:0092-8674(94)90573-8 [pii] (1994).
17. Yang, G. et al. Elevated Skp2 protein expression in human prostate cancer: association with loss of the cyclin-dependent kinase inhibitor p27 and PTEN and with reduced recurrence-free survival. Clin Cancer Res 8, 3419-3426 (2002).
18. Osoegawa, A. et al. Regulation of p27 by S-phase kinase-associated protein 2 is associated with aggressiveness in non-small-cell lung cancer. J Clin Oncol 22, 4165-4173, doi:22/20/4165 [pii]
10.1200/JCO.2004.01.035 (2004).
19. Chen, L. & Tweddle, D. A. p53, SKP2, and DKK3 as MYCN Target Genes and Their Potential Therapeutic Significance. Front Oncol 2, 173, doi:10.3389/fonc.2012.00173 (2012).
20. Bochis, O. V., Fetica, B., Vlad, C., Achimas-Cadariu, P. & Irimie, A. The Importance of Ubiquitin E3 Ligases, SCF and APC/C, in Human Cancers. Clujul Med 88, 9-14 (2015).
21. Pernicova, Z. et al. Androgen depletion induces senescence in prostate cancer cells through down-regulation of Skp2. Neoplasia 13, 526-536 (2011).
22. van Duijn, P. W. & Trapman, J. PI3K/Akt signaling regulates p27(kip1) expression via Skp2 in PC3 and DU145 prostate cancer cells, but is not a major factor in p27(kip1) regulation in LNCaP and PC346 cells. Prostate 66, 749-760, doi:10.1002/pros.20398 (2006).
23. Shim, E. H. et al. Expression of the F-box protein SKP2 induces hyperplasia, dysplasia, and low-grade carcinoma in the mouse prostate. Cancer Res 63, 1583-1588 (2003).
24. Lin, H. K. et al. Skp2 targeting suppresses tumorigenesis by Arf-p53-independent cellular senescence. Nature 464, 374-379, doi:10.1038/nature08815
nature08815 [pii] (2010).
25. Liao, C. P. et al. Mouse prostate cancer cell lines established from primary and postcastration recurrent tumors. Horm Cancer 1, 44-54, doi:10.1007/s12672-009-0005-y (2010).
26. O'Neill, A. J. et al. Characterisation and manipulation of docetaxel resistant prostate cancer cell lines. Mol Cancer 10, 126, doi:10.1186/1476-4598-10-1261476-4598-10-126 [pii] (2011).
27. Slabakova, E. et al. Opposite regulation of MDM2 and MDMX expression in acquisition of mesenchymal phenotype in benign and cancer cells. Oncotarget 6, 36156-36171, doi:10.18632/oncotarget.53925392 [pii] (2015).
28. Tellmann, G. The E-Method: a highly accurate technique for gene-expression analysis. Nat. Methods 3, i-ii, doi:doi:10.1038/nmeth894 (2006).
29. Mosmann, T. Rapid colorimetric assay for cellular growth and survival: application to proliferation and cytotoxicity assays. J Immunol Methods 65, 55-63, doi:0022-1759(83)90303-4 [pii] (1983).
30. Remsik, J. et al. Plasticity and intratumoural heterogeneity of cell surface antigen expression in breast cancer. Br. J. Cancer 118, 813-819, doi:10.1038/bjc.2017.497 (2018).
31. Vargova, J. et al. Hypericin affects cancer side populations via competitive inhibition of BCRP. Biomed Pharmacother 99, 511-522, doi:10.1016/j.biopha.2018.01.074 (2018).
32. Bray, M.-A. et al. Cell Painting, a high-content image-based assay for morphological profiling using multiplexed fluorescent dyes. Nat. Protocols 11, 1757-1774, doi:10.1038/nprot.2016.105
http://www.nature.com/nprot/journal/v11/n9/abs/nprot.2016.105.html#supplementary-information (2016).
33. Carpenter, A. et al. CellProfiler: image analysis software for identifying and quantifying cell phenotypes. Genome Biology 7, R100 (2006).
34. Brunger, A. T. Crystallography & NMR system: A new software suite for macromolecular structure determination. Acta Crystallogr. D 54, 905-921 (1998).
35. Taylor, B. S. et al. Integrative genomic profiling of human prostate cancer. Cancer Cell 18, 11-22, doi:10.1016/j.ccr.2010.05.026 S1535-6108(10)00238-2 [pii] (2010).
36. Remšík J. et al. Trop-2 plasticity is controlled by epithelial-to-mesenchymal transition. Manuscript submitted for publication (2018).
37. Yang, Q. et al. Acquisition of epithelial-mesenchymal transition is associated with Skp2 expression in paclitaxel-resistant breast cancer cells. Br J Cancer 110, 1958-1967, doi:10.1038/bjc.2014.136
bjc2014136 [pii] (2014).
38. Qu, X. et al. A signal transduction pathway from TGF-beta1 to SKP2 via Akt1 and c-Myc and its correlation with progression in human melanoma. J Invest Dermatol 134, 159-167, doi:10.1038/jid.2013.281
S0022-202X(15)36471-X [pii] (2014).
39. Yan, W., Chen, Y., Yao, Y., Zhang, H. & Wang, T. Increased invasion and tumorigenicity capacity of CD44+/CD24- breast cancer MCF7 cells in vitro and in nude mice. Cancer Cell Int 13, 62, doi:10.1186/1475-2867-13-62
1475-2867-13-62 [pii] (2013).
40. Li, W. et al. Unraveling the roles of CD44/CD24 and ALDH1 as cancer stem cell markers in tumorigenesis

and metastasis. Sci Rep 7, 13856, doi:10.1038/s41598-017-14364-2
10.1038/s41598-017-14364-2 [pii] (2017).
41. Meng, E. et al. CD44+/CD24- ovarian cancer cells demonstrate cancer stem cell properties and correlate to survival. Clin Exp Metastasis 29, 939-948, doi:10.1007/s10585-012-9482-4 (2012).
42. Ghuwalewala, S. et al. CD44(high)CD24(low) molecular signature determines the Cancer Stem Cell and EMT phenotype in Oral Squamous Cell Carcinoma. Stem Cell Res 16, 405-417, doi:10.1016/j.scr.2016.02.028
S1873-5061(16)00070-2 [pii] (2016).
43. Klarmann, G. J. et al. Invasive prostate cancer cells are tumor initiating cells that have a stem cell-like genomic signature. Clin Exp Metastasis 26, 433-446, doi:10.1007/s10585-009-9242-2 (2009).
44. Cremers, N. et al. CD24 Is Not Required for Tumor Initiation and Growth in Murine Breast and Prostate Cancer Models. PLoS One 11, e0151468, doi:10.1371/journal.pone.0151468
PONE-D-15-18809 [pii] (2016).
45. Lu, W. et al. SKP2 inactivation suppresses prostate tumorigenesis by mediating JARID1B ubiquitination. Oncotarget 6, 771-788, doi:2718 [pii]
10.18632/oncotarget.2718 (2015).
46. Zhao, H. et al. Skp2 deletion unmasks a p27 safeguard that blocks tumorigenesis in the absence of pRb and p53 tumor suppressors. Cancer Cell 24, 645-659, doi:10.1016/j.ccr.2013.09.021
S1535-6108(13)00428-5 [pii] (2013).
47. Puhr, M. et al. PIAS1 is a crucial factor for prostate cancer cell survival and a valid target in docetaxel resistant cells. Oncotarget 5, 12043-12056 (2014).
48. Mulholland, D. J. et al. Pten Loss and RAS/MAPK Activation Cooperate to Promote EMT and Metastasis Initiated from Prostate Cancer Stem/Progenitor Cells. Cancer Research 72, 1878-1889, doi:10.1158/0008-5472.can-11-3132 (2012).

Grant Acknowledgment

This work was supported by grants GA CR P301/12/P407, IGA MZD NT13573-4/2012, and AZV ČR 15-28628A & 15-33999A, and supported by project no. LQ1605 from the National Program of Sustainability II (MEYS CR) and by European Union project ICRC-ERA-HumanBridge (No. 316345) and HistoPARK (CZ.1.07/2.3.00/20.0185) from the European Regional Development Fund.

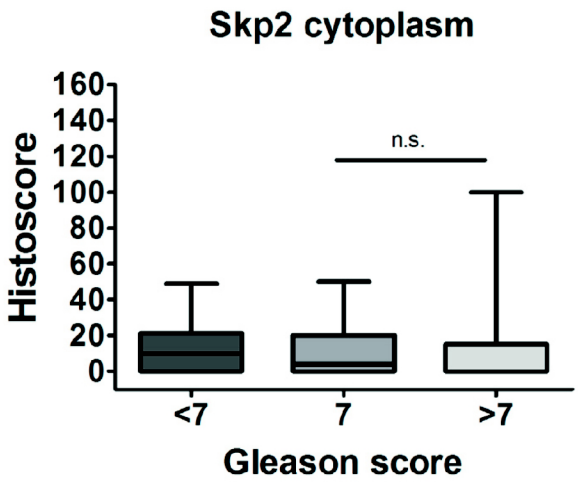

Supplementary Figure 1. Cytoplasmic Skp2 expression does not correlate with high Gleason score (≥ 7) in patients with prostate cancer. Data were plotted, reanalyzed using Prism (v6, GraphPad), and statistics was calculated using the Student's t-test.

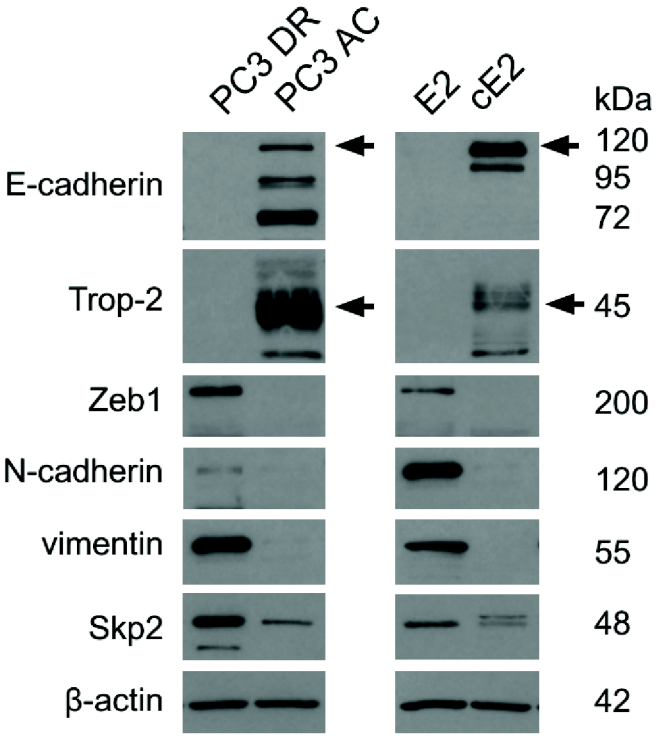

Supplementary Figure 2. Western blot analysis for Skp2 expression of prostate cancer cell lines [PC3 docetaxel-resistant (DR), PC3 age-control (AC), and mouse prostate adenocarcinoma cells] with mesenchymal (E2) and epithelial (cE2) phenotypes. Representative results from three independent repetitions are shown. β-actin was used as a loading control.

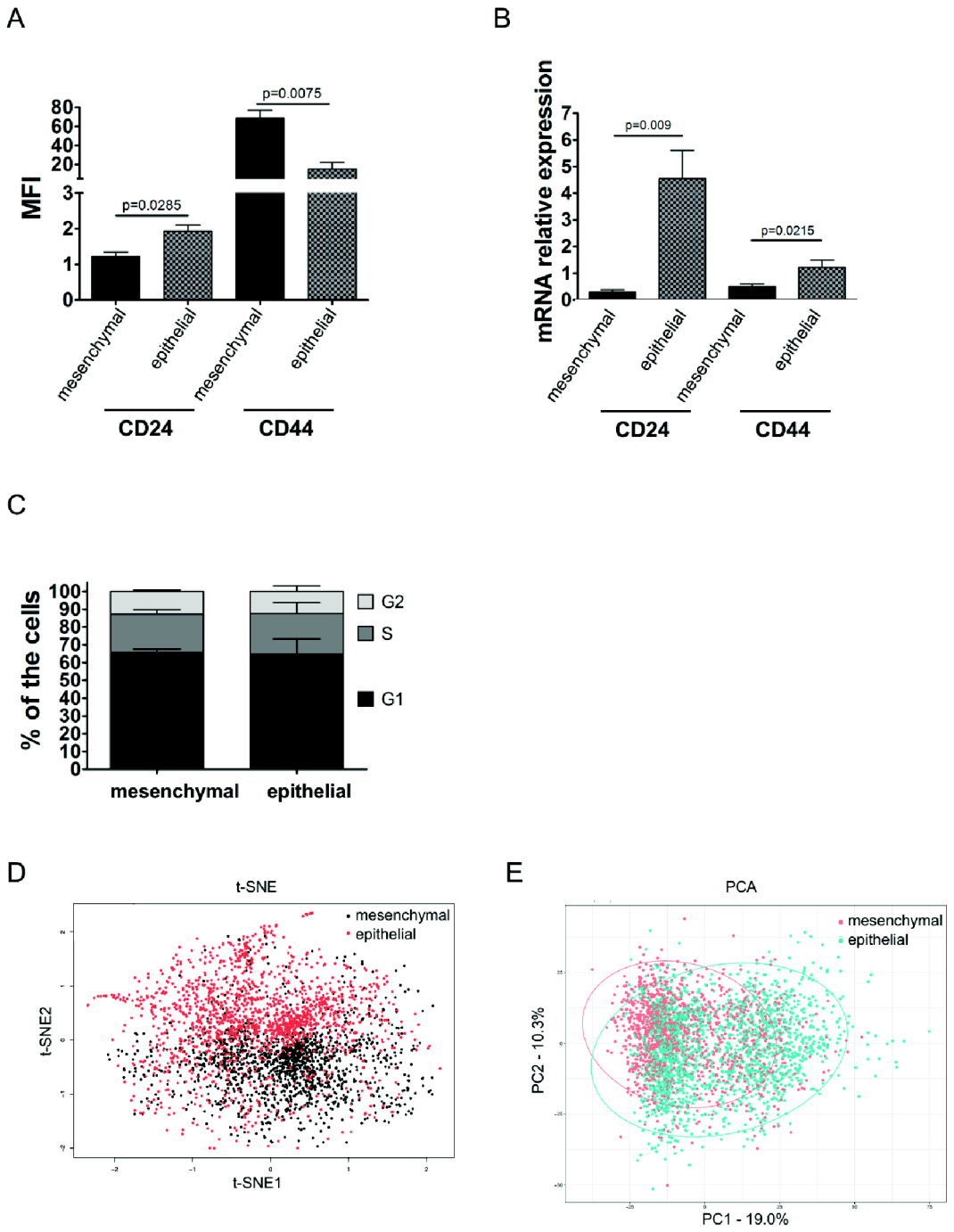

Supplementary Figure 3. Proliferation in DU 145 mesenchymal and epithelial cells is equal but expression of CD24 and CD44 is increased in DU145 epithelial cells. (A) Expression of CD24 and CD44 measured as the median fluorescence index (MFI) in DU 145 mesenchymal and epithelial cells. Bars show the mean ± SD values for the MFI of selected markers from three independent experiments. (B) qRT-PCR analysis of CD24 and CD44 markers. Data represent the mean ± SD of five independent experiments. The relative expression of the markers was normalized to *POLR2A* expression. (C) Cell cycle analysis. Results are from three independent experiments. (D) Principal component and t-SNE analysis from 1761 morphology parameters of mesenchymal and epithelial cells. (E) Ellipse in principal component analysis plot marks 95% confidence interval. Partial separation of confidence intervals in PCA and objects clustering into 2 groups in t-SNE plot shows different phenotype based on morphology of mesenchymal and epithelial cell lines.

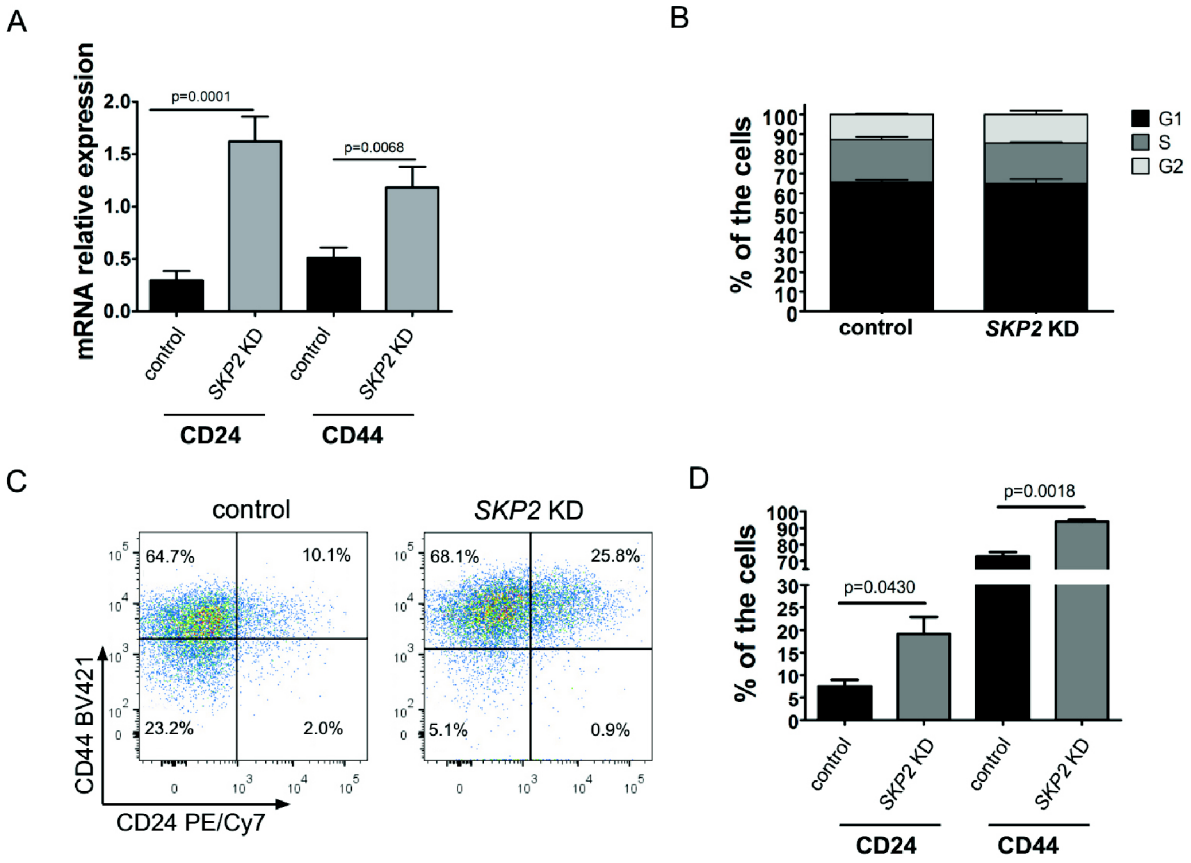

Supplementary Figure 4. Decreased expression of Skp2 in accompanied with increased expression of CD24, CD44, but no change in proliferation in mesenchymal DU 145. (A) qRT-PCR analysis of CD24 and CD44 markers in DU 145 *SKP2* KD cells and control cells. Data represent the mean ± SD of three independent experiments. The relative expression of the markers was normalized to POLR2A expression. (B) Cell cycle analysis. Data are from three independent experiments. (C) The expression of CD24 and CD44 in DU 145 *SKP2* KD cells and control cells cultivated in anchorage-independent conditions. Representative images are from three independent experiments. Bars show the mean ± SD of the percentage of positive cells for both markers. Results are from three independent repetitions. (D) Quantitation of results shown in (C).

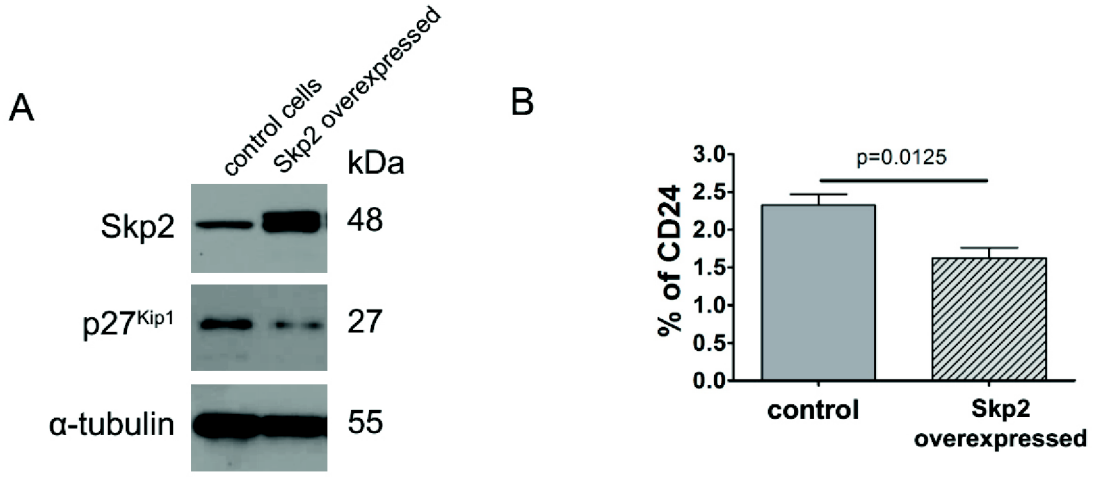

Supplementary Figure 5. CD24 is decreased in DU 145 cells after Skp2 overexpression. (A) Skp2 and $p27^{Kip1}$ protein expression by western blot. Representative images are from three independent experiments. α-tubulin was used as a loading control. (B) Expression of CD24 in DU 145 cells overexpressing Skp2 and control cells. Data are presented as the mean ± SD of the percentage of CD24-positive cells. Results are from three independent experiments.

Supplementary Table S1 List of primary and secondary antibodies used for western blot

Primary Antibody	**Supplier**	**Source**	**Cat. No.**	**Dilution**
α-tubulin	Sigma-Aldrich	Mouse	T9026	1:4000
β-actin	Sigma-Aldrich	Mouse	A5441	1:8000
E-Cadherin	BD Pharmingen	Mouse	610182	1:5000
N-Cadherin	BD Pharmingen	Mouse	610920	1:2500
$p27^{Kip1}$	Santa Cruz	Rabbit	SC-528	1:500
$p27^{Kip1}$	Cell Signaling	Rabbit	2552	1:1000
Skp2	Cell Signaling	Rabbit	4313	1:1000
Trop-2	R&D	Mouse	AF650	1:250
Trop-2	R&D	Goat	AF1122	1:250
vimentin	Sigma-Aldrich	Mouse	V6389	1:500
vimentin	Sigma-Aldrich	Rabbit	SAB300676	1:500
Zeb1	Bethyl	Rabbit	A301-922A	1:500
Zeb2	Bethyl	Rabbit	A302-474A	1:500
Secondary Antibody	**Supplier**		**Cat. No.**	**Dilution**
[HRP]-linked anti-rabbit IgG1,	Amersham	Sheep	NA934V	1:3000
HRP-linked anti-mouse IgG1	Amersham	Sheep	NA931	1:4000

Supplementary Table S2 Human gene expression assays

Gene	**Accesion #**	**F primer**	**R primer**	**Probe**
CD24	NM_013230.2	TGGATTTGACATTGCATTTGA	TGGGGGTAGATTCTCATTCATC	#37
CD44	NM_000610.3	TCACATTAAGTTTGCATGACCTG	AATAGGGCCAGCCTCTATGAA	#57
POLR2A	NM_000937.3	CACGTCGACAGGAACATCAG	GCAAATTCACCAAGAGAGACG	#1

Supplementary Table S3 List of primary antibodies, Isotype controls and probes used for for flow cytometry

Antibody	Fluorochrome	Source	Supplier	Cat. No	Dilution
Surface markers					
CD24	Briliant Violet 421	Mouse	BioLegend	311122	1:20
CD24	PE/Cy7	Mouse	BioLegend	311122	1:20
CD44	APC/Cy7	Rat	BioLegend	103 028	1:100
Isotype controls					
IgG2a	Briliant Violet 650	Mouse	BioLegend	711-126-152	1:20
IgG2a	PE/Cy7	Mouse	BioLegend		1:20
IgG2b	APC/Cy7	Rat	BioLegend	400624	1:100
Viability					
LIVE/DEAD® Fixable Dead Cell Stain Kit	Far Red	-	Thermo Fisher Scientific	L10120	1:1000

Supplementary Table S4 List of antibodies used for immunohistochemistry

Primary Antibody	Supplier	Source	Clone	Cat. No.	Dilution	Method
Skp2	Invitrogen	Mouse	2C8D9	18-7334	1:75	Ventana
Slug	Cell Signaling	Rabbit	C19G7	9585	1:100	MW, citrate, pH 6.0
E-cadherin	Dako	Mouse	NCH-38	IR05961-2	1:50	MW, citrate, pH 6.0
vimentin	Dako	Mouse	V9	IR63061-2	1:10	MW, citrate, pH 6.0

Supplementary Table S5 Clinical data related to patient samples

prostate cancer patients	age at diagnosis	PSA total [ng/mL]	Gleason score	TNM		stage	risk
patient 1	56	5,86	<7	pT2b	pN0	local	low
patient 2	60	14,70	<7	pT4	pN0	advanced	high
patient 3	66	20,40	<7	pT4	pN0	advanced	high
patient 4	55	3,66	<7	pT2b	pN0	local	low
patient 5	65	4,22	<7	pT2a	pN0	local	low
patient 6	51	6,01	<7	pT2b	pN0	local	low
patient 7	66	14,10	<7	pT3b	pN0	advanced	high
patient 8	65	4,40	<7	pT2b	pN0	local	low
patient 9	65	9,80	<7	pT2b	pN0	local	low
patient 10	69	n/a	<7	pT4	pN0	advanced	high
patient 11	70	17,40	<7	pT2b	pN0	local	low
patient 12	63	7,06	<7	pT2c	pN0	local	low
patient 13	55	8,35	<7	pT3b	pN0	advanced	high
patient 14	57	33,60	<7	pT3b	pN0	advanced	high
patient 15	62	3,59	<7	pT2c	pN0	local	low
patient 16	64	17,30	<7	T2c	pN0	local	low
patient 17	62	7,77	<7	T2c	pN0	local	low
patient 18	60	8,21	<7	pT2c	pN0	local	low
patient 19	56	7,60	<7	pT2c	pN0	local	low
patient 20	72	10,20	<7	pT3a	pN1	metastatic	high
patient 21	58	6,40	<7	pT2c	pN1	metastatic	high
patient 22	58	3,20	<7	pT2b	pNx	local	low
patient 23	65	21,50	7	pT3b	pN0	advanced	high
patient 24	70	n/a	7	pT4	pN0	advanced	high
patient 25	62	35,00	7	pT3b	pN0	advanced	high
patient 26	61	18,00	7	pT3b	pN0	advanced	high
patient 27	68	28,00	7	pT2b	pN0	local	high
patient 28	60	6,60	7	pT2b	pN0	local	low
patient 29	58	6,15	7	pT3b	pN0	advanced	high
patient 30	68	7,40	7	pT2a	pN0	local	low
patient 31	59	4,80	7	pT2b	pN0	local	low
patient 32	61	16,81	7	pT2b	pN0	local	low
patient 33	51	13,68	7	pT2b	pN0	local	low
patient 34	60	28,50	7	pT2b	pN0	local	high

patient 35	53	1,89	7	pT2a	pN0	local	low
patient 36	72	1,46	7	pT2a	pN0	local	low
patient 37	66	9,02	7	pT3b	pN0	advanced	high
patient 38	57	12,50	7	pT3b	pN0	advanced	high
patient 39	60	15,90	7	pT3a	pN0	advanced	high
patient 40	66	19,50	7	pT2c	pN0	local	low
patient 41	71	18,80	7	pT3b	pN0	advanced	high
patient 42	61	4,28	7	pT2a	pN0	local	low
patient 43	61	10,80	7	pT2c	pN0	local	low
patient 44	64	11,16	7	pT3b	pN0	advanced	high
patient 45	69	6,50	7	pT3b	pN0	advanced	high
patient 46	66	14,70	7	pT3b	pN0	advanced	high
patient 47	62	6,04	7	pT3b	pN0	advanced	high
patient 48	49	9,13	7	T2c	pN0	local	low
patient 49	66	7,17	7	pT2c	pN0	local	low
patient 50	51	9,64	7	pT2a	pN0	local	low
patient 51	66	3,11	7	pT2a	pN0	local	low
patient 52	50	8,30	7	pT2c	pN0	local	low
patient 53	65	6,70	7	pT2c	pN0	local	low
patient 54	52	3,90	7	pT2b	pN0	local	low
patient 55	64	5,13	7	pT2c	pN0	local	low
patient 56	73	11,99	7	pT2c	pN0	local	low
patient 57	64	n/a	7	pT2c	pN1	metastatic	high
patient 58	63	n/a	7	pT3b	pN1	metastatic	high
patient 59	56	n/a	7	pT3b	pN1	metastatic	high
patient 60	56	35,00	7	pT3b	pN1	metastatic	high
patient 61	56	12,70	7	pT3b	pN1	metastatic	high
patient 62	57	2,78	7	pT3a	pN1	metastatic	high
patient 63	62	15,44	7	pT4	pN1	metastatic	high
patient 64	61	25,46	7	pT2c	pN1	metastatic	high
patient 65	68	33,16	7	pT3b	pN1	metastatic	high
patient 66	59	40,00	7	pT3b	pN1	metastatic	high
patient 67	63	41,00	7	pT3b	pN1	metastatic	high
patient 68	63	10,30	7	pT3b	pNx	advanced	high
patient 69	62	8,53	7	pT3b	pNx	advanced	high
patient 70	68	6,29	7	pT3b	pNx	advanced	high
patient 71	63	9,80	7	pT2c	pNx	local	low
patient 72	69	4,00	>7	pT3b	pN0	advanced	high

Supplementary Table S5 continued

patient 73	55	31,20	>7	pT3b	pN0	advanced	high
patient 74	57	12,12	>7	pT3b	pN0	advanced	high
patient 75	58	13,74	>7	pT4	pN0	advanced	high
patient 76	73	3,06	>7	pT3b	pN0	advanced	high
patient 77	55	3,60	>7	pT3b	pN0	advanced	high
patient 78	61	7,48	>7	pT3b	pN0	advanced	high
patient 79	67	6,05	>7	pT3b	pN0	advanced	high
patient 80	59	6,03	>7	pT3b	pN0	advanced	high
patient 81	74	5,20	>7	pT3b	pN0	advanced	high
patient 82	71	15,10	>7	pT3b	pN0	advanced	high
patient 83	64	n/a	>7	pT4	pN1	metastatic	high
patient 84	62	13,60	>7	pT3b	pN1	metastatic	high
patient 85	69	3,10	>7	pT3b	pN1	metastatic	high
patient 86	68	7,90	>7	pT3b	pN1	metastatic	high
patient 87	59	12,00	>7	pT3b	pN1	metastatic	high
patient 88	62	12,49	>7	pT2b	pN1	metastatic	high
patient 89	57	6,70	>7	pT2b	pN1	metastatic	high
patient 90	61	n/a	>7	pT4	pN1	metastatic	high
patient 91	63	9,37	>7	pT3b	pN1	metastatic	high
patient 92	60	9,51	>7	pT3b	pN1	metastatic	high
patient 93	67	n/a	>7	pT3b	pN1	metastatic	high
patient 94	56	28,00	>7	pT3b	pN1	metastatic	high
patient 95	64	12,20	>7	pT3b	pN1	metastatic	high
patient 96	76	30,77	>7	pT3b	pN1	metastatic	high
patient 97	70	11,00	>7	pT3b	pN1	metastatic	high
patient 98	69	10,30	>7	pT3b	pN1	metastatic	high
patient 99	66	8,29	>7	pT2b	pNx	local	low
patient 100	61	4,51	>7	pT3b	pNx	advanced	high
patient 101	66	11,66	>7	pT4		advanced	high

Supplementary Table S5 continued

Supplementary Table 6 Clinical characteristics of the patients - summarization

Number of patients	101			
Age	49-60	61-70	71-76	
	36	57	8	
Serum PSA (ng/ml)	<4	4–10	>10	missing
	11	40	45	5
Gleason scores	<7	7	>7	
	22	49	30	
Cancer stages	pT2a-c	pT3a-b	pT4	
	42	50	9	
Lymph node status	pN1	pN0	pNx*	
	29	65	7	
*without lymphadenectomy or no information				

Appendix II

TECHNICAL NOTE

Cytometry PART A
Journal of the International Society for Advancement of Cytometry

MIFlowCyt

Multiparameter Cytometric Analysis of Complex Cellular Response

Šárka Šimečková,[1,2] Radek Fedr,[1,3] Ján Remšík,[1,2,3] Zuzana Kahounová,[1,3] Eva Slabáková,[1] Karel Souček[1,3]*

[1]Department of Cytokinetics, Institute of Biophysics of the Czech Academy of Sciences, Brno, Czech Republic

[2]Department of Experimental Biology, Faculty of Science, Masaryk University, Brno, Czech Republic

[3]Center of Biomolecular and Cellular Engineering, International Clinical Research Center, St. Anne's University Hospital Brno, Brno, Czech Republic

Received 5 June 2017; Revised 22 October 2017; Accepted 10 November 2017

Grant sponsor: Czech Science Foundation, Grant number: 15–11707 S

Grant sponsor: Ministry of Health of the Czech Republic, Grant numbers: 15–28628 A; 15–33999 A; 17-28518A

Grant sponsor: Ministry of Education, Youth and Sports, Grant number: 7AMB16AT022

Grant sponsor: National Program of Sustainability II (MEYS CR, LQ1605)

Grant sponsor: European Union (ICRC-ERA-HumanBridge, No. 316345)

Grant sponsor: European Regional Development Fund (HistoPARK), Grant number: CZ.1.07/2.3.00/20.0185

Additional Supporting Information may be found in the online version of this article.

*Correspondence to: Karel Souček, Ph.D., Institute of Biophysics of the Czech Academy of Sciences, Královopolská 135, CZ-612 65 Brno, Czech Republic. E-mail: ksoucek@ibp.cz

ISAC
International Society for Advancement of Cytometry

Abstract

Complex analysis of cellular responses after experimental treatment is important for screening, mechanistic understanding of treatment effects, and the identification of sensitive and resistant cell phenotypes. Modern multicolor flow cytometry has demonstrated its power for such analyses. Here, we introduce a multiparametric protocol for complex analysis of cytokinetics by the simultaneous detection of seven fluorescence parameters. This analysis includes the detection of two surface markers for immunophenotyping, analysis of proliferation based on the cell cycle and the measurement of incorporated nucleoside analogue 5-ethynyl-2′-deoxyuridine (EdU) in newly synthesized DNA, analysis of DNA damage using an anti-phospho-histone H2A.X (Ser139) antibody, and determination of cell death using a fixable viability probe and intracellular detection of caspase-3 activation. To demonstrate the applicability of this protocol for the analysis of heterogeneous and complex cell responses, we used different treatments and model cell lines. We demonstrated that this protocol has the potential to provide complex and simultaneous analysis of cytokinetics and analyze the heterogeneity of the response at the single-cell level. © 2017 International Society for Advancement of Cytometry

Key terms

flow cytometry; multiparametric analysis; DNA damage; apoptosis; proliferation; immunophenotyping

Introduction

Modern multicolor flow cytometry has been used effectively in almost every field of cell biology. It can provide detailed information about the phenotype of the cells at the single-cell level and elucidate the functions of identified cell populations by analyzing a variety of parameters (e.g., viability, proliferation, intracellular cytokine detection). Flow cytometers are now routinely capable of measuring up to 10 parameters, and state-of-the-art research flow cytometers can acquire signal from 20 fluorescent channels (1). Nevertheless, design and optimization challenges remain in multiparametric flow cytometry protocols to detect markers present in various cellular compartments (e.g. surface and/or nucleus), targeted to different types of molecules (protein or nucleic acids), and that are either detected by miscellaneous fluorescent probes (e.g. conjugated antibodies or free small organic fluorescent dyes) or require labeling under viable conditions followed by fixation and membrane permeabilization steps (2,3). For these protocols, it is critical to not only acquire good compensation control data to determine accurate spillover coefficients, but to consider the selection of appropriate markers and probes that are technically and biologically compatible with the staining procedure. For example, in case of the combined detection of surface and intracellular markers, labeling of surface epitopes is recommended prior to cell fixation and permeabilization, to avoid potential false positivity

Published online 00 Month 2017 in Wiley Online Library (wileyonlinelibrary.com)
DOI: 10.1002/cyto.a.23295

© 2017 International Society for Advancement of Cytometry

due to the cross reactivity of antibodies with intracellular proteins, as described in the case of surface CD133 (AC141) antibody cross-reacting with intracellular cytokeratin 18 (4). The proper protocol for fixation and permeabilization needs to be gentle on the labeled surface markers, but simultaneously sufficient to provide access to intracellular antigens (5).

Complex analysis of the cellular response and cell fate (cytokinetics) following experimental treatment is important not only for screening and gaining a basic understanding of treatment (drug) effects but also for the identification of sensitive or resistant cell types with a characteristic phenotype. For such analyses, a variety of methodological approaches might be used. Typically, these can involve the adaptation of several methods performed in parallel, which may have different types of readouts. Most of the frequently used single-readout methods (e.g., western blot or qPCR) cannot detect cell-to-cell heterogeneity in response to the tested compound, unless performed at the single-cell level (6). A modern cytokinetic analysis method should take full advantage of the multicolor character of flow cytometry to measure several different types of cell responses simultaneously, and analyze both the phenotype and functional characteristics of the treated cells. In our work, we used cell lines that represent most of the cell types that are routinely used in cancer research (both human and mouse cells, adherent and non-adherent cells to show the universality of the protocol and its utilization for wide spectrum of applications.

Material and Methods

Materials

MLN-4924 was obtained from Active Biochem (Hong Kong, China); dimethyl sulfoxide (DMSO), MG-132, Triton X-100, and phosphate-buffered saline (PBS) were obtained from Sigma-Aldrich; TRAIL was kindly provided by Dr. Ladislav Anděra, Institute of Molecular Genetics, CAS, Prague, Czech Republic; and Click-iT® Flow Cytometry Assays Kits were obtained from Thermo Fisher Scientific. The staining buffer was 1% bovine serum albumin (BSA; Serva Electrophoresis GmbH, Heidelberg, Germany) in PBS with 0.1% NaN_3 (Sigma-Aldrich). A buffered, 4% formaldehyde solution in PBS was prepared in-house from powder (Fluka). The antibodies, concentrations, and dilutions used are listed in Supporting Information Table S2.

Cells and Cell Culture

DU 145 human cancer cells (ATCC) derived from brain metastases of prostate cancer were cultivated in RPMI 1640 (Thermo Fisher Scientific, Waltham, MA) supplemented with 10% fetal bovine serum (FBS) (Thermo Fisher Scientific), penicillin (100 U/ml), and streptomycin (0.1 mg/ml; Biosera, Nuaille, France). HCT 116 human colon adenocarcinoma cells (a generous gift from Dr. Bert Vogelstein, Johns Hopkins University, Baltimore, MD) were cultivated in McCoy's medium (Thermo Fisher Scientific) containing 10% heat-inactivated FBS, penicillin, and streptomycin. cE2 mouse prostate adenocarcinoma cells (7) (a generous gift from Dr. Pradip Roy Burman, University of Southern California, Los Angeles, CA), were cultivated in Dulbecco's modified Eagle medium (DMEM) (Thermo Fisher Scientific) supplemented with recombinant human (rh) epidermal growth factor (rh-EGF) (6 ng/ml; Sigma-Aldrich, St. Luis, MO), rh-insulin (5 μg/ml; Sigma-Aldrich), bovine pituitary extract (25 μg/ml; Hammond Cell Tech, Windsor, CA), 10% FBS, penicillin, and streptomycin. Human diffuse large B-cell lymphoma, SU-DHL-4 cells (a kind gift from Dr. Martin Trbušek, Masaryk University, Czech Republic), were cultivated in RPMI 1640 supplemented with 10% FBS, penicillin, and streptomycin.

Cells were cultivated in TPP cultivation flasks and dishes (Trasadingen, Switzerland) in a humidified incubator at 37°C with an atmosphere of 5% CO_2. The cells (except SU-DHL-4 growing in suspension) were harvested by washing with 1.35 mM ethylene diamine tetraacetic acid (EDTA) in PBS followed by trypsinization (0.05% w/v trypsin, 0.02% EDTA). Cells were routinely tested for mycoplasma contamination.

For the induction of DNA damage and/or apoptosis, exponentially growing cells were subsequently treated with experimental drugs. cE2 and SU-DHL-4 were treated with lethal concentrations of MG-132 (1 μM and 5 μM, respectively) for 24 hours. DU 145 and HCT 116 were treated with lethal concentration of TRAIL (50 ng/ml) for 2 hours. All cell lines were treated with MLN-4924 (DU 145 and HCT 116 0.33 μM, SU-DHL-4 1 μM, cE2 5 μM) for 24 hours. Concentrations were selected based on pilot experiments. In all cases, corresponding vehicle at the appropriate dilution was applied in the control groups.

Western Blot

Samples for western blot were prepared as described previously (8). Proteins were separated using sodium dodecyl sulfate polyacrylamide gel electrophoresis (SDS-PAGE) and visualized with specific primary antibodies (Nedd8, Cell Signaling #2754, 1:1,000; cleaved caspase-3, Cell Signaling #9661 1:500; γH2A.X [Ser139], Cell Signaling #9718, 1:1,000 and α-tubulin, Sigma, T9026, 1:4,000) and secondary antibodies (horseradish peroxidase [HRP]-linked anti-rabbit IgG1, Amersham, NA934V, 1:3,000; HRP-linked anti-mouse IgG1, Amersham, NA931, 1:4,000). Signals were detected using the Immobilon Western HRP Substrate (Merck Millipore, Billerica, MA) and visualized on X-ray films (Agfa, Mortsel, Belgium).

Instrumentation, Data Analysis, Software, and Compensations

The acquisition was performed on a BD FACSAria II Sorp system (BD Biosciences, Franklin Lakes, NJ) equipped with five lasers (excitation wavelengths: 355, 405, 488, 561, and 639 nm). Cytometric data were recorded using FACSDiva software (Version 6.1.3; BD Biosciences). Optimization experiments were recorded on a BD FACSVerse (BD Biosciences) equipped with three lasers (excitation wavelengths: 405, 488, and 640 nm) where cytometric data were recorded using FACSuite software (Version 1.0.5.3841 and 1.0.6; BD Biosciences). The quality of the instrument was regularly tested using BD FACSuite CS&T Research Beads (BD Biosciences) before each measurement. The instrument set-up and procedure of data recording is described in Supporting Information protocol (section Instrument set-up and analysis). Data analysis was performed using FlowJo software (Version 10.0.7, Tree Star, Ashland, OR). List mode data were uploaded into the FlowRepository database of flow cytometry experiments (http://flowrepository.org/id/FR-FCM-ZZS3). Instrument configuration details are shown in Supporting Information Table S2. For compensation setup, single color controls (beads or cells) were recorded on a BD FACSAria II Sorp system and compensation matrix was calculated by FACSDiva software.

For single color controls, compensation beads or cells (positive controls) stained with appropriate antibodies and probes were used. Anti-rat and anti-hamster Ig,κ/negative control, anti-mouse Ig,κ/negative control compensation beads (BD Biosciences), Sphero™ Goat anti-Rabbit and Sphero™ Biotin Polystyrene Particles (Spherotech, Lake Forest, IL) labeled with specific antibodies in the appropriate dilutions were used. Arc™ Amine Reactive Compensation Bead Kit beads (Thermo Fisher Scientific) were stained using the LIVE/DEAD® Fixable fluorescent reactive dye kit according to manufacturer's recommendation. As compensation control for DNA staining, fixed and permeabilized cells with and without the appropriately diluted DNA probe was used. As a compensation control for DNA proliferation, cell pretreated with EdU were stained with Click-iT reaction cocktail. Cells were stained under the same conditions (time, temperature) as samples in protocol. Compensation beads were stained with primary antibodies for 20 min at 4°C. In case of secondary detection, beads were stained with primary antibodies (20 min, 4°C) following with secondary detection (20 min, 4°C).

Isotype controls (ISO) were prepared and recorded for all samples. Gates were set according to the isotype controls or untreated cells (for γH2A.X and cleaved caspase-3). Isotype controls are shown in Supporting Information Figure S5 A-D.

Statistical Analysis

Raw data were processed and statistical analysis was performed in Prism (v6, GraphPad, La Jolla, CA, United States). P values were calculated using paired t test (two-tailed) or multiple comparison t test with Holm-Sidak correction.

Results

A detailed description of the cellular response to a drug treatment is important to gain a better understanding of the mechanisms of action of anticancer drugs. In this respect, flow cytometry is an irreplaceable methodology, not only in experimental biology but also in clinical and diagnostic applications. The advantage of flow cytometry over many other methods is the capability to perform multiparametric analysis at the single-cell level in a single tube/assay.

The goal of our work was to introduce a multiparametric protocol for the assessment of complex cellular responses to experimental treatments. Therefore, we established the simultaneous detection of fluorescence parameters to detect surface markers for immunophenotyping, analyze proliferation based on the cell cycle and measurement of DNA synthesis, analyze DNA damage, and determine cell death using viability and apoptosis markers. By utilizing various cell lines (mouse and human, suspension, and adherent) and experimental treatments, we demonstrated the feasibility and robustness of our protocol. An overview of the experimental workflow is depicted in Figure 1.

Optimization Steps Required for Establishment of Final Assay

Several optimization steps were performed before we reached the above described final workflow and protocol. The initial step in our design was the selection of fluorescently labeled antibodies for surface marker detection that are compatible with subsequent azide-alkyne coupling (Click-iT EdU) reaction. During our optimization procedure, we realized that the performance of Click-iT EdU compatible antibody conjugates (e.g., allophycocyanin [APC]) might be significantly affected on permeabilization followed by the Click-iT EdU reaction. For example, when we detected the surface marker Prominin-1 in cE2 cells using APC-labeled anti-Prominin-1 antibody, we observed a visible drop in both the number of positive cells and mean fluorescence intensity (MFI) after the permeabilization and Click-iT EdU reaction steps (Supporting Information Figure S1A-C).

For successful detection of intracellular markers, fixation and permeabilization are crucial steps during sample processing (9,10). Here, we tested several permeabilizing agents, such as 0.25% Triton X-100, digitonin (300 μg/ml), and saponin-based reagents from two different commercial kits (Mouse Pluripotent Stem Cell Transcription Factor Analysis Kit, BD 560585, kit 1; and Click-iT detection kit). In case of saponin permeabilization, we followed the manufacturer's recommendation (dilution, incubation time). Under these experimental conditions, saponin was not sufficient for the detection of intracellular markers, such as cleaved caspase-3 (CC3) or γH2A.X (Figs. 2A and 2B, and Supporting Information Figure S4). The best results in the detection of the intracellular markers γH2A.X and CC3 (i.e., a good separation of positive and negative populations) in cells treated with a high dose of the proteasome inhibitor MG-132 occurred when 0.25% Triton X-100 was used (Figs. 2A and 2B; Supporting Information Figure S4). Because we aimed to simultaneously

analyze intracellular markers with surface markers, we also examined how the tested agents affect the detection of the surface marker Trop-2 (11) in cE2 cells. Cells treated with all permeabilization reagents exhibited 100% positivity for Trop-2, however, based on MFI, the most gentle permeabilization reagent was 0.25% Triton X-100 (Fig. 2C and Supporting Information Figure S4). 0.2% and 0.15% Triton X-100 concentrations were insufficient for sensitive detection of intracellular markers (data not shown).

Optimization of permeabilization conditions was a prerequisite for successful implementation of intracellular markers of apoptosis induction: cleaved PARP (cPARP), a substrate of executive caspases, and cleaved caspase-3 (CC3), both of which are commonly used as indicators of ongoing apoptosis (12,13). Positivity for both markers was detected in cells treated with MG-132; however, CC3 exhibited better separation of positive and negative populations (Supporting Information Figure S2). Therefore, we decided to use CC3 as a marker of ongoing apoptosis in our protocol.

Surprisingly, one of the most challenging steps in the assay optimization was to find an appropriate DNA stain to use in combination with other selected parameters. For our application, we found that the fluorescent signal of some DNA dyes is too strong, with high background, and impossible to compensate (e.g., FxCycle Far Red and APC/Cy7; data not shown). In our experimental setup, we found the most convenient employment of the dye PO-PRO-1, which is a bright and photostable cyanine monomer that intercalates nonspecifically into DNA (14).

Examination of Various Cell Lines Demonstrates Versatility of the Assay

Having optimized all the crucial steps, we aimed to demonstrate the ability of our assay to examine the complex cellular response to the experimental treatment. We treated cells with selected concentrations of well-established inducers of cell cycle arrest or apoptosis MLN-4924, MG-132, or TRAIL (Supporting Information Table S1) and applied the complete staining procedure (Fig. 1). Changes in cellular viability, expression of surface markers, cell cycle progression and markers of apoptosis induction are depicted in Figure 3, and described in Supporting Information Table S3. Altogether, most effects were in accordance with expected outcomes of drug treatment, but our analysis revealed several interesting phenomena. An apparent lack of effect of TRAIL on cellular viability probably results from the sustained integrity of the

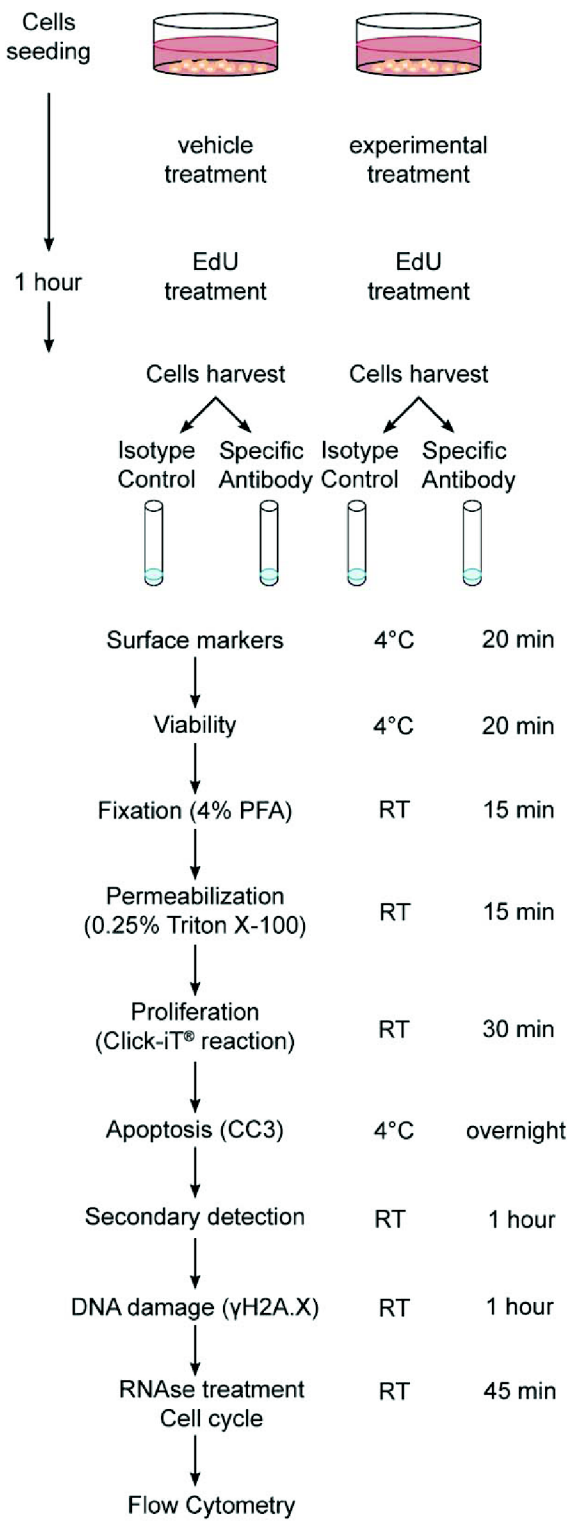

Figure 1. Scheme of experimental design and procedure. Cells were seeded and treated with experimental drugs as described in the Material and Methods section. One hour before harvesting, all cells were treated with EdU (10 μM). Cells were then harvested, split, and stained with isotype controls or specific antibodies. First, cells were stained with surface markers antibodies followed by viability stain. Next, cells were fixed (4% PFA), permeabilized (0.25% Triton X-100), and the Click-iT® reaction was performed. Subsequently, cells were stained with cleaved caspase-3 (CC3) followed by secondary antibody stain to detect apoptosis and afterwards with γH2A.X for the detection of DNA damage. Lastly, cells were stained with DNA-binding dye PO-PRO-1 with RNAse (100 μg/ml) and analyzed with a flow cytometer. Sample acquisition was performed on a BD FACSAria II Sorp instrument. The final optimized protocol was applied to SU-DHL-4, DU 145, cE2, and HCT 116 cells and measured at least twice for each cell line. [Color figure can be viewed at wileyonlinelibrary.com]

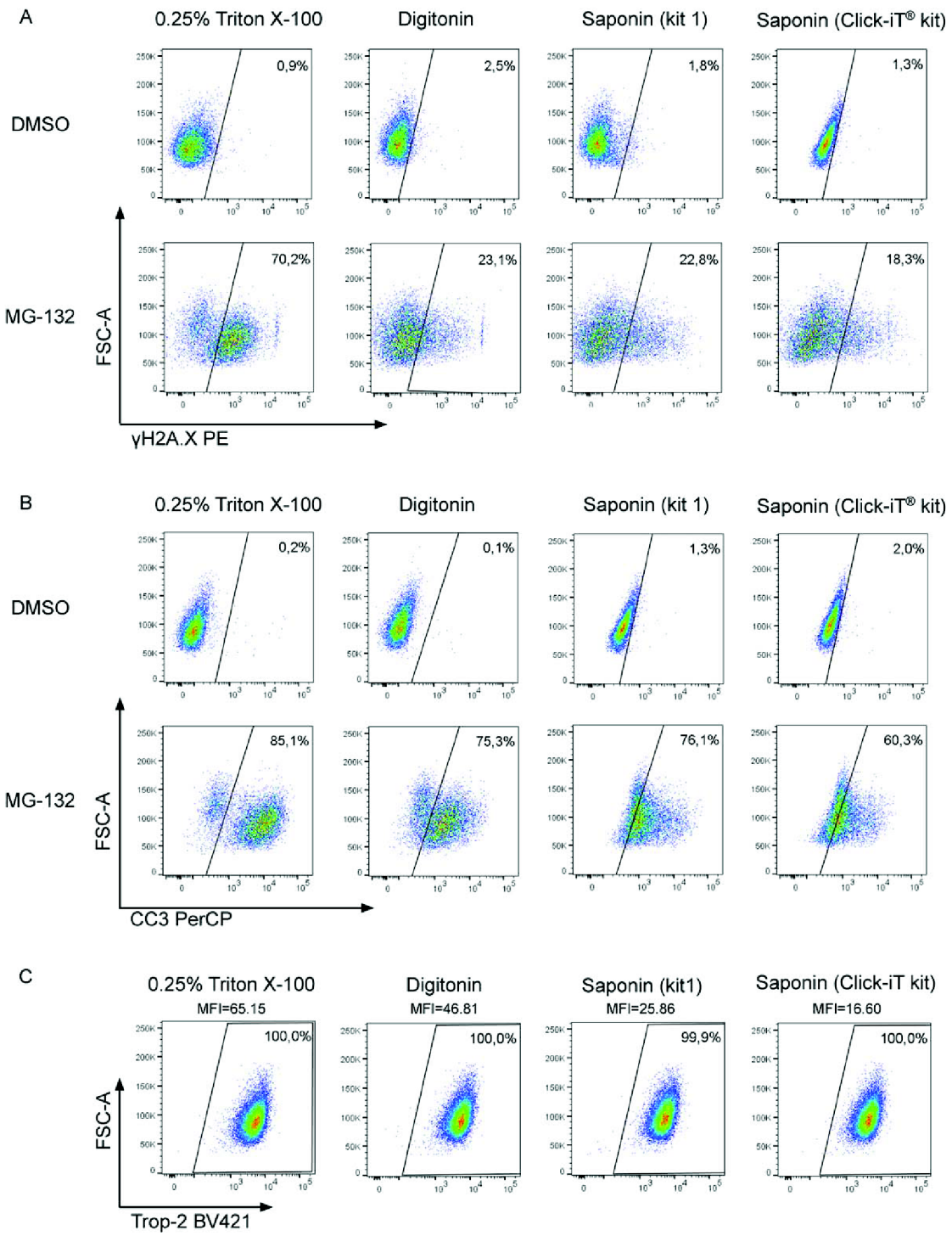

Figure 2. Optimization of permeabilization step and DNA staining. Permeabilization agents (0.25% Triton X-100, digitonin [300 μg/ml], or saponin-based reagents from the Mouse Pluripotent Stem Cell Transcription Factor Analysis Kit [BD Biosciences 560585; kit 1] or the Click-iT® detection kit [Thermo Fisher Scientific 405231]) were tested in cE2 cells to obtain a convenient agent that is sufficient for cell permeabilization and detection of intracellular markers such as γH2A.X (**A**) and CC3 (**B**), and simultaneously gentle for surface markers for example, Trop-2 (**C**). The positivity for Trop-2 was similar in all tested conditions. However, the MFI was decreased in cells permeabilized with Digitonin or Saponin Based kits compared to 0.25% Triton X-100, giving the best results for all tested markers. Sample acquisition was performed on BD FACSVerse. The corresponding isotype controls are presented in Supporting Information Figure S4. [Color figure can be viewed at wileyonlinelibrary.com]

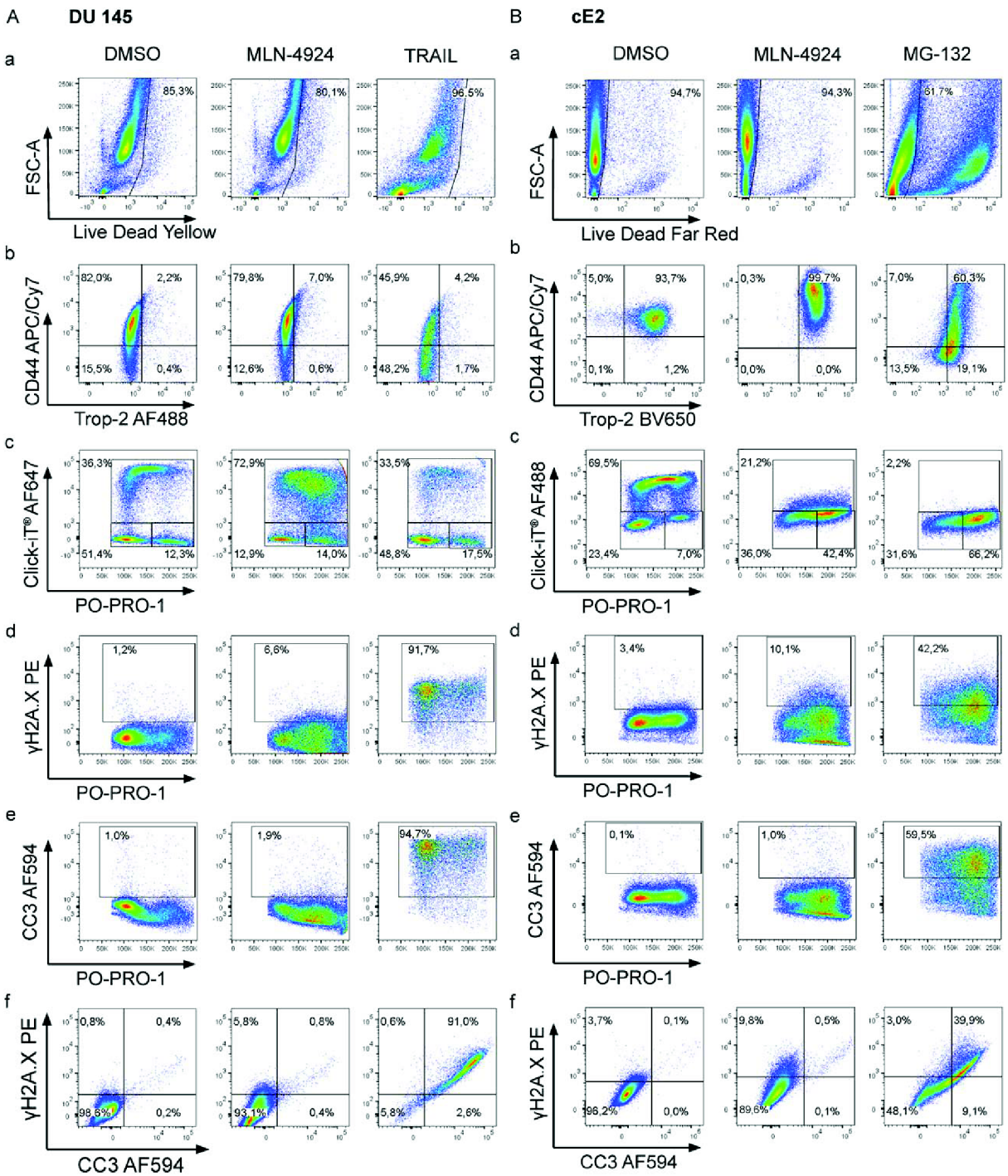

Figure 3. Complex analysis of cellular response to MLN-4924 and TRAIL or MG-132 treatment. Cells negative for the LIVE/DEAD® Fixable Dead stain (row a in **A**–**D**) were selected for further analysis to differentiate dead cells and to avoid false positivity in the detection of surface markers. cE2 and DU 145 cells were characterized by non-uniform expression of CD44 and Trop-2 (A-B, row b), SU-DHL-4 cells were characterized by the expression of differentiation markers CD20 and CD19 (C, row b) and HCT 116 cells were stained for markers CD133 and CD44 (D row b). The accumulation of cells in distinct phases of the cell cycle is defined in dot plots with PO-PRO-1/Click-iT® EdU (row c). To evaluate DNA damage, cells were stained with γH2A.X (row d, f). Induction of apoptosis was determined by CC3 (row e, f). Sample acquisition was performed on a BD FACSAria II Sorp instrument. The corresponding isotype controls are presented in Supporting Information Figure S5. (**E**) Western blot analysis of cells treated with DMSO, MLN-4924, TRAIL or MG-132. Samples are paired to those analyzed by flow cytometry. The activity of the MLN-4924 inhibitor was confirmed by abrogated NEDD8 binding to Cullins. Induction of DNA damage was confirmed by detection of γH2A.X, apoptosis was detected by CC3. α-tubulin was used as a loading control. [Color figure can be viewed at wileyonlinelibrary.com]

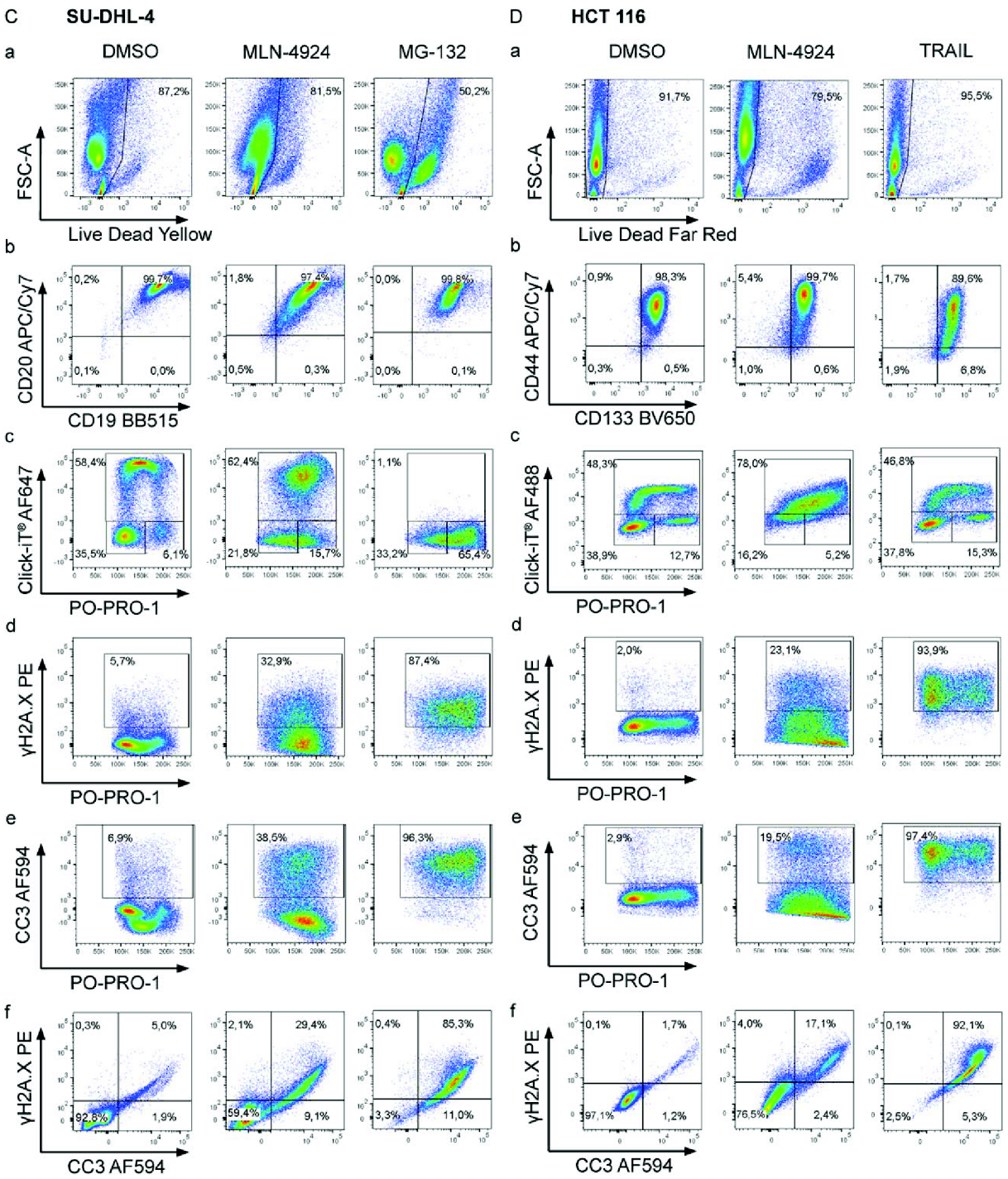

Figure 3. (Continued).

cellular membrane in the early phases of apoptosis in DU 145 and HCT 116 cells (Figs. 3A and 3D, row a) (15). In terms of surface marker expression, we detected an effect of particular treatments on expression of surface markers in all studied cell lines (Figs. 3A–3D, row b; and Supporting Information Table S3). Cell cycle analysis based on the DNA amount stained with probe PO-PRO-1 indicated changes in the cell cycle progression; however, the cell cycle profile showed relatively high coefficient of variation. Alternatively, cell cycle phases can be visualized and determined accurately in a dot plot showing a combination of DNA stain versus DNA synthesis (Click-iT EdU).

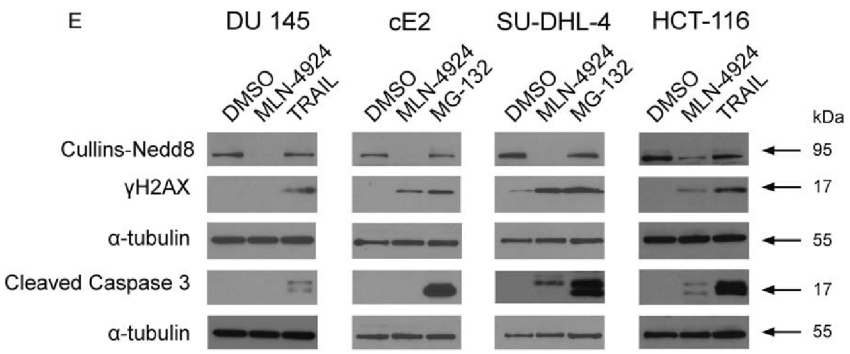

Figure 3. (Continued).

Our analysis revealed different responses of selected cell lines to the MLN-4924 inhibitor, as depicted in Figures 3A–3D, row c, and Supporting Information Table S3. Proliferation was abolished in cE2 and SU-DHL-4 treated with MG-132 (Figs 3B and 3C, row c, and summarized in Supporting Information Table S3) and interestingly, proliferation was not affected in DU 145 and HCT 116 cells following TRAIL treatment, and these cells exhibited a normal cell cycle profile as seen in control (Figs. 3A and 3D, row c).

Our analysis confirmed the ability of MLN-4924 to induce DNA damage in all studied cell lines (Figs. 3A–3D, rows d, f and Supporting Information Table S3), and to induce apoptosis in SU-DHL-4 and HCT 116 cells (Figs. 3C and 3D, rows e, f). Both induction of DNA damage and apoptosis was observed in samples treated with MG-132 or TRAIL (Figs. 3A–3D, rows d-f, Supporting Information Table S3) and confirmed also on protein level by western blot (Fig. 3E). These results demonstrated the robustness of our assay and its capability to describe a broad spectrum of cell responses using a complex set of different parameters at the single-cell level.

Assay Application—Analysis of Response to Experimental Treatment in a Heterogeneous Sample

Finally, we wanted to demonstrate the applicability of our protocol in the complex analysis of heterogeneous samples. We took advantage of the DU 145 cell line, where we observed the consistent presence of a subpopulation of cells expressing Trop-2 (Fig. 3A, row b). Therefore, we used the established protocol to investigate the response of cells that differ in Trop-2 expression status to MLN-4924 or TRAIL treatment. We observed that the expression of Trop-2 itself did not change following MLN-4924 or TRAIL treatment (Fig. 4A and Supporting Information Figure S3A, and Supporting Information Table S4), but we noted differences in cell cycle progression in Trop-2 positive and negative subpopulations (Fig. 4B, Supporting Information Figure S3B and Supporting Information Table S4), while the induction of DNA damage was proportionate in Trop-2^- and Trop-2^+ cells following TRAIL and MLN-4924 treatment (Figs. 4C and 4E; Supporting Information Figure S3C, and Supporting Information Table S4). Induction of apoptosis was significantly increased in Trop-2^- cells compared to Trop-2^+ cells following TRAIL treatment (Figs. 4D and 4E, Supporting Information Figure S3D, and Supporting Information Table S4). Thus, these data demonstrate that our approach is useful in complex analysis of cellular responses in a heterogeneous sample, and has the potential to reveal differences in the responses of precisely defined phenotypic subpopulations.

Discussion

Although flow cytometry is an irreplaceable approach for multiparametric single-cell analyses, it is not frequently used for "single-tube" analysis of complex cellular response to the experimental therapy. This type of analysis can be very useful in case of limited amount of biological material, such as clinical samples or end-point in vivo studies. Major obstacle for simple multiplex detection of different biomarkers of cellular functions is the necessity to perform several optimizing steps and verifications. In this study, we aimed to use full advantage of the multicolor flow cytometry to establish a protocol for complex analysis of cellular response together with the immunophenotype and functional characteristics of the treated cells.

The crucial step is the selection of fluorescently labeled antibodies for surface marker detection that are compatible with subsequent azide-alkyne coupling (Click-iT EdU) reaction. Azide-alkyne coupling (click chemistry) has become a powerful coupling method for chemoselective ligation (16). However, copper and reactive oxygen species-mediated damage to fluorescent proteins prevents the simultaneous detection of EdU with GFP or R-phycoerythrin (R-PE) fluorescence. Moreover, here we showed that fluorescent intensity of Click-iT EdU compatible APC conjugate is affected on permeabilization followed by the Click-iT EdU reaction. This limitation might be overcome in second-generation Click-iT Plus EdU kits with "copper-safe" catalysis of the click reaction (17). With respect to the compatibility with the Click-iT chemistry, the protocol allows high degree of customization by the end user. For instance, other antibodies for apoptosis detection (such as cPARP) can be suitable for different experimental models.

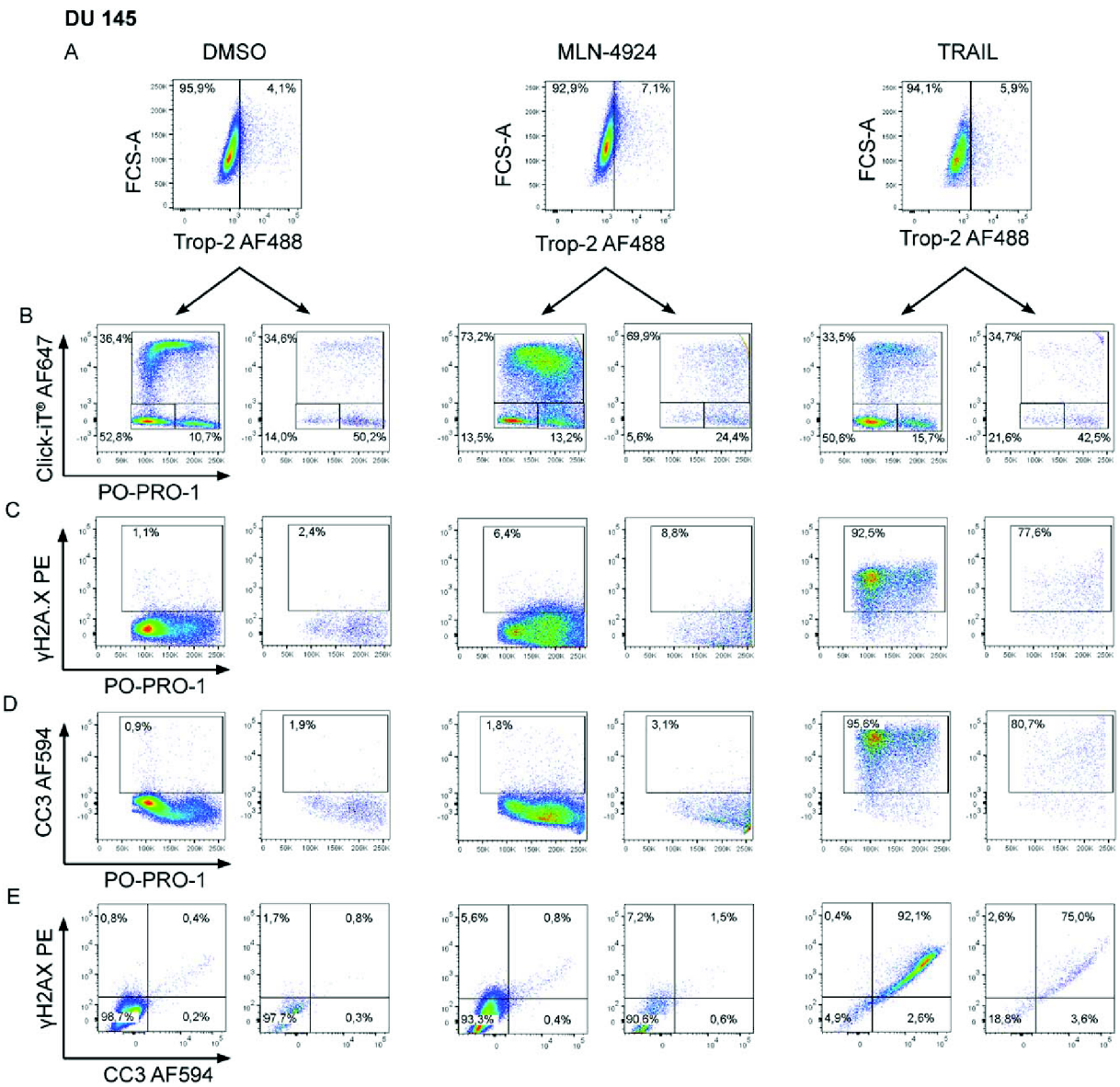

Figure 4. Comparison of complex responses to treatment among Trop-2$^-$ and Trop-2$^+$ subpopulations. Response to treatment was analyzed separately in the Trop-2$^-$ and Trop-2$^+$ subpopulations in the DU 145 cell line (**A**). Differences in proliferation (**B**), DNA damage (**C**, **E**), and induction of apoptosis (**D**, **E**) were examined. Gates shown in Figure 3A were applied to Trop-2 subpopulations of DU 145 cells in Figure 4. Sample acquisition was performed on a BD FACSAria II Sorp instrument. [Color figure can be viewed at wileyonlinelibrary.com]

Detergents such as saponin, Triton X-100, and Tween-20 are widely used to permeabilize cells in flow cytometry (18). Saponin has been described as a favorable permeabilization reagent for simultaneous detection of surface antibodies and proliferation in T cells with no alteration of membrane antigens. In addition, saponin has been described as a sensitive reagent for the detection of intranuclear antigens (19). Seminal study comparing different cellular fixation and permeabilization techniques for intracellular stainings published by Krutzik and Nolen is not systematically dealing with permeabilization in combination with surface antigen detection (20). Therefore, we concentrated in our work on finding a condition which will preserve the surface antigen pattern and give optimal result of intracellular stainings not only in the intact cells but also in drug treated groups. Triton X-100 in 0.25% concentration was gentle enough to the tested surface proteins and at the same time provided a good separation of positive and negative populations for the intracellular markers γH2A.X and CC3. This result is in line with a recent study, where Triton X-100 was shown to be a more convenient permeabilization reagent compared to saponin in the immunocytochemical detection of phospho-specific antibodies (21).

Analysis of the perturbation of cell cycle progression using flow cytometry is a frequently used technique. Nowadays, a

broad spectrum of DNA-binding fluorescent dyes is available, including intercalating dyes (ethidium bromide, propidium iodide, 7AAD) and minor groove binders (DAPI and Hoechst 33342). In our case, the fluorescent signal of FxCycle Far Red stain was impossible to compensate with some other fluorochromes. Therefore, we searched for a dye suitable for our experimental setup. As the result, we implemented PO-PRO-1 dye (14,22) into our protocol. It gave suitable results of cell cycle analysis when it was combined with Click-iT EdU assay and in overall it was functional in our multiparametric assay. However, we are aware of the existing scope for further improvement of DNA staining in this protocol.

In summary, we have established a multiparametric flow cytometric assay for the complex analysis of cellular phenotypes in response to experimental therapy. Using this assay, we are able to simultaneously detect changes in viability, cell cycle profile, DNA synthesis and damage, and apoptosis in cells characterized by the expression of two surface markers. Obviously, the main benefit of this approach is that various biological responses to a specific treatment can be evaluated in a single assay on a single-cell level. Furthermore, we demonstrate the possible application of this established procedure to analyze heterogeneous samples and to compare the effects of drugs on different subsets of cell lines. Moreover, the protocol can be applied to both human and mouse cells, and to adherent and non-adherent cells. This creates an opportunity to efficiently analyze mixed cell populations including infiltrating host cells in xenografts. We propose that this protocol (described in detail in the Supporting Information Protocol) will be useful for complex phenotype analysis of specifically defined cell populations and for investigations of their responses to drug treatment in a single assay.

Acknowledgments

The authors would like to thank Dr. Jaromír Mikeš for helpful and critical comments on the manuscript, anonymous reviewers for their valuable comments and suggestions to improve the quality of the article, Prof. Bert Vogelstein (John Hopkins University, Baltimore, MA) for providing the HCT 116 cells, Dr. Pradip Roy Burman for providing the cE2 cells, Dr. Martin Trbušek (Masaryk University, Brno, Czech Republic) for providing the SU-DHL-4 cells, Ladislav Anděra (Institute of Biotechnology of the Czech Academy of Sciences, Prague, Czech Republic) for providing TRAIL, and Iva Lišková, Kateřina Svobodová, and Martina Urbánková for superb technical assistance.

Conflicts of Interest

The authors declare that there are no potential conflicts of interest.

Authors Contributions

Conception and design: K. Souček, Š. Šimečková, Z. Kahounová

Cell line experiments: Š. Šimečková, R. Fedr

Writing, review, and/or revision of the manuscript: Š. Šimečková, Z. Kahounová, J. Remšík, E. Slabáková, K. Souček

Study supervision: K. Souček

Literature Cited

1. Silveira GF. Evolution of flow cytometry technology. Microb Biochem Technol 2015; 7:216.
2. Donnenberg VS, Donnenberg AD. Coping with artifact in the analysis of flow cytometric data. Methods 2015;82:3–11.
3. Filby A. Sample preparation for flow cytometry benefits from some lateral thinking. Cytometry Part A 2016;89A:1054–1056.
4. Potgens AJ, Schmitz U, Kaufmann P, Frank HG. Monoclonal antibody CD133-2 (AC141) against hematopoietic stem cell antigen CD133 shows crossreactivity with cytokeratin 18. J Histochem Cytochem 2002;50:1131–1134.
5. Jamur MC, Oliver C. Permeabilization of cell membranes. In Oliver C, Jamur CM, editors. Immunocytochemical Methods and Protocols. Totowa, NJ: Humana Press; 2010. pp 63–66.
6. Heath JR, Ribas A, Mischel PS. Single-cell analysis tools for drug discovery and development. Nat Rev Drug Discov 2016;15:204–216.
7. Liao CP, Liang M, Cohen MB, Flesken-Nikitin A, Jeong JH, Nikitin AY, Roy-Burman P. Mouse prostate cancer cell lines established from primary and postcastration recurrent tumors. Horm Cancer 2010;1:44–54.
8. Slabakova E, Pernicova Z, Slavickova E, Starsichova A, Kozubik A, Soucek K. TGF-beta 1-induced EMT of non-transformed prostate hyperplasia cells is characterized by early induction of SNAI2/slug. Prostate 2011;71:1332–1343.
9. Pollice AA, Philip Mccoy J, Shackney SE, Smith CA, Agarwal J, Burnolt DR, Janocko LE, Hornicek FJ, Singh SG, Hartsock RJ. Sequential paraformaldehyde and methanol fixation for simultaneous flow cytometric analysis of DNA, cell surface proteins, and intracellular proteins. Cytometry 1992;13:432–444.
10. Schmid I, Uittenbogaart CH, Giorgi JV. A gentle fixation and permeabilization method for combined cell surface and intracellular staining with improved precision in DNA quantification. Cytometry 1991;12:279–285.
11. Goldstein AS, Lawson DA, Cheng D, Sun W, Garraway IP, Witte ON. Trop2 identifies a subpopulation of murine and human prostate basal cells with stem cell characteristics. Proc Natl Acad Sci USA 2008;105:20882–20887.
12. Kaufmann SH, Desnoyers S, Ottaviano Y, Davidson NE, Poirier GG. Specific proteolytic cleavage of poly(ADP-ribose) polymerase: An early marker of chemotherapy-induced apoptosis. Cancer Res 1993;53:3976–3985.
13. Miura M, Zhu H, Rotello R, Hartwieg EA, Yuan J. Induction of apoptosis in fibroblasts by IL-1 beta-converting enzyme, a mammalian homolog of the C. elegans cell death gene ced-3. Cell 1993;75:653–660.
14. Hoshi H, O'Brien J, Mills SL. A novel fluorescent tracer for visualizing coupled cells in neural circuits of living tissue. J Histochem Cytochem 2006;54:1169–1176.
15. Wlodkowic D, Telford W, Skommer J, Darzynkiewicz Z. Apoptosis and beyond: Cytometry in studies of programmed cell death. Methods Cell Biol 2011;103:55–98.
16. Breinbauer R, Köhn M. Azide–alkyne coupling: A powerful reaction for bioconjugate chemistry. ChemBioChem 2003;4:1147–1149.
17. Deveny R, DeMarco C, Bradford J, Clarke S, Grecian S, Singh U, Gee K. Improved click chemistry demonstrating EdU cell proliferation with GFP expressing cells and R-PE based immunophenotyping. (P3299). J Immunol 2013;190:211.7–211.7.
18. Koester SK, Bolton WE. Strategies for cell permeabilization and fixation in detecting surface and intracellular antigens. In: Wilson L, Matsudaira PT, Darzynkiewicz Z, Robinson JP, Crissman HA, editors. Methods in Cell Biology. Chapter 12. Academic Press. vol. 63, p 253–268; 2001. http://www.sciencedirect.com/science/article/pii/S0091679X01630164
19. Jacob MC, Favre M, Bensa JC. Membrane cell permeabilization with saponin and multiparametric analysis by flow cytometry. Cytometry 1991;12:550–558.
20. Krutzik PO, Nolan GP. Intracellular phospho-protein staining techniques for flow cytometry: Monitoring single cell signaling events. Cytometry Part A 2003;55A:61–70.
21. Molgaard S, Ulrichsen M, Olsen D, Glerup S. Detection of phosphorylated Akt and MAPK in cell culture assays. MethodsX 2016;3:386–398.
22. Sabnis RW. PO-PRO 1. Handbook of Fluorescent Dyes and Probes. Wiley; 2015. pp 324–325.

Supplementary figures

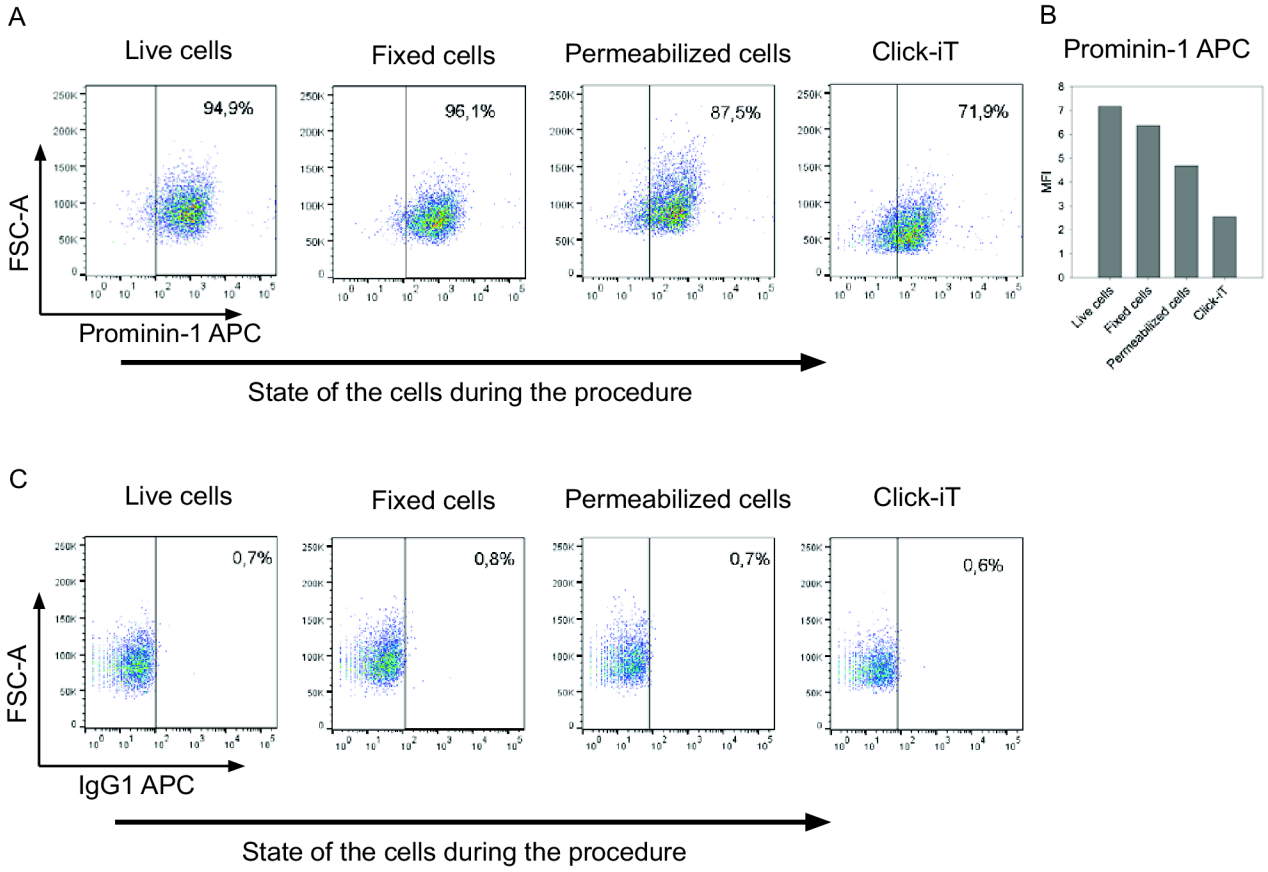

Supplementary Figure 1. Stability of surface marker Prominin-1 in particular steps during the procedure The signal stability of the Prominin-1 APC antibody during the procedure was examined. Decreased positivity of cE2 cells for prominin-1 APC after permeabilization and the Click-iT® reaction was observed (A), and was confirmed by a decrease in MFI (B). Isotype controls related to panel A are shown in panel C. Samples acquisition was performed on a BD FACSVerse.

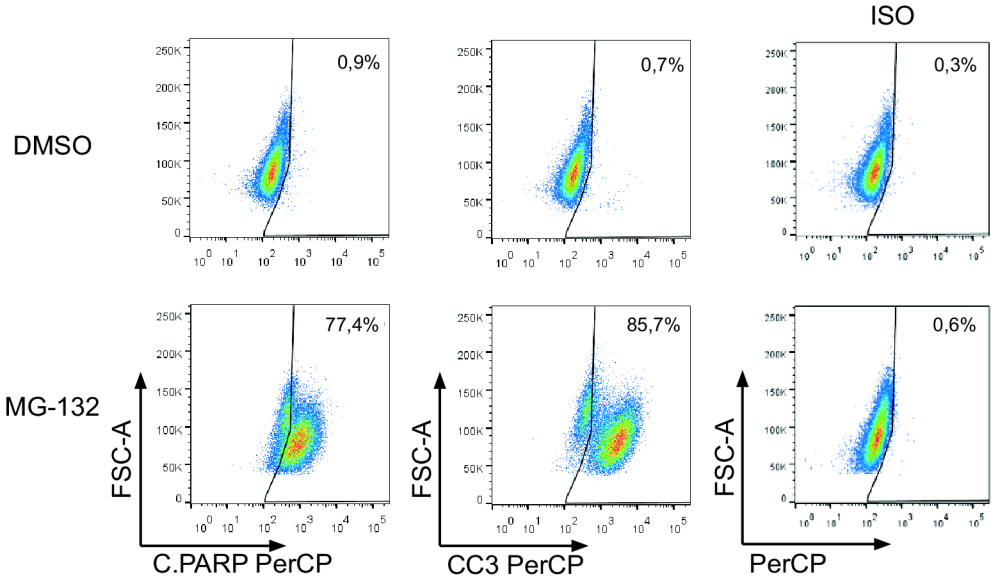

Supplementary Figure 2. Apoptosis marker selection
cE2 cells were treated with DMSO or MG-132 (5 µM for 24 hours). Cells were fixed in 4% PFA and permeabilized by 0.25% Triton X-100. Next, cells were stained with primary antibody to cleaved PARP or CC3 overnight, subsequently stained with secondary antibody for 1 hour at room temperature, and analyzed on BD FACSVerse. Better separation of positive or negative cell populations was observed in cells stained with CC3, compared to cells stained with cleaved PARP. In isotype controls (ISO), cells were stained with secondary antibody only.

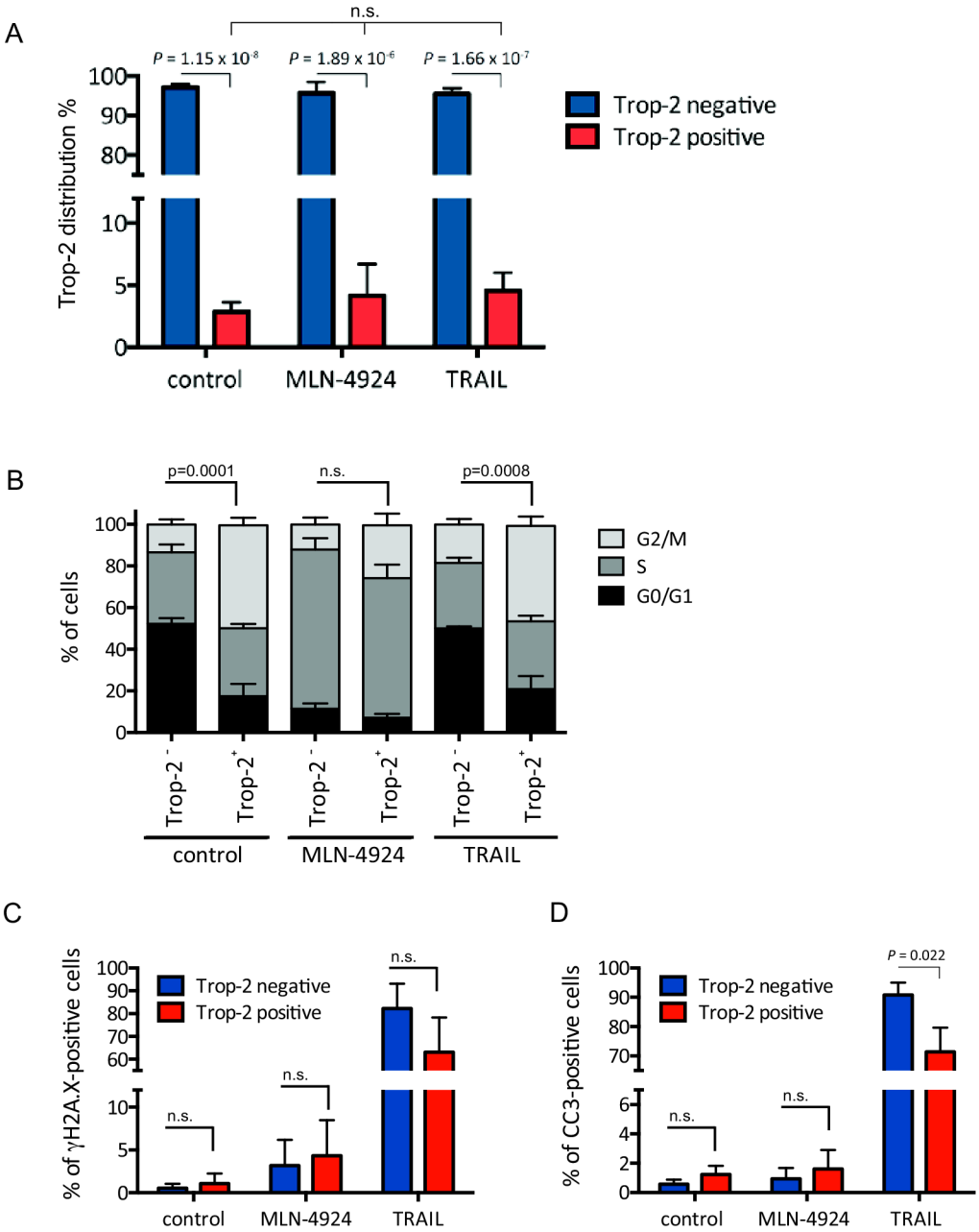

Supplementary Figure 3. Quantitative analysis of complex responses to treatment among Trop-2$^-$ and Trop-2$^+$ subpopulations

(A) The phenotype of DU 145 cells in term of Trop-2 expression is not significantly changed after MLN-4924 or TRAIL treatment. (B) cell cycle analysis of Trop-2$^-$ and Trop-2$^+$ subpopulations reveals their different state in G0/G1 and G2/M phase. MLN-4924 increases S phase in both subpopulations. (C) Induction of DNA damage (γH2A.X) was proportionate in both subpopulations after both MLN-4924 and TRAIL treatment. (D) Induction of Caspase-3 cleavage was minimal after MLN-4924 treatment with no significant difference in Trop-2 subpopulations. In cells treated with TRAIL, induction of Caspase-3 cleavage was significantly increased in Trop-2- cells compared to Trop-2+ cells. Statistical analysis was performed from three independent experiments.

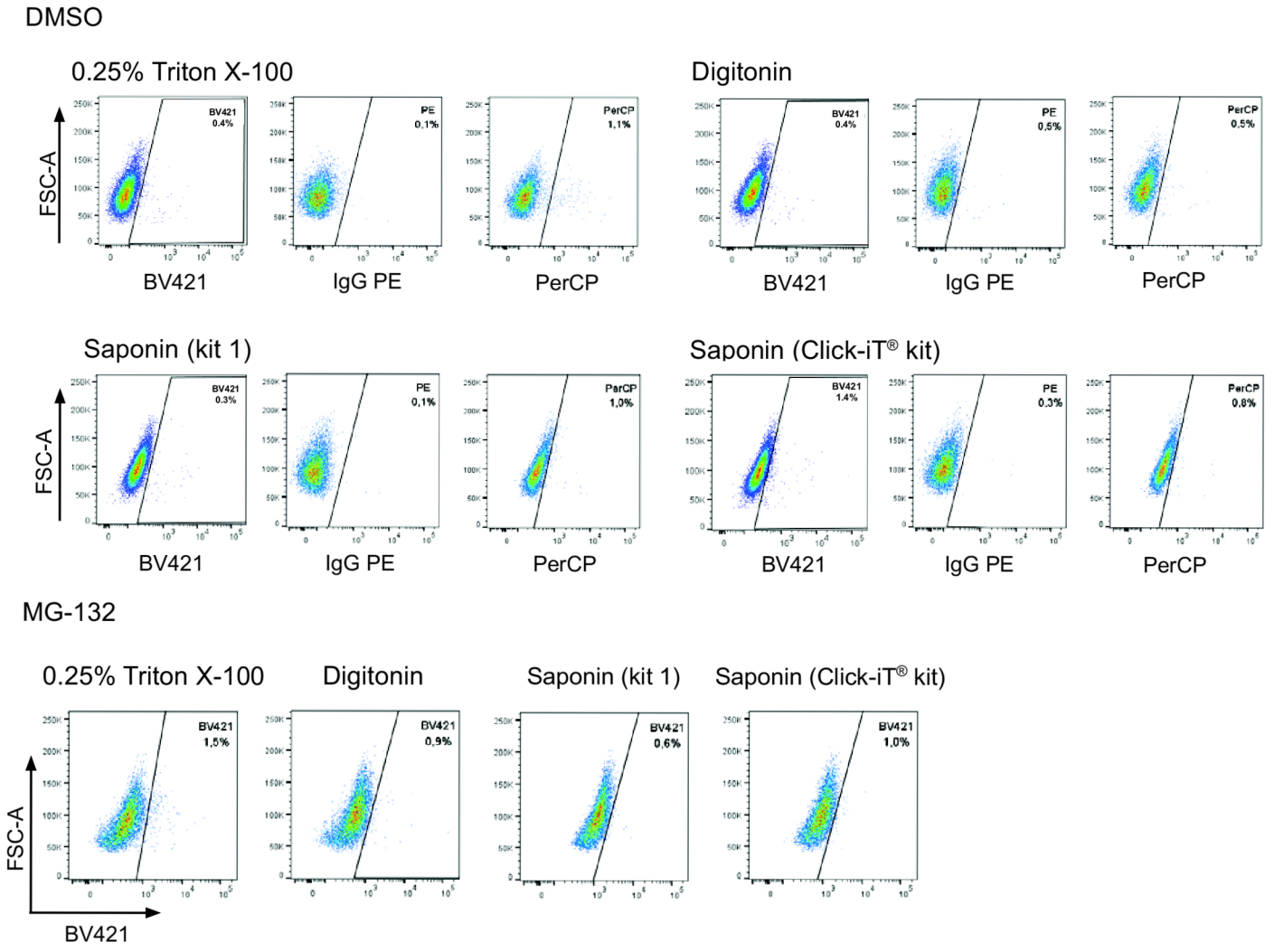

Supplementary Figure 4. Isotype controls gating
Graphs represent isotype control gating. Isotype controls are related to the samples displayed in Figure 2 A-C. Sample acquisition was performed with a BD FACSVerse.

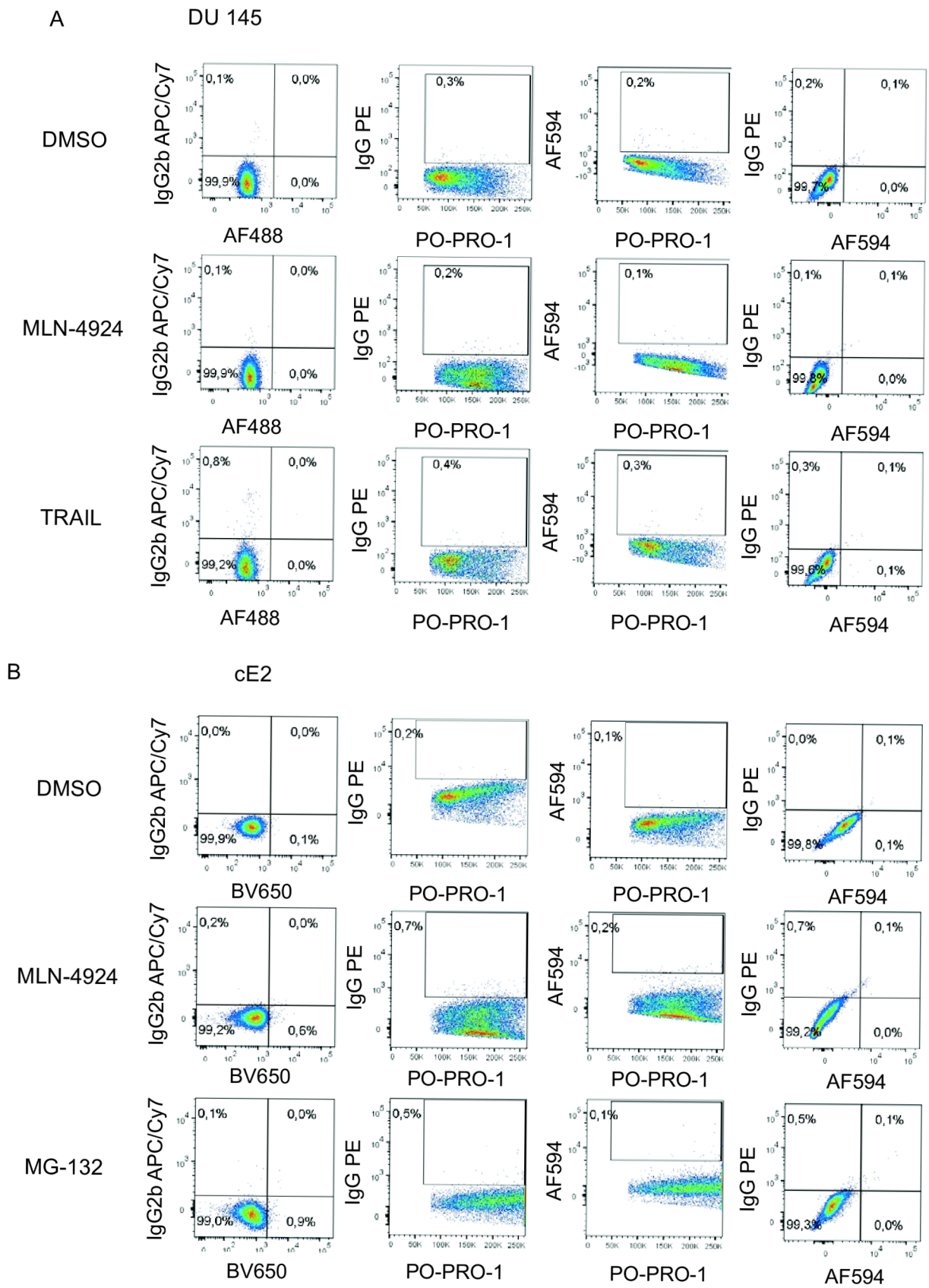

Supplementary Figure 5. Isotype controls gating
Isotype controls of DU 145 (A) and cE2 (B) SU-DHL-4 (C) and HCT 116 (D) cells related to the samples shown in Figure 3 A-D and Figure 4. Sample acquisition was performed with a BD FACSAria II Sorp instrument.

Supplementary Figure 5 cont.

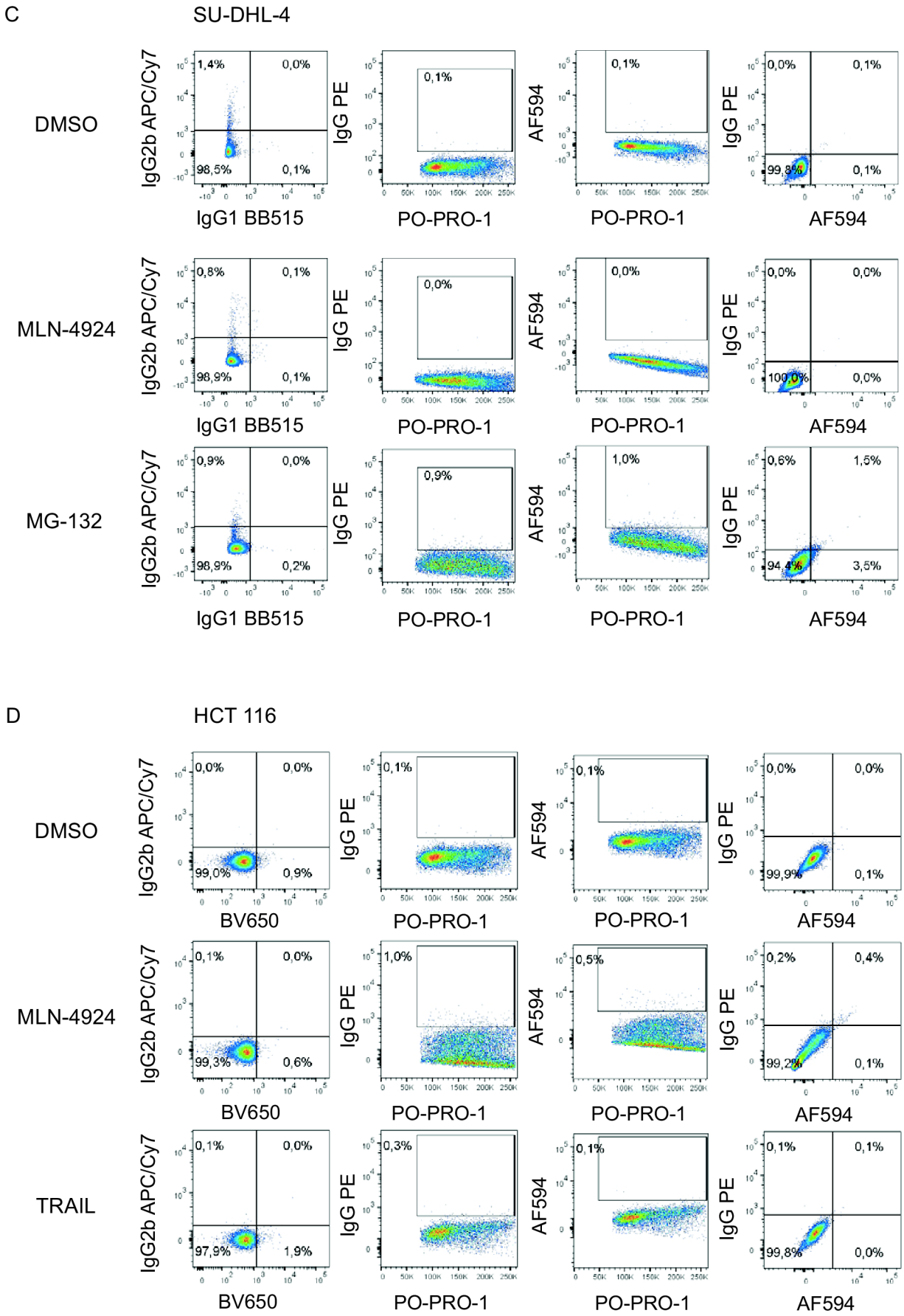

Supplementary Table S1 Treatment of the cells

cell line	control treatment	MLN-4924 24 hrs	TRAIL 2 hrs	MG-132 24 hrs
DU 145	DMSO	0,33 µM	50 ng/ml	-
SU-DHL-4	DMSO	1 µM	-	1 µM
HCT 116	DMSO	0,33 µM	50 ng/ml	-
cE2	DMSO	5 µM	-	1 µM

Supplementary Table S2 Antibodies used and Instrument settings

cE2 cells															
Marker	**Fluorochrome**	**Source**	**Company**	**Catalog Number**	**Antibody concentration**	**Dilution**	**Laser**	**Excitation maxima (nm)**	**Emission maxima (nm)**	**Manufacturer**	**Power**	**Instalation date**	**Detector**	**Dichroic Mirror // Band Pass Filter (nm)**	**Instrument**
Trop-2	biotin	Mouse	R&D	BAF1122	50 µg/ml	1:50	-	-	-	-	-	-	-	-	FACSAria II Sorp
CD44	APC/Cy7	Rat	BioLegend	103028	200 µg/ml	1:100	639	650; 755	785	Coherent Cube	40 mW	2009	C - Red Trigon	750LP // 780/60	FACSAria II Sorp
Viability	LIVE/DEAD Fixable Far Red Dead Cell Stain Kit	-	ThermoFisher Scientific	L10120	-	1:1000	639	650	665	Coherent Cube	40 mW	2009	C - Red Trigon	Empty // 670/14	FACSAria II Sorp
Proliferation	Click-iT® EdU Alexa Fluor® 488	-	ThermoFisher Scientific	C10420	-	-	488	495	519	Coherent Sapphire	100 mW	2009	B - Blue Octagon	505LP // 525/50	FACSAria II Sorp
Cell Cycle	PO-PRO-1	-	ThermoFisher Scientific	P3581	1 mM	1:10000	405	434	456	Coherent Cube	100 mW	2009	F - Violet Octagon	Empty // 450/50	FACSAria II Sorp
Cleaved Caspase 3	-	Rabbit	Cell Signalling	9661S	-	1:800	-	-	-	-	-	-	-	-	-
γH2AX	PE	Rabbit	Cell Signalling	5763S	50 µg/ml	1:50	561	565	575	Coherent Sapphire	100 mW	2013	E - Yellow Green Octagon	570LP // 585/15	FACSAria II Sorp
Isotype Controls and secondary detection															
IgG2b	APC/Cy7	Rat	BioLegend	400624	200 µg/ml	1:100	639	650; 755	785	Coherent Cube	40 mW	2009	C - Red Trigon	750LP // 780/60	FACSAria II Sorp
IgG XP®	PE	Rabbit	Cell Signaling	5742S	100 µg/ml	1:100	561	565	575	Coherent Sapphire	100 mW	2009	E - Yellow Green Octagon	570LP // 585/15	FACSAria II Sorp
anti-Rabbit	Alexa Fluor 594	Donkey	ThermoFisher Scientific	A-21207	2000 µg/ml	1:500	561	590	617	Coherent Sapphire	100 mW	2013	D - Yellow Green Octagon	600LP // 610/20	FACSAria II Sorp
Streptavidin	Briliant Violet 650	-	BioLegend	405231	100 µg/ml	1:1500	405	407	650	Coherent Cube	40 mW	2009	C - Blue Octagon	630LP // 660/20	FACSAria II Sorp
Antibodies used for optimization steps															

Prominin-1	APC	Rat	Miltenyi Biotec	130-102-197	30 µg/ml	1:11	640	660	650		40 mW	2012	B - Red Digon	660/10 // 660/10	FACSVerse
Trop-2	biotin	Mouse	R&D	BAF1122	50 µg/ml	1:50	-	-	-	-	-	-	-	-	FACSVerse
Viability	LIVE/DEAD Fixable Violet Dead Cell Stain Kit	-	ThermoFisher Scientific	L34955	-	1:1000	405	416	451		40 mW	2012	B - Violet Digon	448/45 // 448/45	FACSVerse
Viability	LIVE/DEAD Fixable Yellow Dead Cell Stain Kit	-	ThermoFisher Scientific	L34959	-	1:500	405	400	575		40 mW	2012	A - Violet Digon	500 LP // 528/45	FACSVerse
Cleaved Caspase3	-	Rabbit	Cell Signalling	9661S	-	1:800	-	-	-	-	-	-	-	-	-
Cleaved PARP	-	Rabbit	Cell Signalling	9544	-	1:25	-	-	-	-	-	-	-	-	-
	DAPI	-	AppliChem	A4099	1000 µg/ml	1:2000	405	358	461	Coherent Cube	100 mW	2009	F - Violet Octagon	Empty // 450/50	FACSAria II Sorp
Isotype Controls and secondary detection															
IgG1	APC	Rat	Miltenyi Biotec	130-102-646	30 µg/ml	1:11	640	660	650		40 mW	2012	B - Red Digon	660/10 // 660/10	FACSVerse
anti-Rabbit	PerCP	Donkey	Jackson ImmunoResearch	711-126-152	500 µg/ml	1:25	488	490	675		20 mW	2012	B - Blue Tetragon	665 LP // 700/54	FACSVerse
Streptavidin	streptavidin PE	-	eBioscience	12-4317	200 µg/ml	1:2000	488	565	575		20 mW	2012	D - Blue Tetragon	560LP // 586/42	FACSVerse
Streptavidin	Briliant Violet 421	-	BioLegend	405226	100 µg/ml	1:1000	405	405	421		40 mW	2012	B - Violet Digon	448/45 // 448/45	FACSVerse
Streptavidin	Briliant Violet 650	-	BioLegend	405231	100 µg/ml	1:1500	405	407	650	Coherent Cube	40 mW	2009	C - Blue Octagon	630LP // 660/20	FACSAria II Sorp
HCT 116 cells															
Marker	**Fluorochrome**		**Source**	**Catalog Number**	**Antibody concentration**	**Dilution**	**Laser**	**Excitation maxima (nm)**	**Emission maxima (nm)**	**Manufacturer**	**Power**	**Instalation date**	**Detector**	**Dichroic Mirror // Band Pass Filter (nm)**	**Instrument**
CD133 (AC133)	biotin	Mouse	Miltenyi Biotec	130-090-664	-	1:11	-	-	-	-	-	-	-	-	-
CD44	APC/Cy7	Rat	BioLegend	103028	200 µg/ml	1:100	639	650; 755	785	Coherent Cube	40 mW	2009	C - Red Trigon	750LP // 780/60	FACSAria II Sorp

Supplementary Table S2 continued

Proliferation	Click-iT® EdU Alexa Fluor® 488	-	ThermoFisher Scientific	C10420	-	-	488	495	519	Coherent Sapphire	100 mW	2009	B - Blue Octagon	505LP // 525/50	FACSAria II Sorp
Viability	LIVE/DEADFixable Far Red Dead Cell Stain Kit	-	ThermoFisher Scientific	L10120	-	1:1000	639	650	665	Coherent Cube	40 mW	2009	C - Red Trigon	Empty // 670/14	FACSAria II Sorp
Cell Cycle	PO-PRO-1	-	ThermoFisher Scientific	P3581	1 mM	1:10000	405	434	456	Coherent Cube	100 mW	2009	F - Violet Octagon	Empty // 450/50	FACSAria II Sorp
γH2AX	PE	Rabbit	Cell Signalling	5763S	50 µg/ml	1:50	561	590	617	Coherent Sapphire	100 mW	2013	D - Yellow Green Octagon	600LP // 610/20	FACSAria II Sorp
Cleaved Caspase 3	-	Rabbit	Cell Signaling	9661S	-	1:800	-	-	-	-	-	-	-	-	-
Isotype Controls and secondary detection															
IgG XP®	PE	Rabbit	Cell Signaling	5742S	100 µg/ml	1:100	561	565	575	Coherent Sapphire	100 mW	2013	E - Yellow Green Octagon	570LP // 585/15	FACSAria II Sorp
IgG2b	APC/Cy7	Rat	BioLegend	400624	200 µg/ml	1:100	639	650; 755	785	Coherent Cube	40 mW	2009	C - Red Trigon	750LP // 780/60	FACSAria II Sorp
anti-Rabbit	Alexa Fluor 594	Donkey	ThermoFisher Scientific	A-21207	2000 µg/ml	1:500	561	565	575	Coherent Sapphire	100 mW	2013	E - Yellow Green Octagon	570LP // 585/15	FACSAria II Sorp
Streptavidin	Briliant Violet 650	-	BioLegend	405231	100 µg/ml	1:1500	405	407	650	Coherent Cube	100 mW	2009	C - Blue Octagon	630LP // 660/20	FACSAria II Sorp
DU 145 cells															
Marker	**Fluorochrome**		**Source**	**Catalog Number**	**Antibody concentration**	**Dilution**	**Laser**	**Excitation maxima (nm)**	**Emission maxima (nm)**	**Manufacturer**	**Power**	**Instalation date**	**Detector**	**Dichroic Mirror // Band Pass Filter (nm)**	**Instrument**
Trop-2	-	Mouse	R&D	MAB650	500 µg/ml	1:50	-	-	-	-	-	-	-	-	-
CD44	APC/Cy7	Rat	BioLegend	103028	200 µg/ml	1:100	639	650; 755	785	Coherent Cube	40 mW	2009	C - Red Trigon	750LP // 780/60	FACSAria II Sorp
Viability	LIVE/DEAD Fixable Yellow Dead Cell Stain Kit	-	ThermoFisher Scientific	L34959	-	1:500	405	400	575		100 mW	2009	E - Violet Octagon	595LP // 605/40	FACSAria II Sorp

Supplementary Table S2 continued

Proliferation	Click-iT® EdU Alexa Fluor® 647	-	ThermoFisher Scientific	C10424	-	-	639	650	667	Coherent Cube	40 mW	2009	C - Red Trigon	Empty // 670/14	FACSAria II Sorp
Cell Cycle	PO-PRO-1	-	ThermoFisher Scientific	P3581	1 mM	1:10000	405	434	456	Coherent Cube	100 mW	2009	F - Violet Octagon	Empty // 450/50	FACSAria II Sorp
Cleaved Caspase 3	-	Rabbit	Cell Signaling	9661S	-	1:800	-	-	-	-	-	-	-	-	-
γH2AX	PE	Rabbit	Cell Signalling	5763S	50 µg/ml	1:50	561	565	575	Coherent Sapphire	100 mW	2013	E - Yellow Green Octagon	570LP // 585/15	FACSAria II Sorp
Isotype Controls and secondary detection															
IgG XP®	PE	Rabbit	Cell Signaling	5742	100 µg/ml	1:100	561	565	575	Coherent Sapphire	100 mW	2013	E - Yellow Green Octagon	570LP // 585/15	FACSAria II Sorp
IgG2b	APC/Cy7	Rat	BioLegend	400624	200 µg/ml	1:100	639	650; 755	785	Coherent Cube	40 mW	2009	C - Red Trigon	750LP // 780/60	FACSAria II Sorp
anti-Mouse	Alexa Fluor 488	Donkey	ThermoFisher Scientific	A21202	2000 µg/ml	1:1500	488	495	519	Coherent Sapphire	100 mW	2009	B - Blue Octagon	505LP // 525/50	FACSAria II Sorp
anti-Rabbit	Alexa Fluor 594	Donkey	ThermoFisher Scientific	A-21207	2000 µg/ml	1:500	561	590	617	Coherent Sapphire	100 mW	2013	D - Yellow Green Octagon	600LP // 610/20	FACSAria II Sorp
SU-DHL-4 cells															
Marker	**Fluorochrome**		**Source**	**Catalog Number**	**Antibody concentration**	**Dilution**	**Laser**	**Excitation maxima (nm)**	**Emission maxima (nm)**	**Manufacturer**	**Power**	**Instalation date**	**Detector**	**Dichroic Mirror // Band Pass Filter (nm)**	**Instrument**
CD19	Briliant Blue 515	Mouse	BD Horizon	564456	-	1:20	488	490	515	Coherent Sapphire	100 mW	2009	B - Blue Octagon	505LP // 525/50	FACSAria II Sorp
CD20	APC/Cy7	Mouse	BioLegend	302314	200 µg/ml	1:20	639	650; 755	785	Coherent Cube	40 mW	2009	C - Red Trigon	750LP // 780/60	FACSAria II Sorp
Viability	LIVE/DEAD Fixable Yellow Dead Cell Stain Kit	-	ThermoFisher Scientific	L34959	-	1:500	405	400	575	Coherent Cube	100 mW	2009	E - Violet Octagon	605/40	FACSAria II Sorp
Proliferation	Click-iT® EdU AF647	-	ThermoFisher Scientific	C10424	-	-	639			Coherent Cube	40 mW	2009		Empty // 670/14	FACSAria II Sorp

Supplementary Table S2 continued

Cell Cycle	PO-PRO-1	-	ThermoFisher Scientific	P3581	1 mM	1:5000	405	434	456	Coherent Cube	100 mW	2009	F - Violet Octagon	Empty // 450/50	FACSAria II Sorp
Cleaved Caspase 3	-	Rabbit	Cell Signaling	9661S	-	1:800	-	-	-	-	-	-	-	-	-
γH2AX	PE	Rabbit	Cell Signaling	5763	50 µg/ml	1:50	561	565	575	Coherent Sapphire	100 mW	2013	D - Yellow Green Octagon	570LP // 585/15	FACSAria II Sorp
Isotype Controls and secondary detection															
IgG1k	Briliant Blue 515	Mouse	BD Horizon	564416	-	1:20	488	490	515	Coherent Sapphire	100 mW	2009	B - Blue Octagon	505LP // 525/50	FACSAria II Sorp
IgG2b	APC/Cy7	Rat	BioLegend	400624	200 µg/ml	1:20	639	650; 755	785	Coherent Cube	40 mW	2009	C - Red Trigon	750LP // 780/60	FACSAria II Sorp
IgG XP®	PE	Rabbit	Cell Signaling	5742	100 µg/ml	1:100	561	565	575	Coherent Sapphire	100 mW	2013	D - Yellow Green Octagon	570LP // 585/15	FACSAria II Sorp
anti-Rabbit	Alexa Fluor 594	Donkey	ThermoFisher Scientific	A-21207	2000 µg/ml	1:500	561	590	617	Coherent Sapphire	100 mW	2013	D - Yellow Green Octagon	600LP // 610/20	FACSAria II Sorp

Supplementary Table S2 continued

Supplementary Table S3 Biological effects of experimental treatments on multiple cellular parameters in different cell lines

	DU 145	**cE2**	**SU-DHL-4**	**HCT 116**
Cell viability				
Figure	3A/a	3B/a	3C/a	3D/a
MLN-2924	Decreased	Decreased	Decreased	Decreased
MG-132		Decreased	Decreased	
TRAIL	Unaffected			Unaffected
Surface markers				
Figure	3A/b	3B/b	3C/b	3D/b
Markers	CD44 + Trop-2	CD44 + Trop-2	CD19 + CD20	CD44 + CD133
MLN-2924	Unaffected	Unaffected	Unaffected	Unaffected
MG-132		Decreased	Unaffected	
TRAIL	Decreased			Unaffected
Cell cycle				
Figure	3A/c	3B/c	3C/c	3D/c
MLN-2924	S phase accumulation	G2 phase arrest	Shift to G2 phase	S phase accumulation
MG-132		G2 phase arrest	G2 phase arrest	
TRAIL	Unaffected			Unaffected
DNA damage				
Figure	3A/d, f	3B/d, f	3C/d, f	3D/d, f
MLN-2924	Induced	Induced	Induced	Induced
MG-132		Induced	Induced	
TRAIL	Induced			Induced
Apoptosis				
Figure	3A/e, f	3B/e, f	3C/e, f	3D/e, f
MLN-2924	Unaffected	Unaffected	Induced	Induced
MG-132		Induced	Induced	
TRAIL	Induced			Induced

Supplementary Table S4 Biological effects of experimental treatments on defined cellular subpopulations

		DU 145 Trop-2-	**DU 145 Trop-2 +**
Trop-2 expression	Figure	4A, S3A	
	MLN-2924	Unaffected	Unaffected
	TRAIL	Unaffected	Unaffected
Cell cycle	Figure	4B, S3B	
	Untreated		G2 accumulation
	MLN-2924		Increased G2, decreased S
	TRAIL		Increased G2, unchanged S
DNA damage	Figure	4C, 4E, S3C	
	MLN-2924	Proportionate	Proportionate
	TRAIL	Proportionate	Proportionate
Apoptosis	Figure	4D, 4E, S3D	
	MLN-2924	Not induced	Not induced
	TRAIL	Increased	Decreased